Synthesis of zinc oxide nanoparticles with different morphologies by wet chemistry routes

SYNTHESIS OF ZINC OXIDE NANOPARTICLES WITH DIFFERENT MORPHOLOGIES BY WET CHEMISTRY ROUTES

by

MICHAEL YOUNG

Doctoral Thesis

Submitted in partial fulfilment of the requirements for the award of Doctor of Philosophy of Loughborough University

28th June 2016

Acknowledgements

First of all, I would like to express my upmost gratitude to my supervisor Dr. Xujin Bao for this guidance, knowledge, time, patience and dedication throughout my time as a research student at the Department of Materials in Loughborough University.

I would also like to extend my thanks to other members of staff in the Department of Materials, in particularly Mr John Bates, Dr David Ross, Mr Ray Owens and Andy Lau for their help and training in the characterisation of samples and other laboratory work. My thanks also go to Miss Xuena Yin, (final year project student) and Miss Wenjing Yu, M.Sc project student

I would also like to express my thanks to all my friends, family and work colleagues who have been invaluable in supporting me through this degree process and in particular helping me get over the finish line. In particular, my wife Rachel whose love, care and support was invaluable to me.

ABSTRACT

The objectives of this project were to synthesise semi-conducting ceramic nanoparticles including zinc oxide (ZnO) and aluminium doped zinc oxide (AZO) through a wet chemistry route to obtain nanoparticles with a controlled size and morphology.

Wet chemistry methods (co-precipitation method and hydrothermal method) were used to synthesise ZnO and AZO particles. In the synthesis, various compounds and morphologies were synthesised. ZnO, $Zn(OH)_2$ and unknown phases were co-precipitated, with only ZnO obtained following hydrothermal treatment. Morphologies ranging from platelets, flower-like, nanorods and microflowers were obtained. Particle sizes as small as 11 nm were characterised. Nanorod and nanosphere AZO particles were also synthesised with the results indicated the average grain size decreasing with increasing Al atomic content.

Three orthogonal arrays were carried out to investigate the effects of the reaction parameters on the size and morphology of ZnO particles. The applicability of the orthogonal array was successful, with the optimum parameters of both hydrothermal experiments showing an increase in aspect ratio. The L/D ratio of ZnO nanorods obtained in the confirmation experiment increased to 9.4 which was larger than the ZnO synthesised using other reaction conditions (1.0 – 8.0).

Scanning electron microscopy, transmission electron microscopy and X-ray diffraction were used to characterise the properties of the obtained particles. Morphology, crystallinity and particle size were all characterised.

Key words: ZnO, AZO, nanoparticles, synthesis, particle size, particle morphology, wet chemistry, co-precipitation method, hydrothermal method, orthogonal method, characterisation.

CONTENTS

ABBREVIATIONS

CTAB	Cetrimonium bromide
CVD	Chemical Vapour Deposition
EA	Ethylenediamine
EDTA	Ethylenediamine tetra-acetic acid
FEGSEM	Field Emission Gun Scanning Electron Microscopy
HMTA	Heaxmethylenetetramine
HT	Hydrothermal
PEG	Polyethylene Glycol
PEI	Polyethyleneimine
SDS	Sodium dodecyl sulfate
SEM	Scanning Electron Microscopy
TEA	Triethanolamine
VLS	Vapour-liquid-solid process
VS	Vapour (solid) Process
XRD	X-ray Diffraction

LIST OF SYMBOLS

°C	Degrees Celcius
µm	Microns
Å	Angstrom
B	The measured broadening of the diffraction line peak at an angle of 2 Θ
D	Crystal size
d	Average grain size of a particle
eV	Electron Volts
GPa	Giga Pascals
k	Kelvin
n	Number of moles
Nm	Nanometers
P	Pressure (Pascals)
R	Ideal gas constant
T	Temperature (Kelvin)
V	Volume (m^3)
λ	X-ray wavelength

LIST OF FIGURES

LIST OF TABLES

Chapter 1 Introduction

1.1 Background

Zinc Oxide (ZnO) has many applications ranging from pharmaceuticals to use as a coating additive [1, 2]. In particular, it is the use of ZnO as a wide-bandgap semiconductor that makes the material a good candidate for many electronic applications [1-3].

Nanomaterials are now an established research field over many different scientific and engineering disciplines and are interesting systems for basic scientific investigations as well as for application within current technologies [4]. It is well reported that nanomaterials have novel properties which differ from micron and bulk properties [5, 6].

In general there are two synthesis methods for ZnO nanostructures, wet chemistry based approach and physical techniques. Physical techniques such as Chemical Vapour Depositions (CVD) can produce high quality single layer and multi-layered ZnO nanostructures. However, the physical vapour methods typically require specific substrates types and high operating conditions both of which lead to increased technique cost. Furthermore the techniques can lead to low product yields [3]. Wet chemistry routes allow morphological and structural control by adjusting the growth process parameter in large scale with low cost.

In this project, co-precipitation and hydrothermal synthesis methods are employed to control the morphology and particles size. This is achieved through changing the synthesis parameters and conditions. The effects of starting reactants (salt, base solution), addition of surfactants and hydrothermal conditions will be investigated.

1.2 General aims & objectives

The aims of the project are (1) to synthesise semi-conducting ceramic nanoparticles including ZnO and aluminium doped zinc oxide (AZO) with controlled particle size and morphology by controlling the reaction conditions via wet chemistry approaches such as co-precipitation and hydrothermal and (2) to understand scientifically the reaction

mechanisms and the effects of synthesis conditions, on the formation of ceramic nanoparticles with different particle sizes and morphologies.

The objectives of the project are to:

1. Investigate the effects of reaction conditions including reaction temperature, reaction time, salt precursors and base solutions on the particle size and morphology of ZnO and AZO nanoparticles by co-precipitation method;

2. Investigate the effects of reaction conditions including reaction temperature, reaction time, salt precursors and base solutions on the particle size and morphology of ZnO and AZO nanoparticles by hydrothermal method;

3. Investigate the effect of the addition of surfactants on the particle size and morphology of ZnO and AZO nanoparticles by co-precipitation method and hydrothermal method;

4. Characterize the nanoparticles synthesized using Scanning Electron Microscopy (SEM) and Transmission Electron Microscopy (TEM). The crystal structures of selected samples will be identified using X-ray Diffraction (XRD).

1.3 Layout of the thesis

Seven chapters are included in this thesis, starting with this chapter, the introduction, which provides the background, aims and objectives and layout of the thesis.

In Chapter 2, the literature review is presented, including a brief introduction of nanomaterials and their applications, the details of the synthesis of ZnO particles by both co-precipitation and hydrothermal methods with or without addition of surfactants.

Chapter 3 provides the experimental details, including the chemicals used, co-precipitation and hydrothermal routes and the setup of the orthogonal arrays. The characterisation techniques are also described.

The results of the synthesis of particles using co-precipitation and hydrothermal methods are provided in Chapter 5 and Chapter 6, respectively. The details on the effects of synthesis conditions on the particle size and morphology of ZnO including starting salt, base solution, addition of non-ionic and ionic surfactants are presented. Each chapter also includes the results of orthogonal arrays. The aim of the orthogonal arrays is to optimise the reaction conditions for the growth of particles with controlled particle size and morphology. Synthesis and characterisation of aluminium doped ZnO by hydrothermal method are also presented in Chapter 6.

Analysis and discussion of the results are provided in Chapter 7, which mainly focuses on the discussion and understanding of the effects of the reaction conditions on the formation mechanisms of the nanoparticles with different particle sizes and morphologies.

Conclusion and further work are presented in chapter 8.

Some details of the calculations using orthogonal arrays, SEM, TEM micrographs and synthesis and characterisation of block polymers using as potential template for synthesis of ceramic nanoparticles are presented in the Appendix.

Chapter 2 Literature Review

2.1 Nanomaterials and their applications

It is well known that nanostructured materials have properties that are defined by features that are smaller than 100nm. As a broad range of properties, such as electrical conductivity, depend on nanometer-scale features, the term “nanostructured material” can include most materials. A reason why this class of materials is considered to be particularly interesting is the opportunity to achieve “materials-by-design” [7, 8].

Nanomaterials can be made using both top-down and bottom-up techniques. Self-assembly bridges these two techniques and can allow materials to be designed with both complex and hierarchical order. Self-assembly of nanostructured materials offers a low-cost, high-yield solution to a wide range of applications [7, 8].

There are generally two approaches for synthesising nanostructures. These are the “top-down” and “bottom-up” techniques. The “top-down” technique can be defined as the formation of nanoscale structures by the removal or subtracting parts of a bulk material. The “bottom-up” technique involve the assembly of sub nanoscale building blocks to build the required nanostructure. The “bottom-up” method has the advantage of being able to fabricate extremely fine features and structures [9 8, 10].

Nanostructured materials can be organised into 3 different groups, different sizes, different functions and different structures, as shown in Figure 2-1.

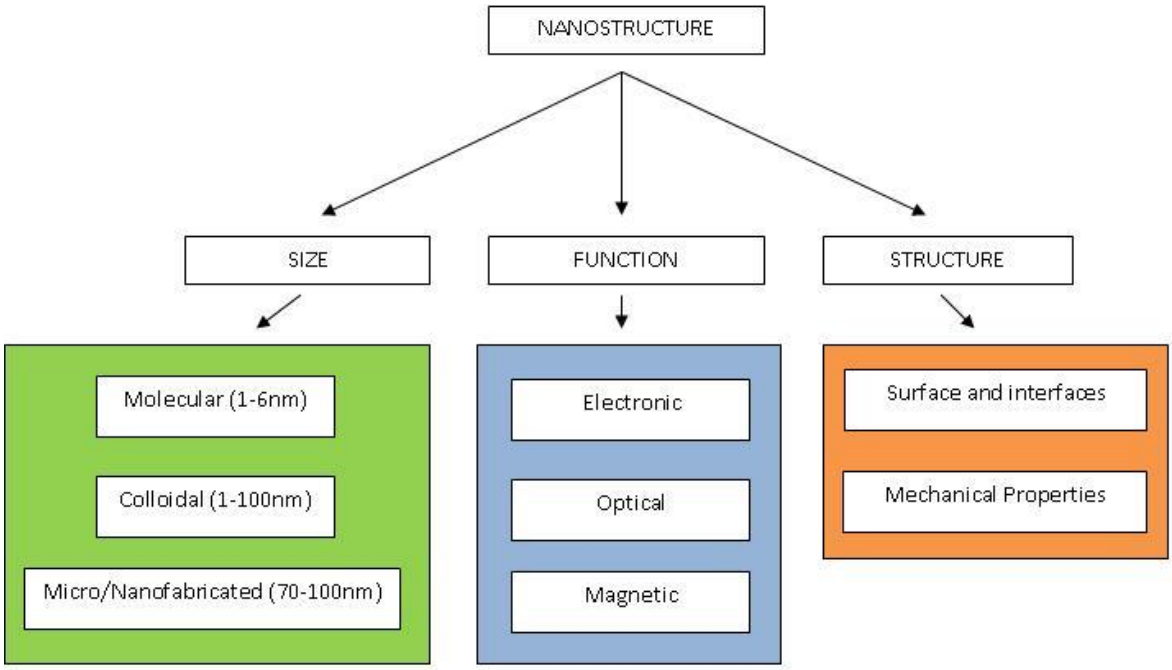

Figure 2-1: Diagram showing the organisation of nanostructures into three different groups; size, function and structure with each group highlighting some parameters from each group.

There are many different uses of nanostructures, including the production of electronic components, sensors, multifunctional materials, structured colloids. They can also be used within manufacturing processes and the manipulation of surface. These uses are summed up in Figure 2-2.

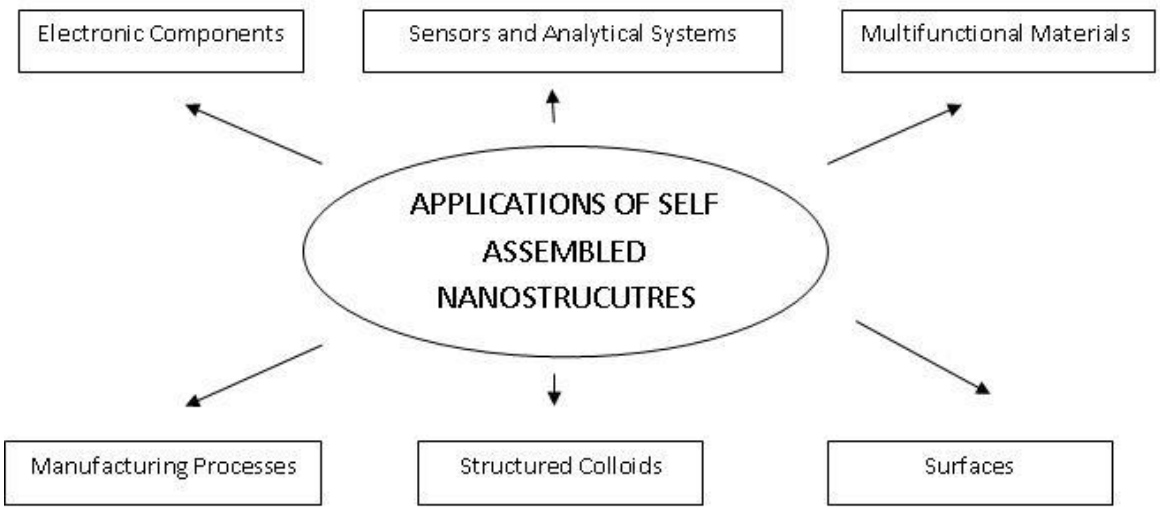

Figure 2-2: Diagram showing a summary of the different areas and applications related to nanostructures

2.2 Structure, properties and applications of ZnO

ZnO nanostructured materials have received significant interest due to their performance in electronics, optics and photonics due to possessing good piezoelectric and pyroelectric properties. With a wide band gap (3.37 eV) it is perfectly suitable for short wavelength optoelectronic applications. The high excitation binding energy (60 meV) allows for efficient excitonic emission at room temperature and can be desirable for photonic applications [11, 12]

The structure of ZnO can be described as a number of alternating planes composed of tetrahedrally co-ordinated oxygen (O^{2-}) and zinc (Zn^{2+}) ions. These ions are stacked alternatively along the c-axis. The tetrahedral coordination in the metal oxide allows for a non-central symmetric structure. This leads to both piezoelectric and pyroelectric properties [11-13].

There are three crystal structures of ZnO that are known of, hexagonal wurtzite, cubic zinc blende and a cubic rock salt (Sodium Chloride type) structure. The hexagonal wurtzite structure (Figure 2-3A) is the most common, with the zinc-blende structure (Figure 2-3B) being metastable and can only be grown on cubic structures [14]. A cubic rock-salt structure (Figure 2-3C) can only be stabilised under extreme pressures (> 2 GPa) [11]. Graphical representations of the structures is given in Figure 2-3.

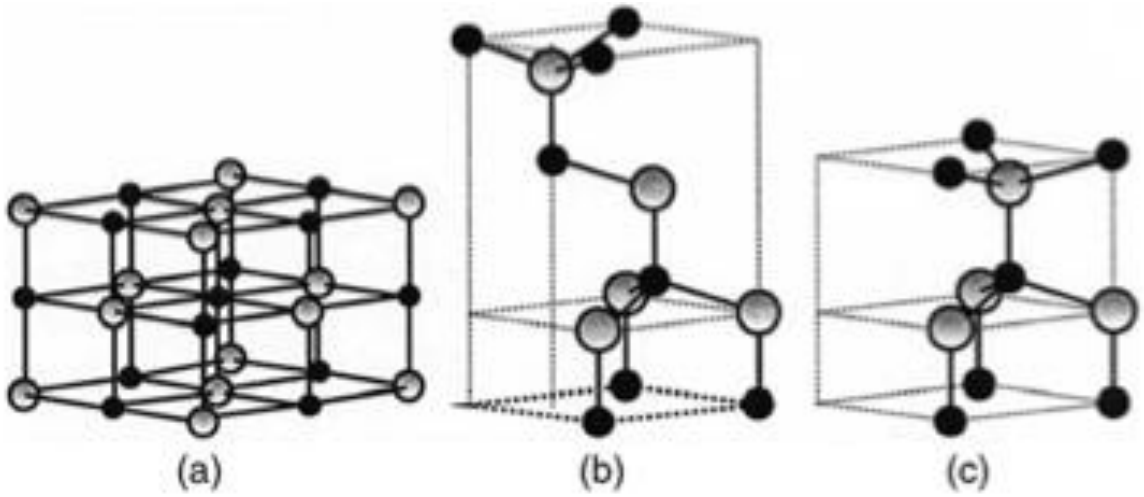

Figure 2-3: Representation of ZnO crystal structures: (a) cubic rocksalt, (b) cubic zinc blende and (c) hexagonal wurtzite structure. The shaded grey and black sphere denote zinc and oxygen atoms respectively [15].

The wurzite structure (Figure 2-3A) is a hexagonal lattice and features non-centrosymmetric symmetry and polar surfaces [16]. The structure belongs to the space group $P6_{3mc}$ and is characterised by two interconnecting sublattices of Zn^{2+} and O^{2-}, such that each zinc ion is surrounded by a tetrahedral of oxygen ions, and vice versa [17]**.**

For crystal structures to remain stable, the polar surfaces within the structure generally have or exhibit surface reconstructions. However, the ZnO crystal structure is different. The ZnO crystal facet ±(0001) is atomically flat, stable and does not exhibit reconstruction. The polar surfaces and other facets of the common ZnO wurtzite crystal structure are shown in Figure 2-4 [11, 12, 15].

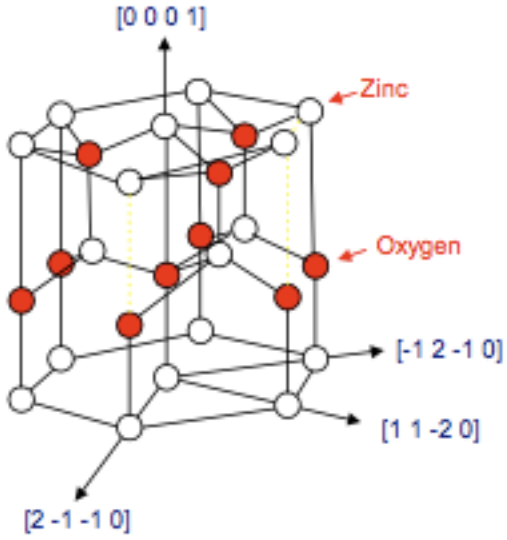

Figure 2-4: The wurzite crystal structure of ZnO with its polar surfaces and various facets represented.

2.2.1 Properties of ZnO

ZnO is considered to have specific optoelectronic, electrical and thermal properties that allow for an assorted range of applications.

The structure (non-centrosymmetric) and polarity found in the ZnO crystal structure can result in good piezoelectric and pyroelectric properties. However, ZnO is also considered to have other advantages to its nanostructure. This includes the potential for high specific surface area, a low toxicity, chemical stability, strong electrochemical activity and high conductivity [15].

The wide band gap exhibited by ZnO (3.37eV) [18] and exciton binding energy (6m meV) allows ZnO to possess some useful optoelectronic properties [12, 19]. The advantages associated with a large band gap include the ability to sustain large electric fields, lower noise generation and the ability to operate under high temperature and high power operation [19]. Electrical conductivity has also been shown to increase with temperature [11]. However, the electrical properties of ZnO are hard to quantify as it depends significantly upon both its stoichiometry and processing conditions [17].

2.2.2 Applications of ZnO

ZnO is used within a wide range of industries in the form as both a bulk product and a nanomaterial. The following table (Table 2-1) represents some of the industries and ZnO use within them [15, 20, 21].

Table 2-1: Summary of industries and subsequent applications in which ZnO is used.

Industry	Application
Electronics	Varistors, Piezoelectric Transducers, sensors, surface acoustic wave devices, solar cell electrodes [15], light emitting devices, memory devices, transparent transistors [11, 22]
Ceramics and concrete	Additive to improve heat capacity, thermal conductivity and high temperature stability of ceramic i.e. tiles. Allows the development of different types and property of surface finish i.e. reduces elasticity in the glaze to reduce cracking and shivering. In concrete, ZnO provides a longer processing time and improves the concretes resistance against water [11].
Rubber	Effect activator of the curing process of natural rubber, increase heat conductivity in tires, retards devulcanization of rubber types, stabilization of latex foam [15].
Plastics	Additive to tune properties such as viscosity, fire-resistance, tensile strength [15].
Coatings	Colour additive, provides sacrificial cathodic protection within coatings [15].
Pharmaceutical	Antiseptic healing creams, sunblock lotions [15]. Antibacterial properties [23].
Agriculture	Source of micronutrient zinc [15]
Oil and Gas	Use as a bulk absorbent for the control of H_2S in drilling fluid formed by the presence of sulphate reducing bacteria [11, 15]

Industry	Application
Catalysts	Use as one of the mixed oxides in catalysts for the production of methanol. Additionally used as a catalyst for the synthesis of *iso*-butyl alcohol, formose sugars and the conversion of cyclohexanol to cylcohexane in the course of the production of caprolactam (a precursor for nylon) [11].

2.3 Synthesis of ZnO

There are various methods that can be used to synthesise ZnO including top-down approaches such as CVD, Spray pyrolysis, Ion beam assisted deposition and sputter deposition and bottom-up approaches such as co-precipitation and hydrothermal synthesis. Unlike the top-down methods, these wet chemical methods involve a lower synthesis temperature, which allows for good control over the size and morphology of the ZnO nanostructures.

2.3.1 Vapour transport methods

A typical vapour transport process involves the reaction of a Zn vapour and O_2 vapour mixture to form nanostructures. The often high processing temperatures involved in these methods can lead to unusual grain growth. Subsequently it becomes harder to prepare a controlled ZnO nanostructure.

The zinc vapours are generated by the decomposition of bulk ZnO or the heating of zinc powder. The decomposition of ZnO also provides the O_2 source, otherwise it is provided from an external tank. The required nanostructures can be achieved the manipulation of the zinc and oxygen vapour ratios and by control of the presence of a metal catalyst e.g. Au, NI, Co and Sn [24, 25]. However, the presence of catalysts in the final product is not always desirable, so two vapor transport methods are used, Catalyst free vapour solid process (VS) and catalysis assisted vapour-liquid-solid process (VLS).

Nano structures, including wires, rods and belts can be synthesised using the VS process and examples are shown in Figure 2-5 [26].

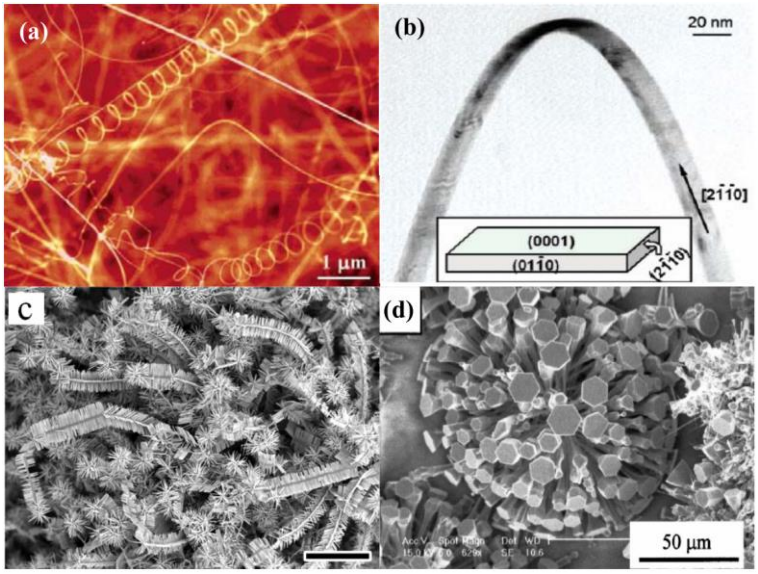

Figure 2-5: Examples of structures formed using the VS process a) spiral b) nanobelt c) Hierarchical d) rods [26].

By using the catalyst assisted VLS method, a more controlled geometry can be achieved. In addition, the alignment and growth location of the nanostructures can be controlled. In the VLS process, elements such Au, Cu, CO and Sn are often used as catalysts. Figure 2-6 represents a flow diagram of a typical VLS method, which in this instance leads to the formation of nanowires. Firstly, the nucleation and growth of ZnO nanowires is caused by the supersaturation of a liquid eutectic alloy droplet. It is from the droplet interface that ZnO nanowire growth occurs. As the catalyst is pushed upwards due to the growth of the wires, further nucleation occurs at each catalytic site as a consequence of this movement [26].

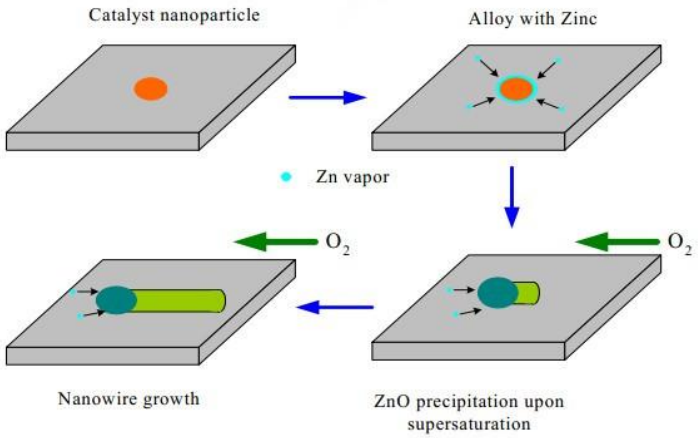

Figure 2-6: Schematic diagram of catalyst assisted VLS process [26]

An example of this method would be the growth of ZnO nanowires. Gold (Au) nanoparticles (the catalyst) and Zn powder were deposited on a substrate and heated in a pre-defined amount of O_2. The as-prepared ZnO nanowires are shown in Figure 2-7. The image shows the uniform diameters and the presence of Au nanoparticles on the end of the wires.

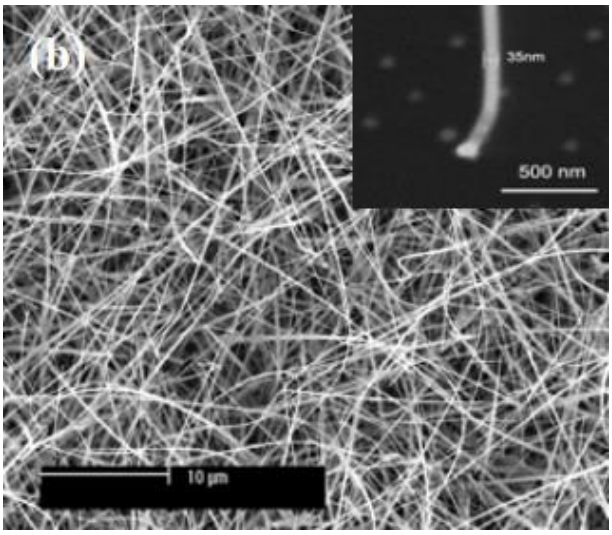

Figure 2-7: SEM image of ZnO nanowires produced via catalyst assisted VLS process [26]

2.3.2 Chemical Vapour Deposition method

CVD is a chemical process popular with the semiconductor industry and is capable of preparing single layer and multi-layered nanostructures. In a typical CVD process, non-volatile materials (e.g. ZnO) are deposited on the surface of a substrate through the

reaction of volatile compounds. This reaction can occur on the growth surface or within the gas phase [27].

An example of ZnO nanostructures prepared by these methods is the spear-like nanostructures shown in Figure 2-8. The source materials were ZnO and carbon powder, the nanostructures were deposited upon a p-Si (100) substrate.

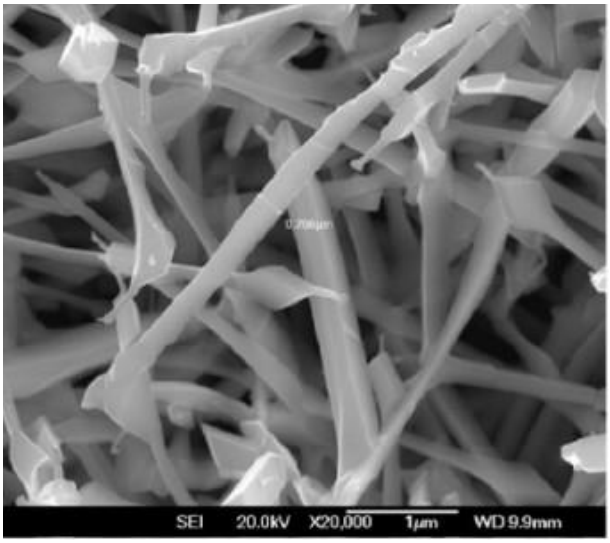

Figure 2-8: SEM image of spear-like ZnO nanostructures deposited via CVD process [27]

2.4 Co-precipitation synthesis method

The co-precipitation method is used to produce solid precipitates via the reaction of two or more chemical solutions. The precipitates are obtained by a cycle of filtering washing and drying. Sometimes further calcination is required to produce desired phase and chemical compositions.[28].

This type of synthesis method is often used due to the simple and rapid nature of the reaction. By varying conditions such as, but not limited to, pH value and reaction temperature the particle size and composition of the particles can be controlled [28].

2.5 Effect of precipitating reagents

The effect of precipitating reagents shows how either a change in the zinc or alkaline source can affect the morphology.

The change in the zinc source represents how the anion in the synthesis reaction can have an effect on particle growth. Hu et al [29] discussed the effect of the anion by comparing three different zinc salts. Zinc acetate dihydrate ($Zn(CH_3COO)_2 \cdot 2H_2O$), zinc bromide ($ZnBr_2$) and zinc perchlorate hexahydrate ($Zn(ClO_4)_2 \cdot 6H_2O$) were reacted with NaOH in propan-2-ol. The reactions were conducted at 65°C.

The aim of the work was to discuss the effects of the anions, acetate ($CH_3CO_2^-$), bromide (Br^-) or perchlorate (ClO_4^-) in the nucleation reaction given below [29]:

$$ZnX_2 + 2NaOH \rightarrow ZnO + 2NaX + H_2O$$

The resultant ZnO particles synthesised included non-faceting spherical particles (Br^-) to spherical with faceting ($CH_3CO_2^-$) to elongated irregular shaped particles (ClO_4^-). From these results, the author showed that the metal salt (anion) had a direct effect on the coarsening rate of the particles. It was found that regardless of the reaction temperature the coarsening rate of the ZnO particles was fastest for the solution synthesised with $Zn(ClO_4)_2 \cdot 6H_2O$ and was the slowest for $ZnBr_2$. The difference in coarsening rates was considered to be due to the tendency for the anion to adsorb on a surface. Halide ions were suggested to adsorb the most strongly on the surface, with acetate ions adsorption weaker still and perchlorate ions exhibiting the weakest surface interactions [29].

The effect of a change in zinc source was also investigated by Xiao et al. and Xu et al, who reported on the use of $Zn(NO_3)_2$, $ZnCl_2$, $ZnSO_4$ and $Zn(CH_3COO)_2$ as the comparable zinc source in a co-precipitating reaction

Xiao et al. reported precipitated morphologies of rod-like ($Zn(NO_3)_2$), sheet-like ($ZnCl_2$ and $ZnSO_4$) and ellipsoidal shapes ($Zn(CH_3COO)_2$). The formation of sheet-like was attributed to the adsorption of sulfate and chloride ions on the surface of the polar c-axis [30].

The resulting morphologies synthesised by Xiao et al. [30] using the same zinc sources were discussed from a kinetic perspective. It was reported that the reaction rate constant of the crystal growth stage decreased with the decreasing electronegativity of the anion from $Zn(NO_3)_2$ (En = 3.91) to $ZnCl_2$ (En = 3.16). The author noted that $Zn(CH_3COO)_2$ was not considered in this conclusion as the compound is known to act as an organic salt in comparison to the inorganic salts discussed.

The effect of the cation or alkaline source is also noted to have an effect on the growth of ZnO. Chittofrati et al [20] discussed the change of alkaline source in a reaction with $Zn(NO_3)_2$. The work demonstrated that the particle shape was strongly dependent upon on the nature of the added base. When reacted with ammonia (NH_3), triethanolamine (TEA) and ethylenediamine (EA) respectively precipitates were only formed when NH_3 was used. In this case the precipitate where irregular in shape. For both TEA and ethylenediamine no precipitate was reported.

Further samples were therefore synthesised at 90^oC to allow the reaction with TEA and EA to occur. At this temperature, the particles synthesised with ammonia coarsened and became intertwined ellipsoidal shaped solids. The use of ethylenediame led to similar particles being formed. When TEA was used spherical particles were formed [20].

A comparison between NH_3 and sodium hydroxide (NaOH) was shown by Shaporev et al. [31]. At room temperature both the compounds and morphology of the precipitated solids were shown to be different. The use of NH_3 yielded zinc hydroxide ($ZnOH_2$), whereas samples prepared with NaOH yielded both wülfingite $ZnOH_2$ and ZnO.

To understand the phase transformation during ZnO formation the same solutions were synthesised in hydrothermal and pre-hydrothermal conditions. The alkaline concentrations and heat treatment were designed to allow a direct comparison between the two alkaline sources. These conditions would also show the major products and intermediated in the synthesis of ZnO [31]. With respect to the specific co-precipitation work, ZnO was only synthesised in both experiments at 80^oC and 85^oC for NaOH and NH_4OH respectively. In both cases platelet like particles were synthesised [31].

2.5.1 Effect of pH

Within the use of the co-precipitation method, the effect of pH would be considered to be one of the most reported. The effect of pH in a co-precipitation reaction is considered an important parameter. For example during a co-precipitation method in water the charge of an oxide or hydroxide surface is dependent upon the pH of the solution. At low pH, hydroxide surface adsorb protons to produce a positively charged complex. At high pH they lose protons to produce negatively charged complex. It is these complexes in the solution that are the precursors to the solid formation (nucleation). As such pH of the solution is considered very important in the formation and final morphology of ZnO [20, 32].

Experimentally, the effect of pH has been reported with respect to the effect of the speed of crystal growth [33] and the surface effects [34]. At high Zn^{2+}/OH^- ratios the nucleation rate is high leading to a large amount of nuclei but a low amount of the subsequent growth unit leading to a relatively slow crystal growth. As the ratio decreases the opposite is found. Li et al reported a change in morphology from monodisperse 1D nanorods to 3D flower like bundle as the pH increased [33]. At a low pH, the individual nuclei allowed for controlled aggregation in the favoured c-axis. At the high pH, the aggregation was uncontrolled and branched, flowerlike structure was formed. This change in morphology is shown in Figure 2-9.

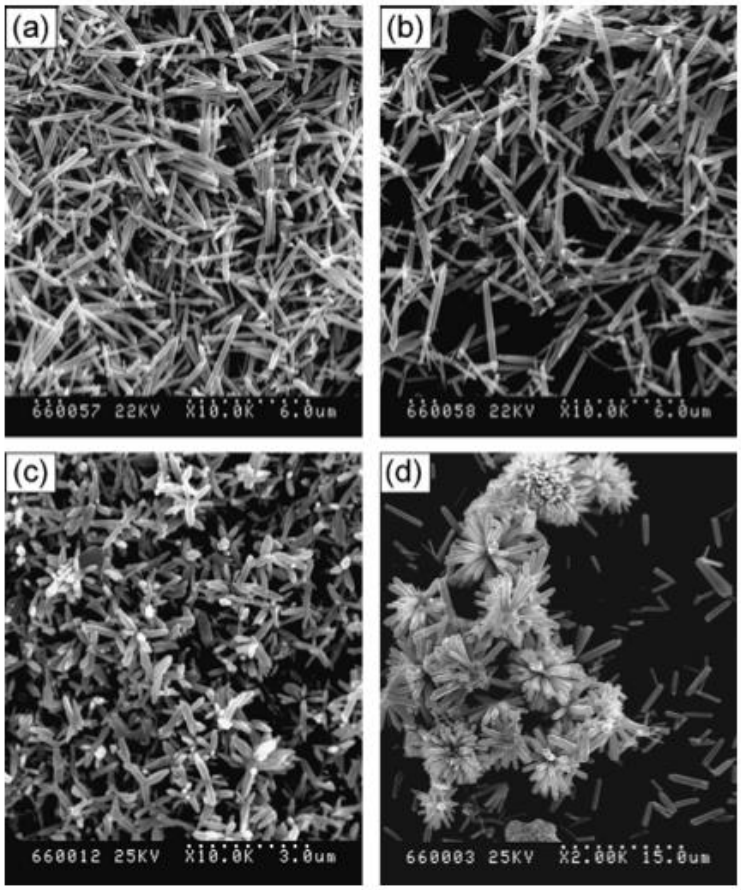

Figure 2-9: SEM images of ZnO microcrystals obtained with different molar ratios of Zn2+/OH− and without any additive (a) 1:6; (b) 1:7; (c) 1:4; (d) 1:8. [33]

Further work by Wahab et al. [34] demonstrated the morphological change when the pH of a precursor varied. Solutions were synthesised with $Zn(CH_3COO)_2 \cdot 2H_2O$ and NaOH with the base added to increase the pH from 6 to 12. The author showed in detail the morphology change and growth from a sheet like structure (pH 6) to a rod like structure (pH 12).

A different study on the effect of pH was present by Vaishampayan et al. [35] who discussed the use of the reaction between $Zn(CH_3COO)_2 \cdot 2H_2O$ and ethanolamine rather than a more traditional alkaline source such as NaOH or NH_3. By control of the molar ratio of the two reagents the pH of the solution was adjusted from 7 to 10.08. It was shown as the pH increased the morphology changed from nano belts to crystalline nanoflowers.

Though not synthesised by a co-precipitation reaction, Degen et al [32] examined the effect of the initial pH on an aqueous suspension of ZnO. It was shown by dissolving ZnO powder

into water and adjusting the pH, that the ZnO suspension could not be electrostatically stabilized in the present pH range between 7.2 and 12 due to the formation of unstable particles of $Zn(OH)_2$. By analysing the pH, it was shown that during this transformation consumption of hydroxyl ions lowered the final pH of the suspension.

A thermodynamic model for the control of the low temperature aqueous synthesis of ZnO was developed by Richardson and Lange [36]. The model was developed to help calculate the solubility and expected ionic species of ZnO as a function of pH, NH_3 concentration and temperature.

At certain ranges of pH and NH_3 concentration, ZnO synthesis can take place under thermodynamic control rather than kinetic control. The model showed that ZnO solubility in NH_3 solutions could be greater that at lower rather than higher temperatures. Due to the fact that it is believed that better crystal growth happens at near equilibrium conditions, the model could help the understanding of a continuous and steady state growth of ZnO in a lower temperature reactor [36].

However the authors warn that care must be taken with the analysis, as the pH of the solution is also dependent on temperature. It was discussed that pH generally decreased with temperature due to the increase de-dissociation of water. To get round this, Richardson and Lange treated pH as an invariant with temperature to be able to obtain an analytically traceable solution. The authors concluded that the model could not be used to provide a quantitative means of prediction of experimental results [36].

2.5.2 Effect of precipitating conditions

The change of the experimental procedure, such as refluxing temperature and time [37-39], pre-stirring [40] and solvent evaporation can have just as much of an effect on the morphology of ZnO as any change in chemicals or concentrations.

The effect of temperature is important for the formation of ZnO. Thermal analysis of a co-precipitation reaction with Zinc Nitrate $(ZnNO_3)_2$ and either NaOH or NH_4OH showed distinct chemical histories. Precipitated samples showed the formation of $Zn(OH)_2$ up to

100°C, with the decomposition to ZnO only occurring above 100°C. The weight loss curve for $Zn(OH)_2$ precipitated at 60°C from both reagents is shown in Figure 2-10 [31].

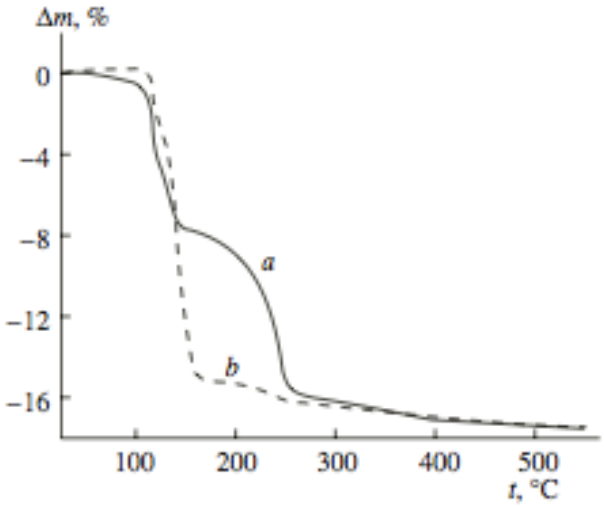

Figure 2-10: Weight loss curve for samples preoperated by the HT treatment of zinc hydroxide compounds with (a) ammonia and (b) NaOH at 60°C for 1 hour [31]

Whereas the effect of temperature is related to the formation of ZnO, the effect of (refluxing) time can be associated to particle size [38, 39, 41]. In general, the increase in time leads to an increase in crystal growth and subsequently crystal size. Even when the co-precipitation reaction was incomplete, Music et al reported, decreases in the specific surface area of the formation complexes indicated an increase in particle size. [41].

Hou et al. reported on a change of morphology due to the change in reaction (refluxing, 90 °C) time between Zinc Nitrate and Heaxmethylenetetramine (HMTA). [42]. Figure 2-11 shows ZnO samples synthesised and collected after 10, 60, 120 and 180 minutes. A change from a lamella aggregate to a dumbbell-like microcrystal was observed as the reaction time increased. The crystallinity also was reported to have steadily increased [42].

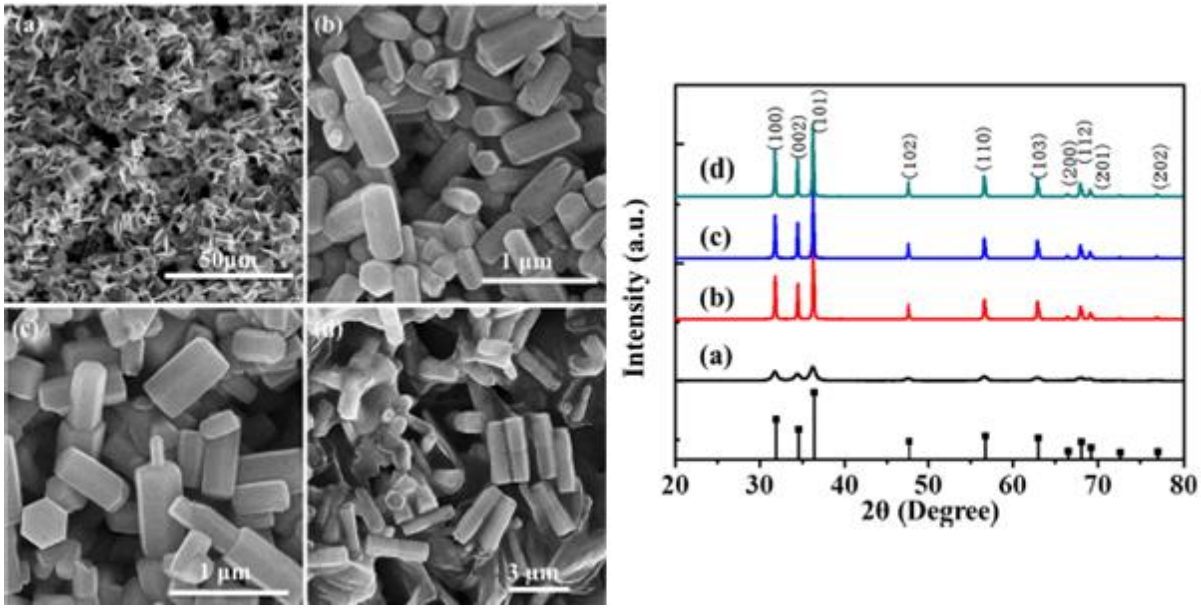

Figure 2-11: (Left) SEM image of synthesised ZnO samples with different reactions times (a) 10 min (b) 60 min, (c) 120 min, (d) 180 min (Right) XRD patterns of the different reaction times. The sequence is the same as the SEM images [42].

In general there are two models for the continual growth of ZnO, Ostwald ripening [43] and oriented attachment. The two models can be summarised as follows:

- Ostwald ripening states that in a particle system with a variation in particles size the larger particles grow at the expense of the smaller particles [38].
- Oriented attachment states that growth stems from spontaneous self-organisation of adjacent particles. This is by sharing a common crystallographic orientation, which leads to joining of the particles at a planar interface [38].

A change in refluxing time can also have an effect on crystal growth. Ge et al. manipulated the length of ZnO nanorods by increasing the refluxing from 24 hours to 176 hours. The nanorods were reported to increase ten-fold in length from 20nm to 100 nm as the time increased. The increase in ZnO nanorods are shown in Figure 2-12 [38].

Though the author discusses other growth mechanism, such as the Bravasis, Freidel, Donnary and Harker (BFDH) and the HP model as possible reasons for the effect of refluxing time, the oriented attachment discussed previously was considered the most likely

mechanism. This was due to the detection of growth from single nanoparticles through Fourier Transform Infrared Spectroscopy (FTIR).

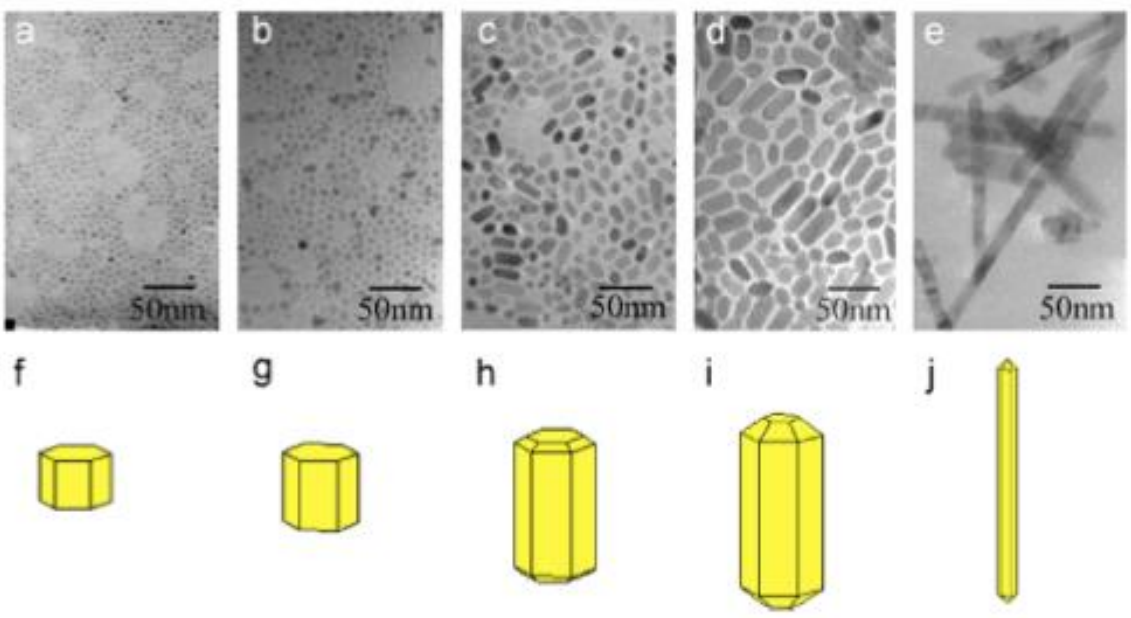

Figure 2-12: TEM images of ZnO nanorods obtained from different reflux times: (a–e) reflux times of 0, 24, 48, 96 and 176 h, respectively; (f–j) the simulated geometries of ZnO during growth process.

McBride et al [40] showed how a pre-stirring step before refluxing in a $Zn(NO_3)_2$ and NaOH precipitating reaction could change the morphology from a star-like particle to a needle-like particle. Further analysis of the pre-stirring step, by withdrawing samples immediately after precipitating and a set stirring time found the particles were initially a rhombic morphology which gradually increased in size and became more uniform over time. However it was noted that there was a limit in the development of the crystal size if samples taken after the mixture were stirred for a further hour; no further change was reported. The work concluded that due to this time restricted growth, and a transient drop in Zn^{2+} ion concentration that the pre-stirring had caused a change to the rate of nucleation.

In contrast, Samanta et al. reported a change in morphology when the pre-stirring step was increased from 4 hours (octahedral shaped) to 6 hours (nanopencils) in zinc acetate (0.1M) and NaOH (1M) reaction [44].

The effect of solvent content, or evaporation of the solvent is discussed by Seow et al. [45]. As the solvent content was reduced, the concentration of Zn^{2+} ions proportional to the solvent increased. The high concentration of the polar growth species (Zn^{2+}) ions led to a fast anisotropic growth of ZnO along the c axis. At a sufficiently high precursor concentration, an oriented attachment mechanism occurred, leading to an increase in crystal size as the amount of solvent decreased. This effect is shown in Figure 2-13.

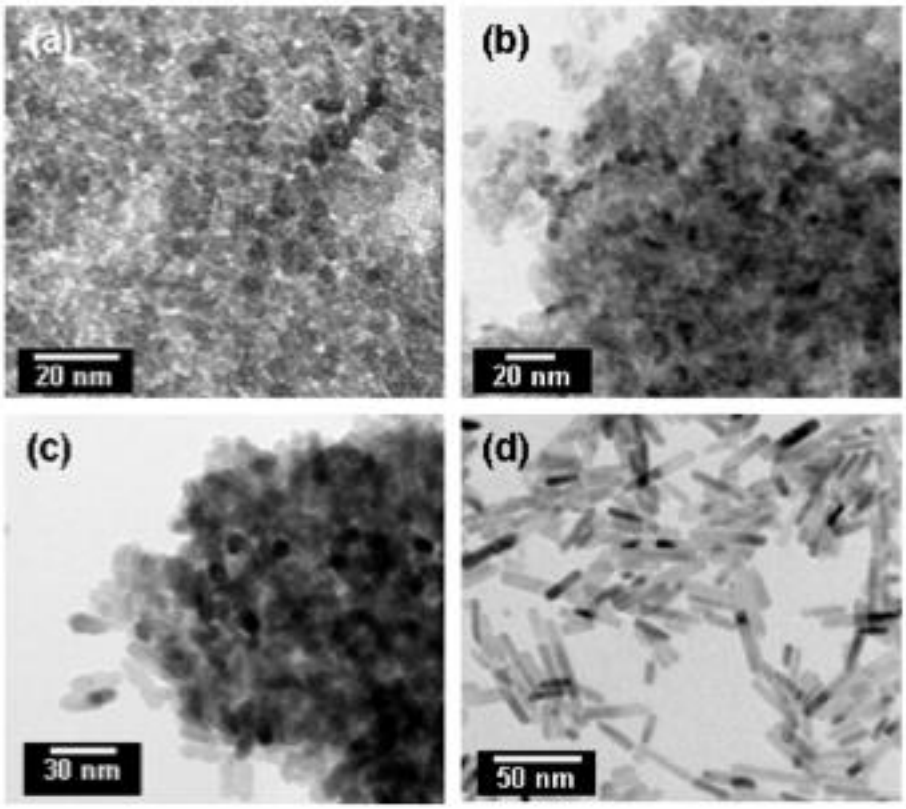

Figure 2-13: TEM images of ZnO nanostructures grown without (a) evaporation and with evaporation to (b) 50, (c) 20 and (d) 10% of its original solvent volume [45].

2.5.3 Effect of surfactant

The effect of surfactants (and polymers in general) on the morphology of ZnO is regarded to be due to the adsorption of the surfactant onto the ZnO crystal during growth [33, 46-48]

Li et al, and Anas et al discussed the difference in ZnO morphology by comparing the effect of two surfactants. Li et al [46] found a change in morphology (Figure 2-14) from rod-like,

when no surfactant was present to nut-like or rice-like when SDS or TEA were used respectively.

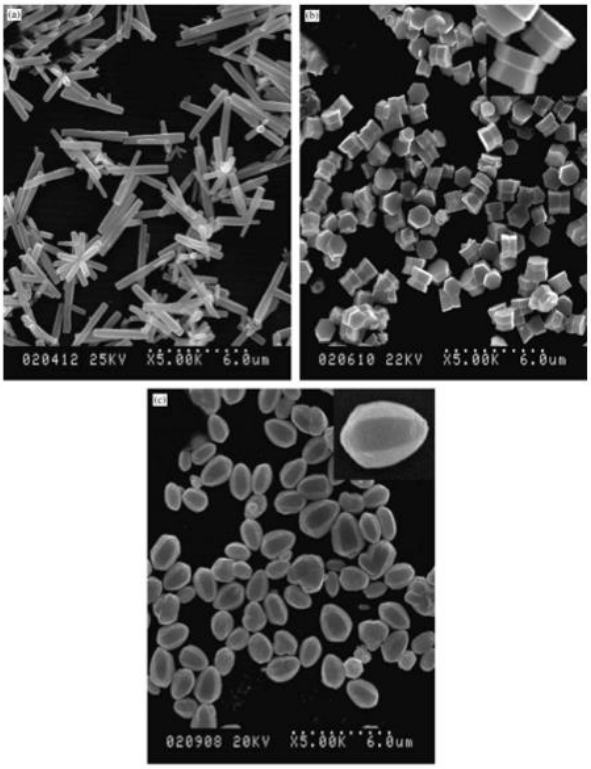

Figure 2-14: SEM images of ZnO microparticles prepared with different additives: (a) no additive; (b) with 0.01 M SDS; and (c) with 0.1 M TEA [46]

The reason for the two distinct morphologies was the adsorption of the surfactant on the ZnO crystal. The rice-like morphology found when TEA was used suggested a non-uniform adsorption compared to SDS. In the case of SDS, its geminal (two active sites) structure was considered to absorb two ZnO nuclei on the (0001) face. This retarded growth in the c-axis forcing growth in the slow $(000\overline{1})$ face and side faces leading to the nut-like shape [46]

Anas et al noted a similar mechanism, with the use of Span-80 in a comparison with CTAB [48]. At high concentrations of Span-80, hexagonal discs of ZnO were synthesised reportedly due to the long chain nature of the polymer suppressing growth along the (0001) direction, inducing growth along the six symmetric hexagonal directions. In a comparison with CTAB, which led to the formation of nanorods, absorption occurred but did not inhibit crystal growth from nucleation. Instead the CTAB is suggested to form a surfactant layer and only prevent

growth when once the crystal reaches a size that allows complete coverage of CTAB. The function of TEA was further discussed by Li et al.[33] where flower-like structures were formed under the co-precipitating conditions. As well as the non-uniform-adsorption, the use TEA caused a decrease in Zn^{2+}/OH^- due to its nature of strong basicity.

The chain length of the surfactant can also have an impact on the morphology. When changing the chain length of PEG from 200, 400, 6000 and 1000, nanoneedles (200) or flowerlike-like (400, 600 & 1000) nanostructures were synthesised. When a short-chain PEG was added, selective adsorption on of some areas of ZnO surface caused restriction of growth in some directions. This led to the needle like structure. When the PEG chain length increased flower-like structures were achieved. This was believed to because of fill adsorption on the surface of ZnO nuclei selected growth from specific active sites covered with PEG.

2.6 Hydrothermal synthesis method

The hydrothermal method has received attention recently as particles can be prepared with desired characteristics. This is achieved by the proper control of variables such as solution pH, reaction time and temperature, inclusion of additives and the type of solvent used (solvothermal method) [28, 49].

The advantage of this process is that it provides a route for homogeneous nucleation which can lead to very small grain sized crystal particles with narrow size distribution, good chemical homogeneity and high purity. This can often be achieved without further calcination being required [28, 50]. The technique has been shown to prepare particles with a higher crystallinity than particles co-precipitated and calcinated [51]..

Other advantages of the method include: [52, 53, 53]

- The method is inexpensive. The costs for the equipment, energy consumption and reactant materials are low. These points are also applicable from an environment perspective. Podrezova et al. provided a comparison between CVD and hydrothermal techniques. Both techqniues led to the synthesis of ZnO nanowires with comparable

growth and crystal quality and highlighted the advantages of operating in mild conditions (and subsequently cheaper production costs) [54].

- For the production of ceramic powders there is less unnecessary mixing and milling required.
- The hydrothermal route is capable of directly precipitating thin film coatings onto the surfaces of the substrate at low temperatures.
- The method can produce single crystals that are hard to synthesis using other approaches.
- Doping elements can be easily incorporated and controlled (Doping can be an effective means of enhancing the properties of the base materials).
- New materials can be prepared by the combination of a hydrothermal synthesis with other processing techniques such as microwaves, electrochemistry and ultrasound.

A disadvantage of the method is the inability to directly manipulate the particles during growth. This is because the reaction occurs in a closed system. For example temperature changes are driven by the heaters (i.e. an oven) around the autoclave. This means that the temperature is unable to change quickly preventing any sharp temperature changes in the solution. One other disadvantage is the lack of visual observation of the reaction due to the construction of the autoclaves [55].

The term “hydrothermal” is derived from geology [55]. Hydrothermal synthesis usually refers to heterogeneous reactions in aqueous media above 100^{o}C under pressure. This normally achieved by the use of a closed high-pressure growth vessel, also known as an autoclave.

This section of the literature review focuses on the synthesis at temperatures above 100^{o}C and conducted within a Teflon lined autoclave. The same parameters discussed in the previous section will also be focussed upon in this literature review. In some cases it has been relevant to discuss the use of a solvothermal method to discuss a parameter.

2.6.1 Effect of precipitating reagents

The effect of precipitating reagents has been widely studied when hydrothermal conditions have been employed.

Chittofrati et al [20] noted the effect of a hydroxide alkaline source (NaOH), lithium hydroxide (LiOH) & potassium hydroxide (KOH) when reacted with $Zn(NO_3)_3$ and then hydrothermally treated. The results showed that when KOH & NaOH were used as the alkaline source rod like particles were synthesised. However under the same conditions LiOH formed irregular particles of no distinct geometry. The author considered Li^+ affected the nature of the nuclei of generated in situ preventing directional crystal growth behaviour.

A comparison between the hydrothermally (150^{o}C, 6 hours) synthesised ZnO formed with zinc chloride ($ZnCl_2$) and alkaline sources hydrazine hydrate (NH_2NH_2) and NaOH respectively was conducted by Zhu et al [56]. ZnO nanorods were found to have been formed with hydrazine as the mineraliser, with irregular nanoparticles forming with NaOH as the alkaline source. The work was an example of the alkaline source acting twofold. The hydrazine was thought to have acted as both an alkaline source and a complexing agent.

Several kinds of ZnO multi-interfacial structures were prepared by changing the zinc source in a precipitation reaction at 373K (100^{o}C) for 20 hours [30]. Sodium hydroxide was used as the alkaline source and the zinc salts were $Zn(NO_3)_2{\cdot}6H_2O$, $Zn(CH_3COO)_2{\cdot}2H_2O$, $ZnSO_4{\cdot}7H_2O$. The SEM image for the respective zinc salts are shown in Figure 2-15.

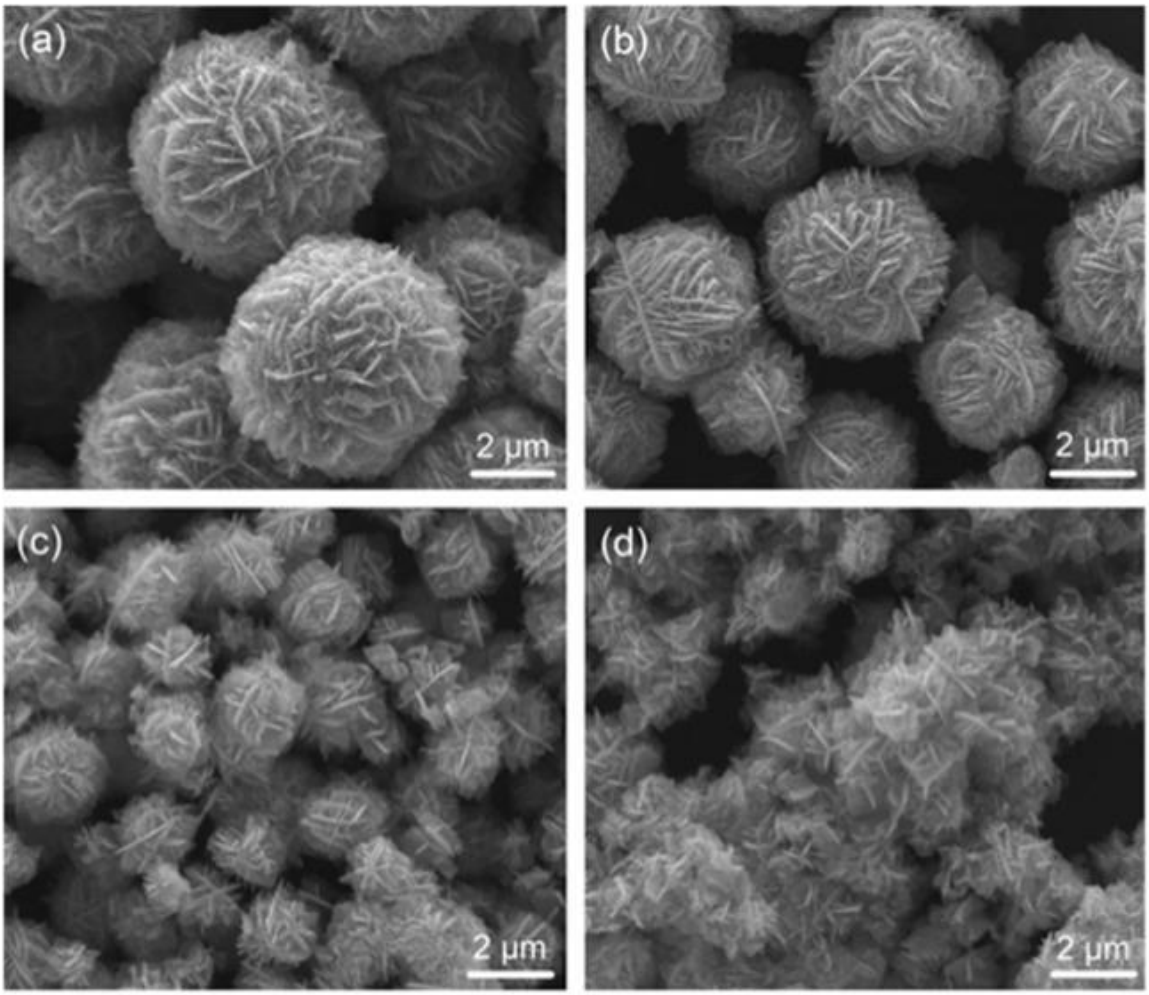

Figure 2-15: SEM images of ZnO crystals from zinc salts with different anions (a) $Zn(NO_3)_2{\cdot}6H_2O$ (b) $Zn(CH_3COO)_2{\cdot}2H_2O$ c (c) $ZnSO_4{\cdot}7H_2O$ (d) $ZnCl_2$ } [30].

The results were discussed around the electronegativity and the hydrated radius of the anions. With the exception of $Zn(CH_3COO)_2{\cdot}2H_2O$, it was noted that the reaction rate constant of the crystal growth stage decreased with the decrease in electronegativity of the anion Table 2-2. This indicated that the anion was the main factor effecting the morphology.

Table 2-2: The electronegativity of the zinc salts and their representative electronegativity

Zinc salt	Electronegativity
$Zn(NO_3)_2•6H_2O$	3.91
$Zn(CH_3COO)_2•2H_2O$	-
$ZnSO_4•7H_2O$	3.83
$ZnCl_2$	3.16

2.6.2 Effect of precipitating concentrations

Xu et al studied the effect of changing the cation source from potassium hydroxide (KOH) to ammonia solution (NH_4OH) [57]. The author also discusses the effect of the change of the molar ratio of both of the cation sources.

With respect to the use of KOH, the change in molar ratio causes a change in the concentration of zinc species (Zn^{2+}) and was thought to cause a variation in the nucleation and growth of ZnO during the hydrothermal process. The results displayed in Figure 2-16 show the different resulting morphologies. These included a twinned pyramidal, shortened prismatic, sheet-like and prismatic-like as the concentration of KOH increased from 0.25 to 2.00 mol/l [57]. When ammonia was used, there was a shape change from ellipsoidal to long prims like with the increasing concentration.

The aspect ratio is also noted to increase. It was proposed that due to the number of complexes and compounds that could be formed in the formation but was not discussed further. The aspect ratio is important as it is a measure of the surface area compared to the volume of materials. In general, the greater the aspect ratio (as subsequently the surface area), the more effective the nanoparticle and the specific parameter being utilised [58].

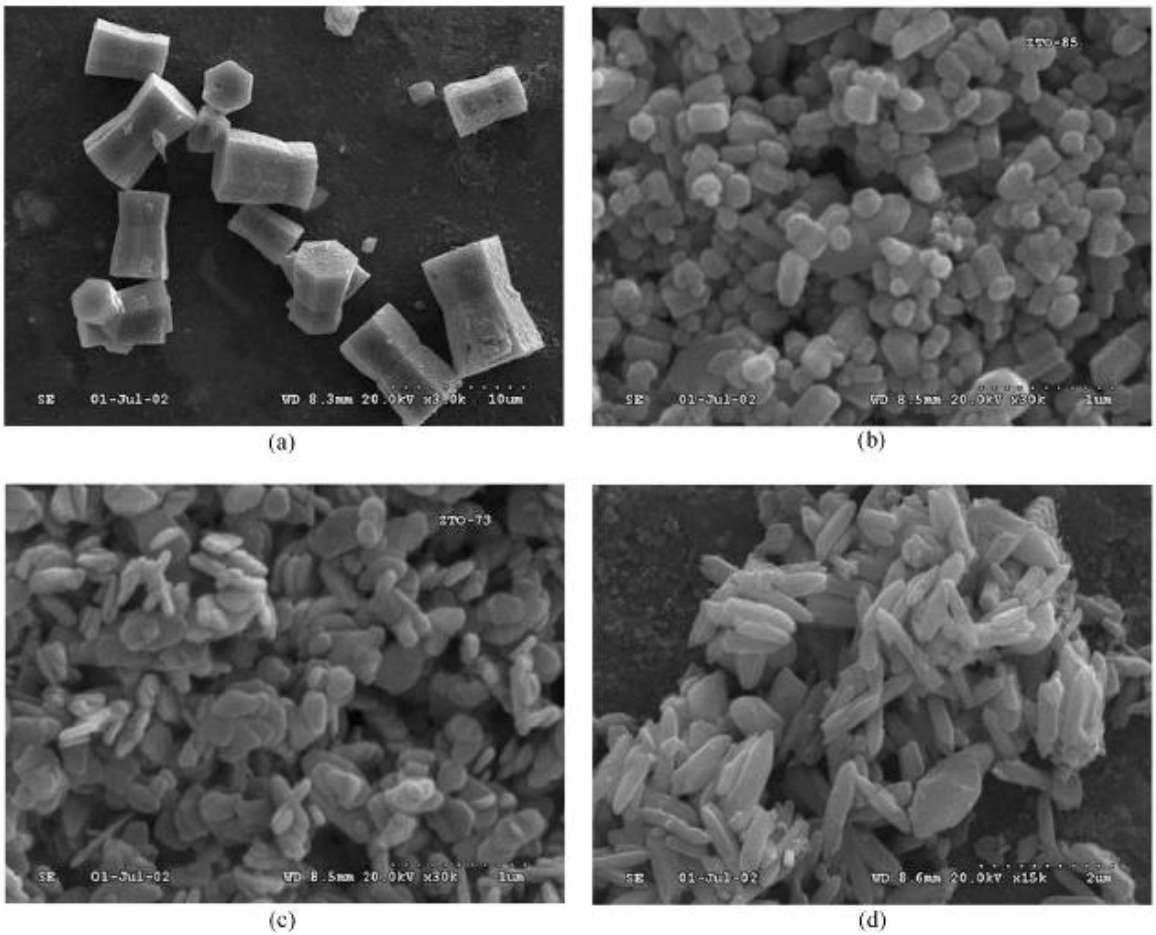

Figure 2-16: SEM micrographs of samples hydrothermally prepared at 200°C for 2h with (a) 0.25 (b) 0.50 (c) 1.00 (d) 2.00 mol/l KOH [57].

Zhang et al. [59] considered the effect on the morphology of ZnO by regulating the ratio of NaOH to $Zn(CH_3COO)_2 \cdot 2H_2O$ within a narrow range under hydrothermal conditions of 120°C for a period of 6. A range of OH^-/Zn^{2+} molar ratio from 8.2 to 11.8 was utilised. The results showed various differently sized shapes and morphologies had been synthesised from flower-like structures approximately 500nm (8.2 molar ratio) in size to micron sized rod-like structures (11.8 molar ratio).

Due to the nature of the experiment and the starting precursors, ZnO was only formed from $Zn(OH)_2$ from the hydrothermal process. By analysing the products of the same experiments at a shorter hydrothermal period of 0.5h it was observed the component of the flower like structures was rod-like. As such Zhang et al considered that the formation of either morphology occurred in the nucleation phase of the formation of ZnO [59]. It was proposed that the level of supersaturation that occurred led to either:

- The formation of spines radiating nuclei that led to a flower like structure

- Single crystal nuclei which led to the formation of rod-like structures.

Polsongkram et al. [60] used $Zn(NO_3)_2$ and hexamethylenetetramine (HMT) solutions as precursors. By varying the concentrations, different morphologies of ZnO nanorods were obtained. These are shown in Figure 2-17.

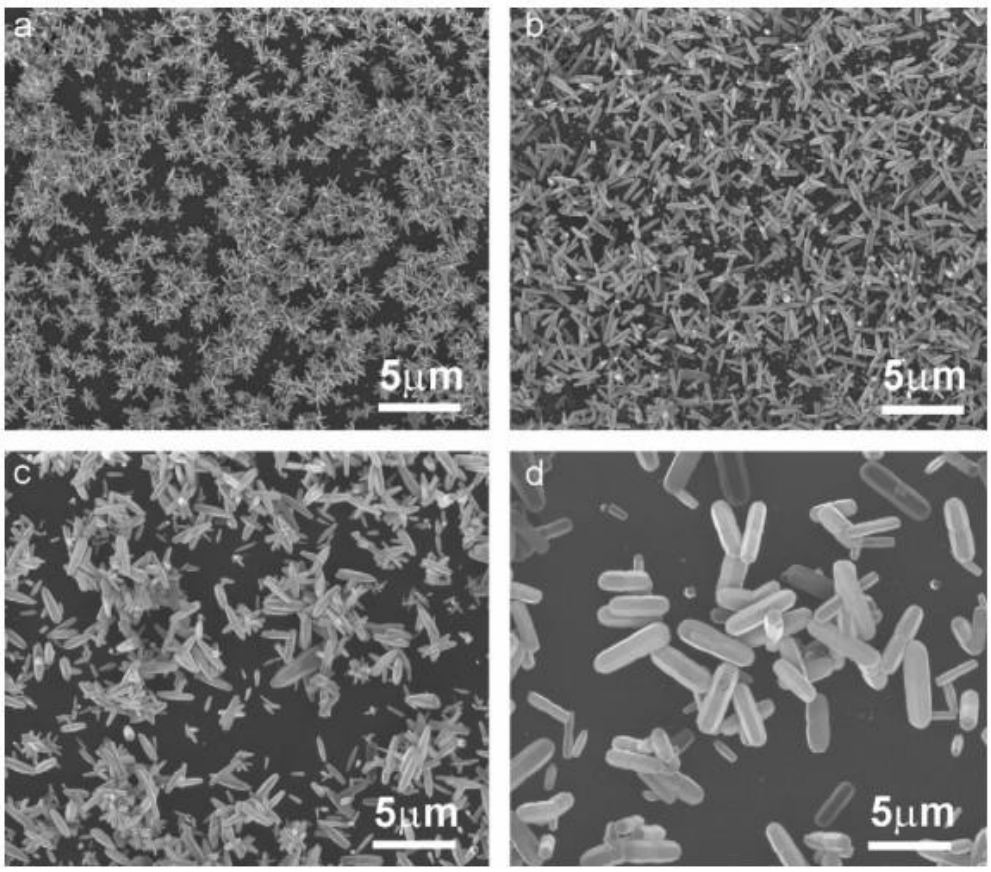

Figure 2-17: SEM images of ZnO nanorods synthesised from (a) $Zn(NO_3)_2$-0.005 M: HMT-0.005 M; (b) $Zn(NO_3)_2$-0.010 M: HMT-0.010 M; (c) $Zn(NO_3)_2$-0.020 M: HMT-0.020 M; (d) $Zn(NO_3)_2$-0.050 M: HMT-0.050 M

As Figure 2-17 shows, the thickness of ZnO nanorods increased with the increasing concentrations of solution. The author explained the following mechanism. High HMT concentrations increased the NH_{4+} concentration. Complex compounds such as as $Zn(OH)_{4-x}(ONH_4)_x^{2-}$ were formed due to the reaction between NH_4^+ and $Zn(OH)_4^{2-}$. This complex could in turn by converted into the growth unit $Zn(OH)_4^{2-}$ which subsequently

caused an acceleration in crystal growth. This endothermic process was considered to inhibit the growth of ZnO nanorods along the <0001> direction. This therefore led to thicker nanorods. [60]. Work by Zhang et al, [61] discussed the effect of the decomposition of HMT to formaldehyde and ammonia. Zhang discussed that when ammonia further decomposed to NH_4^+, the growth of ZnO was interrupted and subsequently nanoparticles were formed as opposed to nanorods [61].

2.6.3 Effect of pH

Investigations into the role of pH have shown the initial solution pH has an influence on the size and morphology of ZnO nanostructures.

By changing the molar ratio of $Zn(CH_3COO)_2 \cdot 2H_2O$ and NaOH solutions from 1:1 to 1:2 it was shown that increase in solution basicity had a similar effect as the when the solvothermal time was increased *i.e.* there was a change in growth rate [62]. For example at the high basicity (pH 10), the morphology of ZnO, aggregates of sheet like branches were formed which was similar, though not identical to the ZnO synthesised when a lower basicity of ZnO was reacted for a longer time.

The effect of pH at various different autoclaving times has been discussed by Music et al. [37] From the perspective of the effect of pH, $Zn(CH_3COO)_2 \cdot 2H_2O$ solutions were neutralized with varying amounts of ammonia solution and then hydrothermally aged at 160^{o}C. Music et al discussed that the exact compositions of the growth units complex ($Zn(OH)_{2-x}(CH_3COO)_x \cdot yNH_3 \cdot zH_2O$) was dependent upon the pH of the suspension. The rate of transformation from the growth unit complex to ZnO increased when the pH increased from 7 to 10 and subsequently a change of morphology was also noted. Brunauer-Emmett-Teller (BET) analysis showed that as the pH increased, regardless of the autoclaving time, the surface area increased, suggesting the precipitation of smaller particles.

An as-obtained ZnO morphology of whiskers were synthesised via a hydrothermal route and different pH values by Shi et al [63]. The precursors were $ZnSO_4$ and Na_2CO_3. Based upon XRD analysis, $Zn_5(CO_3)_2(OH)_6$ particles and ZnO whiskers were both present in the hydrothermal produce under the experimental conditions. This indicated incomplete conversion of ZnO from $Zn_5(CO_3)_2(OH)_6$. The reaction for the conversion was reported as:

$$Zn_5(CO_3)_2(OH)_6 + 4OH \rightarrow 5ZnO + 2CO_3^{2-} + 5H_2O$$

Figure 2-18 showed that at pH 6.5, no ZnO whiskers were observed. This indicated that no $Zn_5(CO_3)_2(OH)_6$ particles were converted into ZnO whiskers. When the pH increased (9.5) both $Zn_5(CO_3)_2(OH)_6$ and ZnO whiskers were observed in the hydrothermal product. The amount of $Zn_5(CO_3)_2(OH)_6$ further decreased at pH 10, until there were no trace of the compound at pH 10.5. At pH 10.5 only ZnO whiskers were observed. The results showed that the higher the solution pH was, the more ZnO whiskers were converted from $Zn_5(CO_3)_2(OH)_6$. The author explained this as follows. As the pH decreased, the amount of H^+ in the hydrothermal solution inhibited the conversion noted above. It was deduced that the increase of the initial solution pH accelerated the decomposition of $Zn_5(CO_3)_2(OH)_6$ in the hydrothermal process. As a result, a high initial pH was preferred for the formation of ZnO whiskers[63].

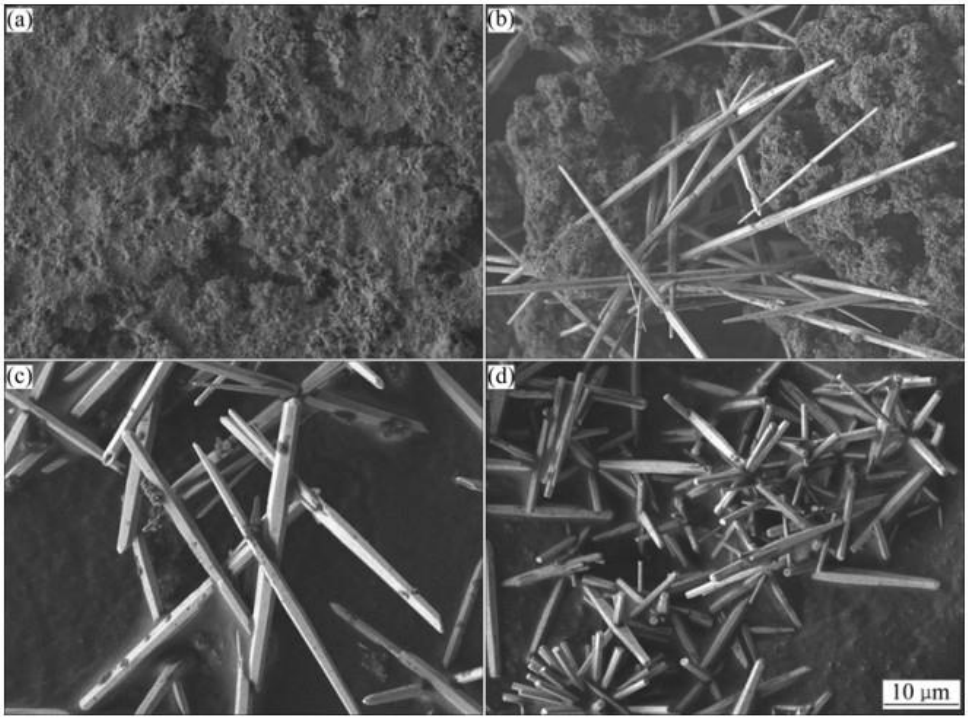

Figure 2-18: SEM images of different morphologies of ZnO whiskers synthesized at (a) pH=6.5; (b) pH=9.5; (c) pH=10.0; (d) pH=10.5 [63]

Wang et al. prepared ZnO nanocrystals using the dissolution of ZnO and the addition of ammonia with different initial solution pH. The size of the resulting ZnO nanocrystals

increased with increasing pH values[64]. The results are shown in Figure 2-19. The following reaction was noted to take place in the synthesis process:

$$Zn^{2+} + 4OH^- = Zn(OH)_4^{2-}$$

$$Zn(OH)_4^{2-} = ZnO + H_2O + 2OH^-$$

Wang et al. considered the low initial solution pH value caused relatively rapid nucleation and slow grain growth. This was due to the low concentration of $Zn(OH)_4^{2-}$ and subsequently there were many nuclei and few growth units. In contary, the high pH resulted in low nucleation and rapid grain growth. Consequently, ZnO prepared with high pH values had a larger size than ZnO prepared with low pH values[64].

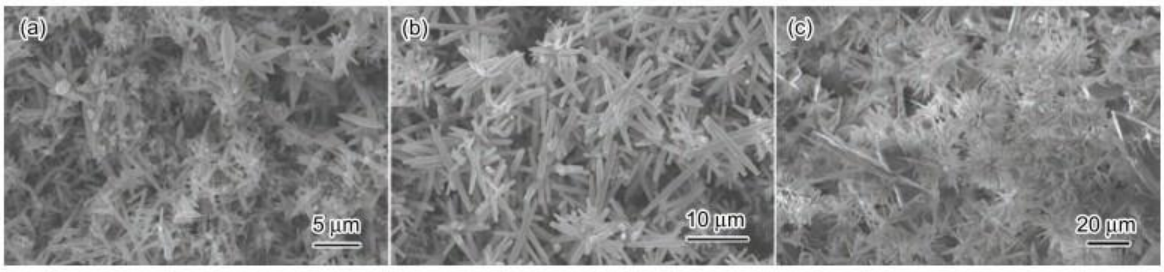

Figure 2-19: SEM images of ZnO nanocrystals synthesized (a) pH=8.0; (b) pH=10.0; (c) pH=12.0 [64]

2.6.4 Effect of precipitating conditions

Zhang et al compared and discussed the effect of a change of alkaline source from NaOH to ammonia in a solvothermal experiment [62]. One of the points made, was the effect of NH_3 byproduct which was suggested to prevent amalgamation of the nucleus during supersaturation period of the reaction process. This therefore would lead to dispersed morphologies such as prism-like rather than (prickly) sphere-like.

During the growth phase of the particles the effect of the ammonia was considered to only provide weak basicity. As such the c-axis was grown slightly faster than any of the other axis leading to a polyhedral shape. However with respect to the use of NaOH,(a stronger

base) the concentration of OH^- was suggested to be the controlling factor for the growth and control of the different crystal faces [62].

2.6.5 Effect of hydrothermal conditions

Increase in ZnO particle size rather than morphology following an increased hydrothermal time is commonly reported [65, 66]. However, Zhang et al investigated the variations in solvothermal conditions with respect to both time and temperature and showed the evolution of ZnO morphologies as the time of the solvothermal process increased from 10 minutes up to 8 hours [62]. This evolution is shown in Figure 2-20

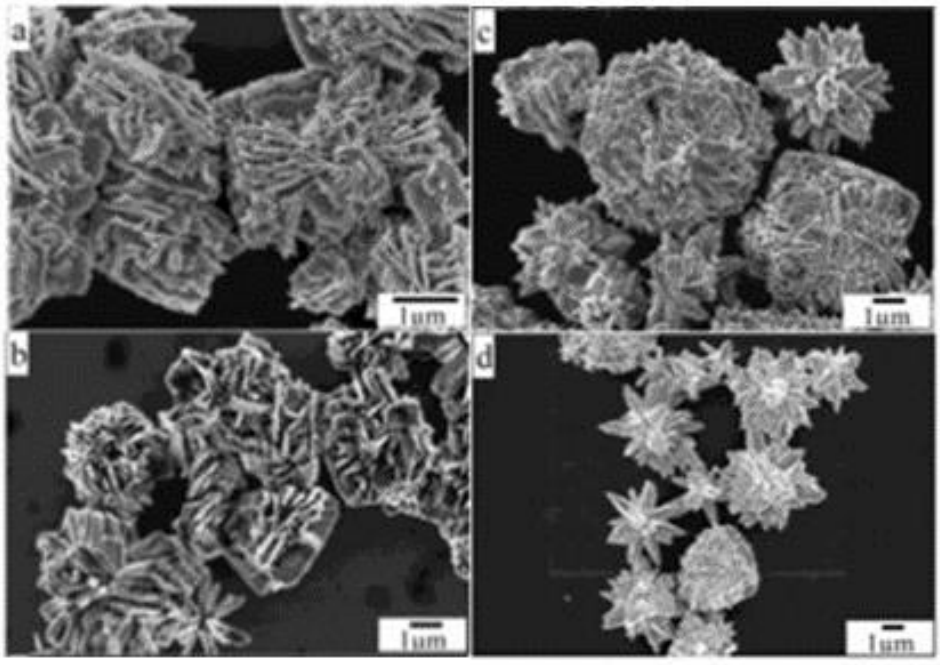

Figure 2-20: SEM images of morphological evolution of ZnO sample with flowerlike shape heated at 180^0C fr (a) 10 min, (b) 2 hours (c) 4 hours and (d) 8 hours [62]

Little discussion though is provided on the evolution of the structures. However the increase in size between the 4 hour to 8 hour samples was noted as an example of Ostwald ripening [43]. When the effect of a temperature increase from 100°C to 140°C was conducted little difference in morphology or size of particle was noted [62].

The effect of hydrothermal time over various final pH was studied by the Music et al. [37] Autoclaving times of 15 minutes, 2 hours and 72 hour were studied at a pH of 7, 8 and 10 using Zn(CH3COO)2·2H2O and ammonia solution precipitation. Under the conditions that synthesised ZnO, it was found that for each pH the surface area of the particles reduced, independently of the pH. The reduction in surface area represents the growth of the particle as autoclaving time increased. This effect of an increase in size due to time was also shown by Nagarju et al [67]. Figure 2-19 shows the change in nanorods size when the time increased from 6 hours to 20 hours. The reactants were $ZnSO_4 \cdot 7H_2O$ and NaOH.

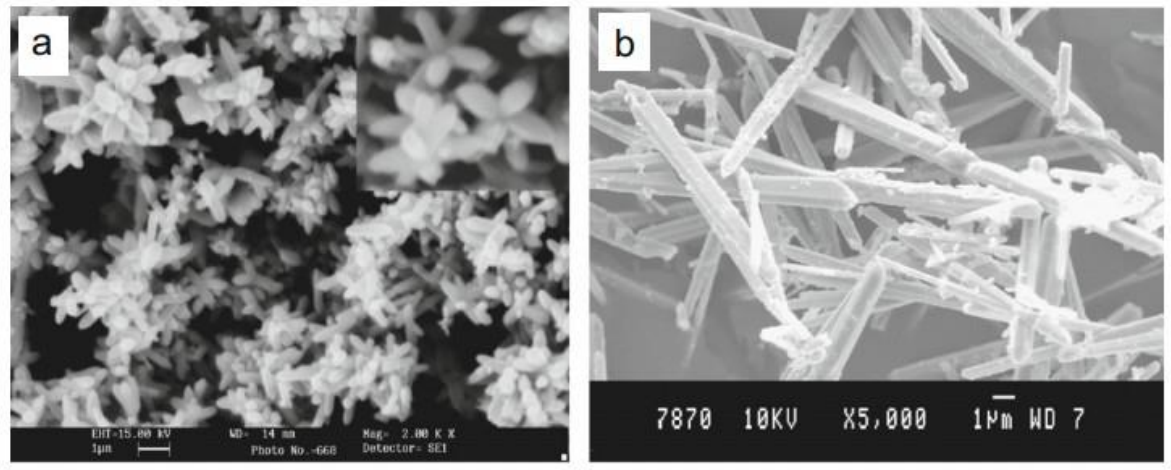

Figure 2-21: SEM images of ZnO rods synthesized for (a) 6 h; (b) 20 h [67]

The author summarised the nanorods (within a star-like structure) in Figure 2-21A were a result of the coalescence of nuclei. Further growth ensued by the nucleation of the reactants onto the particle surface after the first nucleation. As the reaction time increased, larger ZnO microrods were reported [67].

In the discussion of the effect of time, many authors report on reaction times of greater than 1 hour. Jiang et al showed the increase in crystallinity over between reactions times of 5 minutes and 6 hour [68]. The results are presented in Figure 2-22 below show when the reaction time was 5 minutes, the as-obtained flower-like structures of ZnO had a rough surface along the c-axis (0001). When analysed at 6 hours, the as-obtained ZnO was shown to be slightly larger and have a smooth surface. This suggested an increase in crystallinity with increasing reaction time.

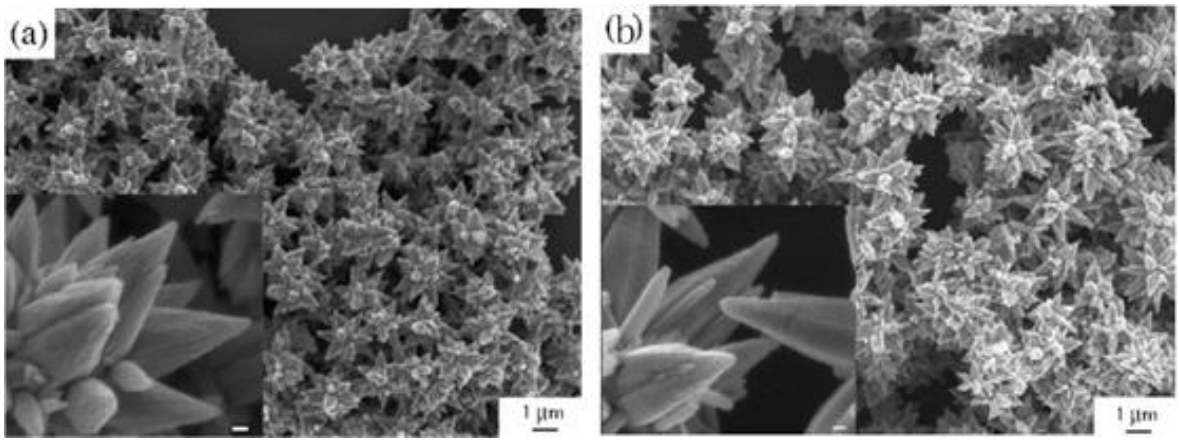

Figure 2-22: SEM images of flower-like ZnO nanostructures formed for: (a) 5 min; (b) 6 hour [68]

Nagarju et al. showed that the "smoothing" of the surface could also be obtained by increasing the reaction temperature. Figure 2-23 shows the increase in crystallinity after an increase in synthesis temperature from 180°C to 200°C. The precursors were $ZnSO_4 \bullet 7H_2O$ and NaOH [67].

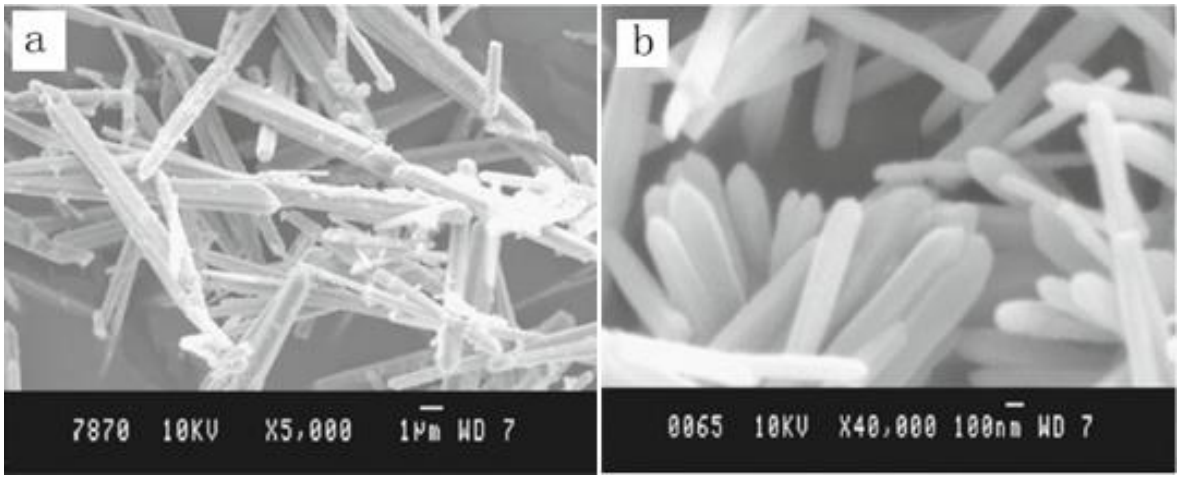

Figure 2-23: SEM images of ZnO nanorods synthesized at (a) 180 °C; (b) 200 °C [67]

Temperature is a key factor to the size and morphology of ZnO nanostructures in hydrothermal synthesis.

Different experimental conditions using $Zn(CH_3COO)_2$ and NaOH as percursors were studied by Zhang et al. A summary of these conditions and the as-obtained ZnO nanostructures are detailed in Table 2-3. The as-obtained morphologies are displayed in Figure 2-24.

Table 2-3: Summary of conditions and as obtained structures following an investigation into the change of pH and temperature.

Temperature (ºC)	As obtained structure (pH=12)	As obtained structure (pH=135
200	Flower-like and nanorods	Flower-like consisting of sword-like nanorods
160	Tip-like anistropic nanoparticles	Flow-like consisting of sword-like nanorods
120	Tip-like anisotropic nanoparticles	Unshaped ZnO nanostructures

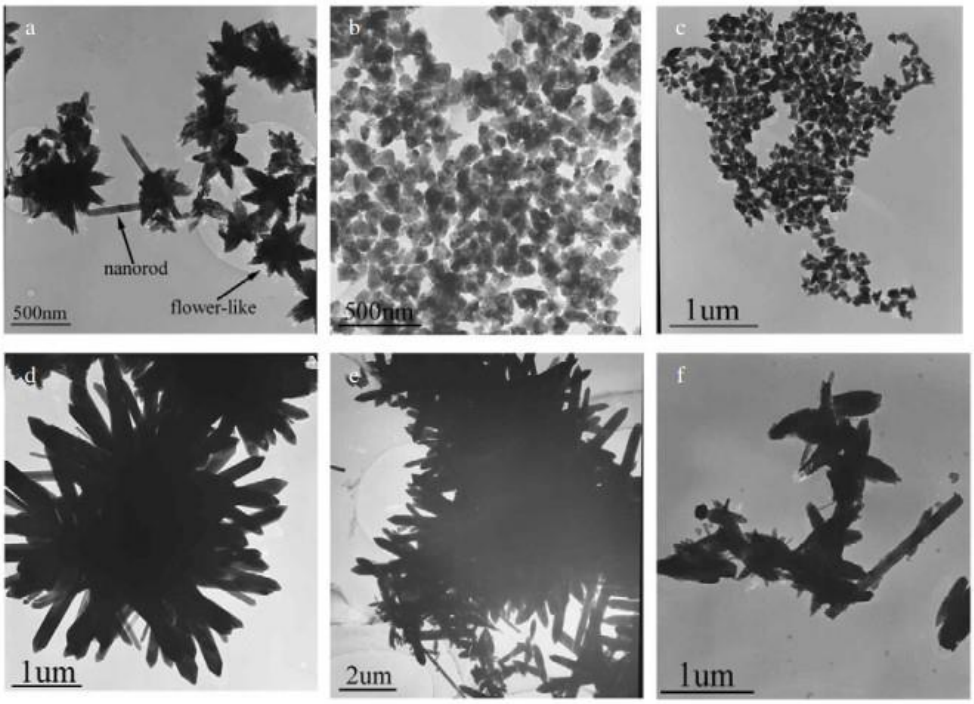

Figure 2-24: TEM images of the ZnO nanostructures synthesized at different temperatures and pH values: (a) 200 °C and pH= 12; (b) 160 °C and pH= 12; (c) 120 °C and pH= 12; (d) 200 °C and pH = 13. 5; (e) 160 °C and pH= 13. 5; (f) 120 °C and pH= 13. 5 [69].

An explanation for the effect of reaction temperature was provided by Zhang et al [69]. The different initial pH values corresponded to different amounts of $Zn(OH)_2$ and $[Zn(OH)_4)]^{2-}$. These two complexes were responsible for the crystal nucleation and subsequent growth. When pH = 12, a large amount of $Zn(OH)_2$ and a small amount $[Zn(OH)_4)]^{2-}$ were formed. Under this condition, there was not enough $[Zn(OH)_4)]^{2-}$ for the growth of ZnO nuclei, though there were large nuclei at 120ºC and 160ºC. Furthermore, at these lower temperatuers the

amount of active sites around the ZnO nuclei was reduced. This was considered to the lead to the tip-like ZnO nanoparticles at 120ºC and 160ºC.

When the reaction temperature was increased to 200ºC, the $Zn(OH)_2$ underwent the following reaction:

$$Zn(OH)_2 + 2OH^- = [Zn(OH_4)]^{2-}$$

This conversion, increasing the amount of $[Zn(OH_4)]^{2-}$ from $Zn(OH)_2$ was thought to promote the growth of ZnO nuclei at the expense of the number of nuclei. Moreover the higher temperature increased the generation of active sites around the ZnO nuclei. However, the amount of $[Zn(OH_4)]^{2-}$ was still not large enough for the formation of nanorods. As such flower-like structures together with some nanorods was found to be the as-obtained structure. When the pH increased to pH = 13.5, a small amount of $Zn(OH)_2$ and a large amount of $[Zn(OH_4)]^{2-}$ was formed. Under this condition, although the number of nuclei was again speculated to reduce, it was considered the growth of ZnO nuclei was promoted. This led to the formation of ZnO nanorods. Flower-like ZnO nanostructure consisting of sword-like nanorods were detected at 160ºC and 200ºC [69].

2.6.6 Effect of surfactant

An early example of the use of surfactants and the hydrothermal treatment of a ZnO precipitation was conducted by Chittofratti et al [20]**.** Three surfactants, SDS, CTAB and PPC were added to hydrothermally treated ZnO solutions. The ZnO was synthesised with $Zn(NO_3)_2$ as the zinc source and NaOH, LiOH and KOH as the alkaline source. CTAB and SDS were reported to have no effect on the morphology. When a PPC was used, the fluorinated surfactant had two effects. The surfactant had prevented aggregation and caused a reduction in particle size of a rod like particle. This was compared to a sample synthesised without surfactant.

The use of CTAB has been recorded to have an effect on the morphology [70]. Zhang et al reported the formation of nanoparticles of ZnO with a flowerlike and swordlike morphology at temperatures of 120ºC and 160ºC respectively. The ZnO was precipitated with $Zn(CH_3COO)_2 \cdot 2H_2O$ and NaOH. Due to weak force interactions between the growth unit

$ZnOH_4^{2-}$ and CTAB a complex agent formed which adsorbed onto the circumference of the ZnO nuclei. This was though to lower the surface energy resulting in an increase in the active surface sites; this allowed the growth of ZnO nanorods. The results of the effect of CTAB were considered to be confirmed by increasing the hydrothermal temperature to 160^{o}C. At this temperature the capsules of CTAB were considered to have been destroyed. Results showed the formation of needle-like nanorods indicating the effect of CTAB.

Increasing the concentration of CTAB resulted in change in synthesised ZnO. When CTAB at varying and increasing concentrations was present within a hydrothermal synthesis between Zinc Nitrate and ammonia solution, Mao et al.[70] reported an increase in crystallinity. However, it should be highlighted that of the three different concentrations (0.62 g, 0.72 g and 0.82g), the best resulting crystallinity was from 0.72g[70].

With regards to the use of SDS, Ni et al showed how the presence of SDS and increasing concentration affect the morphology. Nano-flakes formed without the presence of SDS and flowerlike structures with the surfactant, but only above a certain concentration [71].

In surfactants, molecules form micelles and micelle agglomerates with various morphologies and structures depending upon the surfactant concentration. These surfactant micelles and micelle agglomerates are soft and can be solidified by the mineralization of inorganic species such as metal ions or metal ion hydrates on the hydrophilic heads of surfactant molecules. With respect to the co-precipitation of ZnO by adjusting the solution condition and inorganic species/surfactant molar ratio, the mineralization of inorganic species can be controlled. [2, 72, 73]

The self assembly of the polymer/surfactant can affect the particle morphology [2, 73, 74] The precipitation and hydrothermal treatment of ZnO in the presence of PEG lead to micronuts and nanorods depending upon the precipitating conditions. Shi et al noted that in the presence of the PEG 300, the growth unit $Zn(OH)_2^{4-}$ interacted with the PEG globules microphase leading to the formation of $Zn(OH)_2^{4-}$-PEG spheres under hydrothermal conditions. After the formation of the sphere and subsequent formation of ZnO nuclei, ZnO nuclei in the interior of the sphere moved to the surface of the PEG globule to form a centre cavity. This led to ZnO growing in the surrounding of PEG globules and the hexagonal nut-like morphology being fabricated. The mechanism is represented in Figure 2-25. Guo et al.

reported on a similar mechanism in the hydrothermal synthesis of ZnO microflowers with PEG-20000[74].

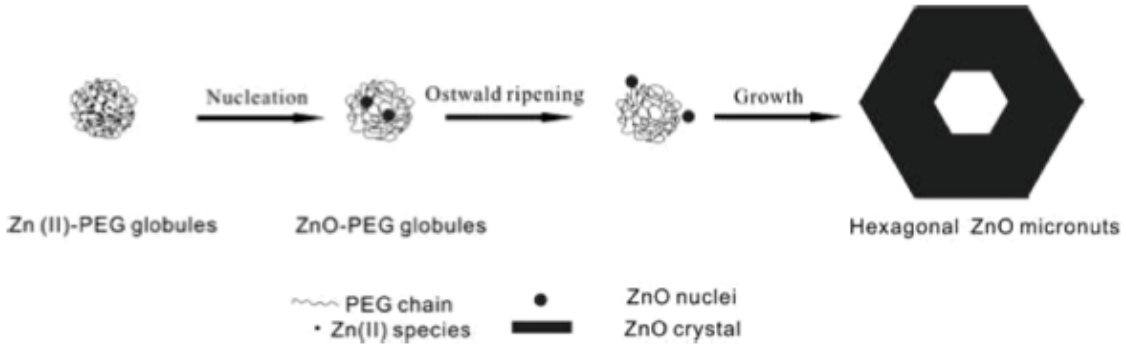

Figure 2-25: Schematic diagram of the growth mechanism of hexagonal nut-like morphology under the direction of Zn(II)-PEG globules.[73]

The self-assembly the PEG molecules into ring pattern and subsequent growth of ZnO was reported to form nanorods. Yogamalar et al. noted that the ZnO growth units were absorbed by the oxygen atom in the C-O-C chain. These can be carried and transformed into ZnO crystalline particles and grow on active sites around the surface of ZnO nuclei. Based on the degree of adsorption, the electrostatic force of attraction and interaction between the PEG and Zn^{2+} ions a morphology with specific orientation is synthesized. The morphologies synthesised by Yogamalar et al. with different zinc salts are shown in Figure 2-26.

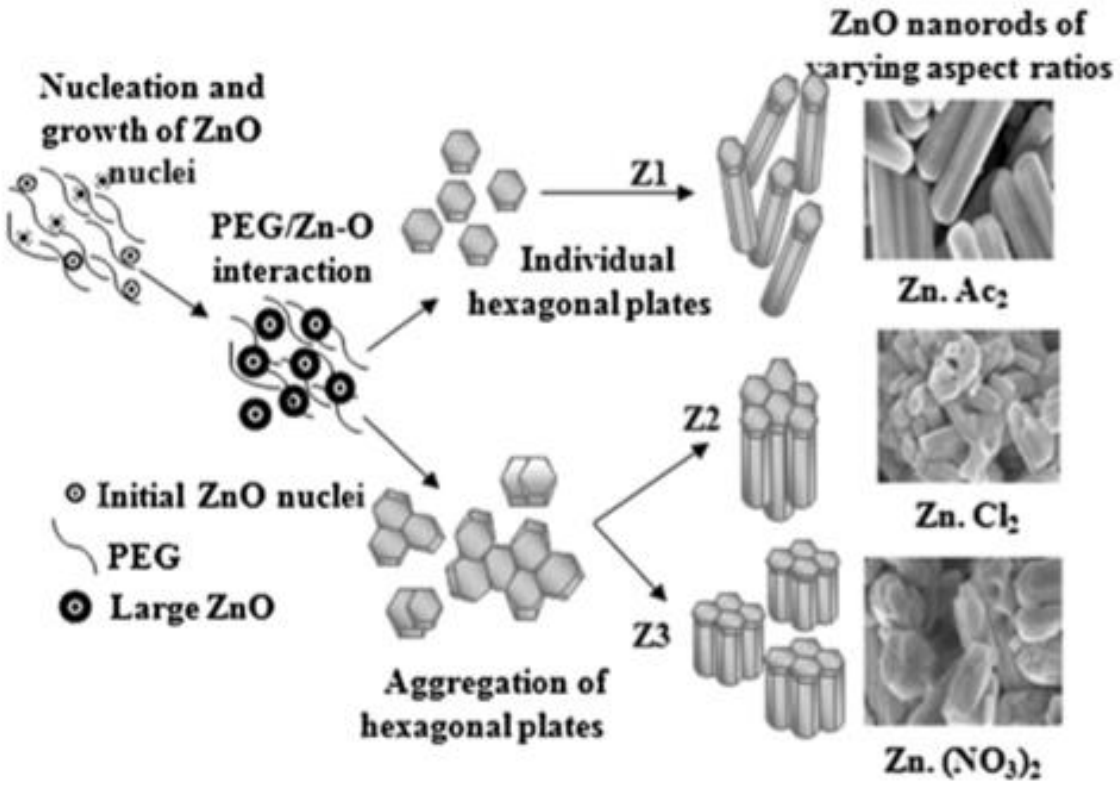

Figure 2-26: Schematic representation of ZnO nanorods and nano-bundles formation under PEG directed hydrothermal synthesis.

ZnO microtubes and nanotubes were synthesised with CTAB and P123 respectively. The difference in size was considered to be due to the critical micelle concentration of the surfactants. As both surfactants were used above their cmc limits there were considered to be formed a lamellar phase (CTAB) and either isolated micelles or agglomerates of micelles (P123), with ZnO growth occurring in conjunction with these templates.

In contrast, two other PEO-PPO-PEO surfactants, F68 and L64 were used to synthesis a prism-like and pyramid like morphology respectively. Microscopy of the particles suggested that the block copolymer enwrapped the $[Zn(OH)_4]^{2-}$ growth units. Under hydrothermal conditions and subsequent nucleation the nuclei are restricted to the hydrophobic (PPO) core and as such any growth is controlled through the micelle. The mechanism is shown in Figure 2-27. The F68 micelle was regarded to be larger due to its longer PEO chain

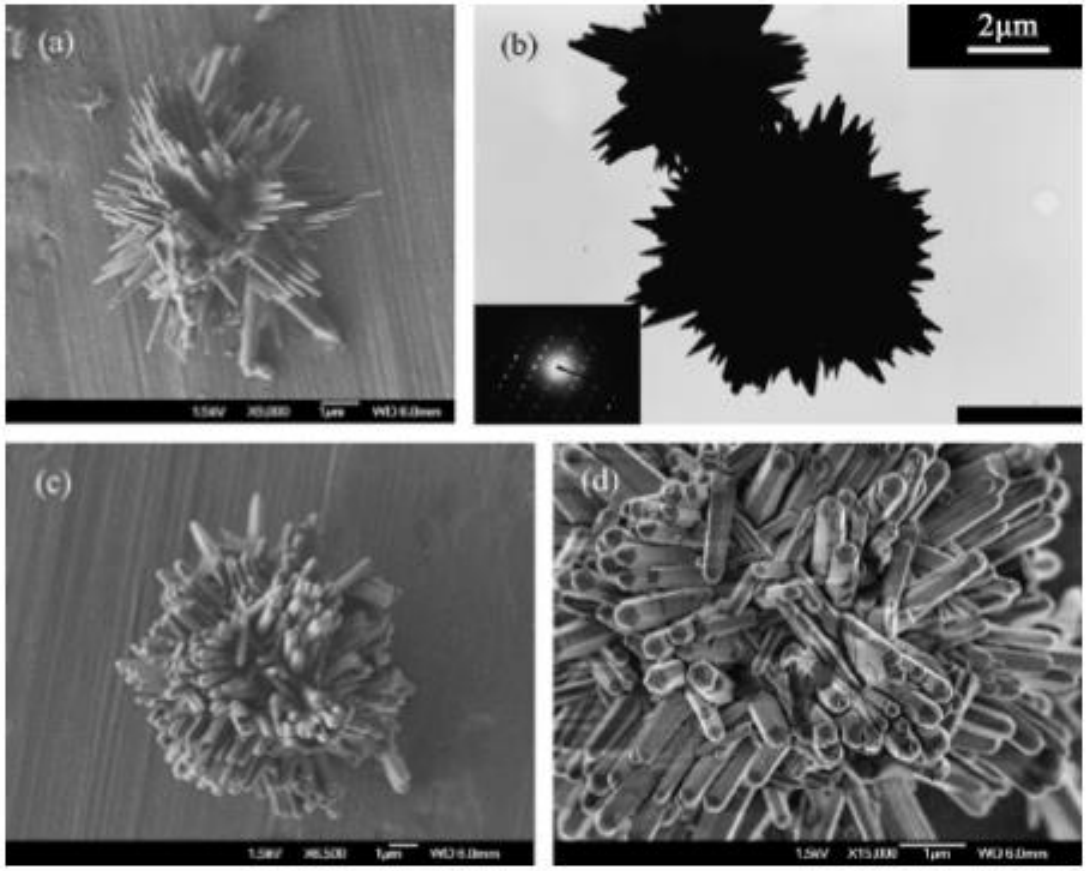

Figure 2-27: SEM and TEM images of ZnO homocentric bundles obtained in block copolymers systems: (a and b) products in L64; (c and d) products in F68.

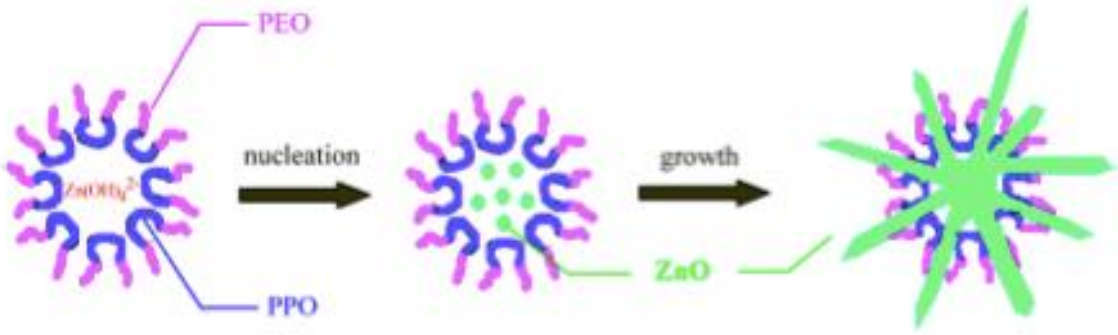

Figure 2-28: Mechanism for the formation of ZnO homocentric bundles

In the presence of PVA, the growth unit could be bonded by PVA at the (0001) plane to form the nucleus of dumbbell-like twinning crystal. This morphology was similar to that formed by a hydrothermal process involving KBr or $NaNO_2$ as the minerlizer and without

surfactant. In this case the K^+ or Na^+ ion formed a bond bridge between the growth units to form a crystal nucleus from which the dumbbell-like twinning crystal could grow from. [75].

An effect on the grain size of ZnO was shown when synthesised with and without the presence of EDTA. Shi et al. synthesised ZnO whiskers by using a hydrothermal process and $ZnSO_4$ and Na_2CO_3 as the precursors. With the addition of EDTA the length of the whiskers grew by approximately 20 – 30 µm. Shi et al. considered the surfactant (EDTA) promoted the growth of ZnO whiskers along one direction. The chelating behaviour of EDTA was thought to account for this promoted growth. It was also considered the growth may have been due to the selective adsorption of EDTA on certain ZnO facets. The change in size of the as-obtained ZnO is shown in Figure 2-29 [63].

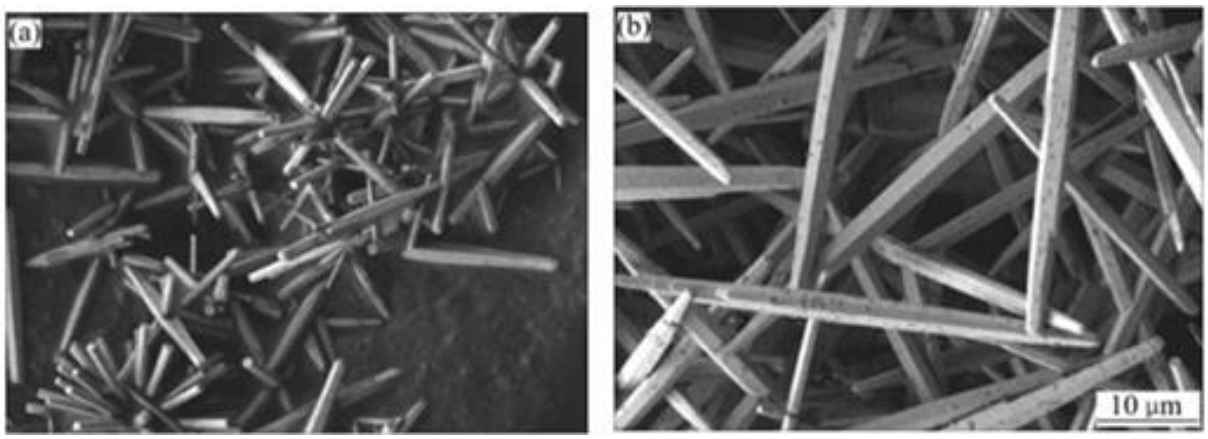

Figure 2-29: SEM images of different morphologies of ZnO whiskers synthesized: (a) without the presence of EDTA; (b) with the presence of EDTA [63]]

ZnO nanorod arrays have been synthesised on a seeded glass substatre by Zhou et al [76]. In this study non-polar polyethyleneimine (PEI) was added to the solution as a surfactant. The repeating unit is shown in Figure 2-30. The repeating unit has side amino groups (-NH_2) attached. These can be protonisated and positively charged under hydrothermal conditions.

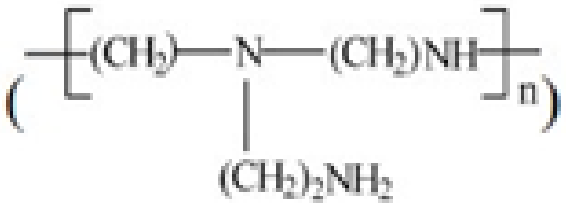

Figure 2-30: Repeating unit of polyethyleneimine [76]

The as-obtained structures shown in Figure 2-31, show the nanorods obtained with 0 ml, 3 ml and 6 ml PEI had diameters of 300 nm, 200 nm and 40 nm, respectively. In addition, the spaces between the nanorods were broadened with the increasing concentration of surfactant. Zhou et al explained that under conditions without surfactant, the positive top Zn^{2+} would have promoted the growth of the nanorods. However, the growth of the nanorods along the later axis was inhibited due to the adsorption of positively charged PEI molecules. This was as a result of electrostatic affinity. It was concluded that the increase in PEI concentration resulted in the formation of small diameter nanorods [76]

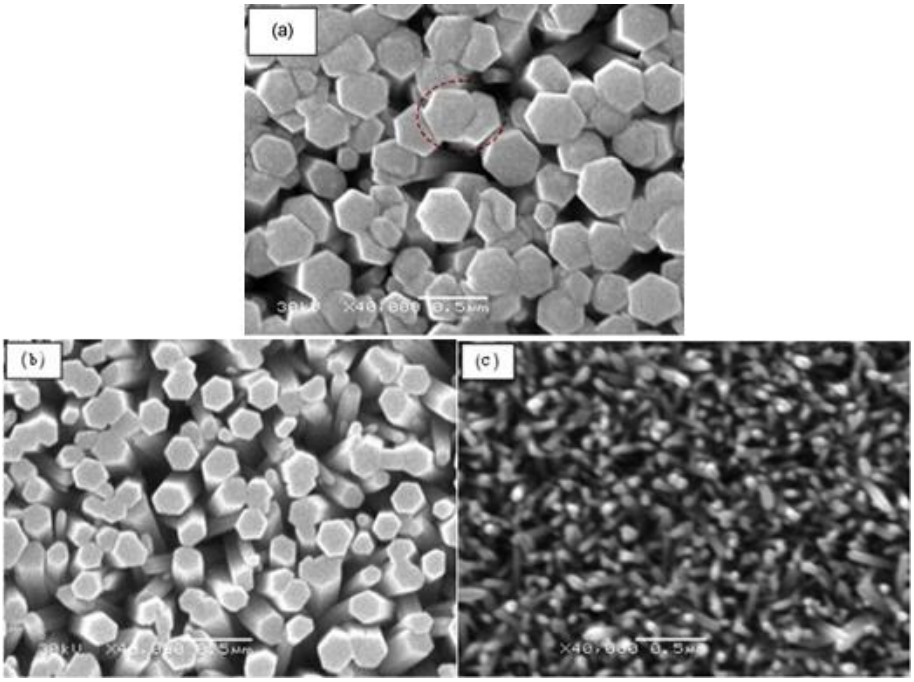

Figure 2-31: SEM images of ZnO nanorods synthesized: (a) without PEI; (b) with 3 ml PEI; (c) with 6 ml PEI [10] [76]

2.7 Aluminium Zinc Oxide

In general, the incorporation of the dopant into the ZnO crystal causes a change in the lattice paramters and defects concentration leading to a change in properties [77]. ZnO doping is achieved by replacing Zn^{2+} atoms with atoms of elements of higher valence. These elements are normally picked from Group III *e.g.* indium, gallium [77, 78].

Another element which can be used to dope ZnO is aluminium, causing the formation of Aluminium doped Zinc Oxide (AZO). AZO has a structure similar to ZnO (hexagonal closed packed) but with Al atoms doped into the lattice. The site of Zn atoms are replaced by Al, but with the replacement only affecting the lattice parameter and not the structure of ZnO[79].

2.7.1 Properties

The electrical and optical properties of ZnO, as discussed in Section 2.2.1 can be tuned by controlling the defects and concentration of the dopant impurity (Al) [80].

The electrical conductivity, charge carrier density, and mobility are improved in AZO. The changes to the ZnO lattice and the replacement of Zn^{2+} with Al^{3+} produces an extra carrier, improving the electrical conductivity [79]. AZO also exhibits a low resistivity [78, 81]. Nunes et al. demonstrated that the resistivity of ZnO thin films (prepared with spray pyrolysis decreased by two orders of magnitude with a dopant concentration up to 1-2 at% [78].

The optical band gap can be widened with the addition of Al [82-84]. For example, Ratana et al demonstrated an increase in band gap of up to 0.17 eV when sol-gel synthesised AZO (8 mol.% Al doped ZnO) was compared with undoped ZnO. The results were reported to be due to the Burstein-Moss band gap widening and band gap narrowing due to the electron-electron and electron-impurtiy scattering [82].

2.7.2 Applications

The main application of AZO is within photovoltaics, where they are used as transparent conducting electrodes. AZO is being sought as an alternative candidate to Sn-doped In_2O_3

(ITO) due to its non-toxicity, low cost, material abundance and a high level of stability under heat cycling. Applications for AZO as a replacement for ITO are, for example, in solar cells where ITO has been extensively studied [85]. Other applications include acoustic devices, gas sensors and micro-machined acutators [81].

2.7.3 Processing Routes

AZO is commonly prepared as a film, using techniques such as sputtering, CVD and sol-gel [77]. Physical deposition routes such as CVD are reported to produce films with good electrical and optical properties. However, the physical deposition approaches are limited by both low deposition rates and expensive equipment [86]. The commonly used processing routes for AZO are described in the following paragraphs. The principles of thermal evaporation methods e.g. CVD have been discussed in Section 2.3

Sputtering deposition is a physical deposition method (Section 2.3). The sputtering process relies on the production of a plasma through electrical discharge and the electrostatic acceleration of ions . Generally, argon is introduced into a vacuum chamber which is then ionised, with the positive ion (Ar^+) accelerated towards a target of material to be deposited. Collision in this material cause atoms to be ejected from the surface onto a substrate [87]. Sputtering yields can be increased by the use of a magnetron, which causes a higher concentration of ions towards the material to be deposited. Techniques such as radio frequency (rf) magnetron [88], alternative current (AC) magnetron [89] and direct current (DC) magnetron [90] are examples of magnetron sputtering.

An advantage of sputtering is that it is simple and allows high deposition rates along with the formation of films with a uniform thickness [91]. Disadvantages of sputter deposition include, but are not limited to [92]:

- Expensive sputtering targets and utilisation of the target may be poor.
- The process can be energy intensive, specifically heat which must be removed
- Film contamination can occur

The sol-gel method is a wet chemical multi-step process in which the selected chemical precursors react to form either colloidal particles or polymeric gels. These gels are then formed into their specific form e.g. thin film coating, powder [93].

The sol–gel process is advantageous because it allows good compositional control, homogeneity of the resulting material(s) due to mixing of liquid precursors and lower crystallisation temperatures [94, 95].

Thin films can be produced using from the sol-gel method through both spin-coating and dip-coating.

Dip coating refers to the immersing of a substrate into a tank containing coating material, removing the piece from the tank, and allowing it to drain. The coated piece can then be dried by force-drying or baking. It is a popular way of creating thin film coated materials along with the spin coating procedure.

The dip coating process can be, generally, separated into 3 stages:

- Immersion: the substrate is immersed in the solution of the coating material at a constant speed preferably judder free
- Dwell time: the substrate remains fully immersed and motionless to allow for the coating material to apply itself to the substrate
- Withdrawal: the substrate is withdrawn, again at a constant speed to avoid any judders. The faster the substrate is withdrawn from the tank the thicker the coating material that will be applied to the board.

Spin coating from a dilute solution is a common method to produce a thin, uniform polymer film and is mostly used within the electronics industry for the production of photo resists. In the spin coating process, the solution is first deposited onto the substrate. The substrate is then rapidly accelerated to the desired rotation speed. The polymer solution flows radially, due to the action of centrifugal force and the excess solution is ejected off the edge of the substrate. The film continues to thin slowly until disjoining pressure effect cause the film to

reach an equilibrium thickness, or until the film viscosity increases from solvent evaporation. Final thinning of the film is then due entirely to solvent evaporation [96].

2.8 Literature Review Summary

This literature review has discussed a wide range of topics. ZnO is an extensively studied material and has wide range of applications from pharmaceuticals to use as a coating additive. The material has many processing routes including CVD, PVD and wet chemistry routes which allow morphological and structural control by adjusting the growth process.

Under a wet chemistry route the review has shown that the morphology of ZnO can be very sensitive to changes in reagents, with changes in metal salt, alkaline source and pH all reporting an effect on the morphology. The effect of alkaline source and pH was also shown to have an effect on the compound synthesised, with $Zn(OH)_2$ reported to be formed under some conditions. The addition of hydrothermal conditions also added further complication to the morphologies formed.

Some of the biggest changes in morphologies and interesting shapes were reported with the addition of surfactant. Particles were morphologies from rod-like particles, mircoflowers and ZnO micro nuts were noted. Changes in properties were also shown by the formation of AZO through doping of the ZnO crystal structure. Improvements in electrical and optical properties were reported.

The review of literature indicates that the resulting morphology is often reported. However, the reported research is often focused to one aspect *e.g.* change in surfactants, change in alkaline source. Multiple changes in reagents and hydrothermal conditions are not discussed. In addition, the resulting compounds and morphology of the precipitate before hydrothermal treatment is not reported, with the focus being solely on the resulting morphology. The reported use of Pluronic (PEO-PPO-PEO) surfactants also allows a different approach to the studying the change in surfactants. Multiple different Pluronics are available with different PEO and PPO block lengths.

The review of literature therefore suggests the following there is scope into the effect of reaction conditions for both ZnO and AZO. This includes, reaction temperature, reaction time, salt precursors and base solutions on the particle size and morphology under both co-precipitation and hydrothermal conditions.

Chapter 3 Experimental

3.1 Chemicals

All the chemicals used in this project are listed in Table 3-1 and were of analytical grade. They were used as received with no further purifying treatment.

Table 3-1: List of chemicals utilised in the project

Chemicals	FW (g/mol)	Purity (%)	Manufacturer
Aluminium Chloride $AlCl_3 \cdot 6H_2O$	241.4	99	Acros Organics
Ammonium hydroxide solution (28 – 30 wt.% solution of NH_3 in water) NH_4OH	35.05		Fisher Scientific
Butan–1–ol C_4H_9OH	74.1		Fisher Scientific
Cetyl trimethylammonium bromide (CTAB) $(C_{16}H_{33})N(CH_3)_3Br$	364.5	-	Aldrich Chemical Company Ltd
Diethanolamine (DEA) $HN(CH_2CH_2OH)_2$	105.1	99	Aldrich Chemical Company Ltd
Ethanol C_2H_5OH	46.1		Fisher Scientific
Ethylene glycol $C_2H_6O_2$	62.1		Fisher Scientific
Iso-propanol C_3H_8O	60.1		Fisher Scientific
Pluronic F68 $(C_3H_6O.C_2H_4O)_x$	8400.0	-	BASF

Chemicals	FW (g/mol)	Purity (%)	Manufacturer
Pluronic L64 (20:70:20 (EO:PO:EO)) $(C_3H_6O.C_2H_4O)_x$	2900.0	-	BASF
Pluronic P123 $(C_3H_6O.C_2H_4O)_x$	5750.0	-	BASF
Poly(ethylene glycol) $C_{2n}H_{4n+2}O_{n+1}$	400.0	--	Aldrich Chemical Company Ltd
Sodium bis(2-ethylhexyl) sulfosuccinate $C_{20}H_{37}O_7SNa$	444.6	96	Acros Organics
Sodium dodecyl sulfate (SDS) $NaC_{12}H_{25}SO_4$	288.4	-	Fisher Scientific
Sodium hydroxide NaOH	40.0	99.2	Fisher Scientific
Tetramethylammonium hydroxide pentahydrate (TMAH) $N(CH_3)^{4+}\ OH^-$	91.2	97+	Aldrich Chemical Company Ltd
Zinc Acetate dihydrate $Zn(CH_3COO)_2•2H_2O$	219.5	98+	Aldrich Chemical Company Ltd
Zinc chloride $ZnCl_2$	136.3	98+	Fisher Scientific
Zinc nitrate hexahydrate $Zn(NO_3)_2·6H_2O$	297.5	97	Fisher Scientific
Zinc Sulfate $ZnSO_4·7H_2O$	287.5	99	Fisher Scientific

The precursors used for the synthesis of ZnO and AZO are reported at the each of the relevant experimental and result sections.

3.2 Synthesis of ZnO

ZnO nanoparticles with different sizes and morphologies were synthesised via the co-precipitation and hydrothermal method. Processing parameters used were zinc salt, alkaline base, surfactant, temperature, time, surfactant amount and pH value.

The synthesis of ZnO was approached in two techniques; singular experiments and orthogonal experiments. The singular experiments were conducted to develop, understand and verify the techniques. The orthogonal experiments where then used to study the effect of reaction conditions on the size and morphology of the ZnO nanoparticles.

3.2.1 Synthesis of ZnO without addition of surfactants in aqueous solutions via the co-precipitation method and hydrothermal method

A flow chart of the synthesis of ZnO without addition of the surfactants by co-precipitation method and hydrothermal method is shown in Figure 3-1.

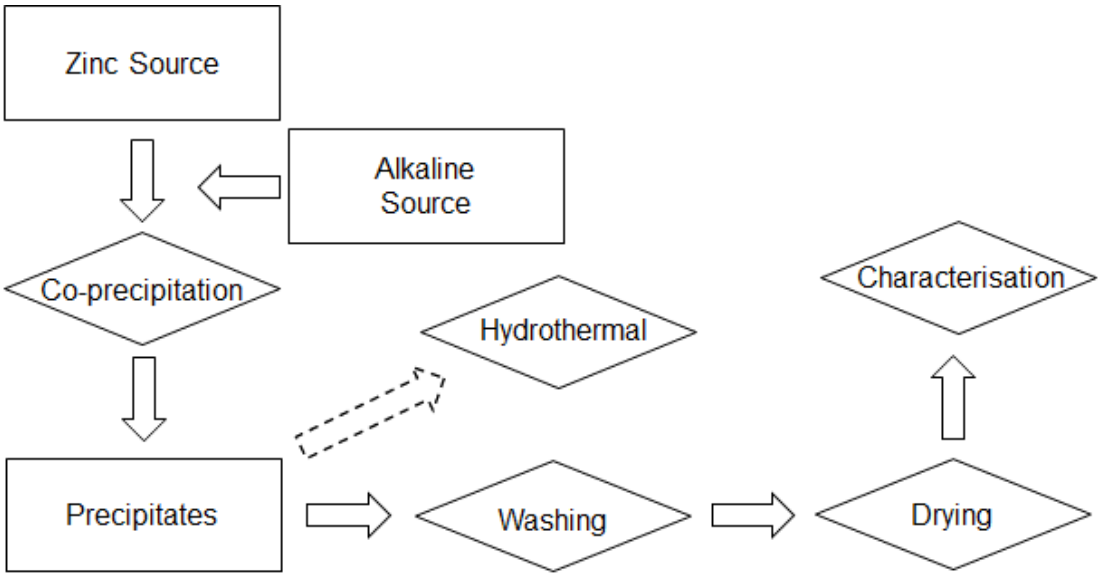

Figure 3-1: A flow chart of the procedure used for the synthesis of ZnO without addition of the surfactants via the co-precipitation method and hydrothermal method

The co-precipitation reaction occurred by adding 10ml of a 0.005 mol/l basic solution dropwise to a 40ml 0.0005 mol/l zinc salt solution. The basic solution was added drop-wise using a peristaltic pump. The solution was then left to stir for 30 minutes with a mechanical stirrer at 4000 RPM to ensure the completion of the reaction. The precipitates were then collected and split into two samples of 20ml. One half was washed thoroughly three times with de-ionized water and three times with iso-propanol to remove any excess ions from the solution. The samples were then put aside for characterisation. The other 20ml of the solution was hydrothermally treated as discussed later in this section.

3.2.2 Synthesis of ZnO with surfactants in aqueous solutions via the co-precipitation method and hydrothermal method

A flow chart of the synthesis of ZnO nanoparticles with addition of surfactants in aqueous solutions by co-precipitation method and hydrothermal method is shown in Figure 3-2.

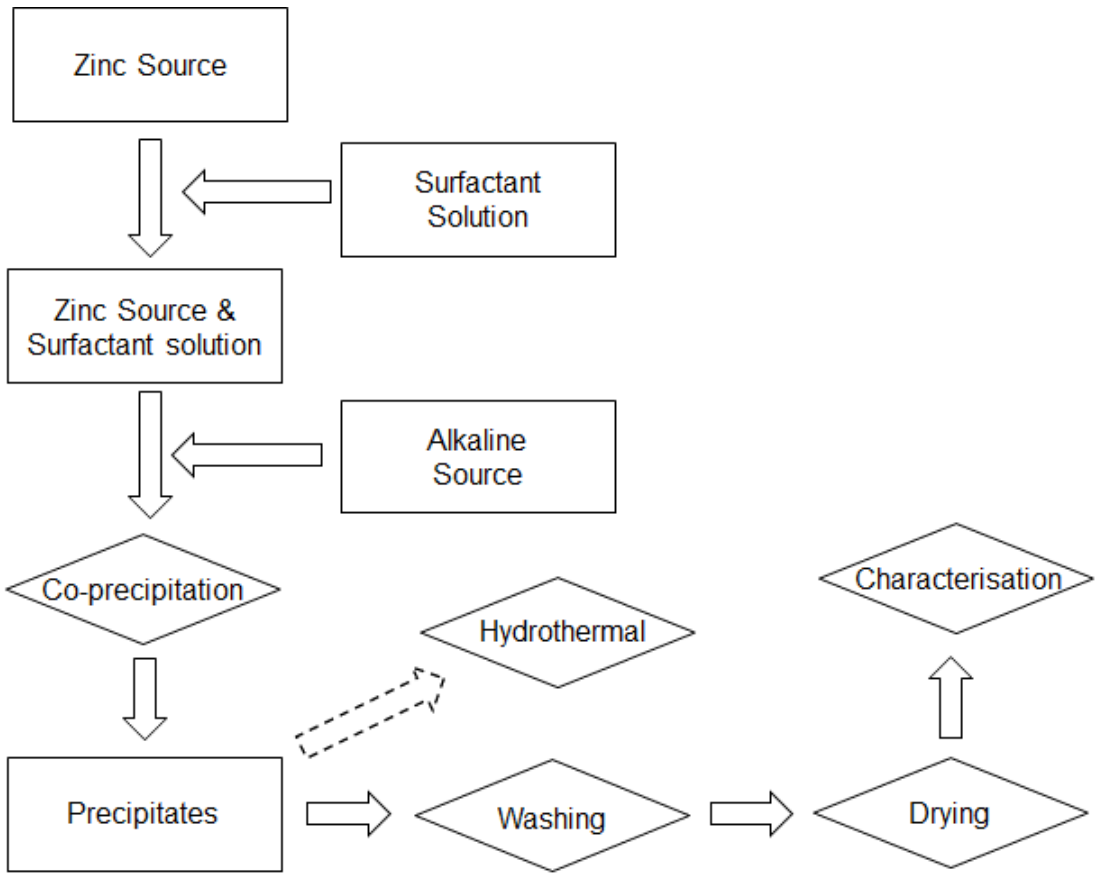

Figure 3-2: Flow chart of the procedure used for the synthesis of ZnO via the co-precipitation method with the addition of surfactants

This experiment used the same method as the previous section except with the addition of surfactant at the start. Firstly, a pre-determined amount of surfactant was dissolved in 30ml H_2O. To this surfactant solution, 18ml of 0.0005 mol/l zinc source solution was added. The solution was then left to stir for 30 minutes with a mechanical stirrer at 4000 RPM to ensure equilibrium of the solution. A 4ml basic solution (0.005 mol/l) was added drop-wise and again allowed 30 minutes of stirring to allow the reaction to complete. The samples were then split, like previously discussed.

The exception to this method was the investigation of surfactant amount. For this experiment, the surfactant solutions were based upon a weight percentage of the final solution amount (50 ml) *e.g.* for the 1% surfactant solution 0.5g of L64 was initially added to 30 ml H_2O.

3.2.3 Hydrothermal method

A flow chart of the hydrothermal method is showed in Figure 3-3.

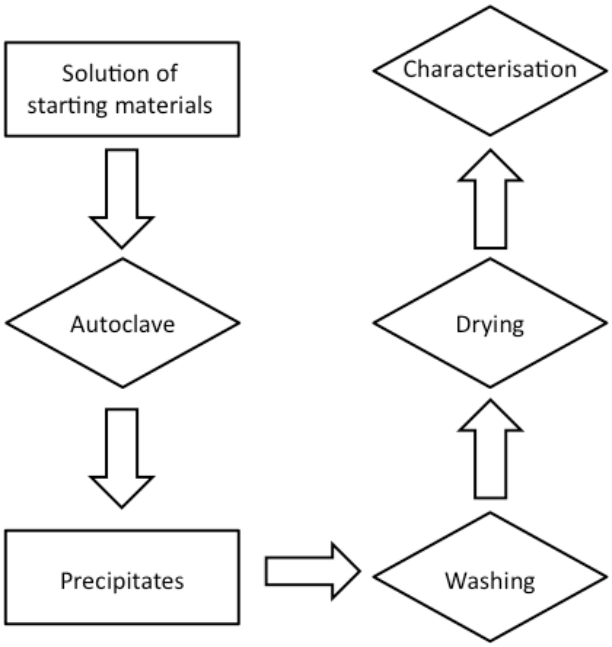

Figure 3-3: Flow chart of the procedure used for the synthesis of ZnO via the hydrothermal method

As stated, all of the experiments carried out in the co-precipitation all underwent a hydrothermal treatment. This involved 20ml of each sample being transferred into a stainless steel autoclave (with the total capacity being 30ml). The autoclave was then placed in a pre-heated oven (UT-6, Heraeus Instruments) at a set time and temperature. Once the heat treatment had been completed, the samples were left to cool at room temperature, washed, dried and characterized.

Unless otherwise stated the majority of the heat treatments were carried out at 140^{o}C for 6 hours. Table 3-2 shows the details of precursors and pH values used in the synthesis of ZnO nanoparticles without addition of surfactants.

Table 3-2: Summary of the precursors and pH values used in synthesis of ZnO nanoparticles without the addition of surfactant.

Zinc Precursor (0.0005 mol)	Base (0.005 mol)	pH
$Zn(CH_3COO)_2•2H_2O$	NaOH	12.8±0.2
$Zn(NO_3)_2•6H_2O$	NaOH	12.8±0.2
$ZnCl_2$	NaOH	12.8±0.2
$Zn(CH_3COO)_2•2H_2O$	TMAH	12.8±0.2
$Zn(NO_3)_2•6H_2O$	TMAH	12.8±0.2
$ZnCl_2$	TMAH	12.8±0.2
$Zn(CH_3COO)_2•2H_2O$	DEA	10.0±0.2
$Zn(NO_3)_2•6H_2O$	DEA	10.0±0.2
$ZnCl_2$	DEA	10.0±0.2
$Zn(CH_3COO)_2•2H_2O$	NH_4OH	10.0±0.2
$Zn(NO_3)_2•6H_2O$	NH_4OH	10.0±0.2
$ZnCl_2$	NH_4OH	10.0±0.2

Table 3-3 shows a summary of the experimental details of the reactions between $Zn(CH_3COO)_2•2H_2O$ and different base solutions with different non-ionic surfactants (L64, L68 and P123).

Table 3-3: Summary of the precursors and pH values used in synthesis of ZnO nanoparticles without the addition of non-ionic surfactant.

Zinc Salt (0.0005 mol)	Base (0.005 mol)	Surfactant (0.00072 mol)	pH
$Zn(CH_3COO)_2•2H_2O$	NaOH	L64	12.8±0.2
$Zn(CH_3COO)_2•2H_2O$	NaOH	F68	12.8±0.2
$Zn(CH_3COO)_2•2H_2O$	NaOH	P123	12.8±0.2
$Zn(CH_3COO)_2•2H_2O$	TMAH	L64	12.8±0.2
$Zn(CH_3COO)_2•2H_2O$	TMAH	F68	12.8±0.2
$Zn(CH_3COO)_2•2H_2O$	TMAH	P123	12.8±0.2
$Zn(CH_3COO)_2•2H_2O$	DEA	L64	10.0±0.2
$Zn(CH_3COO)_2•2H_2O$	DEA	F68	10.0±0.2
$Zn(CH_3COO)_2•2H_2O$	DEA	P123	10.0±0.2
$Zn(CH_3COO)_2•2H_2O$	NH_4OH	L64	10.0±0.2
$Zn(CH_3COO)_2•2H_2O$	NH_4OH	F68	10.0±0.2
$Zn(CH_3COO)_2•2H_2O$	NH_4OH	P123	10.0±0.2

Table 3-4 shows a summary of the experimental details of the reactions between $Zn(CH_3COO)_2•2H_2O$ reacted with NaOH with addition of different concentration of non-ionic surfactant L64

Table 3-4: Summary of the precursors and pH values used in synthesis of ZnO nanoparticles without the addition of various concentrations of non-ionic surfactant.

Zinc Salt (0.0005 mol)	Base (0.005 mol)	Surfactant	pH
$Zn(CH_3COO)_2•2H_2O$	NaOH	L64 (1 wt% total solution, 50ml)	12.8±0.2

Zinc Salt (0.0005 mol)	Base (0.005 mol)	Surfactant	pH
$Zn(CH_3COO)_2•2H_2O$	NaOH	L64 (11 wt% total solution, 50ml)	12.8±0.2
$Zn(CH_3COO)_2•2H_2O$	NaOH	L64 (28 wt% total solution, 50ml)	12.8±0.2
$Zn(CH_3COO)_2•2H_2O$	NaOH	L64 (53 wt% total solution, 50ml)	12.8±0.2

Table 3-5 shows a summary of the experimental details of the reactions between $Zn(NO3)_2•6H_2O$ and $ZnCl_2$ as the salt precursors, NaOH (pH = 12.8±0.2) as the base solution and non-ionic surfactants L64, F68 and P123.

Table 3-5: Summary of the different starting salts and pH values used in synthesis of ZnO nanoparticles without the addition of various non-ionic surfactant

Zinc Salt (0.0005 mol)	Base (0.005 mol)	Surfactant (0.00072 mol)	pH
$Zn(NO_3)_2•6H_2O$	NaOH	L64	12.8±0.2
$Zn(NO_3)_2•6H_2O$	NaOH	F68	12.8±0.2
$Zn(NO_3)_2•6H_2O$	NaOH	P123	12.8±0.2
$ZnCl_2$	NaOH	L64	12.8±0.2
$ZnCl_2$	NaOH	F68	12.8±0.2
$ZnCl_2$	NaOH	P123	12.8±0.2

Table 3-7 shows a summary of the experimental details of the reactions between $Zn(CH_3COO)_2•2H_2O$ as the zinc salt precursor and different base solutions with addition of different ionic surfactants

Table 3-6: Summary of the precursors and pH values used in synthesis of ZnO nanoparticles without the addition of ionic surfactant.

Zinc Salt (0.0005 mol)	Base (0.005 mol)	Surfactant (0.00072 mol)	pH
$Zn(CH_3COO)_2•2H_2O$	NaOH	SDS	12.8±0.2
$Zn(CH_3COO)_2•2H_2O$	NaOH	CTAB	12.8±0.2
$Zn(CH_3COO)_2•2H_2O$	TMAH	SDS	12.8±0.2
$Zn(CH_3COO)_2•2H_2O$	TMAH	CTAB	12.8±0.2
$Zn(CH_3COO)_2•2H_2O$	DEA	SDS	10.0±0.2
$Zn(CH_3COO)_2•2H_2O$	DEA	CTAB	10.0±0.2
$Zn(CH_3COO)_2•2H_2O$	NH_4OH	SDS	10.0±0.2
$Zn(CH_3COO)_2•2H_2O$	NH_4OH	CTAB	10.0±0.2

Table 3-7 and Table 3-8 details the effects of synthetic conditions including hydrothermal time and hydrothermal temperature on the particle size and morphology, respectively.

Table 3-7: Effect of hydrothermal time – details of experiment

Zinc Salt (0.005 mol)	Base (0.05 mol)	Surfactant (0.00072 mol)	Time (h)
$Zn(CH_3COO)_2•2H_2O$	NaOH	L64	2
$Zn(CH_3COO)_2•2H_2O$	NaOH	L64	4
$Zn(CH_3COO)_2•2H_2O$	NaOH	L64	12
$Zn(CH_3COO)_2•2H_2O$	NaOH	F68	2
$Zn(CH_3COO)_2•2H_2O$	NaOH	F68	4
$Zn(CH_3COO)_2•2H_2O$	NaOH	F68	12
$Zn(CH_3COO)_2•2H_2O$	NaOH	P123	2
$Zn(CH_3COO)_2•2H_2O$	NaOH	P123	4
$Zn(CH_3COO)_2•2H_2O$	NaOH	P123	12

Table 3-8: Effect of hydrothermal temperature – details of experiment

Zinc Salt (0.005 mol)	Base (0.05 mol)	Surfactant (0.00072 mol)	Temperature (°C)
$Zn(CH_3COO)_2 \cdot 2H_2O$	NaOH	L64	120
$Zn(CH_3COO)_2 \cdot 2H_2O$	NaOH	L64	160
$Zn(CH_3COO)_2 \cdot 2H_2O$	NaOH	L64	200
$Zn(CH_3COO)_2 \cdot 2H_2O$	NaOH	F68	120
$Zn(CH_3COO)_2 \cdot 2H_2O$	NaOH	F68	160
$Zn(CH_3COO)_2 \cdot 2H_2O$	NaOH	F68	200
$Zn(CH_3COO)_2 \cdot 2H_2O$	NaOH	P123	120
$Zn(CH_3COO)_2 \cdot 2H_2O$	NaOH	P123	160
$Zn(CH_3COO)_2 \cdot 2H_2O$	NaOH	P123	200

3.2.4 Synthesis of AZO

Co-precipitation and hydrothermal methods were employed to synthesise AZO nanoparticles. A flow chart of the method used to synthesis of AZO nanoparticles is shown in Figure 3-4.

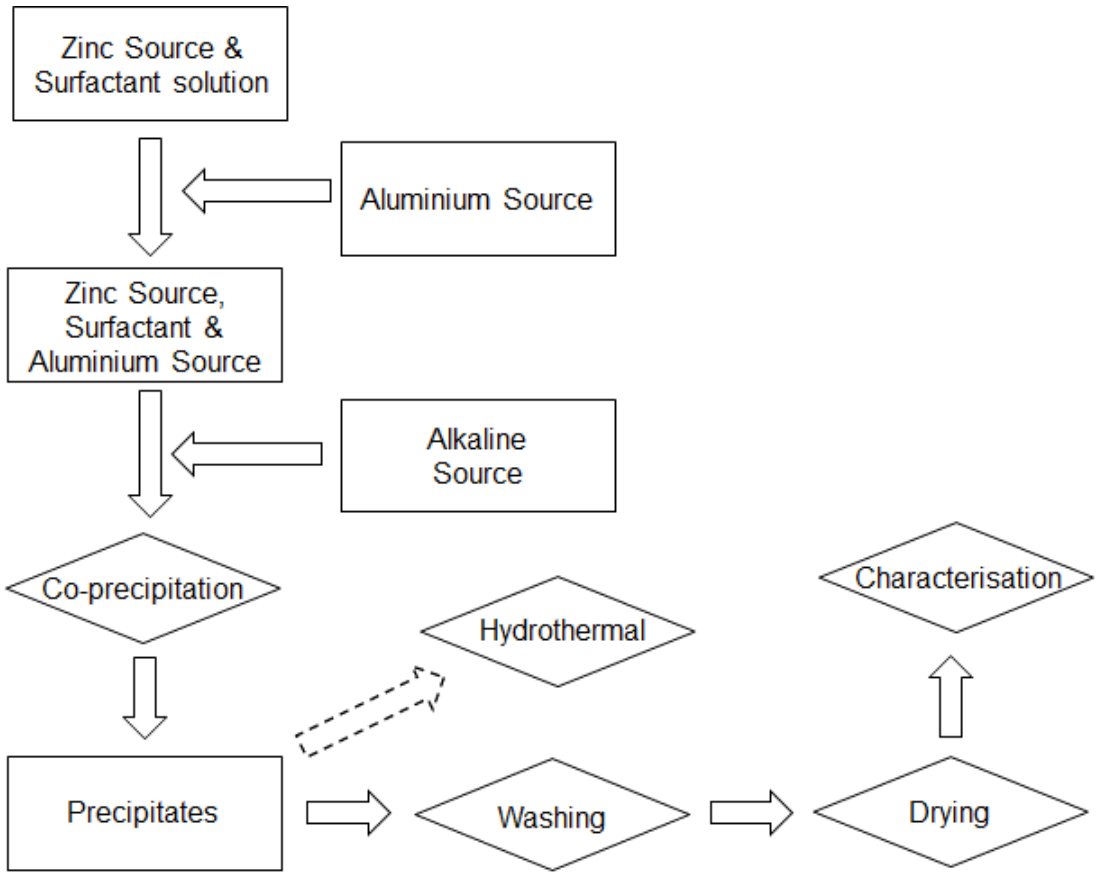

Figure 3-4: Flow chart of the procedure used for the synthesis of ZnO via the hydrothermal method

In a typical synthesis process of ZnO nanoparticles, 0.005 mol zinc salt and 0.0005 mol surfactant were weighed and then dissolved in 30ml deionized water. The solution was vigorously stirred with a magnetic stirrer at room temperature. After 10 min stirring, 20ml alkaline solution was introduced into the aqueous solution drop by drop to keep the pH at a pre-determined value. The resulting solution was constantly stirred for 30 min.

In the synthesis of AZO nanoparticles, 0.005 mol $ZnSO_4 \cdot 7H_2O$ and 0.0005 mol PEG were used. Additionally, $AlCl_3 \cdot 6H_2O$ was added as aluminium source. The pH value was fixed around 10.5.

After 30 minutes synthesis, the solution was split into two parts. One was kept without hydrothermal treatment. The other one was transferred into a Teflon-lined stainless steel autoclave with an inner volume of 30ml and sealed. The autoclave was then moved into an oven (UT-6, Heraeus Instruments) and maintained at different temperatures (140, 180, 220 °C) for different times (2h, 4h and 6h), and then allowed to naturally cool down to room temperature.

In the synthesis of AZO nanoparticles, the hydrothermal treatment was carried out at 220 °C for 6 h. Three experiments were carried out by fixing Al/Zn ratios at 3 at.%, 5 at.% and 10 at.% as shown in Table 3-9.

Table 3-9: AZO synthesis with three different Al/Zn ratios

Sample	Zinc salt	Base	Surfact	Temp (℃)	Time (h)	pH	Dopant
AZO-1HT	0.005 mol	NaOH	0.0005 mol	220	6	10.0±0.2	0.00015 mol
AZO-2HT	0.005 mol	NaOH	0.0005 mol	220	6	10.0±0.2	0.00025 mol
AZO-3TH	0.005 mol	NaOH	0.0005 mol	220	6	10.0±0.2	0.0005 mol

3.3 Orthogonal experimental design and analysis

Orthogonal experimental design was used in this project to study the effect of reaction conditions on the size and morphology of the ZnO nanoparticles in both co-precipitation and hydrothermal approaches.

3.3.1 Procedure of orthogonal experimental design

A typical orthogonal experiment design consists of the following steps [97]

- Identification of the main aims of the experiment
- Determination of factors and the corresponding levels at which they vary
- The design of the appropriate orthogonal array(s)
- Execution of the designed experiment
- Analysis of the obtained results
- Determination of further work from the results.

The effects of reaction conditions on the formation of nanoparticles were investigated by the orthogonal experiment design based upon the morphology (qualitative) and the aspect ratio (length/width) (quantitative) of the prepared ZnO nanoparticles.

All the experiments carried out in this project were based upon a L4 or a L9 orthogonal experimental array.

3.3.2 Principle of L9 orthogonal design

The term solution space is employed to describe the ranges of the varying factors in the orthogonally designed experiments. The selection of levels at which the factors vary is described as building up a network within the solution space. Each node on the network represents a combination of factors with their corresponding levels. A full-scale experiment would require all the nodes on the network to be tested. An orthogonally designed experiment only examines fewer selected nodes.

The solution space of L9 (3^3) orthogonal array can be expressed by a cubic. In an L9 array the three levels correspond to the three dimensional coordinates. The three levels at which the factors vary correspond to the three nodes on each dimension. This cubic model with its all 27 nodes of combinations is illustrated in Figure 3-4 [97, 98]

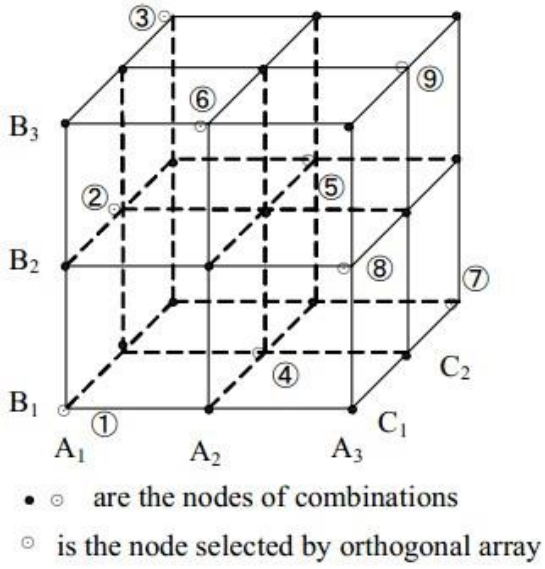

Figure 3-4: Cubic model of L9 (3^4) orthogonal experimental design [98]

This cubic model with 27 nodes would indicate that 27 experiments would be required to study a three or four factors and three levels situation. However, the 9 "⊙" nodes marked in the figure represent the chosen combinations in the L9 orthogonal array and are orthogonal with each other. As such only these 9 experiments are required to be carried out. The 9 combinations of L9 orthogonal experiment are:

(1)$A_1B_1C_1$; (2) $A_1B_2C_2$; (3) $A_1B_3C_3$;

(4) $A_2B_1C_2$; (5) $A_2B_2C_3$; (6) $A_2B_3C_1$;

(7) $A_3B_1C_3$; (8) $A_3B_2C_1$; (9) $A_3B_3C_2$;

These 9 combinations are the same as the 9 experiments listed in Table 3.2. Only 9 experimental runs instead of 27 are needed in L9 orthogonal experiments. The orthogonal

arrays, $L_M(Q^N)$, are used to arrange a small but representative experiments combinations [97, 98].

3.3.3 Experimental design

Orthogonal experimental design is a methodology used to investigate how different factors and the levels at which they vary affect a process performance using the least experimental run]. The adoption of orthogonal arrays in experimental design allows examining selected combination of factors with their corresponding levels instead of testing all possible conditions and therefore saves time and cost [99].

In this project, Both $L_9(3^3)$ and $L_9(3^4)$ array were exploited to study how different processing parameters such as zinc salt, alkaline base, surfactant, temperature, time, surfactant amount and pH value affect the sizes and morphologies of the synthesized ZnO nanoparticles. If orthogonally planned experiment had not been adopted, three factors with three levels would require 3^3=27 experimental runs and four factors with three levels would require 3^4=81 runs. The exploitation of $L_9(3^4)$ array requires only 9 experimental runs for either three factors with three levels or four factors with three levels as shown in Table 3-10 and Table 3-11, respectively.

Table 3-10: $L_9(3^4)$ array

Expt. number	Factor		
	A	B	C
1	A1	B1	C1
2	A1	B2	C2
3	A1	B3	C3
4	A2	B1	C2
5	A2	B2	C3
6	A2	B3	C1
7	A3	B1	C3
8	A3	B2	C1
9	A3	B3	C2

Table 3-11: $L_9(3^4)$ array

Expt. number	Factor			
	A	B	C	D
1	A1	B1	C1	D1
2	A1	B2	C2	D2
3	A1	B3	C3	D3
4	A2	B1	C2	D3
5	A2	B2	C3	D1
6	A2	B3	C1	D2
7	A3	B1	C3	D2
8	A3	B2	C1	D3
9	A3	B3	C2	D1

In the synthesis of ZnO nanoparticles via co-precipitation method, three factors which are starting salts, alkaline solutions and surfactants with their three corresponding levels are listed in Table 3-12.

Table 3-12: The three factors with their corresponding levels of Orthogonal design

	1	**2**	**3**
1-A: Zinc salt	$Zn(NO_3)_2 \cdot 6H_2O$	$ZnSO_4 \cdot 7H_2O$	$Zn(C_2H_4O_2)_2 \cdot 2H_2O$
1-B: Alkaline base	NaOH	NH_4OH	DEA
1-C:Surfactant	CTAB	PEG	AOT

In the first orthogonal experiment, Therefore, the L9 (3^3) orthogonal array in this project was established by combining the factors in Table 3-12 with the array given in Table 3-10. The resulting experimental details are shown in Table 3-13.

Table 3-13: The experimental details of orthogonal array.

1-A Starting salts (0.005 mol)	**1-B Alkaline bases (0.05 mol)**	**1-C Surfactants (0.0005 mol)**
$Zn(NO_3)_2 \cdot 6H_2O$	NaOH solution	CTAB
$Zn(NO_3)_2 \cdot 6H_2O$	NH_4OH solution	PEG
$Zn(NO_3)_2 \cdot 6H_2O$	DEA	AOT
$ZnSO_4 \cdot 6H_2O$	NaOH solution	PEG
$ZnSO_4 \cdot 6H_2O$	NH_4OH solution	AOT
$ZnSO_4 \cdot 6H_2O$	DEA	CTAB
$Zn(Ac)_2 \cdot 2H_2O$	NaOH solution	AOT
$Zn(Ac)_2 \cdot 2H_2O$	NH_4OH solution	CTAB
$Zn(Ac)_2 \cdot 2H_2O$	DEA	PEG

For the synthesis of ZnO nanoparticles via hydrothermal approach, two groups of orthogonal experimental arrays were used. In the first group, zinc salt, alkaline base, surfactant type and temperature were chosen as the four factors and each of them had 3 different levels as listed in Table 3-14.

Table 3-14: Four factors with their corresponding levels chosen in the 1st group

		Level		
		1	**2**	**3**
Factor	**Zinc salt**	$Zn(NO_3)_2 \cdot 6H_2O$	$ZnSO_4 \cdot 7H_2O$	$Zn(C_2H_4O_2)_2 \cdot 2H_2O$
	Alkaline base	NaOH	NH_4OH	DEA
	Surfactant	CTAB	PEG	AOT
	Temperature	140 °C	180 °C	220 °C

Therefore the $L_9(3^4)$ array for the first group was generated in Table 3-15. The 9 experiments were conducted for 6h and the pH value was fixed at about 10.5.

Table 3-15: $L_9(3^4)$ array designed for the 1st group

Zinc salt	Base	Surfactant	Temperature (°C)
$Zn(NO_3)_2 \cdot 6H_2O$	NaOH	CTAB	140
	NH_4OH	PEG	180
	DEA	AOT	220
$ZnSO_4 \cdot 7H_2O$	NaOH	PEG	220
	NH_4OH	AOT	140
	DEA	CTAB	180
$Zn(C_2H_4O_2)_2 \cdot 2H_2O$	NaOH	AOT	180
	NH_4OH	CTAB	220
	DEA	PEG	140

Similarly, time, surfactant amount and pH value were chosen as the three factors in the second group and each of them had 3 different levels as listed in Table 3-16 and the subsequent $L_9(3^3)$ array for the second group was presented in Table 3-17. These 9 experiments used $ZnSO_4 \cdot 7H_2O$, NaOH and PEG as starting materials and were conducted at 180 °C.

Table 3-16: Three factors with their corresponding levels chosen in the 2nd group

		Level		
		1	**2**	**3**
Factor	**Time**	2h	4h	6h
	Surfactant amount	0.00025mol	0.0005 mol	0.001 mol
	pH value	≈ 11.5	≈ 10.5	≈ 12.5

Table 3-17: $L_9(3^3)$ array designed for the 2nd group

Time (h)	Surfactant Amount (mol)	pH value
2	0.00025	11.5±0.2
	0.0005	10.0±0.2
	0.001	12.8±0.2
4	0.00025	10.0±0.2
	0.0005	12.8±0.2
	0.001	11.5±0.2
6	0.00025	12.8±0.2
	0.0005	11.5±0.2
	0.001	10.0±0.2

3.4 Other experimental treatments

3.4.1 Washing

A centrifuge (Biofuge Primo, Heraeus Instruments) was used for the separation of solid precipitates from their solutions. The precipitates were washed with de-ionized water and iso-propanol to remove any excess surfactant and ions produced during the reaction. Each cycle involved 10ml of each washing solution being added to the precipitate, mixed and then spun at 3000 RPM in the centrifuge for 5 minutes. Each sample was washed three times with each washing solution. After the final cycle the precipitates were kept in 20ml de-ionized water ahead of the drying and characterisation stages.

3.4.2 Silicon/Glass cleaning

Silicon and glass slides that were used as substrates for some characterisations were cleaned before use. Firstly the substrate was immersed in a 10% hydrochloric acid solution for 10 minutes. After being rinsed in water the glass was then transferred to a 50/50%

solution of Ethanol and acetone and ultrasonically cleaned for 30 minutes. After a further rinse in de-ionised water the samples were covered and left to dry overnight at room temperature.

3.4.3 Drying

All samples for characterisation were dried at 60°C for 4 to 24 hours in an oven to remove retained water. For AZO samples a vacuum oven was used.

3.5 Characterisation

The sizes and morphologies of the as-synthesized ZnO and AZO nanomaterials were characterised by TEM and Field Emission Gun Scanning Electron Microscopy (FEGSEM). The crystallinity and phase analysis of the products was carried out using X-Ray Diffraction (XRD). The crystallite size was also measured on some samples using XRD.

3.5.1 X-Ray Diffractomery

XRD is a non-destructive technique which can reveal information about the physical properties, chemical composition and crystallographic structure of materials. XRD is based on the observing the scattered intensity of an x-ray beam hitting a sample as a function of incident and scattered angle, polarisation and wavelength or energy.

The resulting XRD patterns are generally used in two main areas; for the identification of crystalline materials and determination of the materials structure. The crystallite size can also be measured using the XRD pattern, respective peaks and the Scherrer equation.

$$\mathrm{D} = \frac{K\lambda}{\beta \cos\theta}$$

Where, λ is the wavelength of X-ray which is 0.1542nm for Copper Kα X-ray; β is the corrected full width at half of the maximum intensity (FWHM) in radians; θ is the Bragg diffraction angle; K Is the Scherrer constant (0.89 in this case) [100].

The crystal structure of the synthesized particles were characterised by a Bruker D8 X-ray diffractometer with CuKα radiation (λ = 1.542 Å) at a scanning rate (step) of 0.02° s^{-1} in the 2θ range from 10° to 70° [101].

3.5.2 Transmission Electron Microscope

TEM is a technique in which a beam of electrons is transmitted through an ultra-thin specimen. An image is formed from the interaction between the sample and the electrons which is magnified and focused by a series of apertures and projected onto an imaging screen, digital camera or photographic film. This technique is widely used to observe the phase structure, defects and morphology of a material in the nanometer scale. The structure of materials can also be analysed by using diffraction patterns.

A transmission electron microscope, TEM (JEM 100CX, JEOL, Japan) was used to examine the size and morphology of the particles. The solutions were cast onto a carbon coated copper grid and left to dry overnight before being transferred into the chamber of the TEM. The elemental analysis was recorded by energy-dispersive X-ray spectroscopy (EDX).

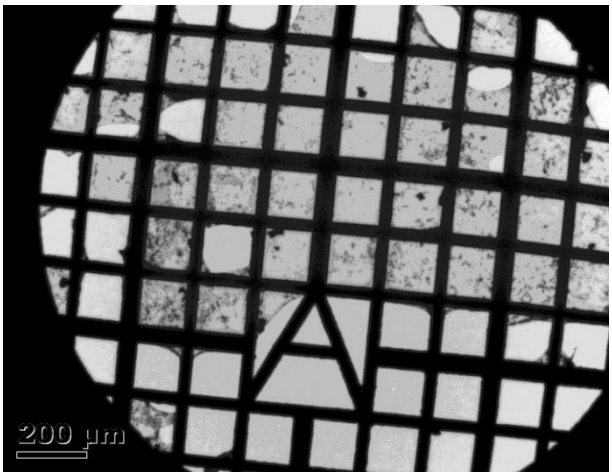

Figure 3-5: TEM image of ZnO particles deposited on a carbon film coated brass grid

3.5.3 Field Emission Gun Scanning Electron Microscope (FEGSEM)

The scanning electron microscope (SEM) is a type of microscope that creates various images by focusing a beam of electrons onto a surface of a material and using the returned interactions to create an image. In this case the electrons are emitted via a field emission gun (FEG) rather than a tungsten cathode and accelerator. Due to the manner in which the image is created, using primary or secondary electron imaging, SEM images have a great depth of field yielding a three dimensional appearance useful for understanding the morphology of many materials.

A scanning electron microscope (FEGSEM, LEO 1530VP) was also used to examine the size and morphology of the particles up to a magnification of 100 K.

The solutions were either cast onto glass slides (1x1cm) subsequently dried and attached to a sample holder using silver paint or a small amount of dry powder was placed onto a carbon paste coated surface.

The samples were then coated with gold in argon gas to improve conductivity. All of the micrographs were taken in the “SE2” mode at electron voltages of between 2-5eV. “SE2” (secondary electron) mode at electron voltages of between 2-5eV. The secondary electron mode allows an image to be displayed and as such the particles to be observed.

Chapter 4 Preparation of ZnO by the co-precipitation method

Co-precipitation is the most direct wet-chemistry approach to synthesise inorganic (ceramic) particles, which is also often used as a reference method for comparison with other wet-chemistry approaches such as hydrothermal method. Various parameters, including different types and amount of zinc salt precursors, the base solutions related to pH values and the additives such as different types and amount of surfactants, will affect the particle size, size distribution and morphology of the particles synthesised. Both orthogonal array and single factor approaches were used to investigate the effects of these parameters.

4.1 Nanoparticles synthesised without addition of surfactants

In order to investigate the effect of surfactants on the crystalline phase, the morphology and the size of particles, the particles were first synthesised by the reactions between the zinc salts and base solutions without addition of the surfactants as the reference for comparison as shown in Table 3-2.

It can be seen that pH value for the reactions was changed from 12.8±0.2 for “strong” base solutions such as NaOH and TMAH to a decreased value of 10.0±0.2 for “weak” base solutions of NH_4OH and DEA. As the same quantity of base solutions and zinc precursors were used for all the reactions, this group of experiments can be considered to look at the effects of both the pH values and different salt precursors on the formation of ZnO compounds.

The X-ray diffractogram for the particles synthesised by the reactions between different zinc salt precursors and different base solutions are shown in Figure 4-1 to Figure 4-3. The XRD patterns indicated that either Zn-O, Zn-O-H or mixture of the two compounds were observed. Zn-O compound was obtained when the reactions were carried out using $Zn(CH_3COO)_2 \cdot 2H_2O$ and $Zn(NO_3)_2 \cdot 6H_2O$ and a “strong base” (pH = 12.0±0.2, NaOH and TMAH) (Figure 4-1A, Figure 4-1B). A mixture of Zn-O and Zn-O-H compounds were observed for the particles synthesised with $ZnCl_2$ and NaOH (Figure 4-1C). Zn-O-H compounds were observed for the particles synthesised between $ZnCl_2$ and TMAH and the

particles synthesised by reactions between “weak” base solution DEA (pH = 10.0±0.2 all of the zinc salts (Figure 4-1C, Figure 4-3,). The XRD results for the resultant compounds synthesised by NH_4OH and the zinc salts were not indicative of either Zn-O-H or Zn-O and were unknown.

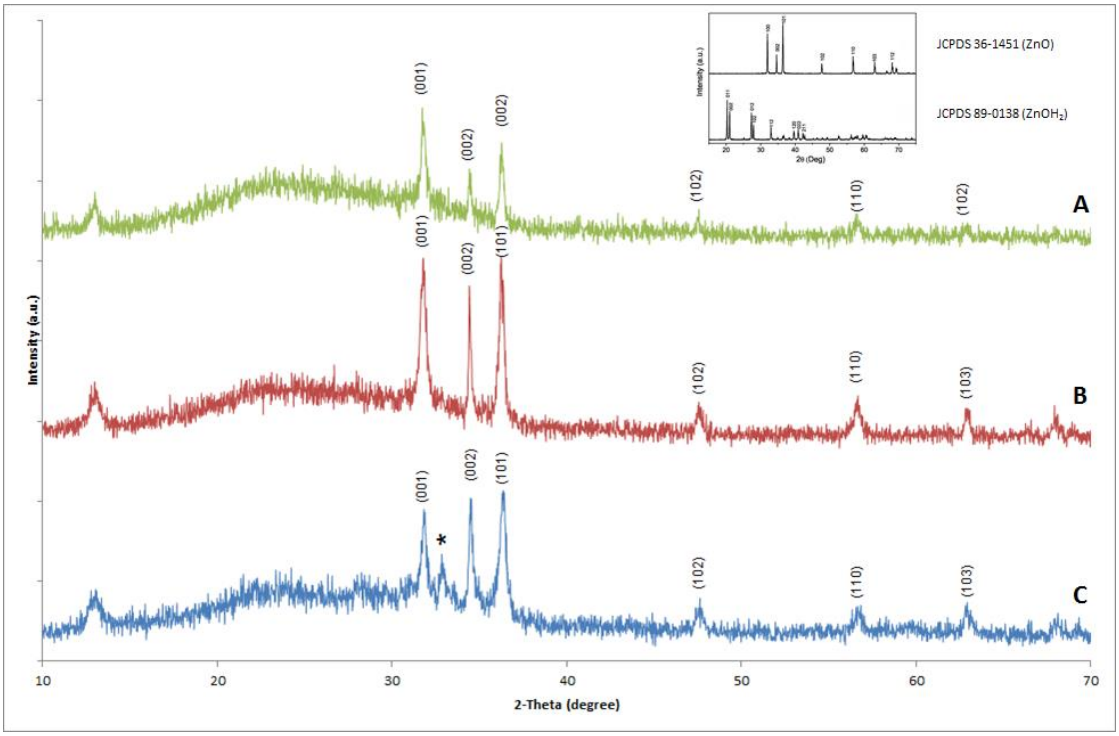

Figure 4-1: X-Ray diffractograms of the particles synthesised by the reactions between NaOH and different salts at room temperature (pH = 12.8±0.2). [A] $Zn(CH_3COO)_2•2H_2O$ [B] $Zn(NO_3)_2•6H_2O$ [C] $ZnCl_2$

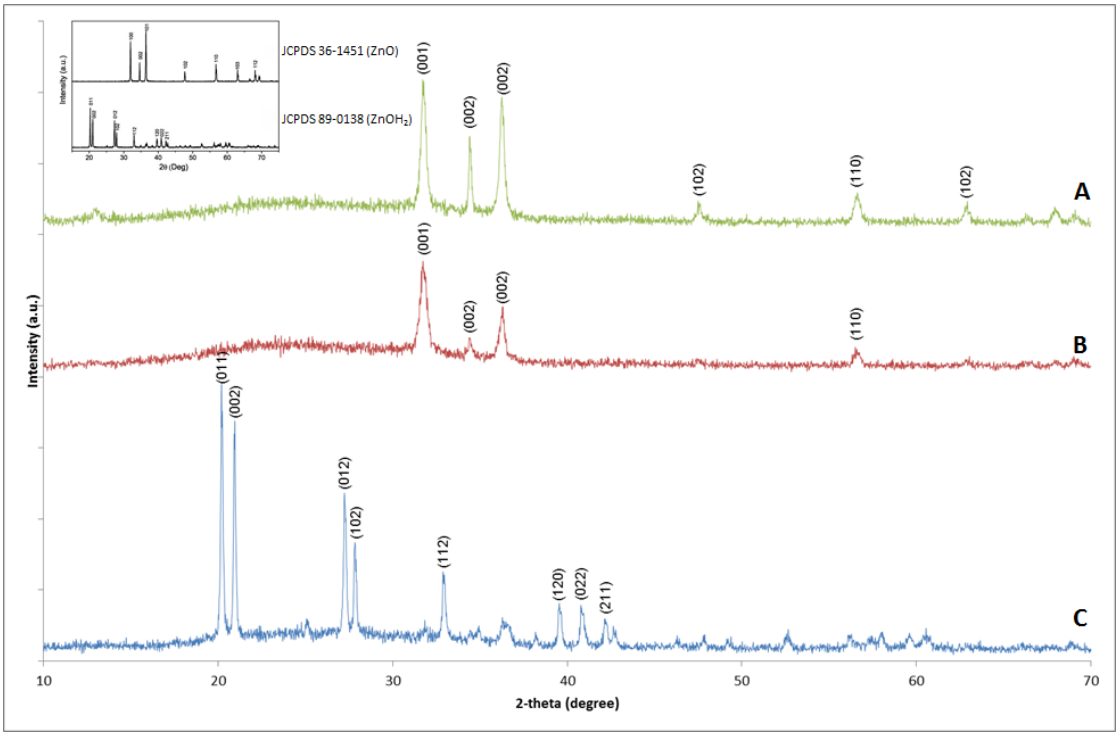

Figure 4-2: X-Ray diffractograms of the particles synthesised by the reactions between TMAH and different salts at room temperature (pH = 12.8±0.2). [A] $Zn(CH_3COO)_2•2H_2O$ [B] $Zn(NO_3)_2•6H_2O$ [C] $ZnCl_2$.

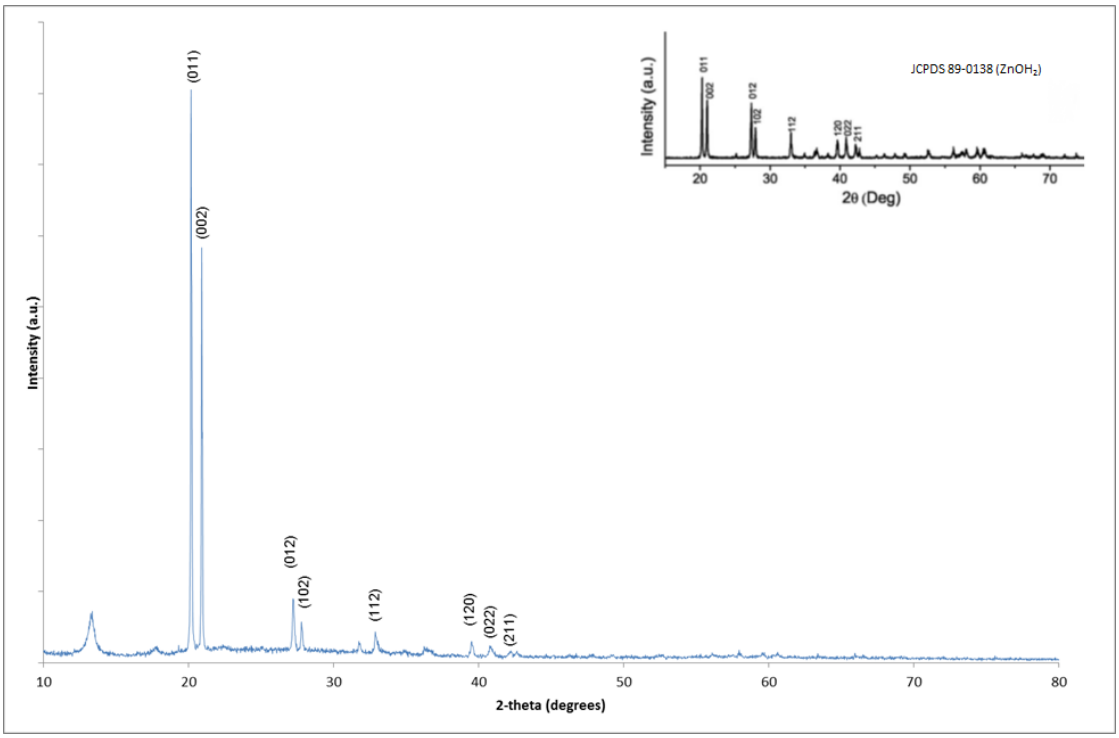

Figure 4-3: X-Ray diffractogram of the particles synthesised by the reaction between DEA and the zinc salt precursor $Zn(CH_3COO)_2•2H_2O$ (pH = 10.0±0.2).

TEM and FEGSEM were used to investigate the effects of zinc salt precursors and different base solutions (pH) on the sizes and morphologies of the particles synthesised. The results are shown in Figure 4-4 to Figure 4-7.

The images show that by using $Zn(CH_3COO)_2•2H_2O$ (Figure 4-4A) or $Zn(NO_3)_2•6H_2O$ (Figure 4-5B) as the salt precursors reacted with NaOH, irregular platelets with a width of 200nm were formed. When $ZnCl_2$ (Figure 4-6C) was used, aggregated bundles of rods with widths of approximately 20nm and a total length of between 200-300nm were formed.

Elongated platelets about approximately 400nm in length were obtained when the particles prepared by the reactions between $Zn(CH_3COO)_2•2H_2O$ (Figure 4-7) and $Zn(NO_3)_2•6H_2O$ (Figure 4-8) as the different precursors salts and TMAH as the base solution. Aggregated bundles of rods of about 200nm in size and a total length of in the range of 150 to 400nm were obtained when $ZnCl_2$ was reacted with TMAH (Figure 4-9).

For the addition of a weak base (pH = 10.0±0.2) spherical particles of $Zn(OH)_2$ approximately 200nm in size were produced following the precipitation reaction between $Zn(NO_3)_2•6H_2O$ and DEA (Figure 4-10B).

No further particles were synthesised with the addition of the other zinc sources and weak bases. Figure 4-11 shows a typical example of the results in this case, with no particles evident. The exception to this were the particles of $Zn(OH)_2$ formed following the reaction with $Zn(CH_3COO)_2•2H_2O$ and DEA and shown in Figure 4-10A. Rectangular particles of roughly 800nm in width and greater than 1000nm in length were synthesised.

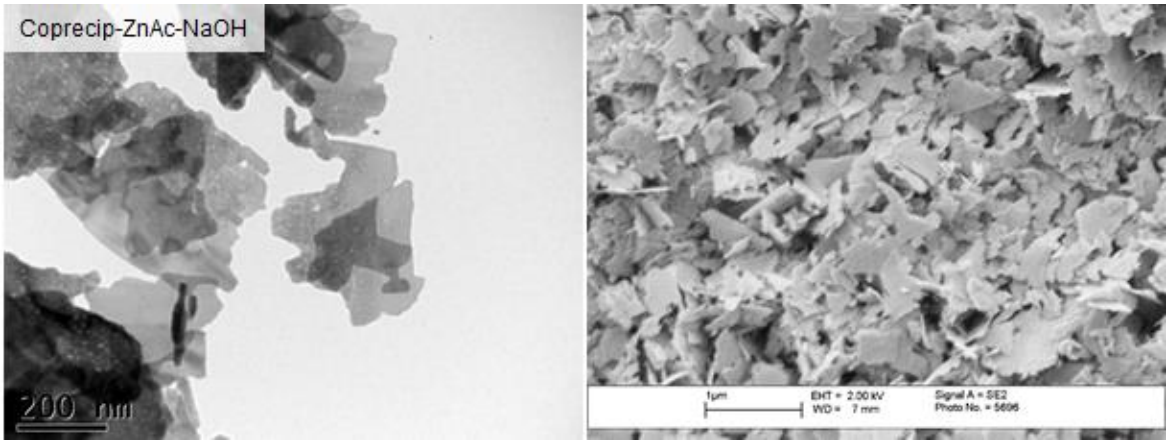

Figure 4-4: TEM (left)/FEGSEM (right) micrographs of the particles prepared by the reactions between NaOH and $Zn(CH_3COO)_2 \bullet 2H_2O$

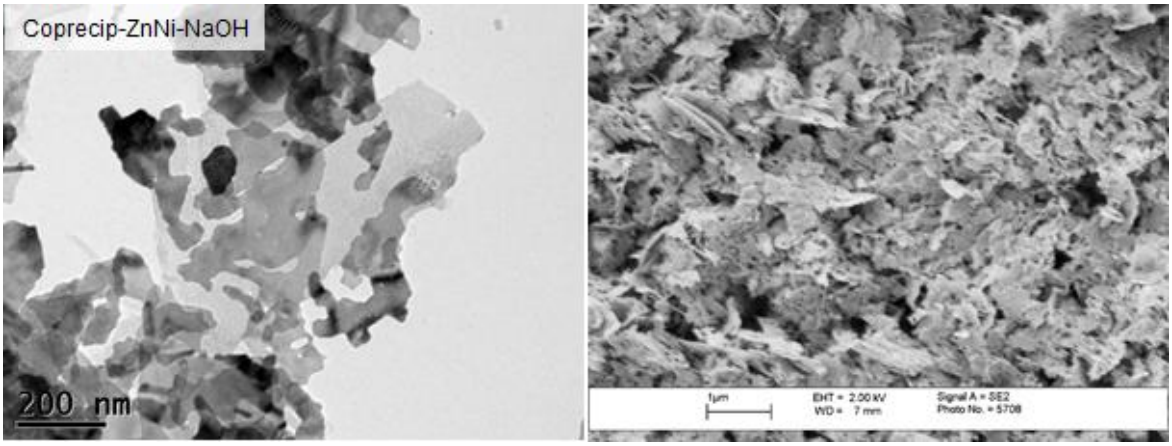

Figure 4-5: TEM (left)/FEGSEM (right) micrographs of the particles prepared by the reactions between NaOH and $Zn(NO_3)_2 \cdot 6H_2O$

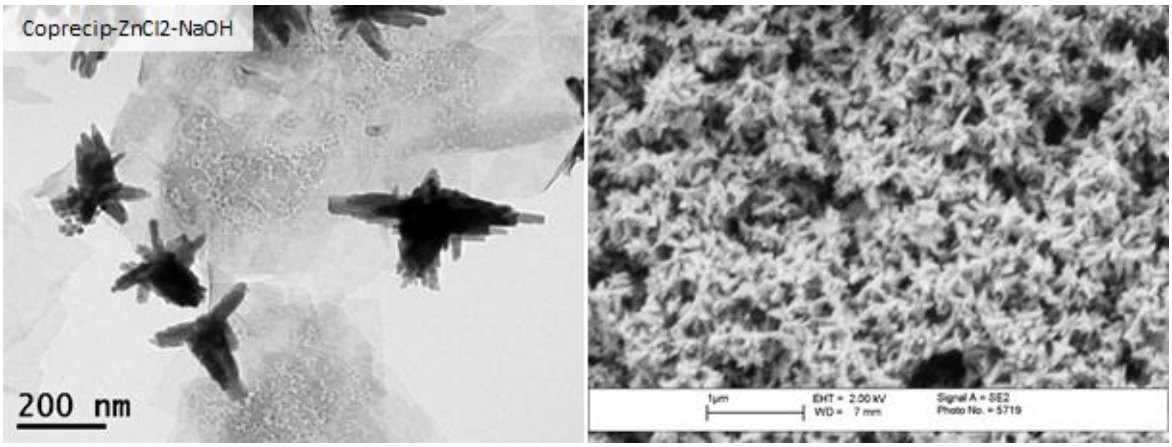

Figure 4-6: TEM (left)/FEGSEM (right) micrographs of the particles prepared by the reactions between NaOH and $ZnCl_2$

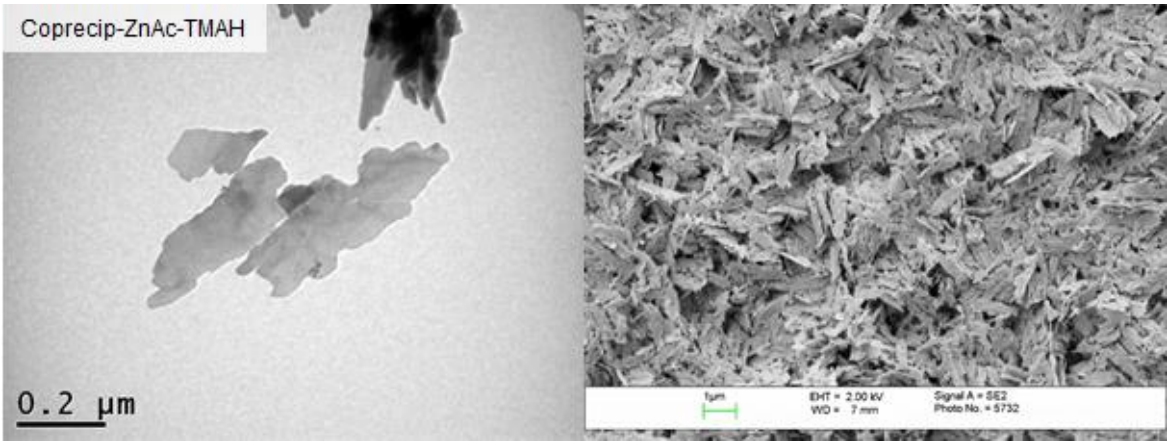

Figure 4-7: TEM (left)/FEGSEM (right) micrographs of the particles prepared by the reactions between TMAH and $Zn(CH_3COO)_2 \cdot 2H_2O$

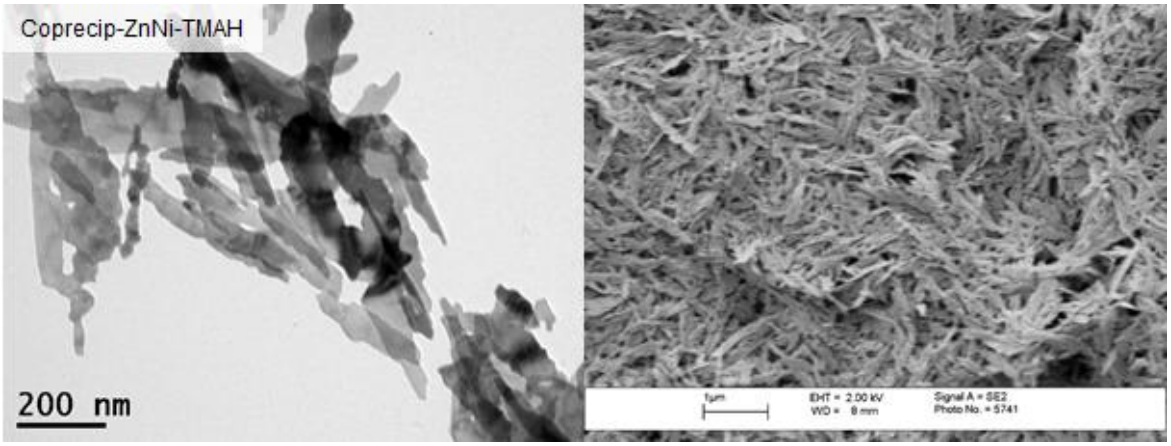

Figure 4-8: TEM (left)/FEGSEM (right) micrographs of the particles prepared by the reactions between TMAH and $Zn(NO_3)_2 \cdot 6H_2O$

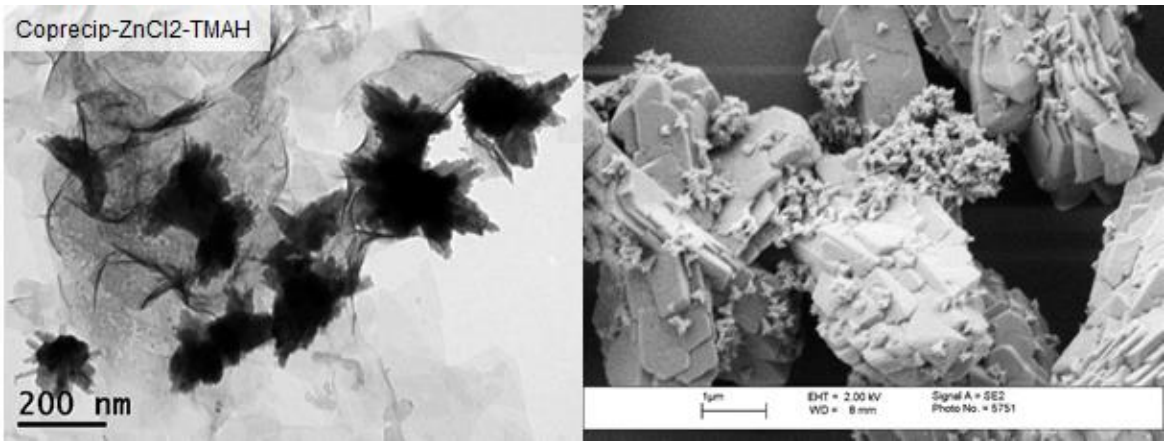

Figure 4-9: TEM (left)/FEGSEM (right) micrographs of the particles prepared by the reactions between TMAH and $ZnCl_2$

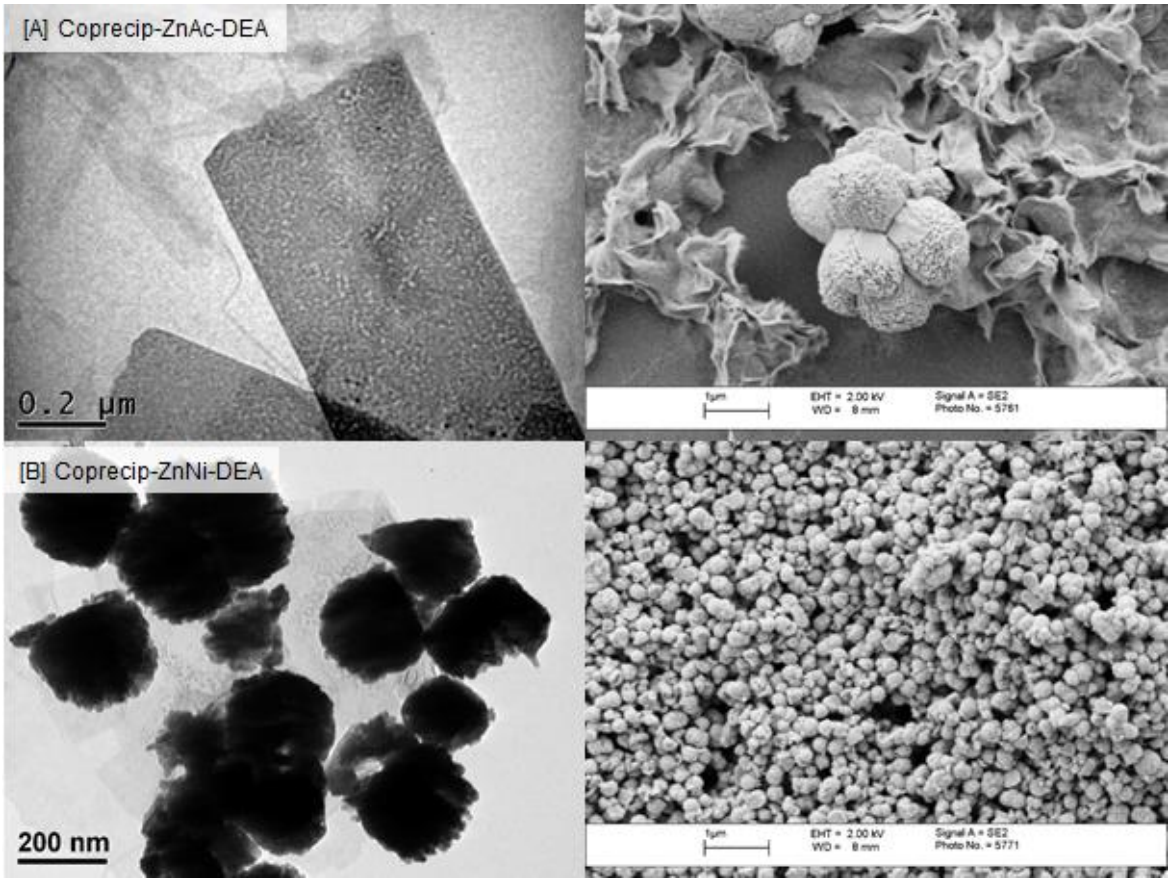

Figure 4-10: TEM (left)/FEGSEM (right) micrographs of the particles prepared by the reactions between DEA and different zinc salts [A] $Zn(CH_3COO)_2$•$2H_2O$ and [B] $Zn(NO_3)_2$·$6H_2O$

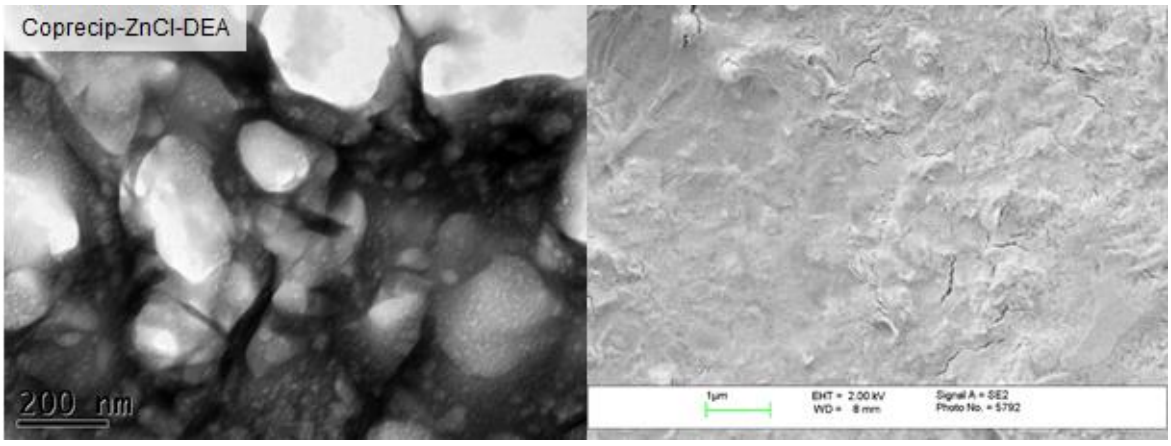

Figure 4-11: TEM (left)/FEGSEM (right) micrographs of the particles prepared by the reactions between NH_4OH and zinc salt of $Zn(CH_3COO)_2$•$2H_2O$

A summary of the shape and size of the particles synthesised through the precipitation of different zinc salt precursors reacted with different bases is given in Table 4-1. In general,

both platelets and aggregated rods were synthesised with the addition of a strong base solution (pH=12.8±0.2). The reaction of $Zn(NO_3)_2$•$6H_2O$ with DEA as the weak base solution (pH = 10.0±0.2), formed spherical particles.

Table 4-1: A summary of the particle size and morphology of ZnO compounds synthesised by using different zinc salt precursors reacted with different base solutions

Zinc Salt	Base	Particle Shape	Size (nm)	Compounds present
$Zn(CH_3COO)_2$•$2H_2O$	NaOH	Irregular Platelets	200	Zn-O
$Zn(NO_3)_2$•$6H_2O$	NaOH	Irregular Platelets	200	Zn-O
$ZnCl_2$	NaOH	Aggregated Bundles of Rods	200 – 300 (length)	Zn-O, Zn-O-H
$Zn(CH_3COO)_2$•$2H_2O$	TMAH	Elongated Platelets	400	Zn-O
$Zn(NO_3)_2$•$6H_2O$	TMAH	Elongated Platelets	400	Zn-O
$ZnCl_2$	TMAH	Aggregated bundles of rods	200 – 300 (length)	Zn-O-H
$Zn(CH_3COO)_2$•$2H_2O$	DEA	No particles synthesised.		Zn-O-H
$Zn(NO_3)_2$•$6H_2O$	DEA	Spherical	200nm	Zn-O-H
$ZnCl_2$	DEA	No particles synthesised.		Zn-O-H
$Zn(CH_3COO)_2$•$2H_2O$	NH_4OH	No particles synthesised.		Unknown
$Zn(NO_3)_2$•$6H_2O$	NH_4OH	No particles synthesised.		Unknown
$ZnCl_2$	NH_4OH	No particles synthesised.		Unknown

4.2 Nanoparticles synthesised with addition of surfactants

The effect of surfactant on the crystal phase, particle size and morphology of the particles was investigated.

4.2.1 The effect of non-ionic surfactant

The X-ray diffractograms of the samples prepared by the reactions of $Zn(CH_3COO)_2 \cdot 2H_2O$ and NaOH with addition of the non-ionic surfactants L64, F68 and P123 are shown in Figure 4-12A, Figure 4-12B and Figure 4-12C respectively. A mixture crystal phases of Zn-O and Zn-O-H compounds were observed when surfactant P123 or F68 was used and mainly the Zn-O compound was identified when the surfactant L64 was added, A mixture of Zn-O and Zn-O-H was also obtained for the particles prepared by the reactions of $Zn(CH_3COO)_2 \cdot 2H_2O$ and TMAH with addition of the non-ionic surfactants L64, F68 and P123, as shown in Figure 4-13.

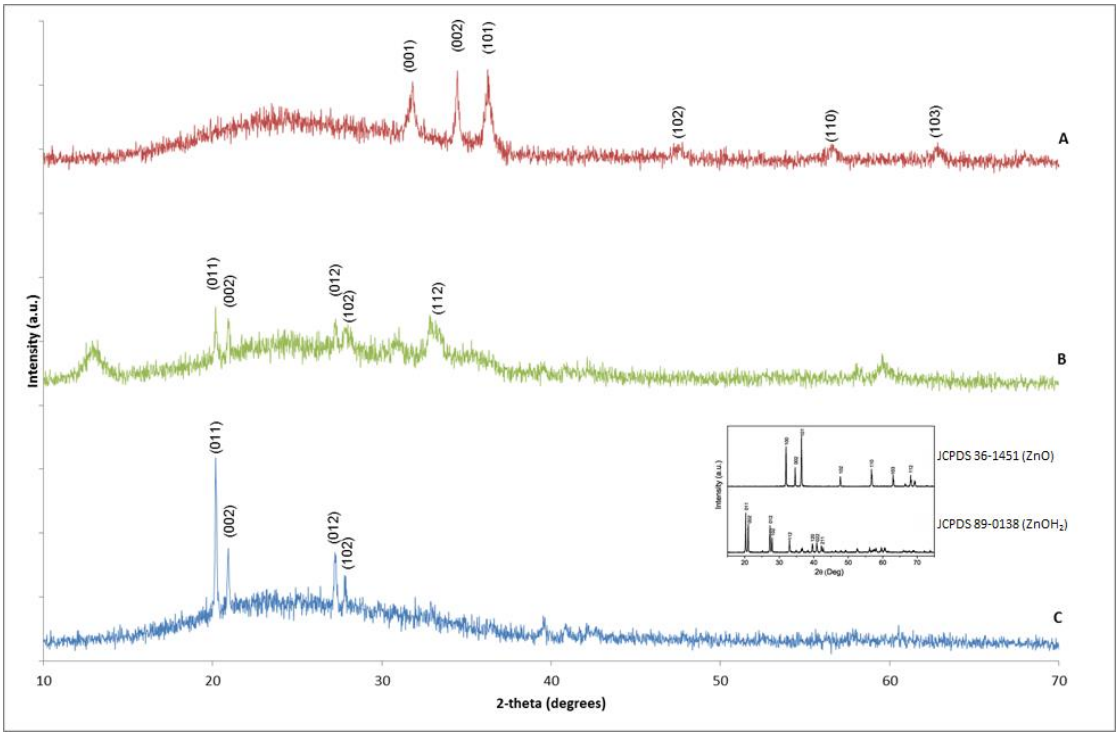

Figure 4-12: X-Ray diffractogram of the particles synthesised by the reactions between $Zn(CH_3COO)_2 \cdot 2H_2O$ and NaOH with different Pluronic surfactants [A] L64 [B] F68 [C] P123

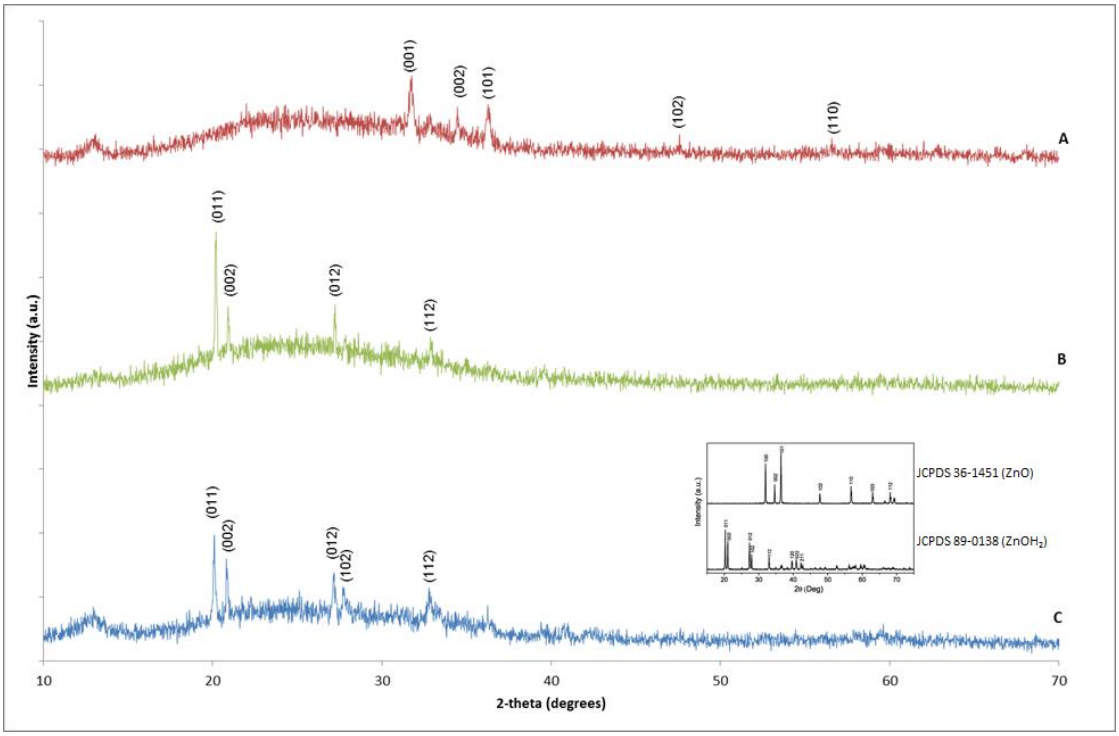

Figure 4-13: X-Ray diffractogram of the particles synthesised by the reactions between $Zn(CH_3COO)_2•2H_2O$ and TMAH with different Pluronic surfactants [A] L64 [B] F68 [C] P123

In comparison with the XRD results for the co-precipitation of $Zn(CH_3COO)_2•2H_2O$ with NaOH and TMAH without surfactants (Figure 4-1A, Figure 4-2A) the addition of surfactant had an effect. The XRD results indicated that with the addition of F68 and P123 surfactants Zn-O-H compound was formed, whereas the Zn-O compound was identified in the resultant precipitates without surfactants.

The morphologies of the co-precipitated particles synthesised by $Zn(CH_3COO)_2•2H_2O$ as the salt precursor reacted with NaOH as the precipitating regents and non-ionic surfactants Pluronic L64, F68 and P123 are shown in Figure 4-14, Figure 4-15 and Figure 4-16 respectively. A star-like particle approximately 1 μm in diameter was formed when L64 was used as the surfactant (Figure 4-14). Aggregated polyol particles were obtained when F68 and P123 were used as the surfactants (Figure 4-15, Figure 4-16). The use of F68 (Figure 4-15), also showed the presence of star-like particles on the surface of the aggregated polyols.

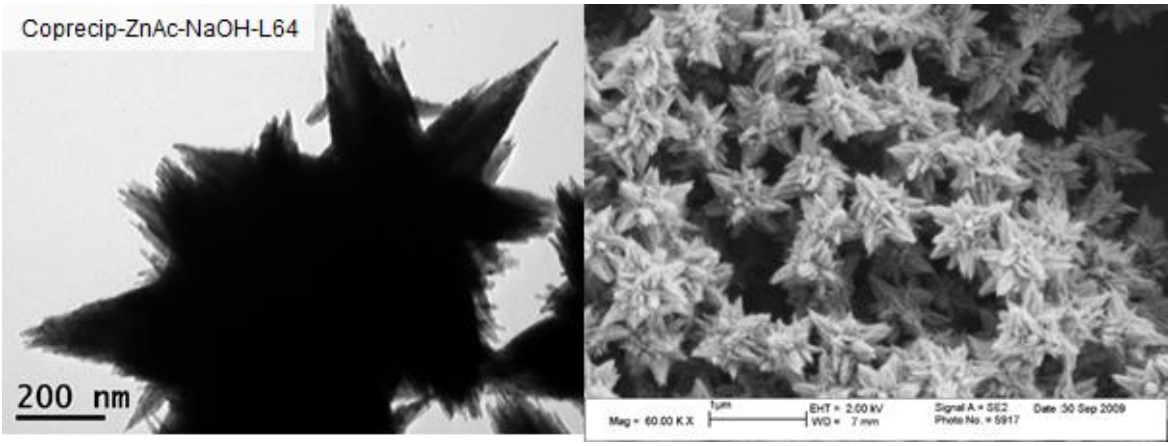

Figure 4-14: TEM (left)/FEGSEM (right) micrographs of particles prepared by the reactions between NaOH and $Zn(CH_3COO)_2 \cdot 2H_2O$ as the salt with addition of different non-ionic surfactants L64

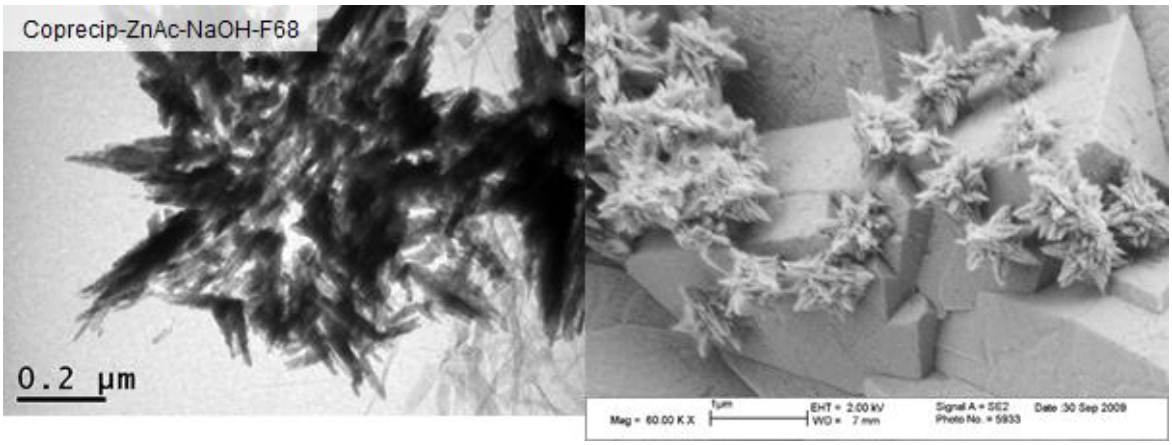

Figure 4-15: TEM (left)/FEGSEM (right) micrographs of particles prepared by the reactions between NaOH and $Zn(CH_3COO)_2 \cdot 2H_2O$ as the salt with addition of different non-ionic surfactants F68

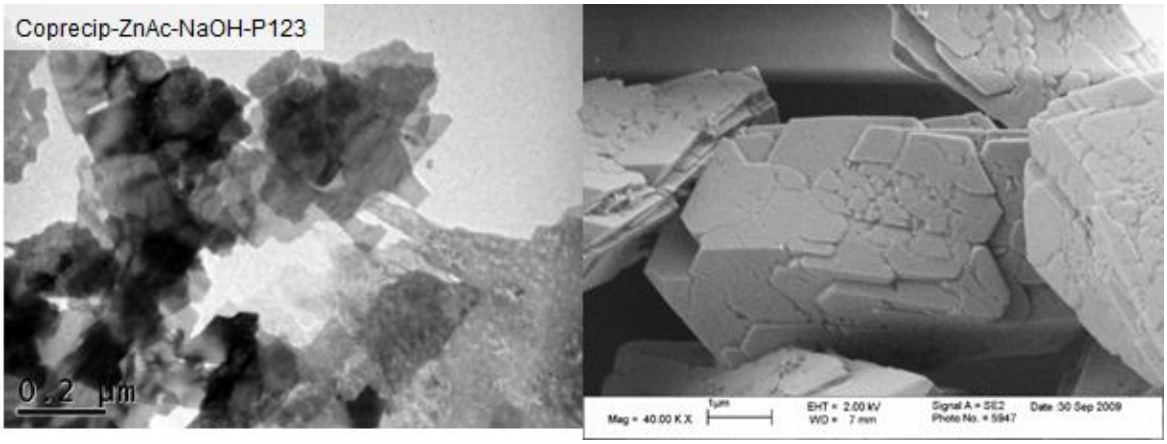

Figure 4-16: TEM (left)/FEGSEM (right) micrographs of particles prepared by the reactions between NaOH and $Zn(CH_3COO)_2 \cdot 2H_2O$ as the salt with addition of different non-ionic surfactants P123

Figure 4-17 shows $Zn(CH_3COO)_2 \cdot 2H_2O$ and TMAH with addition of the non-ionic surfactants. The micrographs show that there is a change in shape from the platelets formed when there is no surfactant presented (Figure 4-7) to aggregated platelets with addition of the surfactant of L64 (Figure 4-17 and aggregated block with surfactant F68 (Figure 4-18) or P123 (Figure 4-19). TEM analysis of the sample with the addition of P123 (Figure 4-19) reported some microflower type morphology present.

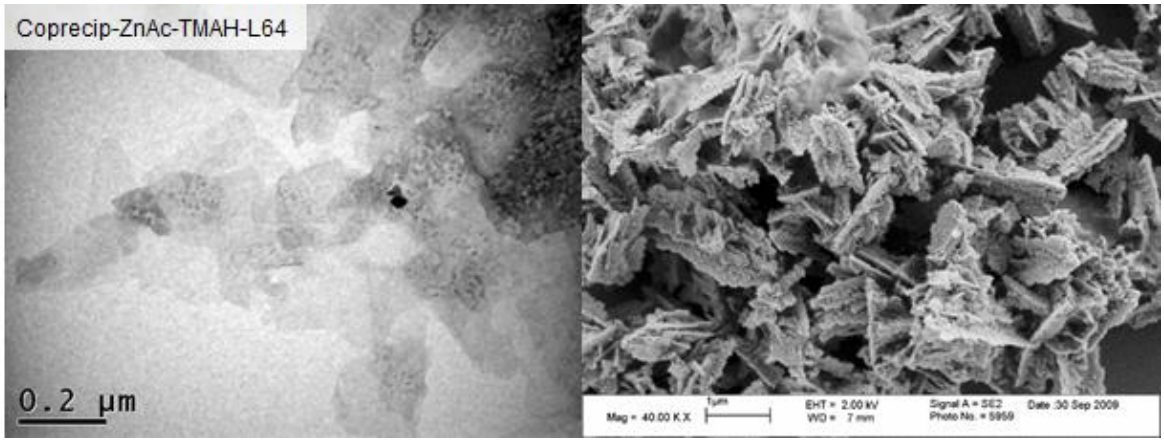

Figure 4-17: TEM (left)/FEGSEM (right) micrographs of particles prepared by the reactions between TMAH and $Zn(CH_3COO)_2 \cdot 2H_2O$ as the salt with addition of different non-ionic surfactant L64

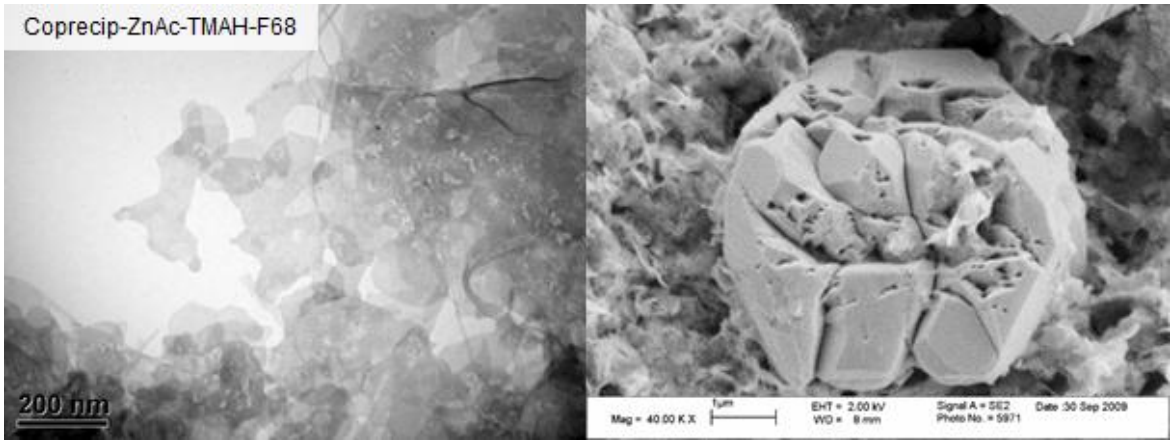

Figure 4-18: TEM (left)/FEGSEM (right) micrographs of particles prepared by the reactions between TMAH and $Zn(CH_3COO)_2 \cdot 2H_2O$ as the salt with addition of different non-ionic surfactant F68

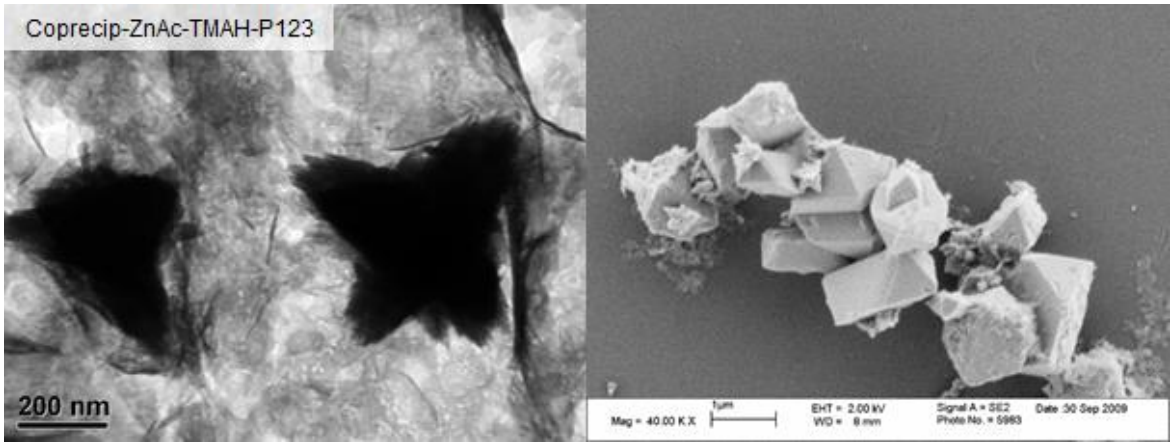

Figure 4-19: TEM (left)/FEGSEM (right) micrographs of particles prepared by the reactions between TMAH and $Zn(CH_3COO)_2 \bullet 2H_2O$ as the salt with addition of different non-ionic surfactant P123

Figure 4-20 shows the micrographs of particles prepared by the reactions between DEA and $Zn(CH_3COO)_2 \cdot 2H_2O$ with different non-ionic surfactants. All the surfactants led to a sheet structure being formed, with very little difference between them.

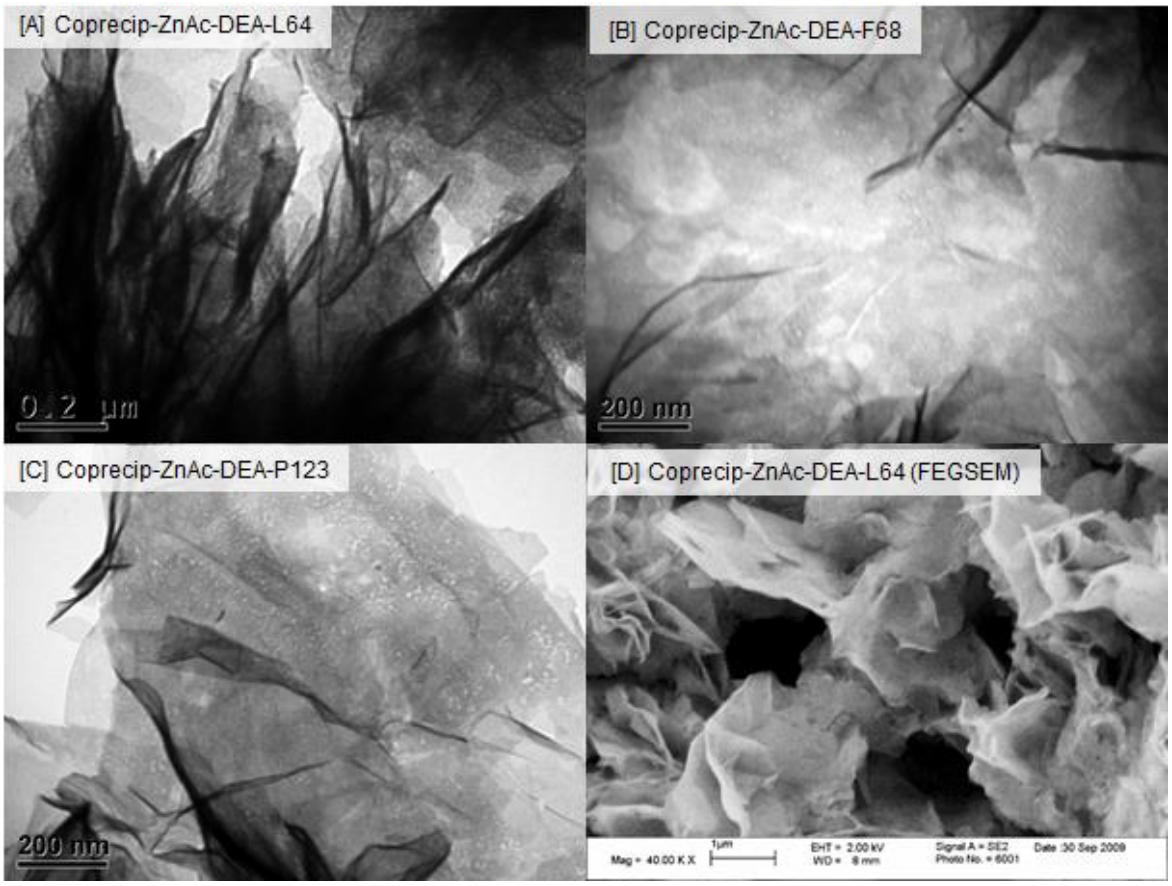

Figure 4-20: TEM micrographs of particles prepared by the reactions between DEA and $Zn(CH_3COO)_2 \cdot 2H_2O$ as the salt with addition of different non-ionic surfactants [A] L64 [B] F68 [C] P123. An FEGSEM micrograph of DEA, $Zn(CH_3COO)_2 \cdot 2H_2O$ and L64 is given bottom right [D]

FEGSEM/TEM micrographs of particles synthesised with NH_4OH, $Zn(CH_3COO)_2 \cdot 2H_2O$ and different non-ionic surfactants are shown in Figure 4-21. Sheet like morphologies were obtained.

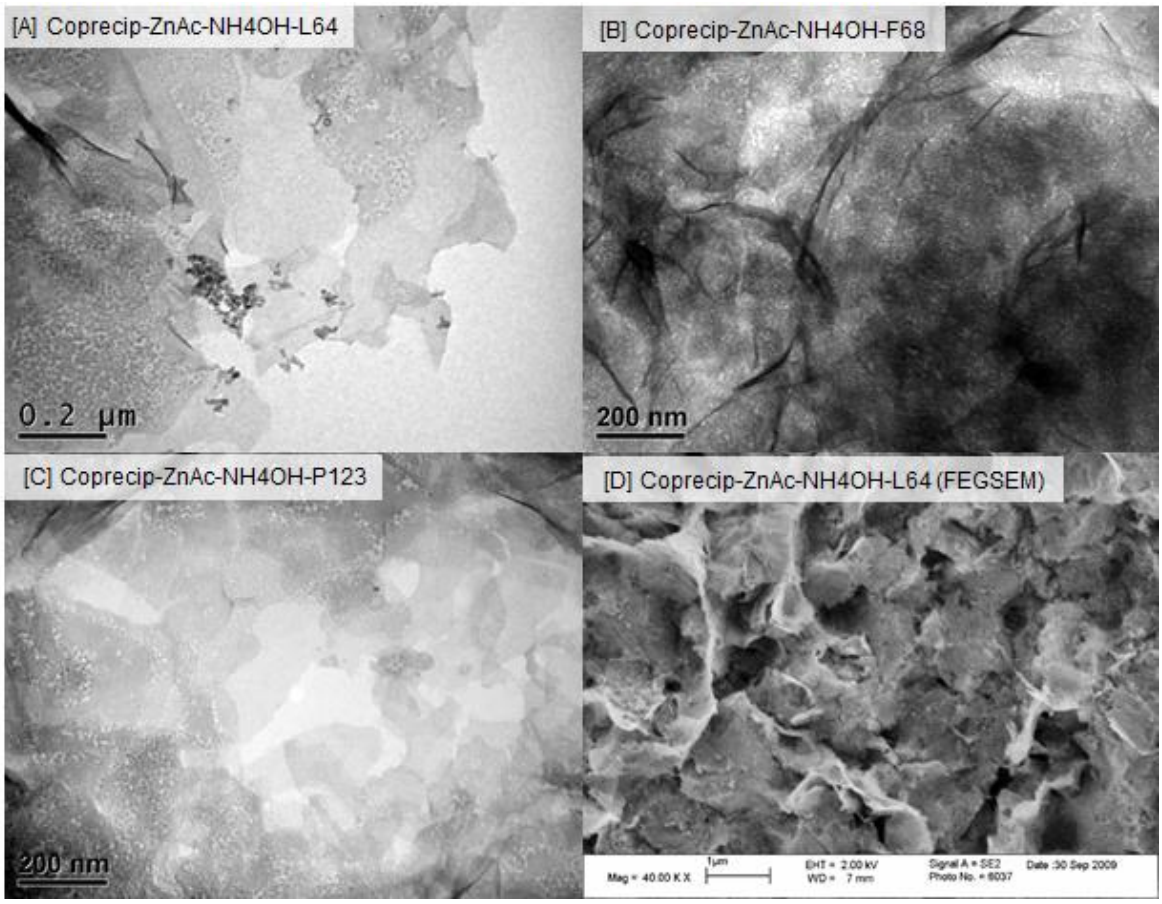

Figure 4-21: TEM (left)/FEGSEM (right) micrographs of particles prepared by the reactions between NH_4OH and $Zn(CH_3COO)_2 \bullet 2H_2O$ as the salt with addition of different non-ionic surfactants [A] L64 [B] F68 [C] P123. An FEGSEM micrograph of NH_4OH, $Zn(CH_3COO)_2 \bullet 2H_2O$ and L64 is given bottom right [D]

4.2.2 The effect of the concentration of non-ionic surfactant

The effect of concentration of the surfactant on the particle size and morphology of the compounds was also investigated.

As showed in Figure 4-22, the increase of the surfactant concentration up to 28% wt. appeared not to have a significant effect on the morphology of the particles. All the particles obtained showed star-like morphology. However, when the surfactant increased to 53% wt. an aggregated platelet morphology was obtained.

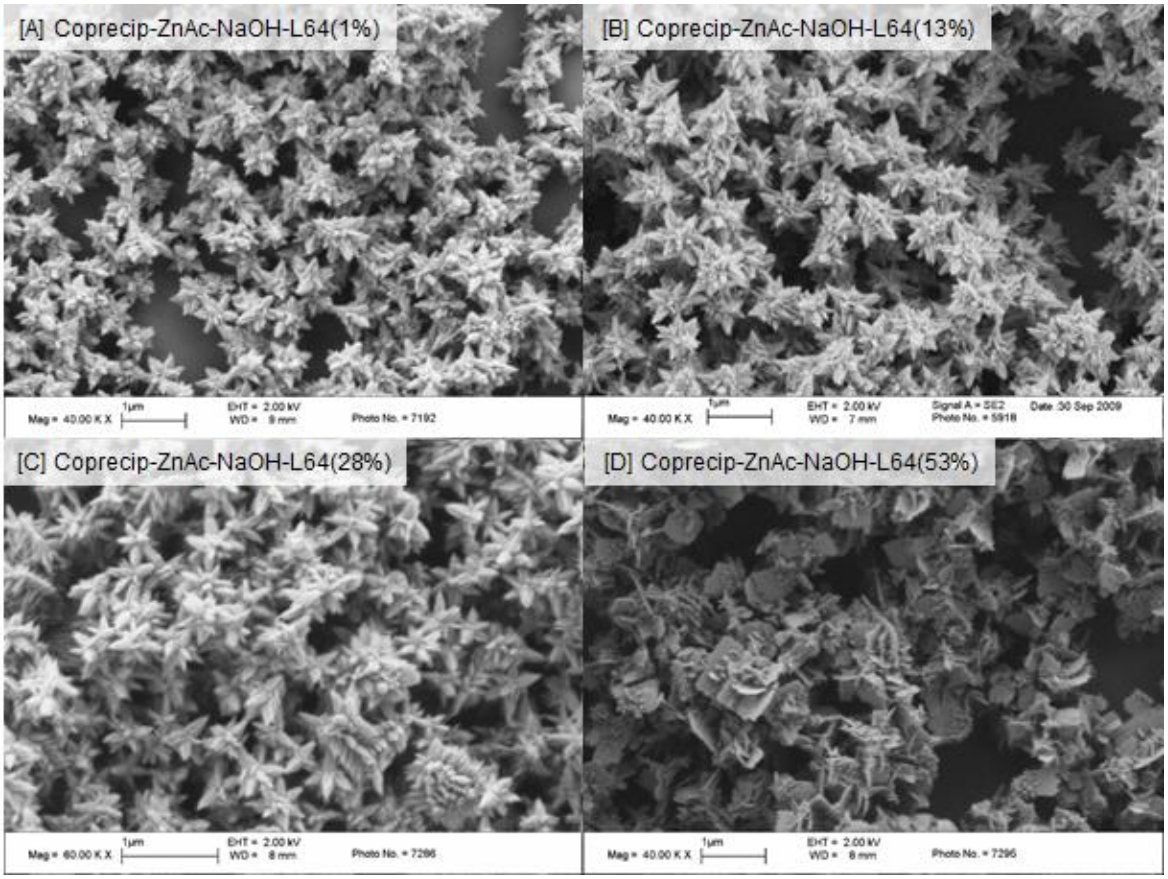

Figure 4-22: FEGSEM micrographs of ZnO particles prepared by the reaction of $Zn(CH_3COO)_2 \cdot 2H_2O$ and NaOH with L64 as the surfactant of [A] 1 wt%; [B] 13 wt% [C] 28 wt% and [D] 53 wt%.

4.2.3 The effect of different zinc salt precursors

The effect of different starting zinc salts on the morphology of particles synthesised was investigated by using $Zn(NO3)_2 \cdot 6H_2O$ and $ZnCl_2$ as the salt precursors reacted with NaOH as the base with addition of non-ionic surfactants L64, F68 and P123.

Figure 4-23 shows the FEGSEM images of the particles synthesised by the reactions between $Zn(NO_3)_2 \cdot 6H_2O$ as the starting salt and NaOH as the base solution with or without addition of surfactants. With no surfactant, platelets were observed (Figure 4-23A). With L64 (Figure 4-23B) and F68 (Figure 4-23C) long thin plank-like structures were formed. When P123 was used aggregates of irregular shaped particles were obtained (Figure 4-23D).

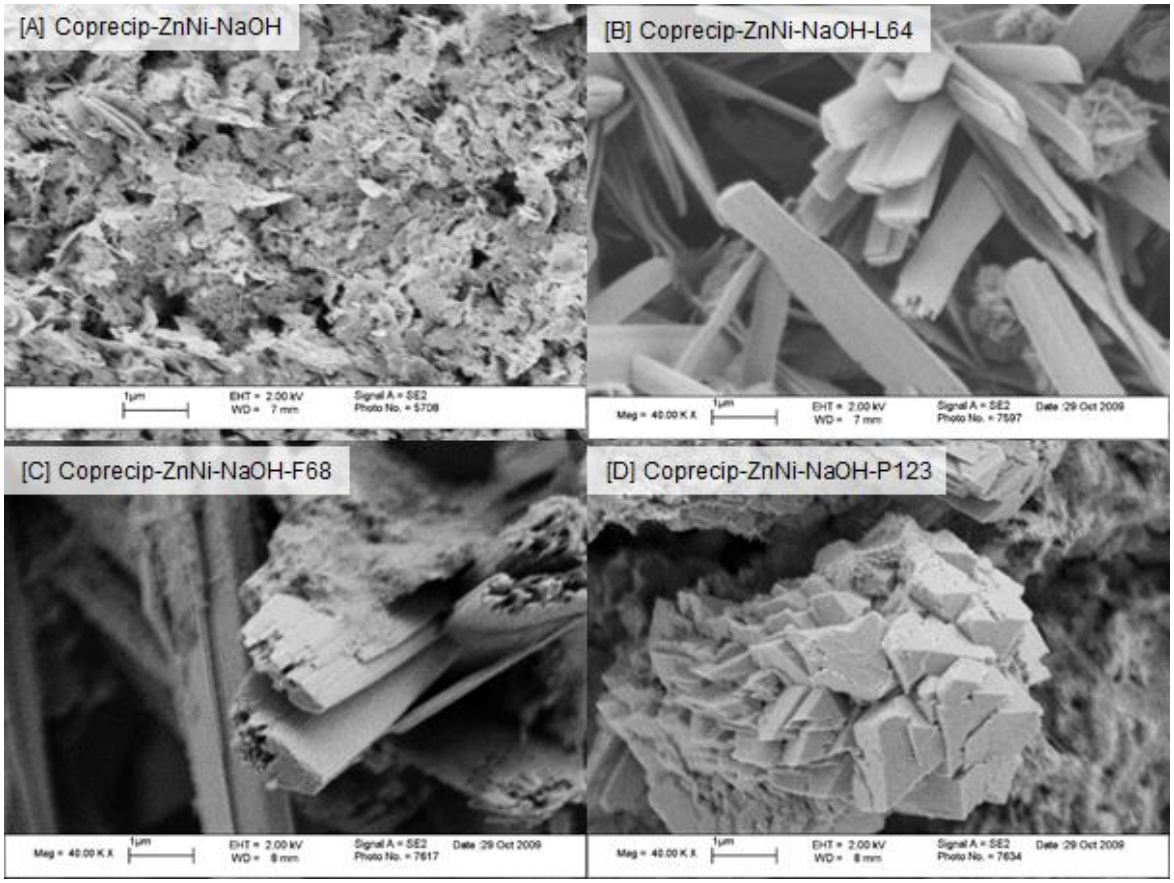

Figure 4-23: FEGSEM micrographs of ZnO compounds synthesised by the reactions between $Zn(NO_3)_2$•6H2O and NaOH with or without addition of surfactants. [A] No surfactant [B] L64 [C] F68 [D] P123.

The morphology of the particles synthesised by the reactions between $ZnCl_2$ as the starting salt and NaOH as the base solution with or without addition of surfactants is shown in Figure 4-24. It can be seen that there is very little difference in the morphology regardless of addition surfactant or not and what kind of surfactant used as well. In each case platelets of approximately 50-100nm were formed.

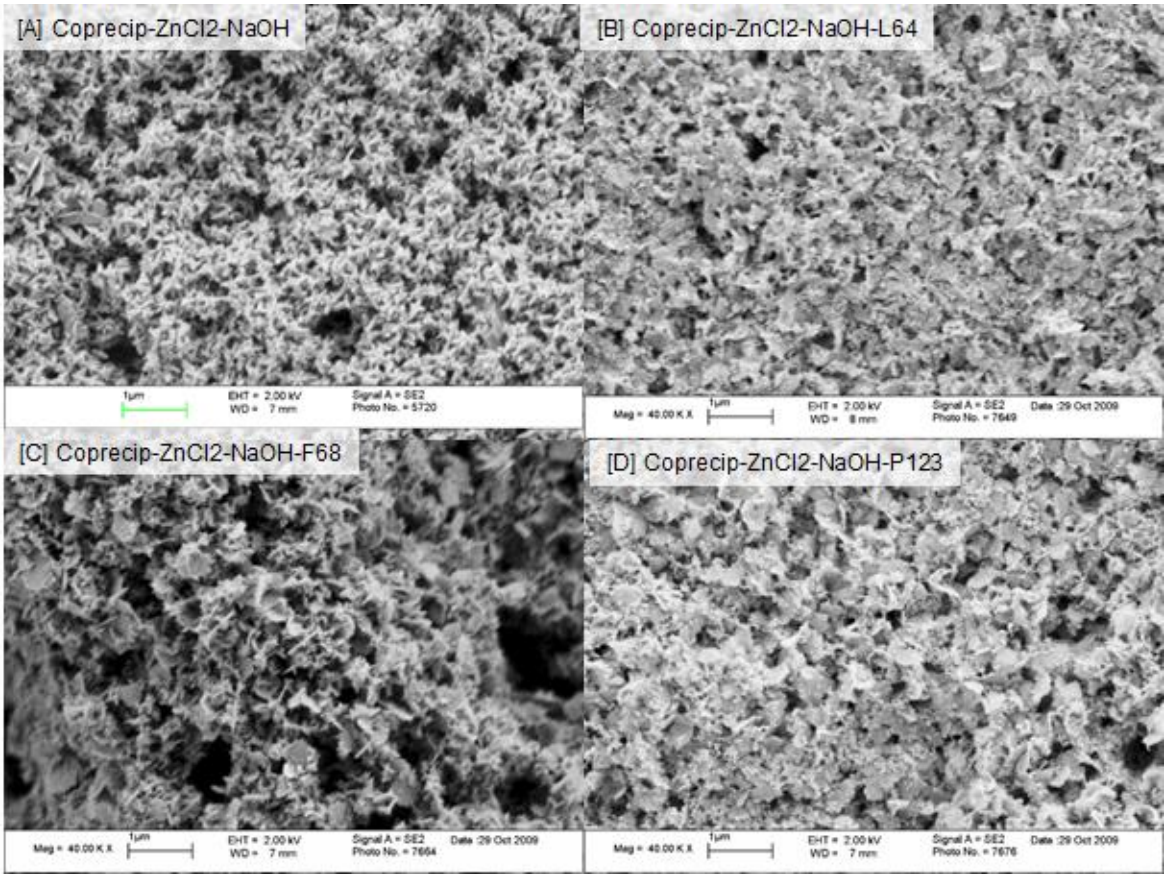

Figure 4-24: FEGSEM micrographs of the particles synthesised by the reactions between $ZnCl_2$ and NaOH with or without addition of surfactants. [A] No surfactant [B] L64 [C] F68 [D] P123.

A summary of the particle size and morphology synthesised by using different zinc salt precursors reacted with NaOH with or without addition of surfactant is given in Table 4-2. It can be seen that there were changes both in particle size and morphology with addition of surfactants compared with these without addition of surfactants.

Table 4-2: A summary of the particle size and morphology of ZnO compounds synthesised by using different zinc salt precursors reacted with NaOH with or without addition of surfactant

Zinc Salt	Surfactant	Particle Shape	Size (nm)	Compounds present
$Zn(CH_3COO)_2 \cdot 2H_2O$	N/A	Platelet	200	Zn-O
$Zn(CH_3COO)_2 \cdot 2H_2O$	L64	Flower	100	Zn-O
$Zn(CH_3COO)_2 \cdot 2H_2O$	F68	Wasps Nest	N/A	Zn-O-H
$Zn(CH_3COO)_2 \cdot 2H_2O$	P123	Agglomerate	<1000	Zn-O-H
$Zn(NO_3)_2 \cdot 6H_2O$	N/A	Platelet	200	Zn-O
$Zn(NO_3)_2 \cdot 6H_2O$	L64	Tape-like	<1000	Zn-O-H
$Zn(NO_3)_2 \cdot 6H_2O$	F68	Tape-like	<1000	Zn-O-H
$Zn(NO_3)_2 \cdot 6H_2O$	P123	Agglomerated	500-1000	Zn-O-H
$ZnCl_2$	N/A	Aggregated rods	200-300	Zn-O, Zn-O-H
$ZnCl_2$	L64	Platelet	100	Zn-O-H
$ZnCl_2$	F68	Platelet	100	Zn-O-H
$ZnCl_2$	P123	Platelet	100	Zn-O-H

4.2.4 The effect of ionic surfactant

Ionic surfactants were also used as the additive to investigate their effects on the particle size and morphology of the ZnO compounds.

Figure 4-25, Figure 4-26, Figure 4-27 and Figure 4-28 show the particles synthesised by the reactions between $Zn(CH_3COO)_2 \cdot 2H_2O$ and NaOH, TMAH, DEA and NH_4OH, respectively, with the addition of ionic surfactant CTAB or SDS. Aggregated blocks were synthesised (Figure 4-25A) when NaOH was used as an base solution and SDS as the

surfactant and a tape like structure was produced with CTAB (Figure 4-25B). With TMAH used as the base, aggregated platelets with a fern like structure was observed using SDS as the surfactant (Figure 4-26A) and flower-like structure was formed with addition of CTAB (Figure 4-27B).

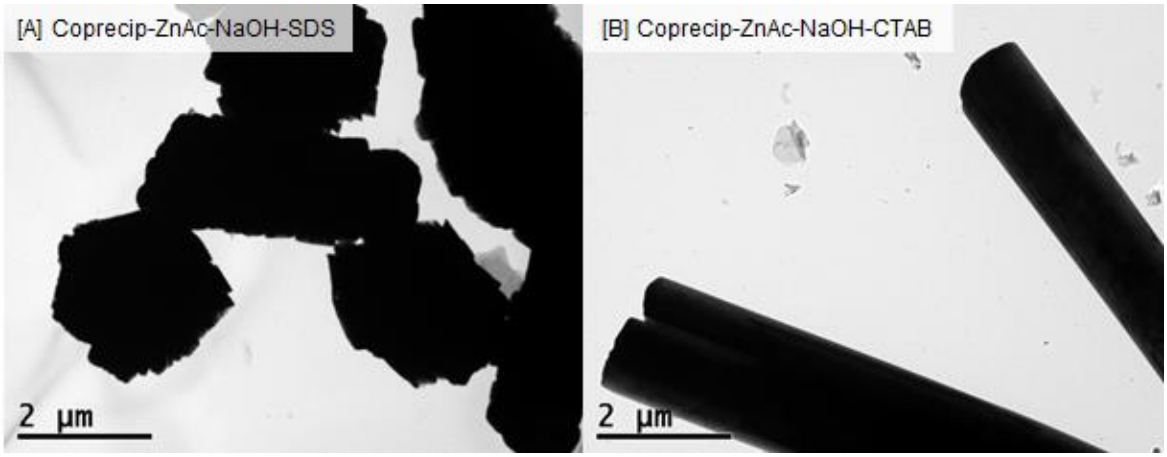

Figure 4-25: TEM micrographs of the particles synthesised by the reactions between $Zn(CH_3COO)_2 \cdot 2H_2O$ and NaOH with addition of surfactants. [A] SDS [B] CTAB

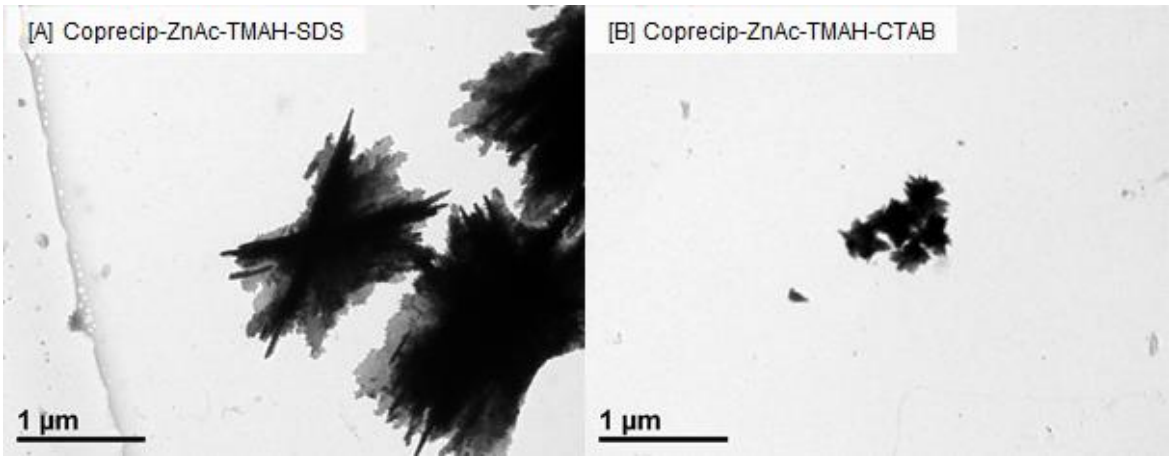

Figure 4-26: TEM micrographs of the particles synthesised by the reactions between $Zn(CH_3COO)_2 \cdot 2H_2O$ and TMAH with addition of surfactants. [A] SDS [B] CTAB

Figure 4-27 and Figure 4-28 show the morphologies of the particles prepared by the reactions of $Zn(CH_3COO)_2 \cdot 2H_2O$ with DEA or NH_4OH, respectively, with SDS or CTAB as the surfactant. In the majority of the cases a sheet like morphology was formed. However when NH_4OH was used with SDS a platelet like structure is evident.

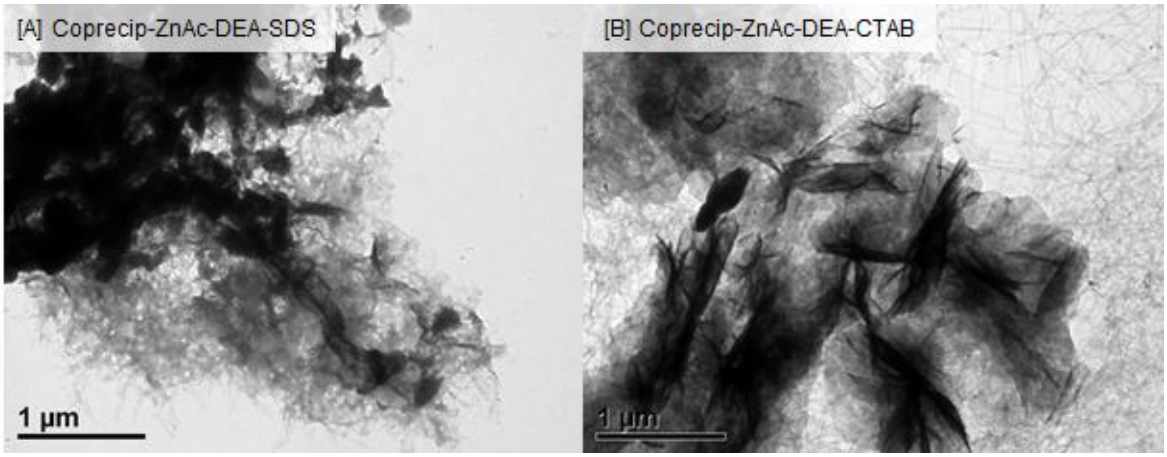

Figure 4-27: TEM micrographs of the particles synthesised by the reactions between $Zn(CH_3COO)_2 \cdot 2H_2O$ and DEA with addition of surfactants. [A] SDS [B] CTAB

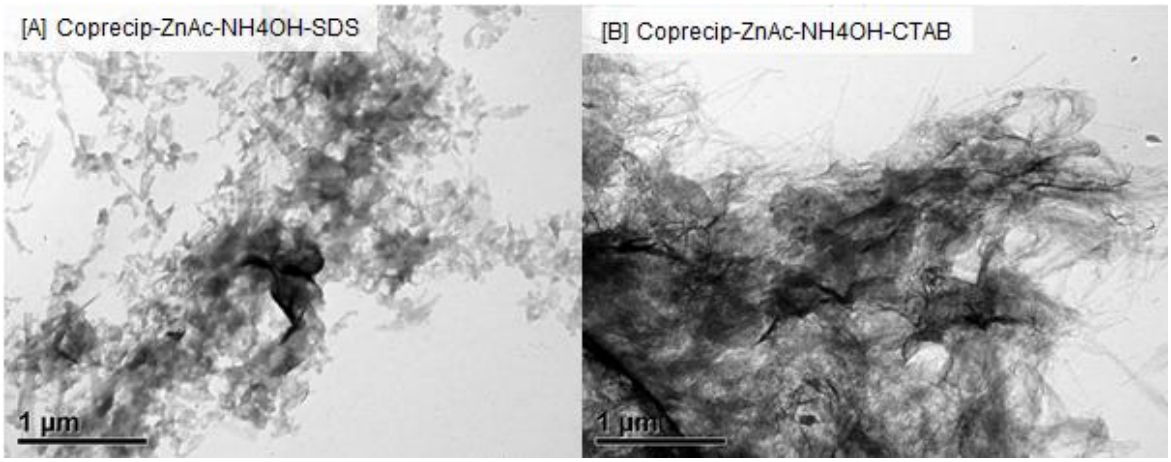

Figure 4-28: TEM micrographs of the particles synthesised by the reactions between $Zn(CH_3COO)_2 \cdot 2H_2O$ and NH_4OH with addition of surfactants. [A] SDS [B] CTAB

It can be seen clearly that various crystal phases, particle sizes and morphologies were obtained when different zinc salt precursors reacted with different base solutions (at different pH values) with or without addition of the surfactant. Therefore, an orthogonal array approach was employed in the experiment to identify factors which have significant influence on the formation of the particles with controlled particle size and morphology.

4.2.5 Co-precipitation experiments using orthogonal design

The effects of starting salt precursors, base solution and the surfactants on the particle size and morphology were investigated using orthogonal array approach. The following commonly available precursors were used:

- Three ZnO salt precursors - $Zn(NO_3)_2$, $ZnSO_4$ and $Zn(CH_3COO)_2 \cdot 2H_2O$
- Three bases solutions - NaOH, NH_4OH solution and DEA
- Three surfactants – CTAB, Sodium bis(2-ethylhexyl) sulfosuccinate (AOT) and Poly (ethylene glycol) (PEG)

The details of the starting salts, base solutions and surfactants with their three corresponding levels with the details of the L9 (3^3) orthogonal array are listed in Table 3-12 and Table 3-13, respectively.

All the reactions were carried out at pH = 10±0.2 at ambient temperature (~22°C) with concentration of the starting salt precursor and surfactant of 0.2M and 3.2mmol, respectively. The micrographs of the particles of these nine samples synthesised are shown in Figure 4-29 to Figure 4-37. A summary of results of the first orthogonal experiments is given in Table 4-3.

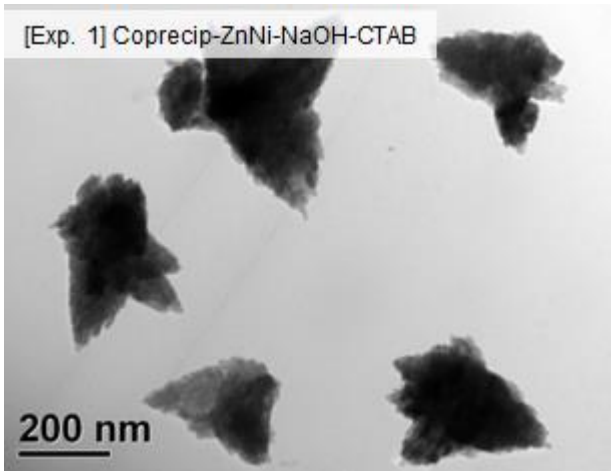

Figure 4-29: TEM micrograph of the particles prepared by the reactions between NaOH and $Zn(NO_3)_2$ in the presence of CTAB (Experiment 1)

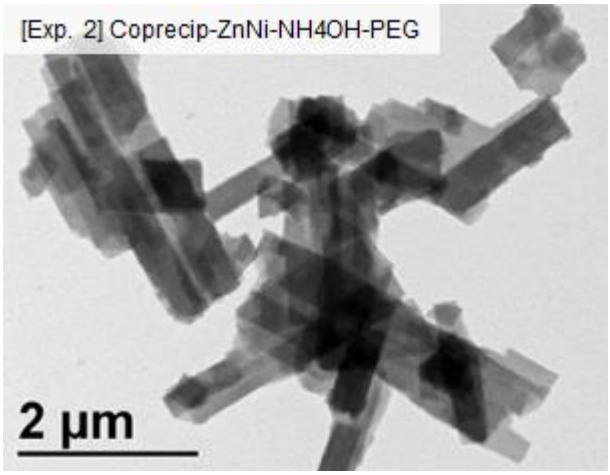

Figure 4-30: TEM micrograph of the particles prepared by the reactions between NH_4OH and $Zn(NO_3)_2$ in the presence of PEG (Experiment 2)

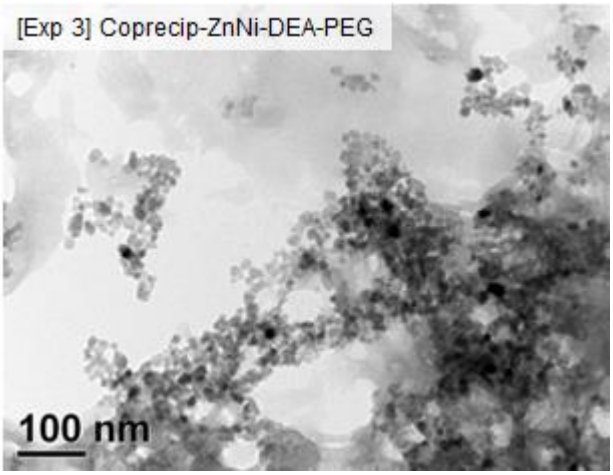

Figure 4-31: TEM micrograph of the particles prepared by the reactions between DEA and $Zn(NO_3)_2$ in the presence of PEG (Experiment 3)

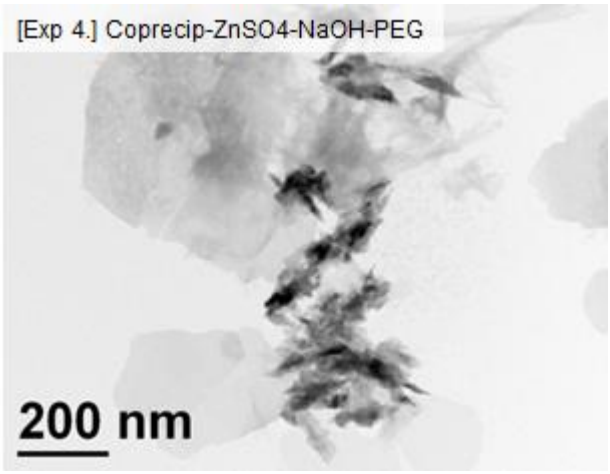

Figure 4-32: TEM micrograph of the particles prepared by the reactions between NaOH and $ZnSO_4$ in the presence of PEG (Experiment 4)

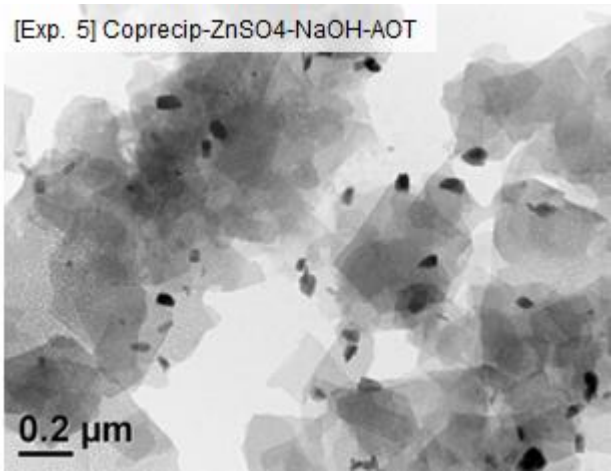

Figure 4-33: TEM micrograph of the particles prepared by the reactions between NaOH and $ZnSO_4$ in the presence of AOT (Experiment 5)

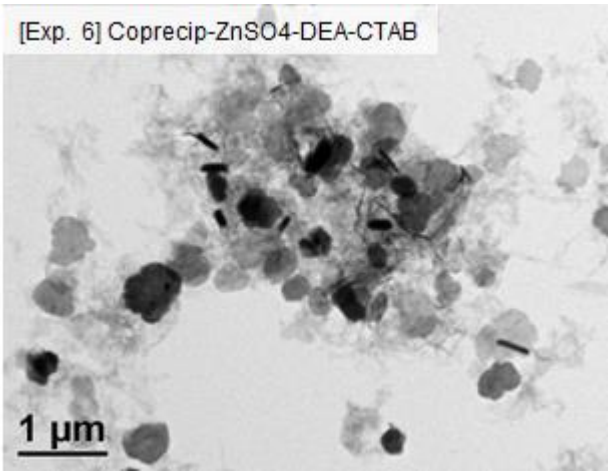

Figure 4-34: TEM micrograph of the particles prepared by the reactions between DEA and $ZnSO_4$ in the presence of CTAB (Experiment 6)

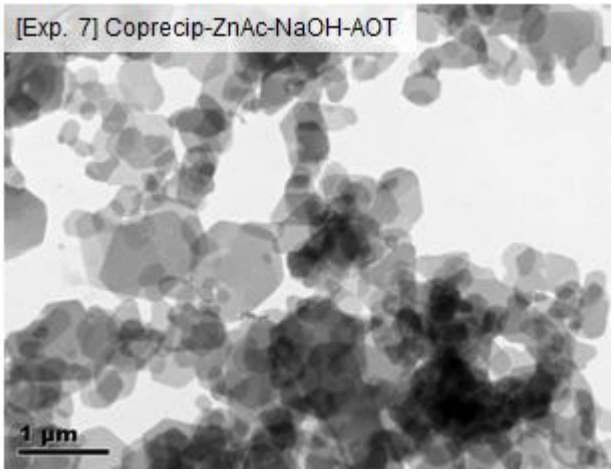

Figure 4-35: TEM micrograph of the particles prepared by the reactions between NaOH and $Zn(CH_3COO)_2 \cdot 2H_2O$ in the presence of AOT (Experiment 7)

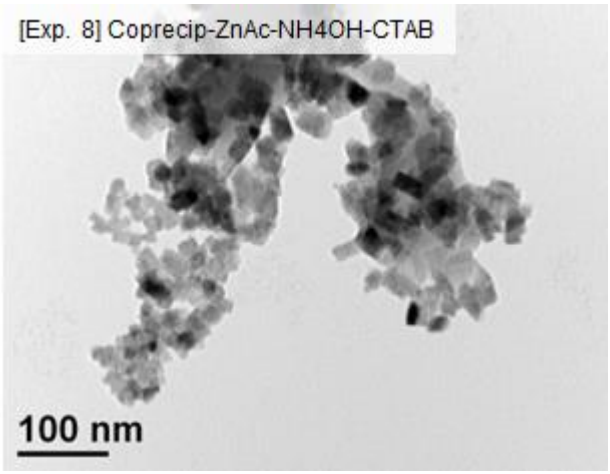

Figure 4-36: TEM micrograph of the particles prepared by the reactions between NH_4OH and $Zn(CH_3COO)_2 \cdot 2H_2O$ in the presence of CTAB (Experiment 8)

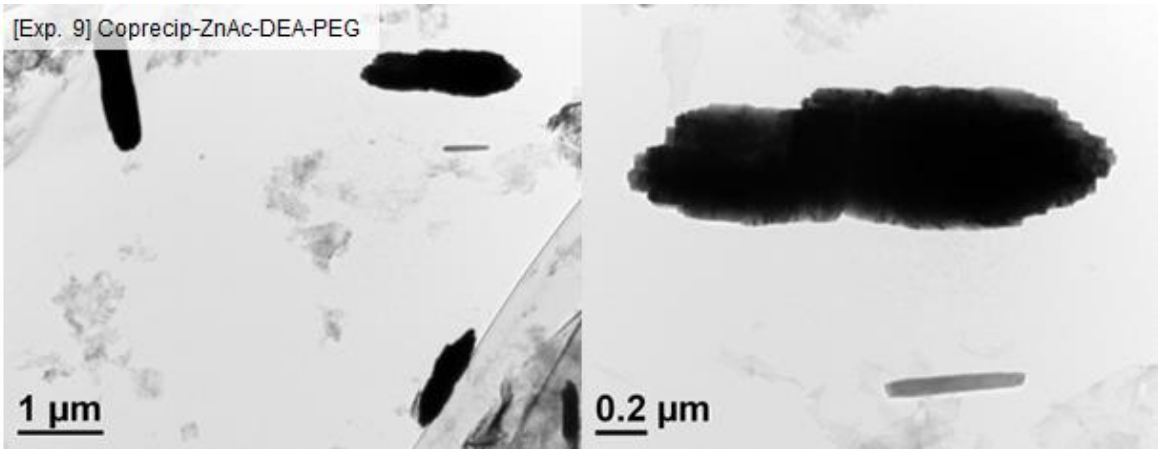

Figure 4-37: TEM micrograph of the particles prepared by the reactions between DEA and $Zn(CH_3COO)_2 \cdot 2H_2O$ in the presence of PEG (Experiment 9)

Table 4-3: Summary of results of the first orthogonal experiments.

Figure	Morphology	Average length (nm)	Average width (nm)	Aspect ratio
Figure 4-29	Spindle/rod-like	400	220	1.8
Figure 4-30	rectangle-like	1670	330	5.1
Figure 4-31	spherical-like	15	12	1.3
Figure 4-32	Small needle/rod-like	115	26	4.4
Figure 4-33	Small rod-like	84	36	2.3
Figure 4-34	spherical-like	500	452	1.1
Figure 4-35	spherical-like	720	600	1.2
Figure 4-36	Spherical /small rod-like	33	16	2.1
Figure 4-37	Spindle/rod-like	1425	357	4.0

The aspect ratio (average length/average width) is used as the criteria to analyse the results of the first orthogonal experiment, which is shown in Table 4-4. The aspect ratio was used as a criteria due its importance with respect to the effectiveness of the nanoparticle property; a greater aspect ratio is related to an increase in the effectiveness of the nanoparticle property being used. The detailed calculation processes of K, *k* and δ in Table 5-8 are given in Appendix A.

Table 4-4: The aspect ratios of the particles and analysis of Orthogonal Array 1.

	1-A Starting salts	1-B Bases	1-C Surfactant	Results
				Aspect Ratio (L/D)
Figure 4-29	$Zn(NO_3)_2 \cdot 6H_2O$	NaOH	CTAB	1.8
Figure 4-30	$Zn(NO_3)_2 \cdot 6H_2O$	NH_4OH	PEG	5.1
Figure 4-31	$Zn(NO_3)_2 \cdot 6H_2O$	DEA	AOT	1.3
Figure 4-32	$ZnSO_4 \cdot 6H_2O$	NaOH	PEG	4.4
Figure 4-33	$ZnSO_4 \cdot 6H_2O$	NH_4OH	AOT	2.3
Figure 4-34	$ZnSO_4 \cdot 6H_2O$	DEA	CTAB	1.1
Figure 4-35	$Zn(Ac)_2 \cdot 2H_2O$	NaOH	AOT	1.2
Figure 4-36	$Zn(Ac)_2 \cdot 2H_2O$	NH_4OH	CTAB	2.1
Figure 4-37	$Zn(Ac)_2 \cdot 2H_2O$	DEA	PEG	4.0
K_1	8.2	7.4	5.0	
K_2	7.8	9.5	13.5	
K_3	7.3	6.3	4.8	
k_1	2.7	2.5	1.7	
k_2	2.6	3.2	4.5	
k_3	2.4	2.1	1.6	
Δ	0.3	1.1	2.9	
Optimum	A1	B2	C2	
Rank of δ	C > B > A			

The rank and value of δ indicates the effect of the change of the parameters on the aspect ratio of the particles synthesised. As shown in Table 4-4, the rank is C > B> A based on the relative values of δ_{kA}, δ_{kB} and δ_{kC}, i.e the change of the surfactant (factor C) has the most significant effect on the aspect ratio of the particles and different salt precursors (factor A) seem to have little effect on the change of the aspect ratio of the particles.

The highest K of 13.5 was observed for K_{c2}, i.e. the effect of second level of factor C, which is surfactant PEG, implying that the surfactant PEG has the most influence on the formation of the particles with high aspect ratio.

Ammonia solution (K = 9.5) and three precursors (K = 8.2, 7.8 and 7.3, respectively) also have a significant effect on the aspect ratio of the synthesised synthesised. The optimum parameters for the formation of particles with highest aspect ratio are A_1 [$Zn(NO_3)_2 \cdot 2H_2O$], B_2 (NH_4OH) and C_2 (PEG) according to the relative values of K_1, K_2 and K_3. Also, the particles with smaller aspect ratio could be obtained when $Zn(Ac)_2 \cdot 2H_2O$ reacted with DEA using AOT as the surfactant (A_3, B_3 and C_3).

The morphologies of particles synthesised by using two “selected” combinations of the synthetic parameters (A_1, B_2, C_2 and A_3, B_3, C_3) are shown in Figure 4-38. It can been seen clearly that the particles with high aspect ratio (needle-like morphology) and low aspect ratio (spherical-like morphology) were synthesised by using selected combination of the different reaction parameters. The details of the morphology and aspect ratio of these two particles are shown in Table 4-5.

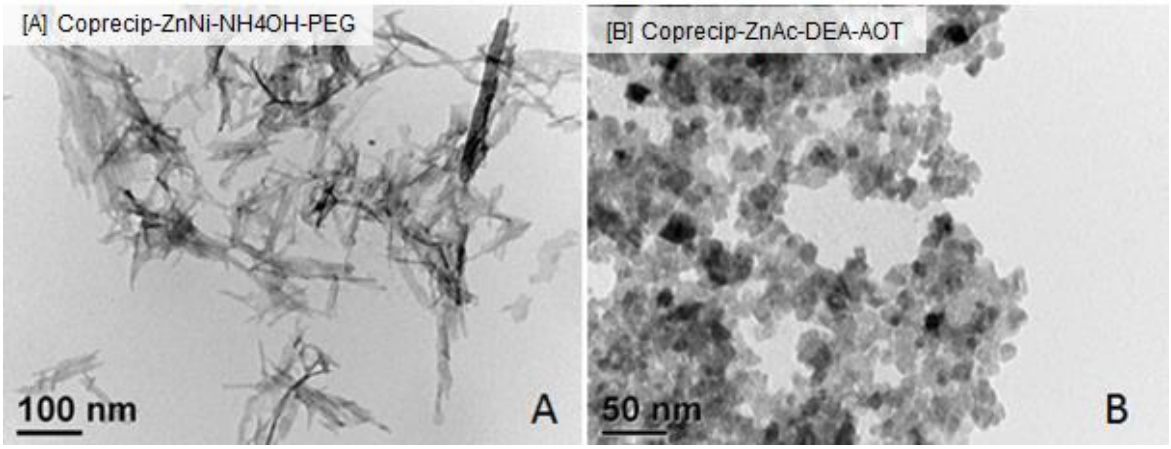

Figure 4-38: TEM images of ZnO particles synthesised by (a) $Zn(NO_3)_2 \cdot 2H_2O$ + (NH_4OH) with PEG as the surfactant; (b) $Zn(Ac)_2 \cdot 2H_2O$ + DEA with AOT as the surfactant

Table 4-5: Summary of results of the selected experiments

Sample number	Morphology	Average length (nm)	Average width (nm)	Aspect ratio
$Zn(NO_3)_2 \cdot 2H_2O$ + (NH_4OH) with PEG (Figure 4-38A)	Needle-like	142	12	11.8
$Zn(Ac)_2 \cdot 2H_2O$ + DEA with AOT (Figure 4-38B)	Spherical-like	20	18	1.1

The crystal phases of the synthesised compounds were characterised by XRD. All the characteristic peaks detected by XRD for compounds synthesised via co-precipitation showed the same positions with approximately the same intensities and indicated a mixture of Zn-O and Zn-O-H compounds.

The XRD pattern of synthesised compounds via co-precipitation between $Zn(Ac)_2 \cdot 2H_2O$ and DEA with AOT is showed in Figure 4-39. The XRD pattern indicated that the ZnO particles obtained had a mixture of the compounds of Zn-O-H and Zn-O. The green circles (●), the horizontal green double triangle peaks (⋈) and the transverse green double triangle peaks (⧗) stand for the standard peaks of $Zn(OH)_2$. The PDF number of the

standard peaks of $Zn(OH)_2$ are JCP 01-0360, JCP 89-0138 and 48-1066 separately. The red squares (■) and the red single triangle peaks in the pattern stand for the standard peaks of ZnO (PDF number: JCP 01-1136 and JCP 03-0888 separately) and the columns stand for the intensity for each peak. The highest intensity of the detected peaks is less than 3000, indicating a low crystallinity of the particles.

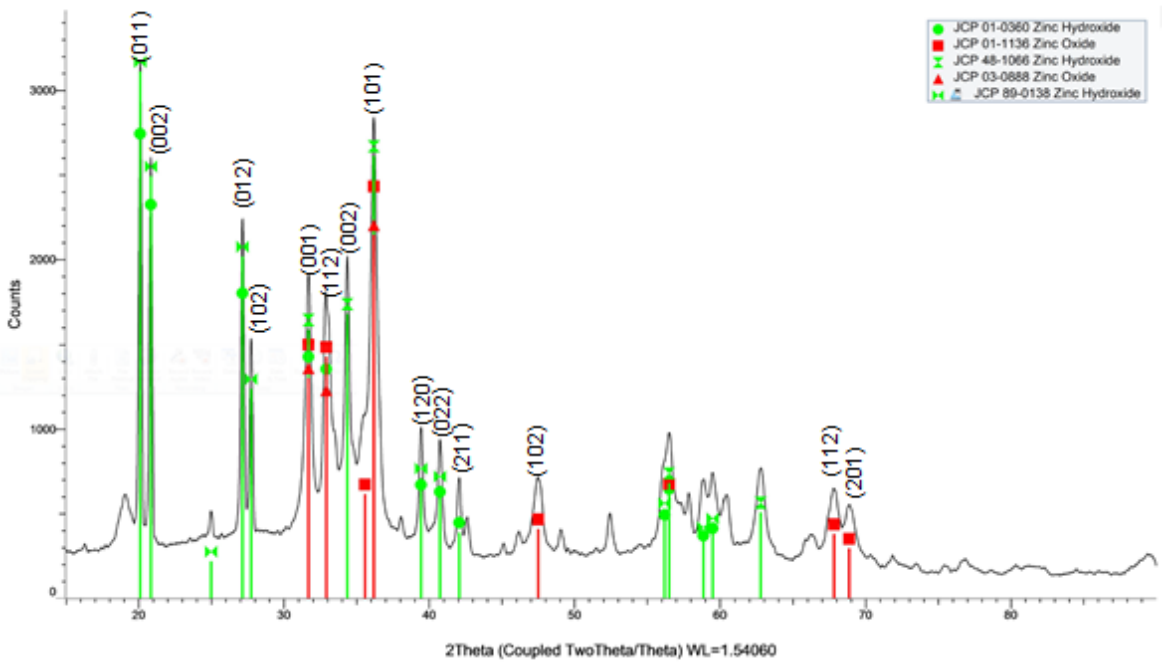

Figure 4-39: XRD pattern of synthesised ZnO compounds ($Zn(Ac)_2 \cdot 2H_2O$, DEA with AOT) via co-precipitation process.

From the matched PDF standard cards of $Zn(OH)_2$ and ZnO, it can be confirmed that orthorhombic and hexagonal $Zn(OH)_2$ was obtained. More specifically, metastable zinc blende (which is a cubic closest-packed structure) and stable wurtzite which is a hexagonal closest-packed structure ZnO were reported from the XRD results.

These mixed phases had also been observed by Li et al [102] as the concentration of Zn^{2+} and OH^- had not fully reached the super saturation degree of forming ZnO. The synthesis temperature and pressure were not high enough to meet that the transformation requirements [102].

The particles synthesised are a mixture of ZnO (red dots in the XRD pattern) and $Zn(OH)_2$ (green dots in the XRD pattern). The highest peak intensity for both compounds at 2θ = 21.1 for $Zn(OH)_2$ and 36.2 for ZnO, respectively are used for the calculation of the particle size using the Scherrer formula. The calculated particle sizes for $Zn(OH)_2$ and ZnO are 28 nm and 11 nm, respectively (Table 4-6), which are similar to the size of the particles measured using TEM images.

Table 4-6: Calculated particle sizes of $Zn(OH)_2$ and ZnO

Compounds	**Morphology**	**Calculated crystal size (nm) (XRD)**
$Zn(OH)_2$	spherical-like	28
ZnO	spherical-like	11

In comparison, the particles measured from the TEM micrographs (20 nm) sits in-between that calculated from the XRD results (Table 4-6). In general, the correlation between particles sizes obtained by XRD and TEM is that the calculated XRD size is usually equal or smaller than that obtained by TEM [103]. Though this is the case for the comparison between the ZnO particle size (-9 nm), the $Zn(OH)_2$ measurement is higher (+8 nm). This may be due to statistical deviation in the number of particles measured or due to inaccuracies in measurement due to the poor definition of the particles within the TEM micrograph. Larger particles may have been present in areas in which single particles were not measurable, as shown in Figure 4-40.

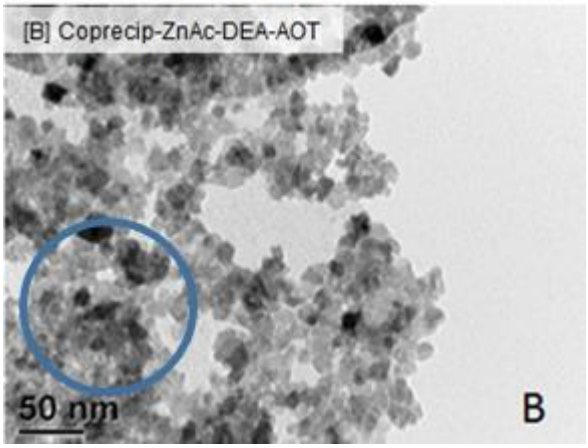

Figure 4-40: Example of an area where large particles could have been present but would have been unmeasurable.

4.3 Summary

The use of co-precipitation method resulted in various compounds and particle morphologies being formed. Without the addition of surfactant, XRD diffractograms for particles synthesis between XRD diffactograms for particles synthesized by reaction between different zinc salt precursors and different base solutions indicated the presence of Zn-O, Zn-O-H compounds and unknown phases. A combination of Zn-O and Zn-O-H compounds were formed with strong bases (pH = 12.0±0.2, NaOH and TMAH) and Zn-O-H and unknown compounds were identified when weak bases (pH = 10.0±0.2, DEA and NH_4OH were used). Different morphologies, including platelets, aggregated bundles of rods and spherical particles were formed.

The addition of surfactant had an effect. In the case of the reactions using NaOH and TMAH, XRD results indicated that with the addition of non-ionic surfactants F68 and P123 Zn-O-H compounds were formed, whereas Zn-O was identified in the resultant precipitates without surfactants. The addition of L64 led to a change in particle shape from platelets to star-like (NaOH) and aggregated platelets (TMAH). The co-precipitation reactions investigating the change in surfactant concentration showed little effect in particle morphology until the concentration increased to 53% wt. The use of ionic surfactants (CTAB and SDS) led to the formation of various different morphologies including platelet, fern-like and flower-like structures.

An orthogonal design was used to investigate the effect of starting precursors and surfactants on the aspect ratio of the formed particles with the change of the surfactant (factor C) having the most significant effect on the aspect ratio of the particles. The morphologies of particles synthesised by using two “selected” combinations of the synthetic parameters showed an increase in aspect ratio. XRD indicated the formation of ZnO and $Zn(OH)_2$ with crystallite sizes calculated using the Scherrer formula as 11 nm and 28 nm, respectively.

Chapter 5 Preparation of ZnO and AZO nanoparticles by the Hydrothermal method

5.1 ZnO nanoparticles synthesised without addition of surfactants

Co-precipitated ZnO particles were synthesised and hydrothermally treated at 140ºC for 6h. Different starting zinc salts including $Zn(CH_3COO)_2•2H_2O$, $Zn(NO_3)_2•6H_2O$ or $ZnCl_2$ with different base solutions of NaOH, TMAH, DEA and NH_4OH were used respectively.

X-ray diffractogram for the particles prepared by the reactions between different zinc salt precursors ($Zn(CH_3COO)_2•2H_2O$, $Zn(NO_3)_2•6H_2O$ or $ZnCl_2$) and NaOH solution, with a hydrothermal heat treatment at 140ºC for 6h is shown in Figure 5-1 (a), (b) and (c) respectively. All three diffractograms showed same patterns, which were the characteristic peaks for ZnO (JCPDS 36-1451).

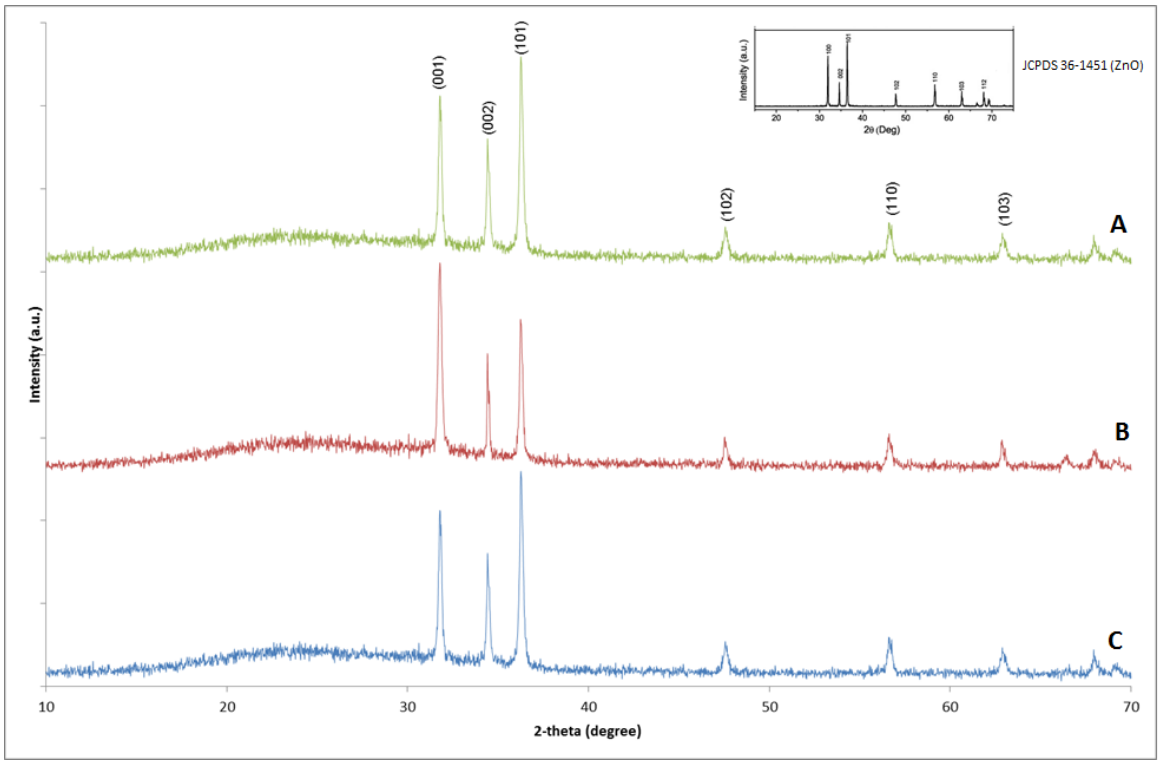

Figure 5-1: X-Ray diffractogram of the particles synthesised by different zinc salts reacted with NaOH then having a hydrothermal treatment at 140ºC for 6H [A] $Zn(CH_3COO)_2•2H_2O$ [B] $Zn(NO_3)_2•6H_2O$ [C] $ZnCl_2$

TEM and FEGSEM images of the hydrothermally treated (140°C/6h) particles prepared with various zinc salts and NaOH are shown in Figure 5-2, Figure 5-3 and Figure 5-4. Like the ZnO particles prepared by co-precipitation method, by using $Zn(CH_3COO)_2•2H_2O$ (Figure 5-2) and (Figure 5-3) as the salt precursors, round edged platelets with a width of 200nm were formed. When $ZnCl_2$ was used (Figure 5-4), round-edged platelets of 200nm in width were synthesised, but these particles also tended to be aggregated. A higher resolution micrograph of the round edged platelets is given in Figure 5-5.

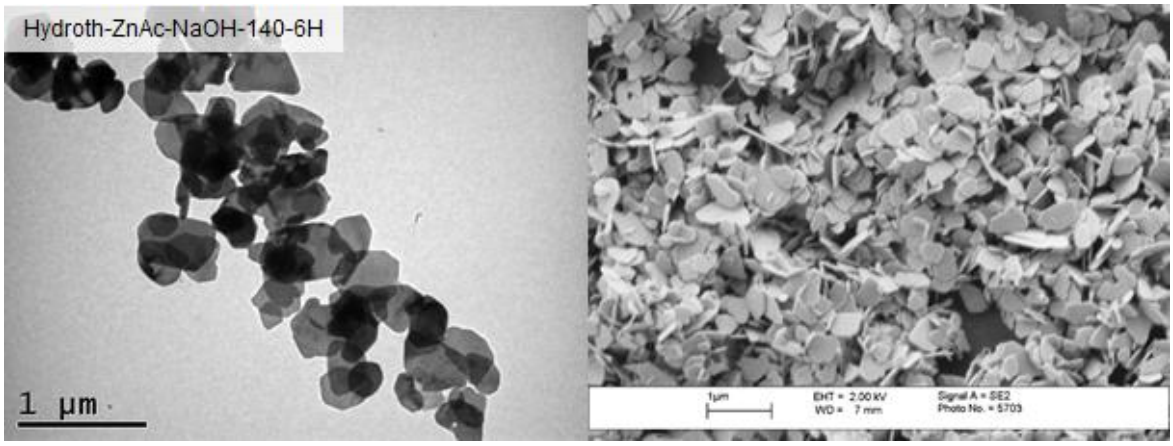

Figure 5-2: TEM (left)/FEGSEM (right) micrographs of hydrothermally treated particles prepared by NaOH reacted $Zn(CH_3COO)_2•2H_2O$

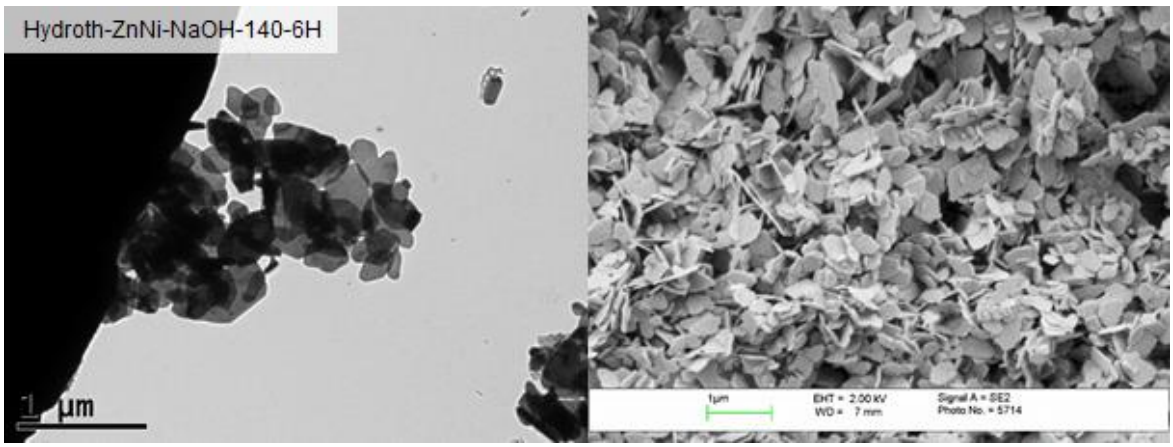

Figure 5-3: TEM (left)/FEGSEM (right) micrographs of hydrothermally treated particles prepared by NaOH reacted with $Zn(NO_3)_2•6H_2O$

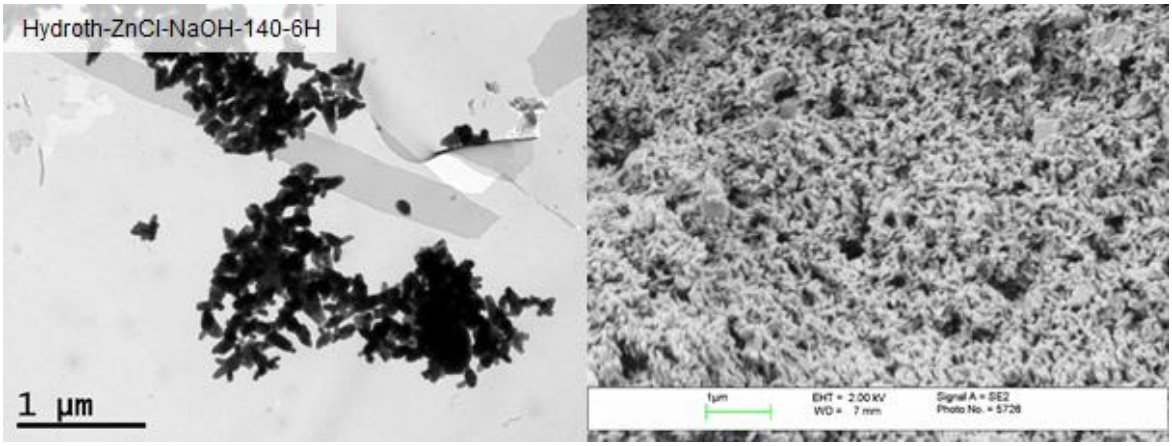

Figure 5-4: TEM (left)/FEGSEM (right) micrographs of hydrothermally treated particles prepared by NaOH reacted with ZnCl2

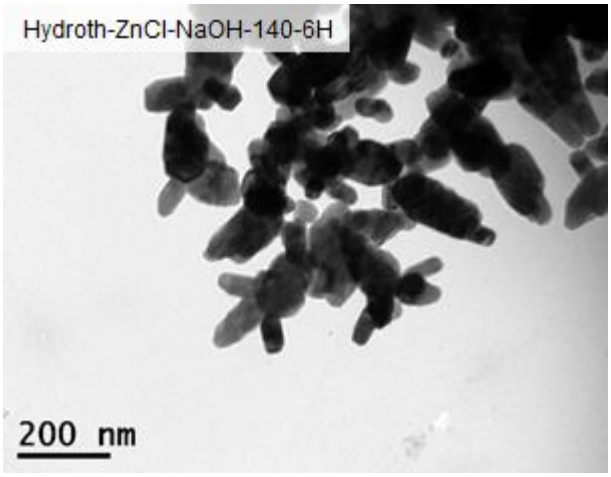

Figure 5-5: Higher resolution TEM micrographs of hydrothermally treated particles prepared by NaOH reacted with $ZnCl_2$

Figure 6-6 shows the X-ray diffractogram for the particles obtained by $Zn(CH_3COO)_2•2H_2O$ (Figure 5-6A), $Zn(NO_3)_2•6H_2O$ (Figure 5-4B) and $ZnCl_2$ (Figure 5-4C) reacted with TMAH as the base solution after hydrothermal treatment at 140°C for 6h. Similar patterns as obtained with NaOH as the base source were observed for all three X-ray diffractograms and were identified as ZnO (JCPDS 36-1451).

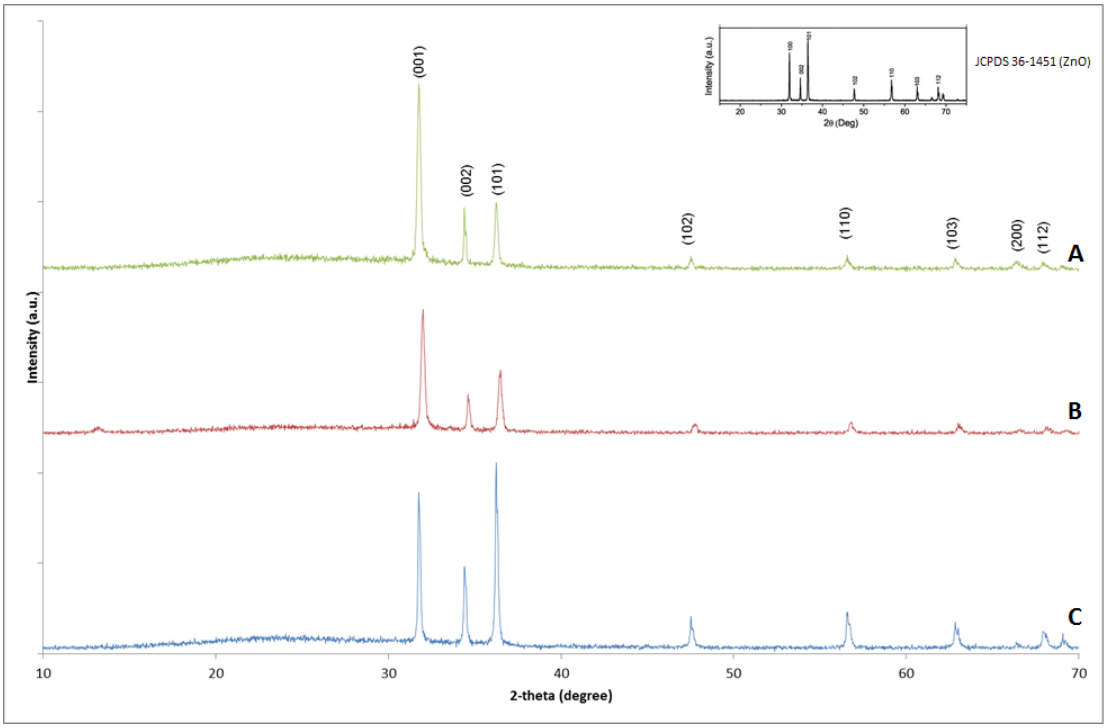

Figure 5-6: X-Ray diffractogram of the particles synthesised by different zinc salts reacted with TMAH and then hydrothermally treatment at 140°C for 6H [A] $Zn(CH_3COO)_2 \cdot 2H_2O$ [B] $Zn(NO_3)_2 \cdot 6H_2O$ [C] $ZnCl_2$

TEM and FEGSEM micrographs of hydrothermally treated samples prepared by different salts reacted with TMAH as the base solution as shown in Figure 6-4. Elongated round edged platelets about approximately 400nm in length were synthesised using $Zn(CH_3COO)_2 \cdot 2H_2O$ (Figure 5-7) and $Zn(NO_3)_2 \cdot 6H_2O$ (Figure 5-8) as the precursor, respectively. When $ZnCl_2$ was used as the salt precursor, ZnO particles with flat-ended columns were synthesised (Figure 5-9, Figure 5-10). The length of the particles was varied but in general were approximately 600nm to 1µm.

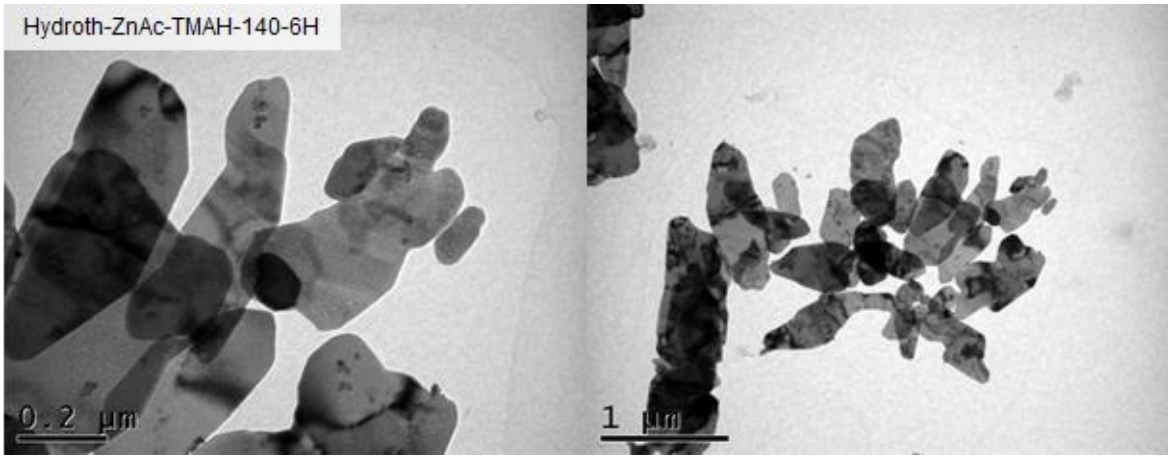

Figure 5-7: TEM micrographs of hydrothermally treated particles prepared by TMAH reacted with $Zn(CH_3COO)_2 \cdot 2H_2O$

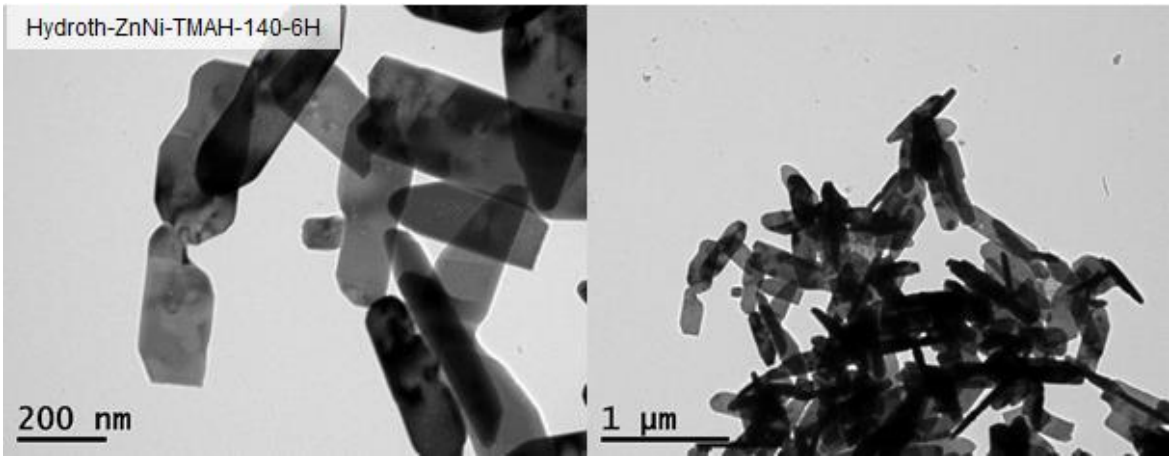

Figure 5-8: TEM micrographs of hydrothermally treated particles prepared by TMAH reacted with Zn(NO3)2•6H_2O

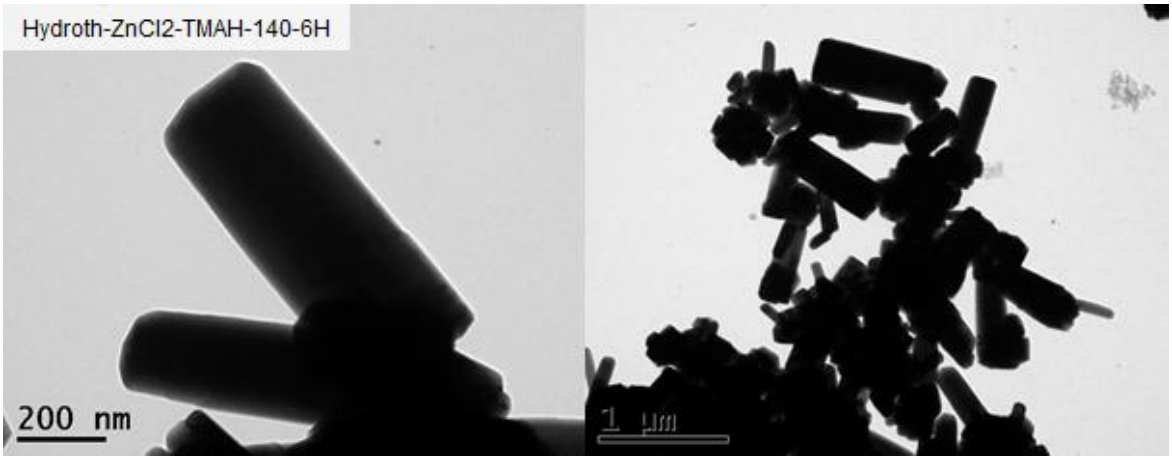

Figure 5-9: TEM micrographs of hydrothermally treated particles prepared by TMAH reacted with $ZnCl_2$

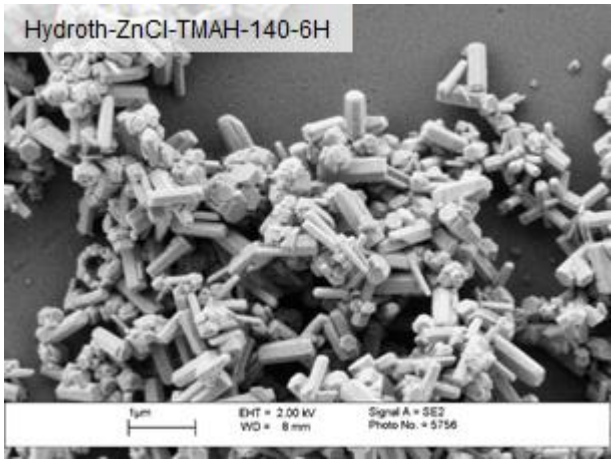

Figure 5-10: FEGSEM micrographs of hydrothermally treated particles prepared by TMAH reacted with $ZnCl_2$

The XRD results shown in Figure 5.1B ($Zn(NO_3)2•6H_2O$/NaOH) and suggest that there has been an increase in the (100) plane and a reduction in the (101) plane when compared to Figure 5.1A ($Zn(CH_3COO)_2•2H_2O$/NaOH) and Figure 5.1C ($ZnCl_2$/NaOH). This would indicate that the synthesised particles should be wider/longer. However this is not indicated in the TEM micrographs (Figure 5-1 to Figure 5-3) . The increase in length is however evident if Figure 5-1 (NaOH) and Figure 5-6 (TMAH) are compared, with the particles synthesised with TMAH being longer.

In addition, the difference between the three XRD patterns in Figure 5-1 is minimal and does not significantly represent the change in morphology seen in the TEM microscopy. This is especially true if Figure 5-1 and Figure 5-6C are compared, where the XRD patterns are similar but (aggregated) platelets (Figure 5-1) instead of columns (Figure 5-6C) were formed. It is suggested that the differences in XRD pattern could to the orientation and alignment of the particles following casting.

Particles were also hydrothermally synthesised by the reactions between different zinc salt precursors and “weak” base solutions (pH = 10.0±0.2) including DEA and NH_4OH. Figure 5-11 shows the X-ray diffractograms of the particles prepared by $Zn(CH_3COO)_2•2H_2O$ reacted with DEA before and after hydrothermal treatment at 140^{o}C for 6h and the corresponding TEM/FEGSEM micrographs of the particles hydrothermally treated are shown in Figure 5-12. Also, the FEGSEM micrographs of the particles synthesized the

reactions between DEA and other two zinc salt precursors $Zn(NO_3)_2 \cdot 6H_2O$ and $ZnCl_2$ are shown in Figure 5-13 (a) and (b), respectively.

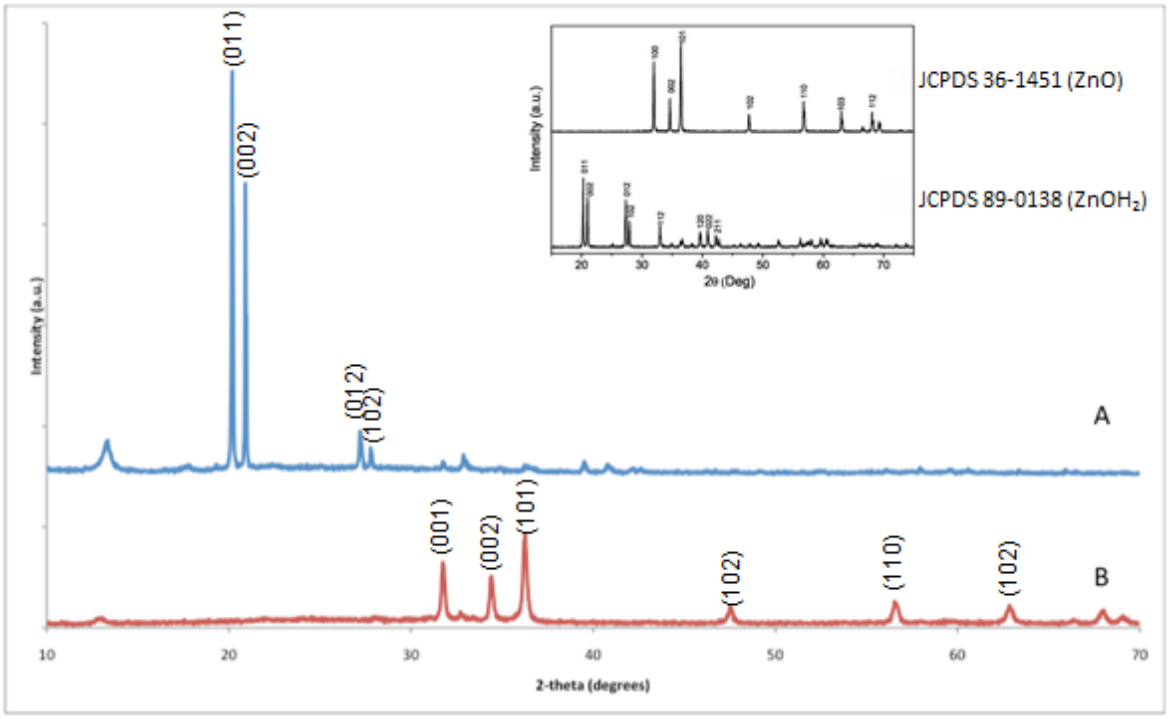

Figure 5-11: X-ray diffractograms of the particles synthesised with a co-precipitation reaction [A] and then subsequently hydrothermally treated [B]. The particles were prepared with $Zn(CH_3COO)_2 \cdot 2H_2O$ and DEA

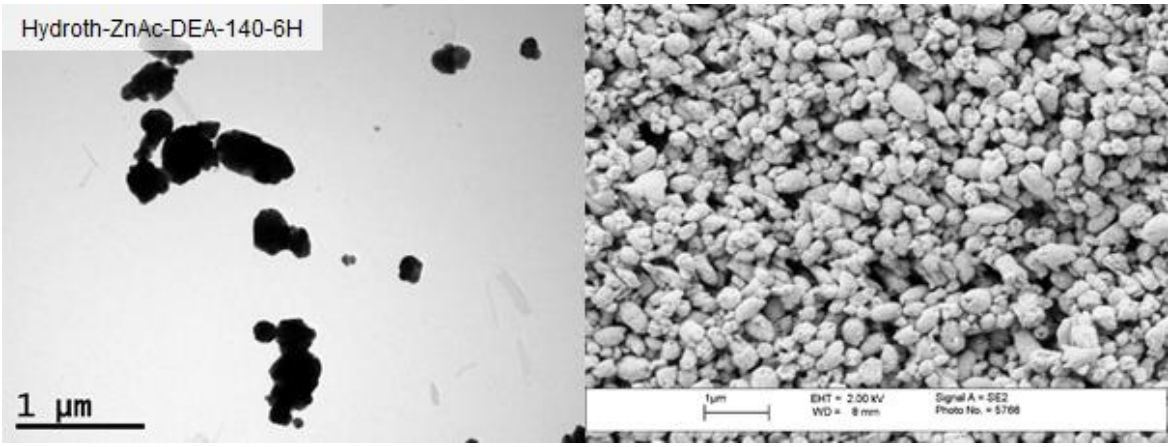

Figure 5-12: TEM (left)/FEGSEM (right) micrographs of particles prepared by $Zn(CH_3COO)_2 \cdot 2H_2O$ reacted with DEA after hydrothermal treatment at 140°C for 6h.

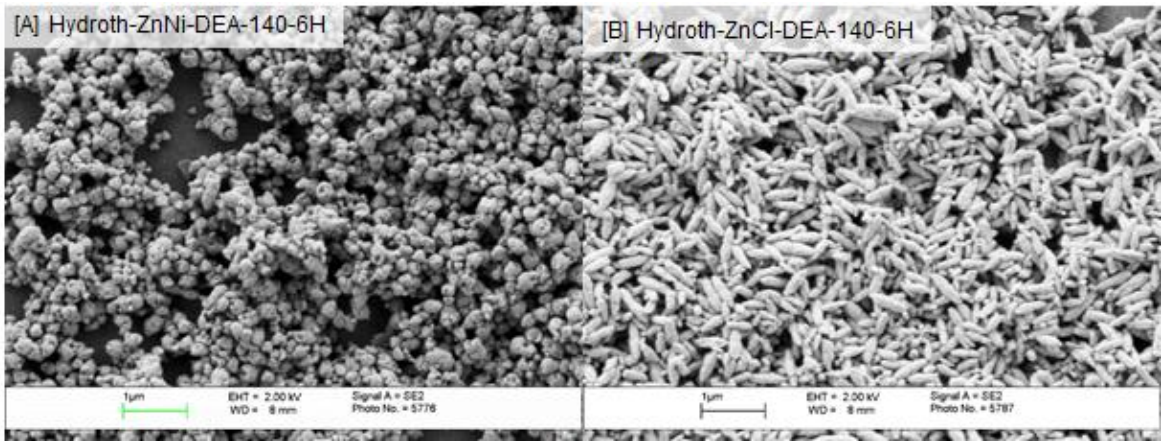

Figure 5-13: FEGSEM micrographs of particles prepared by DEA reacted with $Zn(NO_3)_2$•$6H_2O$ [A] $ZnCl_2$ [B] after hydrothermal treatment at 140°C for 6h.

From the XRD results given in Figure 5-11, it can be seen there is a change from a Zn-O-H compound to a Zn-O compound after hydrothermal treatment at 140°C for 6h for particles prepared by the by the co-precipitation of $Zn(CH_3COO)_2$•$2H_2O$ and DEA. TEM and FEGSEM images of the hydrothermally treated particles (Figure 5-12) indicated elliptical and spherical particles of approximately 200 nm.

Spherical particles of 100 nm and elliptical particles 1um in length were observed following the hydrothermal treatment of particles precipated following a reaction between $Zn(NO_3)_2$·$6H_2O$ (Figure 5-13) and DEA and $ZnCl_2$ and DEA (Figure 5-14), respectively

The morphologies of the ZnO particles synthesized using NH_4OH as a “weak” base solution (pH =10.0±0.2) reacted with different zinc salt precursors were also characterized by using TEM and FEGSEM as shown in Figure 5-14 and Figure 5-15.

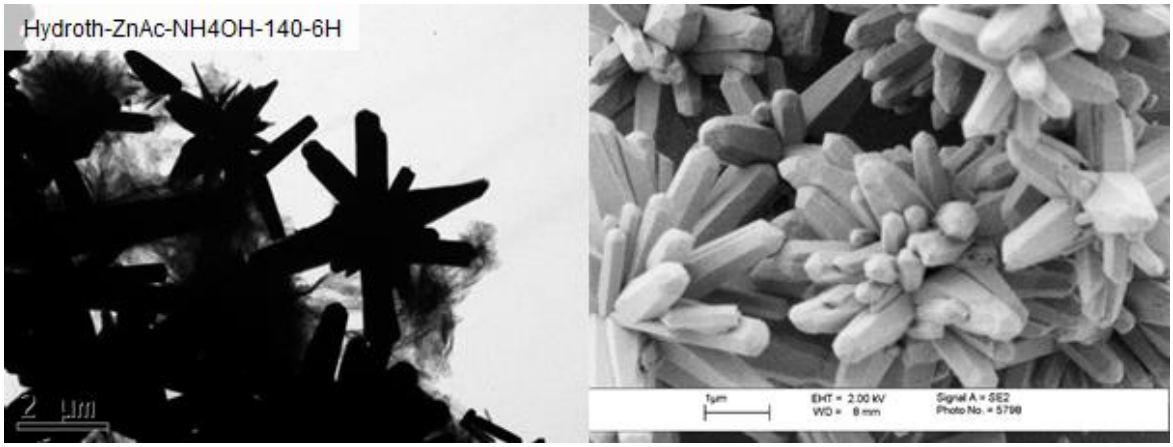

Figure 5-14: TEM (left)/FEGSEM (right) micrographs of particles prepared by $Zn(CH_3COO)_2 \cdot 2H_2O$ reacted with NH_4OH after hydrothermal treatment at 140°C for 6h.

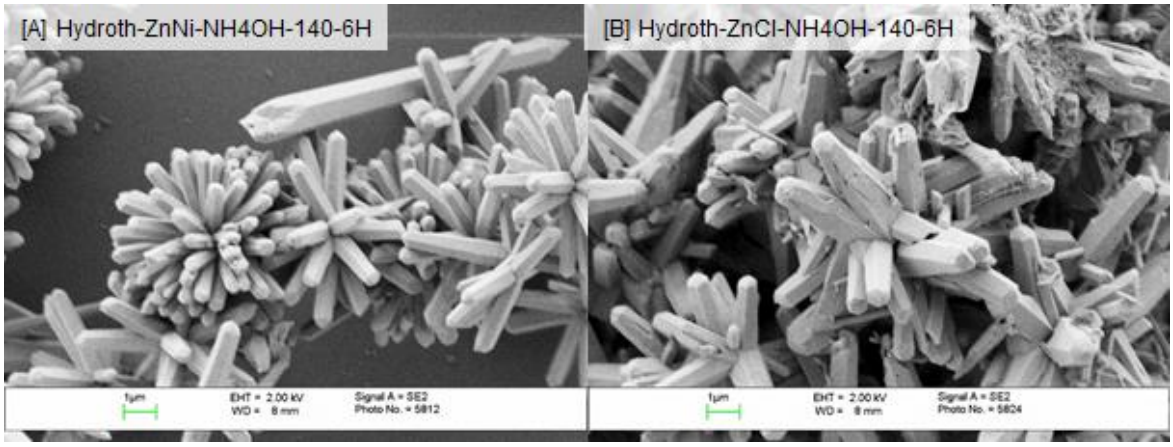

Figure 5-15: FEGSEM micrographs of particles prepared by NH_4OH reacted with [A] $Zn(NO_3)_2 \cdot 6H_2O$ [B] $ZnCl_2$ after hydrothermal treatment at 140°C for 6h.

The micrographs show that varying sizes of aggregated bundles of rod-like structures were formed of the particles prepared with all the zinc salt precursors. The micrographs for the particles formed with NH_4OH show a significant increase in particles size compared to the particles formed with NaOH, TMAH and DEA. This suggests that the nucleation rate lowered and the crystal growth rate increased with the use of NH_4OH. In the case of TMAH and DEA this could be due to a templating effect induced. Both compounds are reported to act as surfactants, which could have inhibited growth [41, 104].

A summary of the particle size and morphology of the particles prepared by using different zinc salt precursors reacted with different base solutions are presented in Table 5-1.

Table 5-1: A summary of the particle size and morphology of ZnO compounds hydrothermally synthesised by using different zinc salt precursors reacted with different bases

Zinc Precursor	Base	Particle size (nm)	Morphology
$Zn(CH_3COO)_2 \bullet 2H_2O$	NaOH	200	Platelet
$Zn(NO_3)_2 \cdot 6H_2O$	NaOH	200	Platelet
$ZnCl_2$	NaOH	200-300	Aggregated rods
$Zn(CH_3COO)_2 \bullet 2H_2O$	TMAH	200	Platelet
$Zn(NO_3)_2 \cdot 6H_2O$	TMAH	200	Platelet
$ZnCl_2$	TMAH	200	Aggregated rods
$Zn(CH_3COO)_2 \bullet 2H_2O$	DEA	400	Spherical
$Zn(NO_3)_2 \cdot 6H_2O$	DEA	200	Spherical
$ZnCl_2$	DEA	500-800	Elliptical
$Zn(CH_3COO)_2 \bullet 2H_2O$	NH_4OH	<1000	Rod-like
$Zn(NO_3)_2 \cdot 6H_2O$	NH_4OH	<1000	Rod-like
$ZnCl_2$	NH_4OH	<1000	Rod-like

5.2 Nanoparticles synthesised with addition of surfactants

Similar to the experiment carried out with the co-precipitation method, both non-ionic surfactants and ionic surfactants were used to investigate the effect on particle size and morphology of particles using different base solutions with hydrothermal treatment. As pervious, single experiments and orthogonal array were used.

5.2.1 Effect of Non-ionic Surfactant

The TEM and FEGSEM micrographs of hydrothermally treated particles prepared by reactions between $Zn(CH_3COO)_2 \cdot 2H_2O$ and NaOH with addition of different non-ionic surfactants are shown below. Aggregated bundles of rod like structures with varying sizes were obtained for all the samples with addition of the surfactants. For L64, flower-like bundles of approximately 500nm in size with rods of 250nm in length were formed (Figure 5-16). For F68, these bundles increased in size to rods of 1um and bundles of 2um in size (Figure 5-17). When P123 was the surfactant, the largest rod was synthesised, with a length of approximately 2um. However, unlike the previous surfactants the rods were less agglomerated (Figure 5-18).

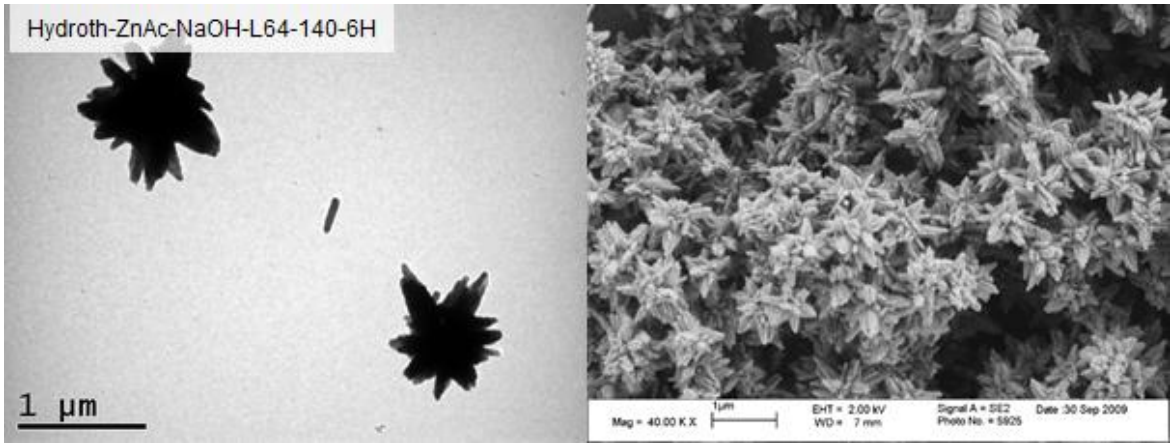

Figure 5-16: TEM (left)/FEGSEM (right) micrographs of particles prepared by the reactions between NaOH and $Zn(CH_3COO)_2 \cdot 2H_2O$ as the salt with addition of different non-ionic surfactants L64

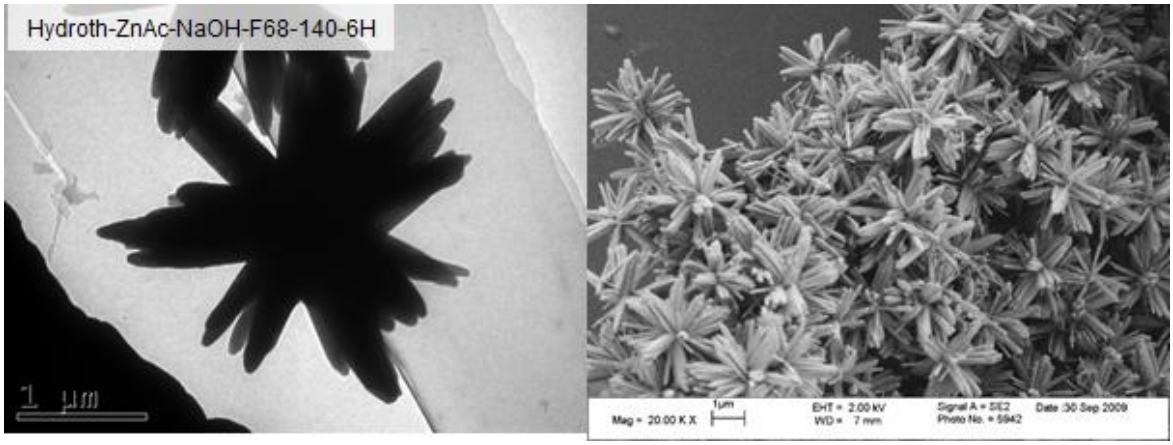

Figure 5-17: TEM (left)/FEGSEM (right) micrographs of particles prepared by the reactions between NaOH and $Zn(CH_3COO)_2•2H_2O$ as the salt with addition of different non-ionic surfactant F68

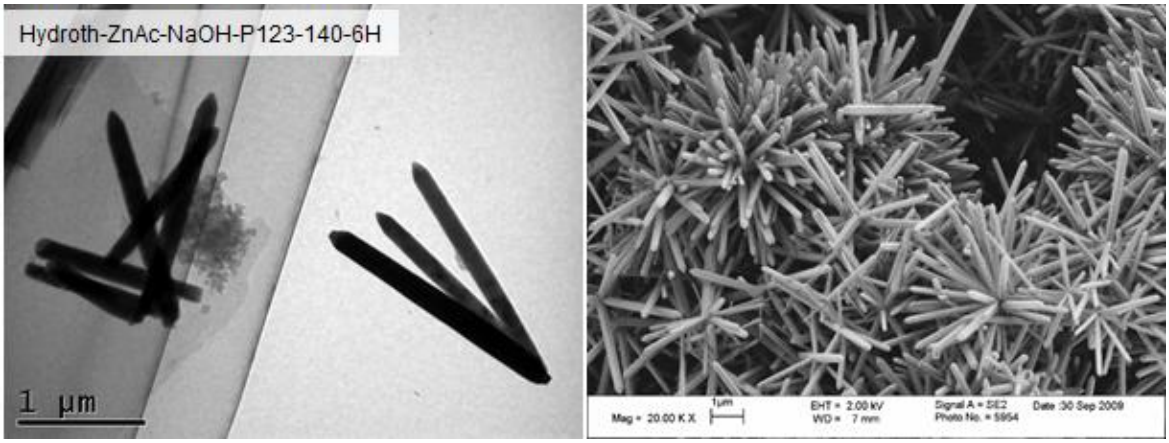

Figure 5-18: TEM (left)/FEGSEM (right) micrographs of particles prepared by the reactions between NaOH and Zn(CH3COO)2•2H2O as the salt with addition of different non-ionic surfactant P123

The particle sizes and morphologies of the ZnO particles synthesised hydrothermally by using $Zn(CH_3COO)_2•2H_2O$ as the precursor reacted with TMAH (pH = 12.8±0.2) are shown in Figure 5-19, Figure 5-20 and Figure 5-21. The micrographs show a change in morphology between L64, F68, and P123. TEM micrographs show platelets were formed with L64 (Figure 5-19) and rods were formed with F68 (Figure 5-20) and P123 (Figure 5-21). FEGSEM micrographs show that the platelets were aggregated and about 1um in length for L64 sample and the rods formed with F68 and P123 were both approximately 500nm in length with overall bundle size of 1um.

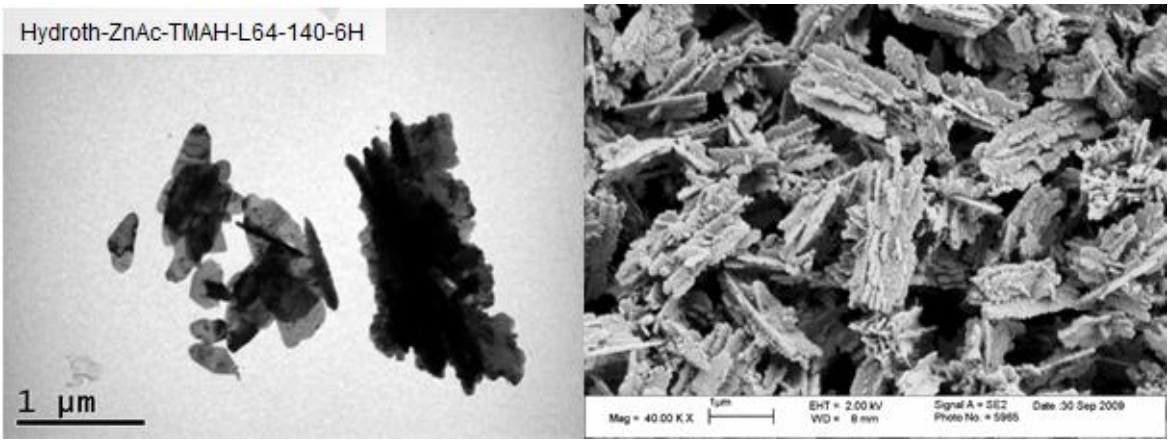

Figure 5-19: TEM (left)/FEGSEM (right) micrographs of particles prepared by the reactions between TMAH and $Zn(CH_3COO)_2 \cdot 2H_2O$ as the salt with addition of non-ionic surfactant L64

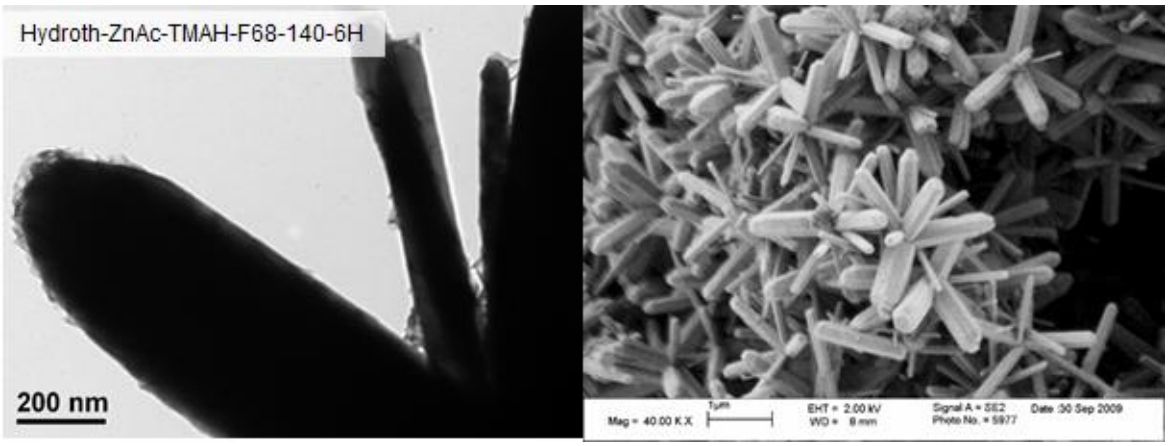

Figure 5-20: TEM (left)/FEGSEM (right) micrographs of particles prepared by the reactions between TMAH and $Zn(CH_3COO)_2 \cdot 2H_2O$ as the salt with addition of non-ionic surfactant F68

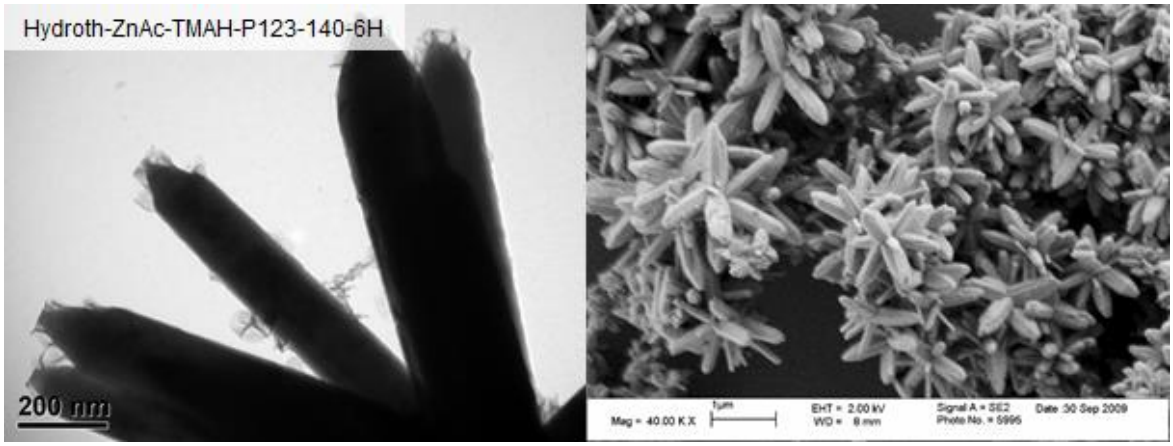

Figure 5-21: TEM (left)/FEGSEM (right) micrographs of particles prepared by the reactions between TMAH and $Zn(CH_3COO)_2$•$2H_2O$ as the salt with addition of non-ionic surfactant P123

Figure 6-12 show the TEM and FEGSEM micrographs of the particles formed using $Zn(CH_3COO)_2$•$2H_2O$ reacted with DEA (pH = 10.0±0.2) after hydrothermal treatment. The micrographs show that all the samples have elliptical shaped structures with the size about 200nm in width and 500-600nm in length.

The FEGSEM/TEM micrographs of ZnO synthesised after hydrothermal treatment when NH_4OH (pH =10±0.2) and $Zn(CH_3COO)_2$•$2H_2O$ were used as the precursor with non-ionic solutions are shown below. The morphology of the ZnO changed from a mixture of platelets and plank-like particles of various size with L64 (Figure 5-26) to sword-like morphology with F68 (Figure 5-27) and P123 (Figure 5-28). The sword like particles were approximately 1-2um in length with F68 and 2-3um with P123.

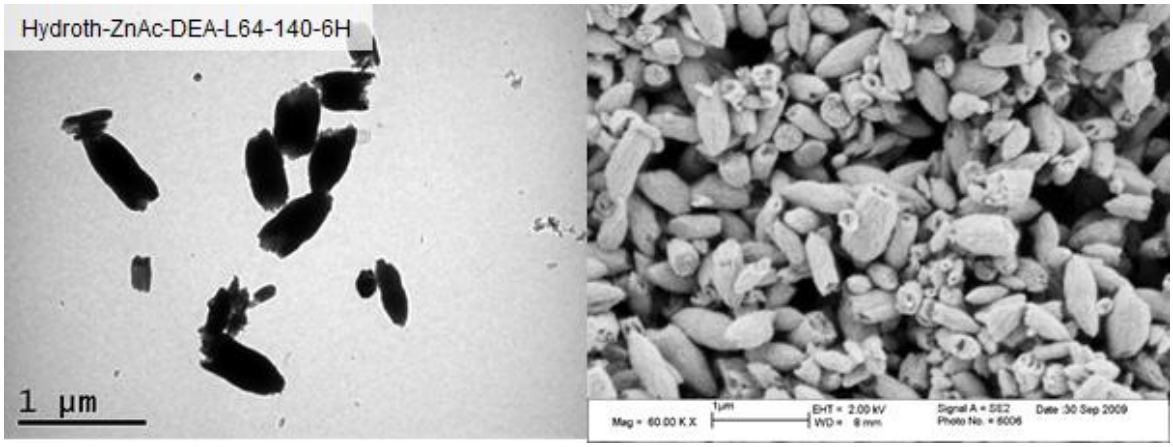

Figure 5-22: TEM (left)/FEGSEM (right) micrographs of particles prepared by the reactions between DEA and $Zn(CH_3COO)_2$•$2H_2O$ as the salt with addition of non-ionic surfactant L64

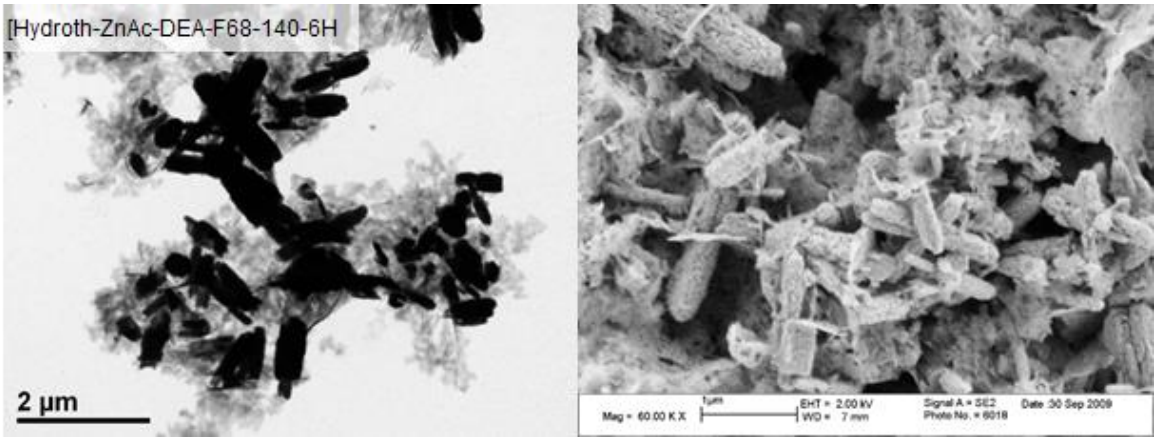

Figure 5-23: TEM (left)/FEGSEM (right) micrographs of particles prepared by the reactions between DEA and Zn(CH3COO)2•2H2O as the salt with addition of non-ionic surfactant F68

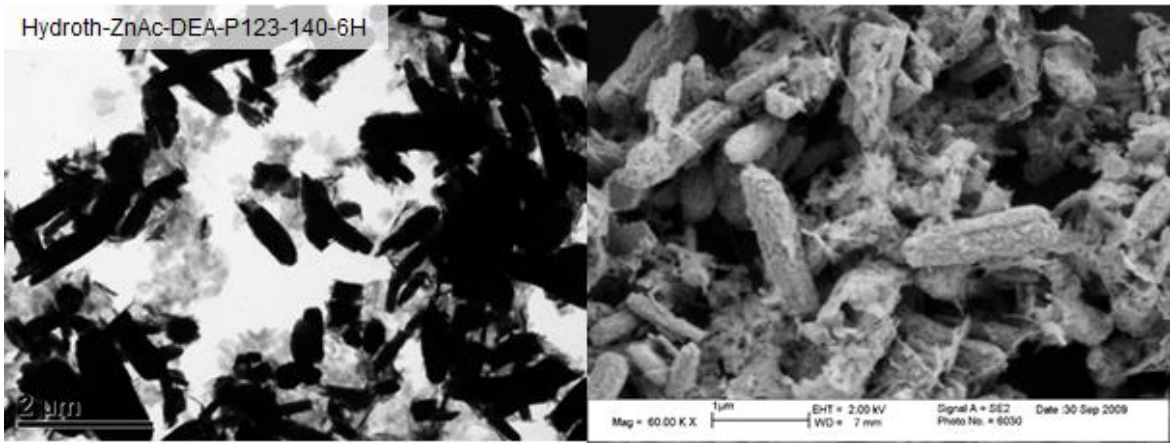

Figure 5-24: TEM (left)/FEGSEM (right) micrographs of particles prepared by the reactions between DEA and Zn(CH3COO)2•2H2O as the salt with addition of non-ionic surfactant P123

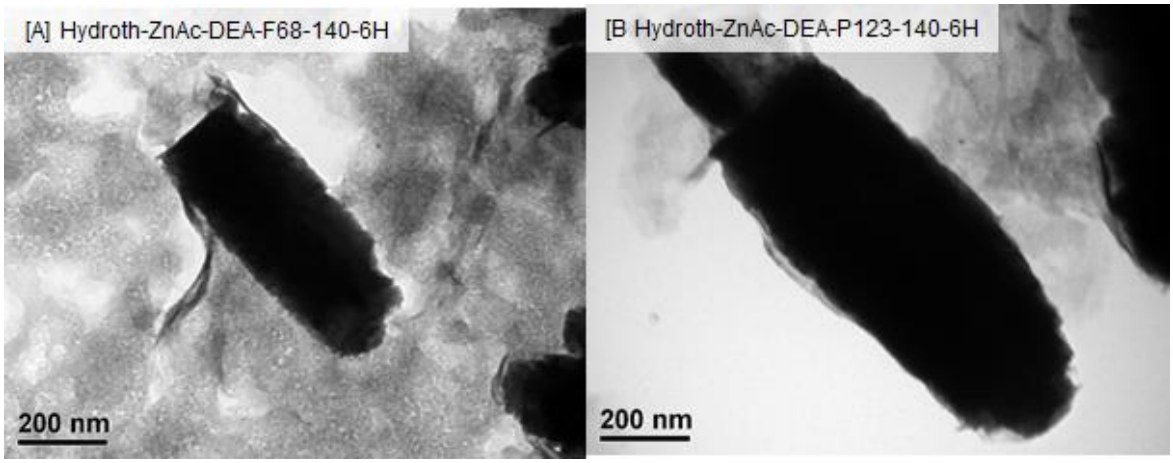

Figure 5-25: TEM (left) micrographs of particles prepared by the reactions between DEA and $Zn(CH_3COO)_2•2H_2O$ as the salt with addition of different non-ionic surfactants [A] F68 [B] P123

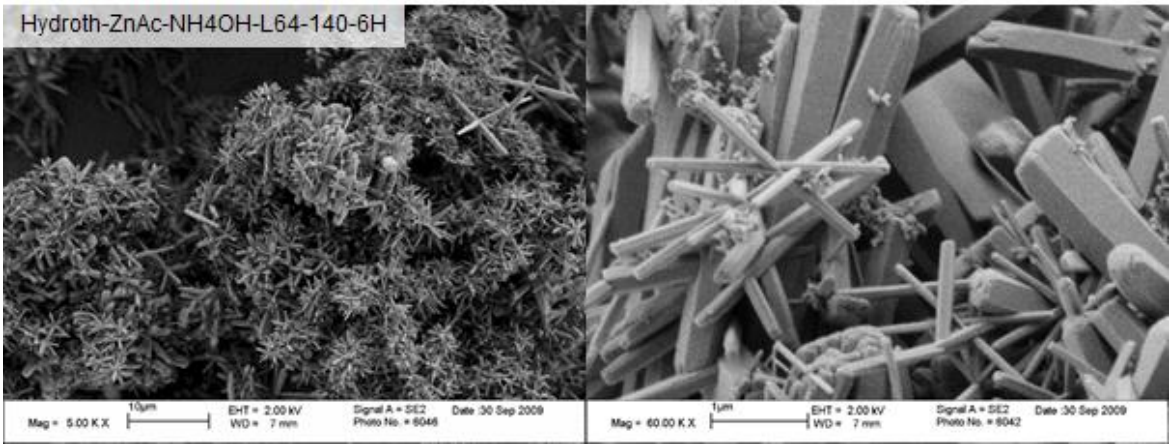

Figure 5-26: FEGSEM micrographs of particles prepared by the reactions between NH_4OH and $Zn(CH_3COO)_2•2H_2O$ as the salt with addition of different non-ionic surfactant L64

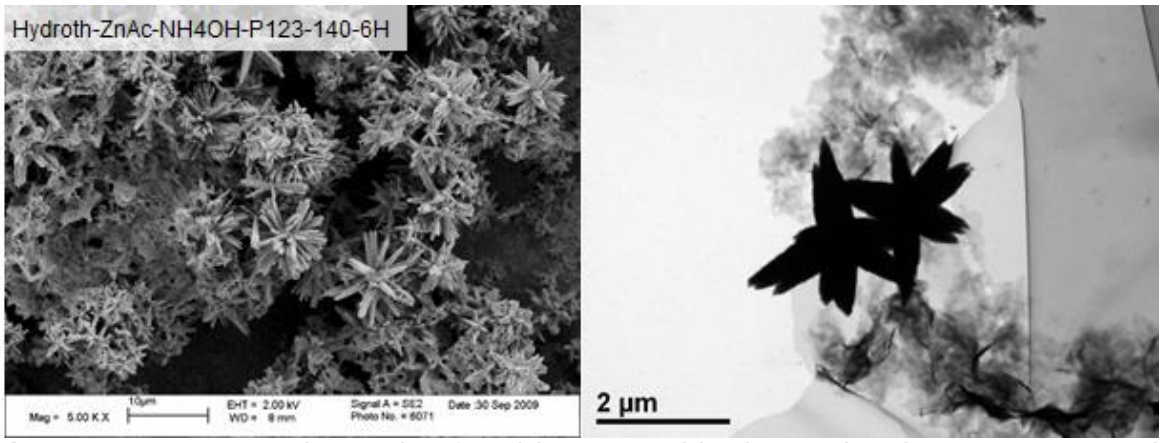

Figure 5-27: FEGSEM micrographs of particles prepared by the reactions between NH_4OH and $Zn(CH_3COO)_2•2H_2O$ as the salt with addition of different non-ionic surfactant F68

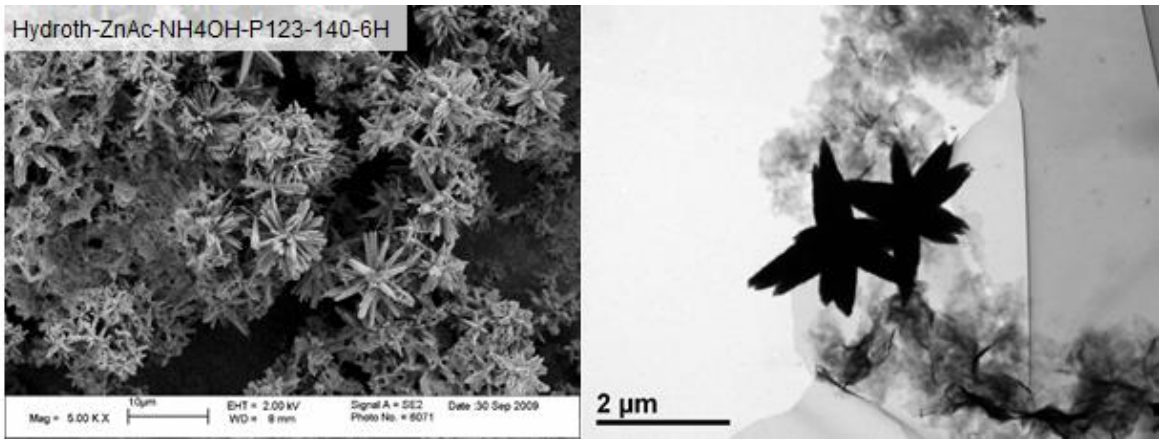

Figure 5-28: FEGSEM micrographs of particles prepared by the reactions between NH_4OH and $Zn(CH_3COO)_2•2H_2O$ as the salt with addition of different non-ionic surfactant P123

A summary of the particle sizes and morphologies of the ZnO particles synthesised by $Zn(CH_3COO)_2 \bullet 2H_2O$ reacted with different base solutions (pH = 12.8±0.2) with the addition of non-ionic surfactants (L64, F68 and P123) is presented in Table 5-2.

Table 5-2: Summary of the precursors used in the hydrothermal synthesis of ZnO nanoparticles without the addition of surfactant

Base solution	Surfactant	Particle Size (nm)	Morphology
NaOH	L64	500	Flower
NaOH	F68	N/A	Aggregated Rods
NaOH	P123	<1000	Aggregated Thin Rods
TMAH	L64	1000	Agglomerated Platelets
TMAH	F68	<1000	Aggregated Rods
TMAH	P123	500-1000	Aggregated Rods
DEA	L64	500	Elliptical
DEA	F68	500-1000	Elliptical
DEA	P123	1000	Elliptical
NH_4OH	L64	<1000	Aggregate rods and Aggregated block
NH_4OH	F68	<1000	Flower
NH_4OH	P123	<1000	Flower

A comparison of Table 5-1 and Table 5-2 indicates that for each reaction, the introduction of surfactant either caused a change in morphology, a change in particle size or a change in both morphology and size. The change in particles size was significant, with micron sized generally particles formed with surfactants compared to the nanosized particles synthesised without. This is likely linked to the fact that the addition of surfactant led to the formation of an aggregated particles (flower-like, aggregated rod-like), whereas more individual morphologies (platelet, elliptical) were formed without surfactants.

5.2.2 Effect of the concentration of non-ionic surfactants

The effect of the concentration of non-ionic surfactant on the particle size and morphology of ZnO particles hydrothermally synthesised was investigated. This was achieved by using $Zn(CH_3COO)_2 \bullet 2H_2O$ reacted with NaOH with addition of different concentration of non-ionic surfactant L64 (140°C for 6h).

The hydrothermally synthesised ZnO particles with different concentrations of surfactant prepared by using $Zn(CH_3COO)_2 \bullet 2H_2O$ as the zinc salt precursor reacted with NaOH (pH =12.8±0.2) are shown in Figure 5-29. The micrographs show that the ZnO particles have a star-like morphology and little change in size or morphology until a platelet morphology was reported with the increase of the surfactant concentration to 53%. At a low concentration (1%) there is also evidence of hexagonal blocks being formed (Figure 5-29 (a)).

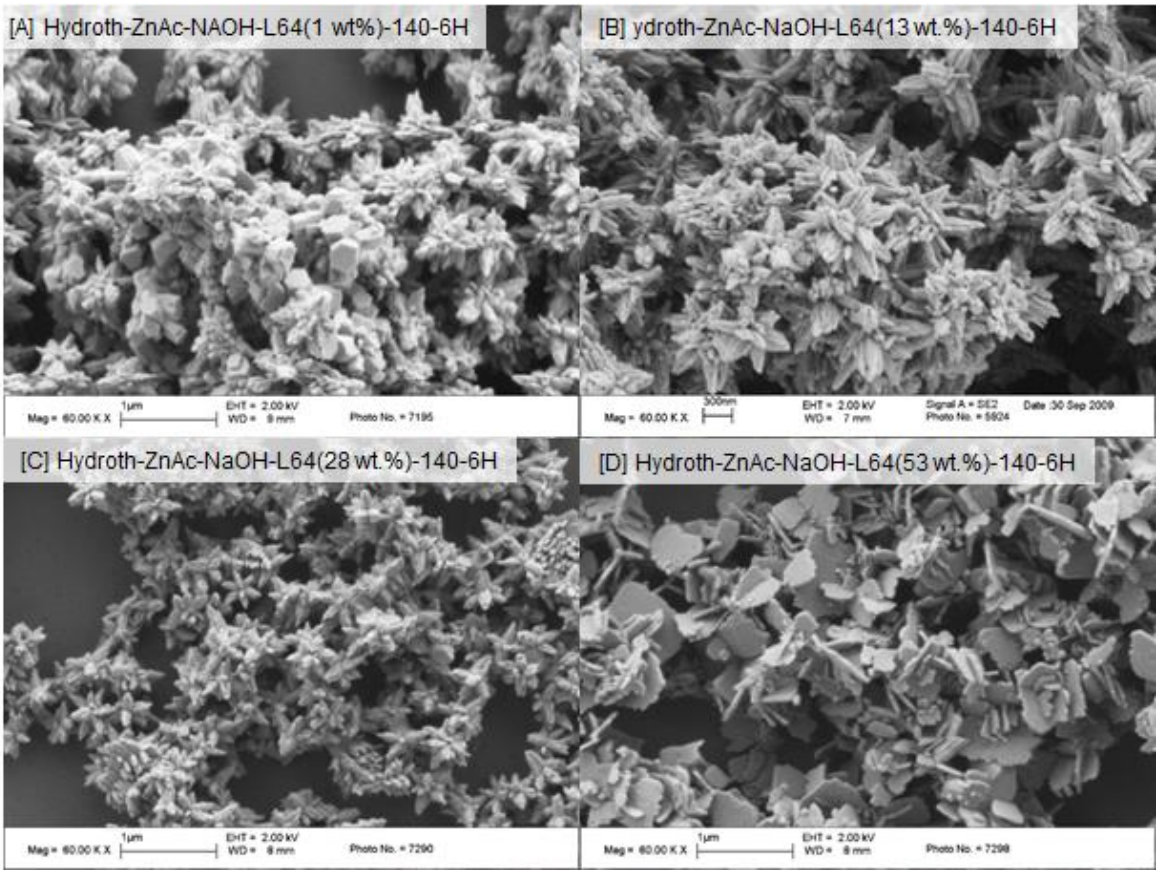

Figure 5-29: FEGSEM micrographs of ZnO particles prepared by the reaction of $Zn(CH_3COO)_2$•$2H_2O$ and NaOH with L64 as the surfactant of [A] 1 wt%; [B] 10 wt% [C] 28 wt% and [D] 53 wt%

5.2.3 Effect of different zinc salt precursors

The effect of different starting zinc salt precursors on the particle size and morphology of ZnO particles synthesised by hydrothermal was investigated by using $Zn(NO3)_2$•$6H_2O$ and $ZnCl_2$ as the salt precursors reacted with NaOH (pH = 12.8±0.2) as the base solution with addition of non-ionic surfactants L64, F68 and P123.

The micrographs of the ZnO particles synthesised using $Zn(NO_3)_2$•$6H_2O$ as the salt reacted with NaOH with addition of various non-ionic surfactants are shown in Figure 5-30. The platelets were formed when there was no surfactant present (Figure 5-30 (a)). Column-like particles were formed with addition of L64 (Figure 5-30. (b)). Rod like particles were observed when F68 (Figure 5-30 (c)) and P123 (Figure 5-30 (d)) were used as the

surfactants, though they varied different size, with the rods synthesised with F68 being about double the size.

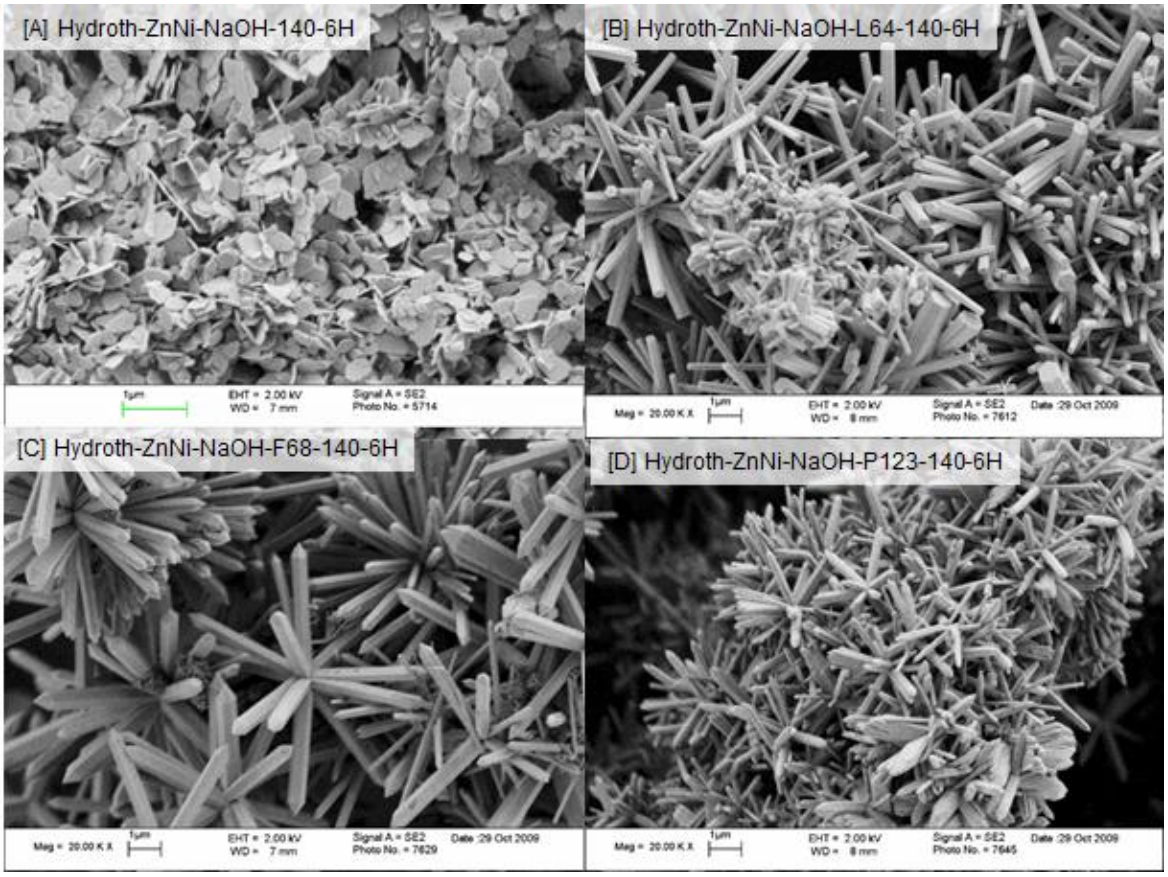

Figure 5-30: FEGSEM micrographs of ZnO compounds synthesised by the reactions between $Zn(NO_3)_2{\cdot}6H_2O$ and NaOH with or without addition of surfactants. [A] No surfactant [B] L64 [C] F68 [D] P123

Figure 5-31 shows the micrographs of ZnO particles hydrothermally prepared by the reactions between $ZnCl_2$ and NaOH with addition of various non-ionic surfactants. Although the morphology of the particles formed did not change compared with those prepared directly by co-precipitation shown in Figure 5-31 (a), there was a noticeable increase in size of the particles when surfactant was used.

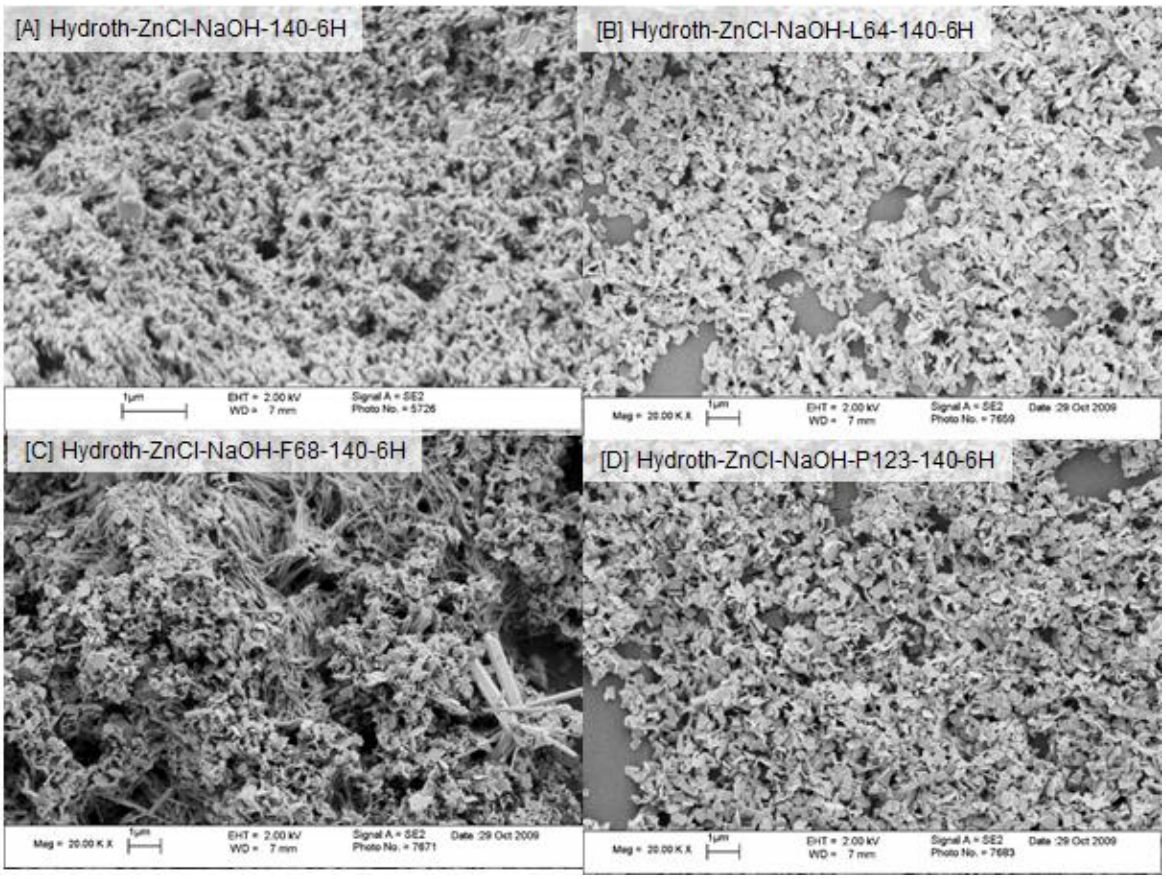

Figure 5-31: FEGSEM micrographs of the particles synthesised by the reactions between $ZnCl_2$ and NaOH with or without addition of surfactants. [A] No surfactant [B] L64 [C] F68 [D] P123

5.2.4 Effect of ionic surfactants

The effect of ionic surfactants on the particle size and morphology of the ZnO particles synthesised by using $Zn(CH_3COO)_2 \cdot 2H_2O$ as the zinc salt precursor reacted with different base solutions with addition of ionic surfactants by hydrothermal at 140ºC for 6 hours was also investigated.

Figure 5-32 and Figure 5-33 show the TEM micrographs of the ZnO particles prepared by $Zn(CH_3COO)_2 \cdot 2H_2O$ reacted with “strong” base solutions (pH =12.8±0.2) NaOH and TMAH, respectively with addition of ionic surfactants SDS or CTAB by hydrothermal at 140ºC for 6 h.

With NaOH as the base solution, particles with a rod like structure (Figure 5-32A) and a small column/star like structure (Figure 5-32B) were obtained when SDS and CTAB were used as the surfactant, respectively. The micrographs in Figure 5-33 show the samples prepared by $Zn(CH_3COO)_2 \cdot 2H_2O$ reacted with TMAH. The TEM micrographs show a large (> 1μm) agglomerated platelet morphology synthesised with SDS (Figure 5-33A) and a microflower-like morphology approximately 400nm in diameter with CTAB (Figure 5-33B).

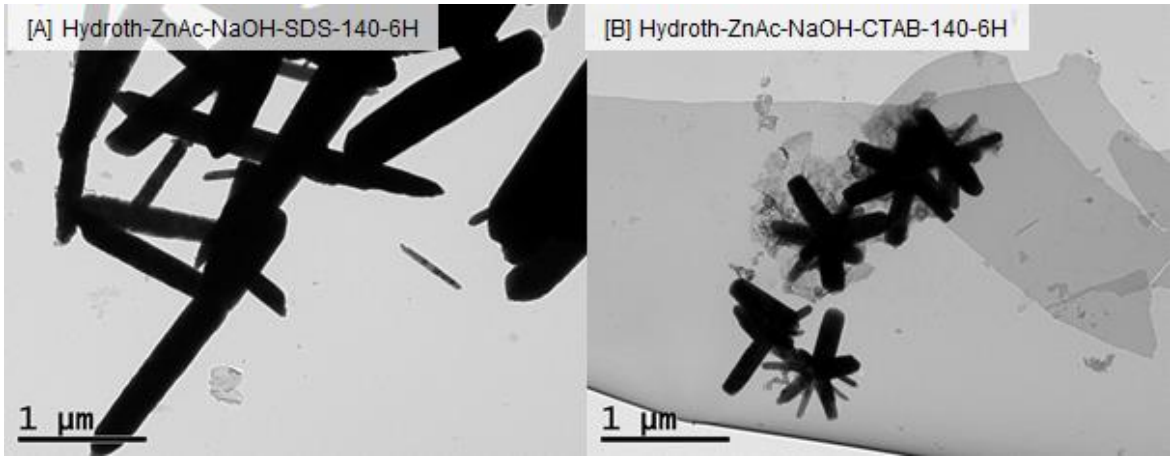

Figure 5-32: TEM micrographs of the particles synthesised by the reactions between $Zn(CH_3COO)_2 \cdot 2H_2O$ and NaOH with addition of surfactants. [A] SDS [B] CTAB

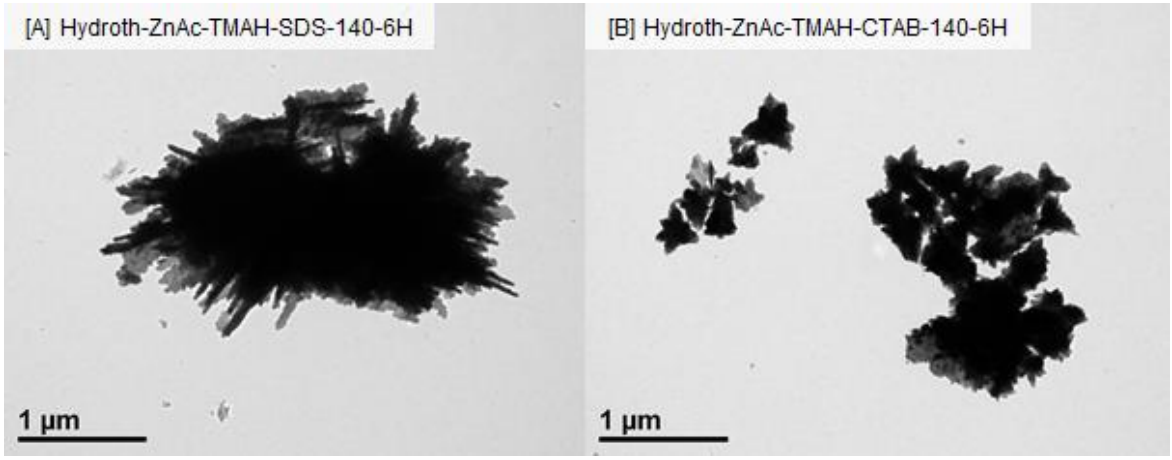

Figure 5-33: TEM micrographs of the particles synthesised by the reactions between $Zn(CH_3COO)_2 \cdot 2H_2O$ and TMAH with addition of surfactants. [A] SDS [B] CTAB

The "weak" base solutions DEA and NH_4OH (pH =10.0±0.2) were also used to react with $Zn(CH_3COO)_2 \cdot 2H_2O$ with addition of ionic surfactants via hydrothermal. The TEM micrographs of the ZnO particles hydrothermally synthesised are shown in Figure 5-34 for

DEA and Figure 5-35 for NH_4OH, respectively. Spherical ZnO particles of between 50-200nm (Figure 5-34A) were synthesised with SDS as the surfactant and elliptical particles of about 200nm in width and 600nm in length were formed with CTAB as the surfactant (Figure 5-34B).

When NH_4OH was used as the base solution (pH =10.0±0.2) and SDS as the surfactant, ZnO particles with hexagonal shape and 800nm in diameter were formed (Figure 5-35A) and a mixture of plank-like and needle-like particles were obtained when CTAB was used as the surfactant (Figure 5-35B).

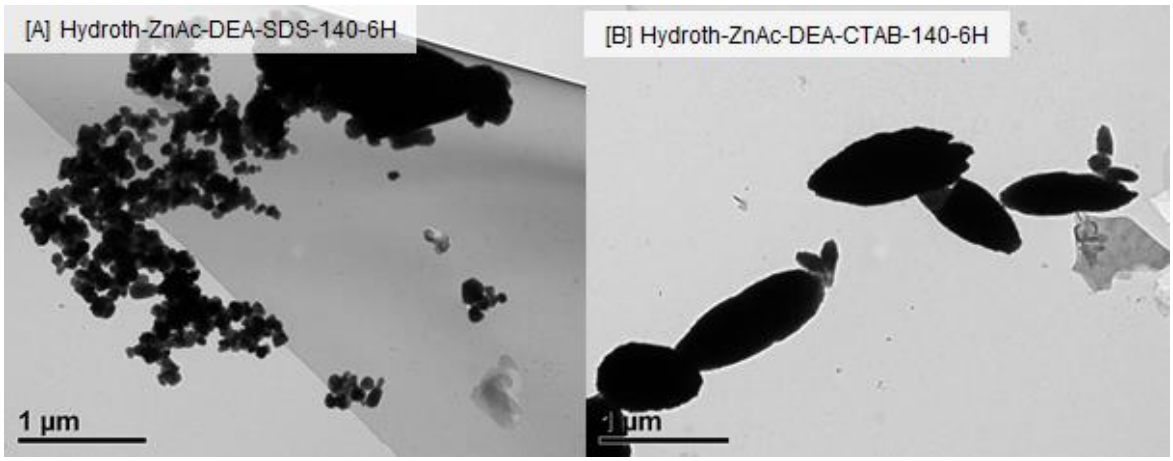

Figure 5-34: TEM micrographs of the particles hydrothermally synthesised by the reactions between $Zn(CH_3COO)_2 \cdot 2H_2O$ and DEA with addition of surfactants. [A] SDS [B] CTAB

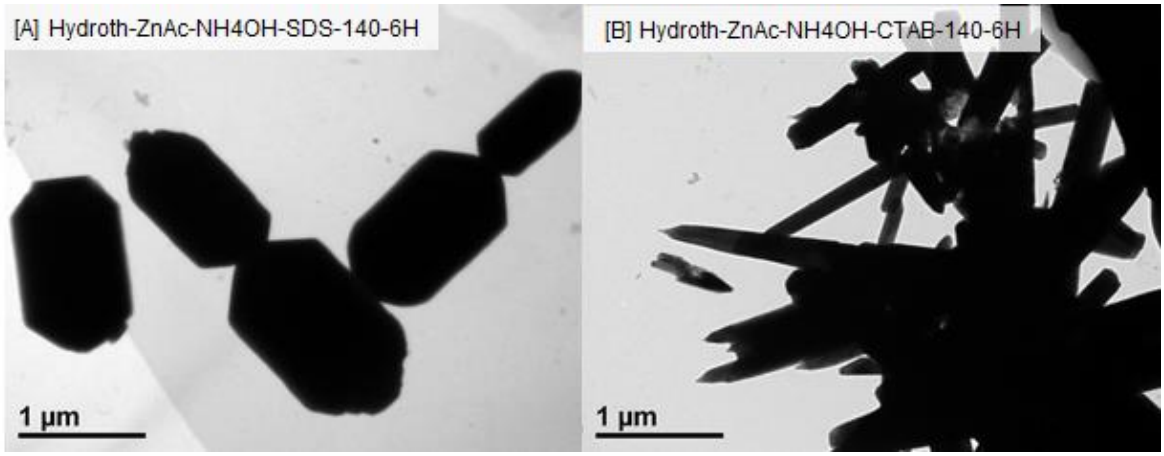

Figure 5-35: TEM micrographs of the particles synthesised by the reactions between $Zn(CH_3COO)_2 \cdot 2H_2O$ and NH_4OH with addition of surfactants. [A] SDS [B] CTAB

5.2.5 Effect of synthesis conditions

The products obtained before and after hydrothermal synthesis (Section 5.3) were characterised by TEM and the micrographs are displayed in Figure 5-36.

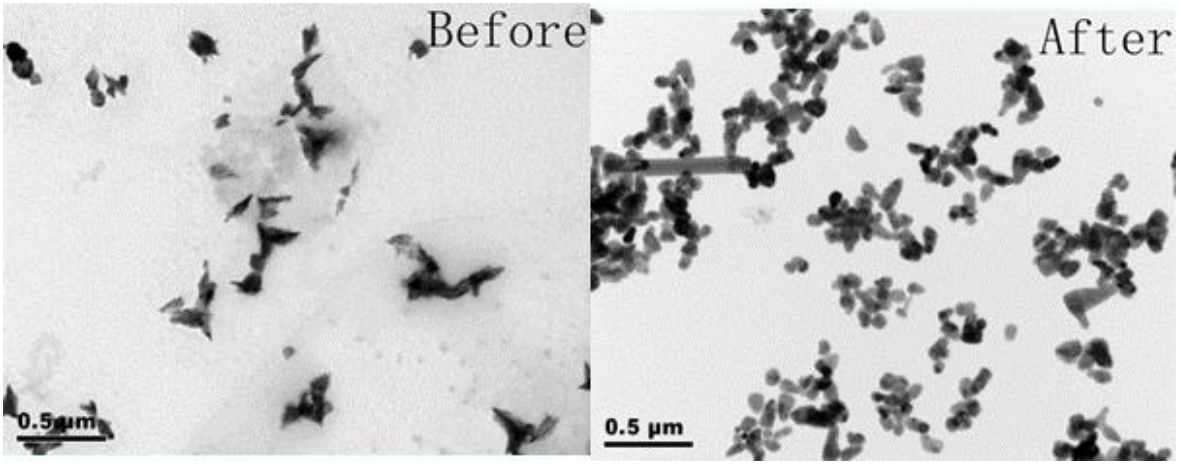

Figure 5-36: TEM micrographs of the products obtained before and after hydrothermal synthesis.

As can be seen from Figure 5-36 the size of the particles with hydrothermal treatment is smaller than that of the particles without hydrothermal treatment. The particles observed before hydrothermal TEM micrograph takes the morphology of tip-like anisotropic nanoparticles; the outline of the particles is rough. The morphology of the hydrothermally synthesized ZnO is anisotropic nanoparticles with very smooth outline. This indicates the size and morphology is modified by the hydrothermal treatment.

Figure 5-37 shows the FEGSEM micrographs of the ZnO particles prepared by using $Zn(CH_3COO)_2 \cdot 2H_2O$ as the zinc salt precursor reacted with NaOH with addition of non-ionic surfactants by hydrothermal at 140°C for various hours. The results show that for all of the experiments a star-like structure of various sizes was synthesised. The structures were between 1µm to 5µm in size. The smallest structures were synthesised with L64 as the surfactant and a hydrothermal time of 2 hours (Figure 5-37 (1)). The largest star-like structures were synthesised by the combination of surfactant P123 and 4 hours of hydrothermal processing (Figure 5-37 (8)).

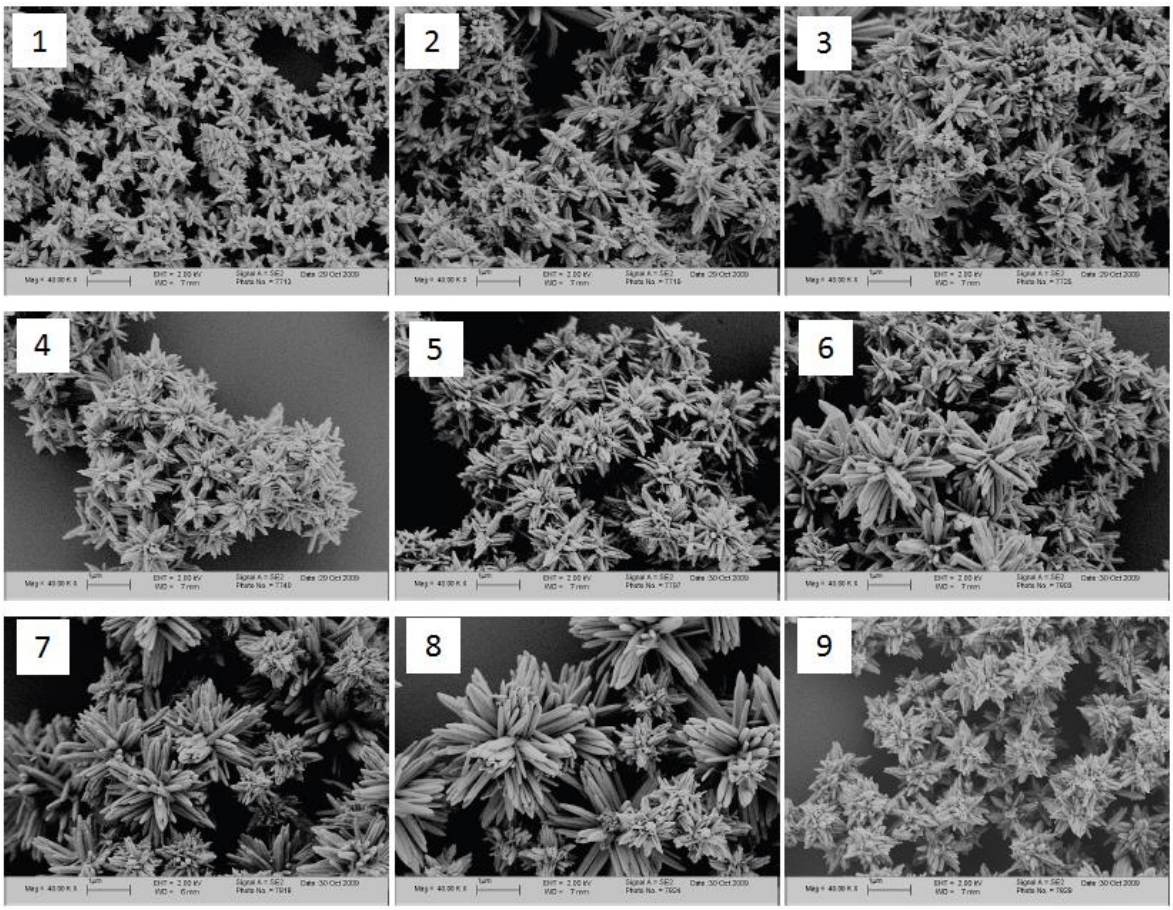

Figure 5-37: FEGSEM micrographs of ZnO particles hydrothermally synthesized by reactions between $Zn(CH_3COO)_2 \cdot 2H_2O$ and NaOH at 140°C for various hours with addition of non-ionic surfactants [1] L64 + 2 hours [2] L64 + 4 hours [3] L64 + 12 hours [4] F68 + 2 hours [5] F68 + 4 hours [6] P123 + 12 hours [7] P123 + 2 hours [8] P123 + 4 hours [9] P123 + 12 hours

5.2.5.1 Effect of hydrothermal temperature

The FEGSEM micrographs of the ZnO particles prepared by the reactions between $Zn(CH_3COO)_2 \cdot 2H_2O$ and NaOH with addition of non-ionic surfactants by hydrothermal at different temperatures for 6h are shown in Figure 5-38. All the experiments led to the synthesis of a star-like structure of varying size. The size of the structures varied from approximately 1µm to 10µm. However, in the use of P123 and 200°C (Figure 5-38 (6)) a whisker morphology was formed. An increase in particle size with increase of the hydrothermal temperature is noticeable for ZnO precipitated with L64 and F68. In the case of P123, no visible increase in size was observed.

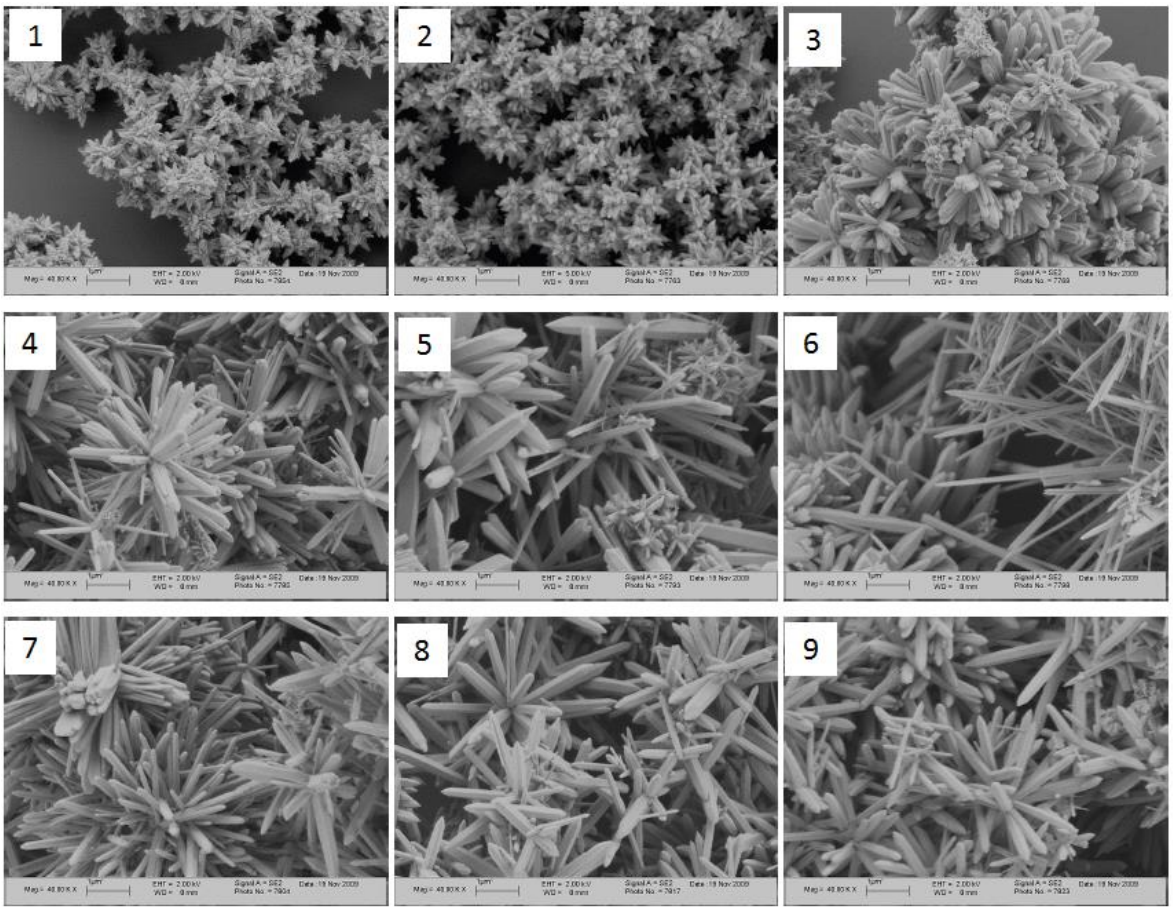

Figure 5-38: FEGSEM micrographs of ZnO particles hydrothermally synthesized by reactions between $Zn(CH_3COO)_2 \cdot 2H_2O$ and NaOH at various temperatures for 6h with addition of non-ionic surfactants [1] L64 + 120^oC [2] L64 + 160^oC [3] L64 + 200^oC [4] F68 + 120^oC [5] F68 + 160^oC [6] F68 + 200^oC [7] P123 + 120^oC [8] P123 + 160^oC [9] P123 + 200^oC

Two further experiments were carried out to compare the effect of temperature on the size and morphologies of the hydrothermally prepared ZnO nanomaterials. These two experiments were carried out under the same synthesizing conditions except for a change in temperature, with the samples prepared at 220 °C (Figure 5-39A) and 140°C (Figure 5-39B), respectively. The synthesizing details are listed in Table 5-3.

Table 5-3: Details of synthesizing conditions to compare the effect of temperature

Zinc salt	Base	Surfactant	Time	pH value	Temperature (°C)
$ZnSO_4 \cdot 7H_2O$	NaOH	PEG	6h	10.0±0.2	220
					140

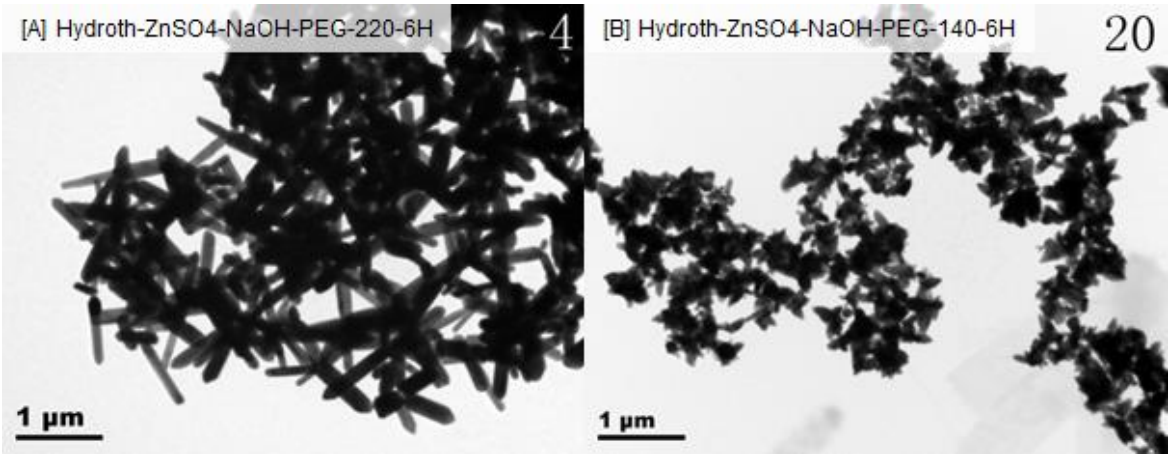

Figure 5-39: TEM micrographs of ZnO nanomaterials synthesized at (a) 220°C (b) 140°C

ZnO nanorods are observed in the Figure 5-39A following synthesis as 220°C and the morphology reported in Figure 5-39B shows tip-like anisotropic nanoparticles following synthesis at 140°C. This indicates hydrothermal temperature has an influence on the morphologies of the synthesized ZnO nanomaterials.

5.2.6 Hydrothermal experiments using orthogonal design

The effects of zinc salt precursors, base solutions, surfactants and synthetic conditions on the particle size and morphology of the ZnO particles synthesised via hydrothermal method were also investigated by using orthogonal design approach.

Table 5-4 shows the four factors (zinc salt, base solution, surfactant and hydrothermal temperature) with their corresponding levels chosen for the orthogonal design and the details of the experiment are given in Table 5-5. The experiments were conducted via hydrothermal for 6h and pH value was fixed at about 10.0±0.2 with the amount zinc salt precursor of 0.005 mol and the addition of the surfactant of 0.0005mol.

Table 5-4: Four factors with their corresponding levels chosen in the 1st group

Level		**1**	**2**	**3**
Factor	Zinc salt	$Zn(NO_3)_2{\cdot}6H_2O$	$ZnSO_4{\cdot}7H_2O$	$Zn(C_2H_4O_2)_2{\cdot}2H_2O$
	Base solution	NaOH	NH_4OH	DEA
	Surfactant	CTAB	PEG	AOT
	Temperature	140 °C	180 °C	220 °C

Table 5-5: The details of the experiments - L9(34) array designed for the 1st group

Expt. number	**Zinc salt**	**Base solution**	**Surfactant**	**Temperature (°C)**
1	$Zn(NO_3)_2{\cdot}6H_2O$	NaOH	CTAB	140
2		NH_4OH	PEG	180
3		DEA	AOT	220
4	$ZnSO_4{\cdot}7H_2O$	NaOH	PEG	220
5		NH_4OH	AOT	140
6		DEA	CTAB	180
7	$Zn(C_2H_4O_2)_2{\cdot}2H_2O$	NaOH	AOT	180
8		NH_4OH	CTAB	220
9		DEA	PEG	140

TEM micrographs of the orthogonally designed and hydrothermally synthesized ZnO nanomaterials are presented in **Figure 5-40** to **Figure 5-48** and a FEGSEM micrograph of Experiment No. 4 is shown in Figure 5-49.

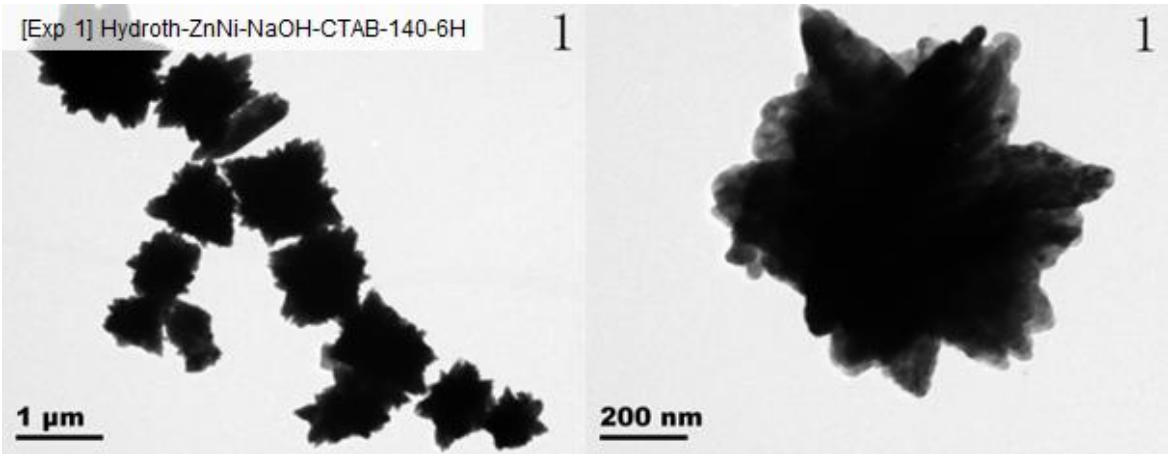

Figure 5-40: TEM micrograph of the particles prepared by the reactions between NaOH and $Zn(NO_3)_2$ in the presence of CTAB followed by hydrothermal treatment at 140°C for 6 hours (Experiment 1)

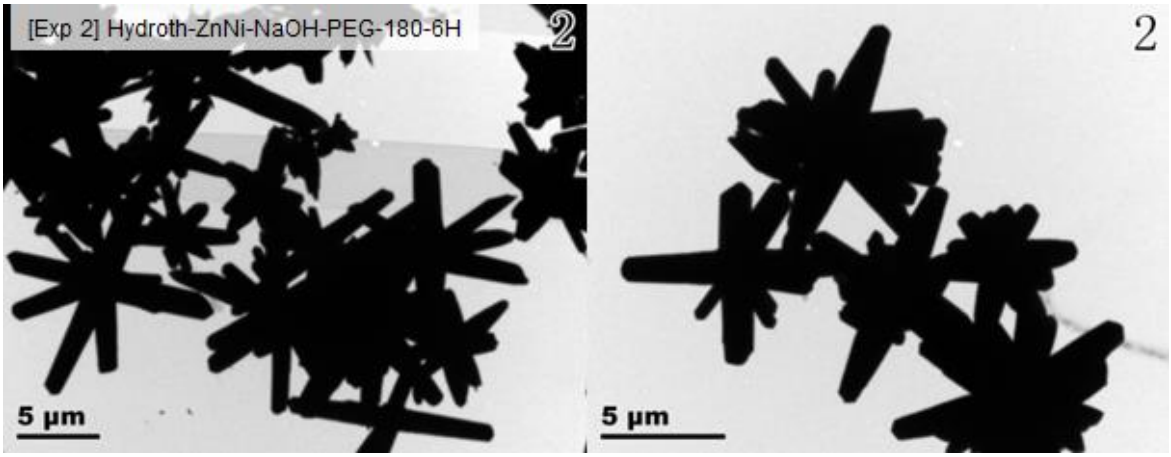

Figure 5-41: TEM micrograph of the particles prepared by the reactions between NH_4OH and $Zn(NO_3)_2$ in the presence of PEG followed by hydrothermal treatment at 180°C for 6 hours (Experiment 2)

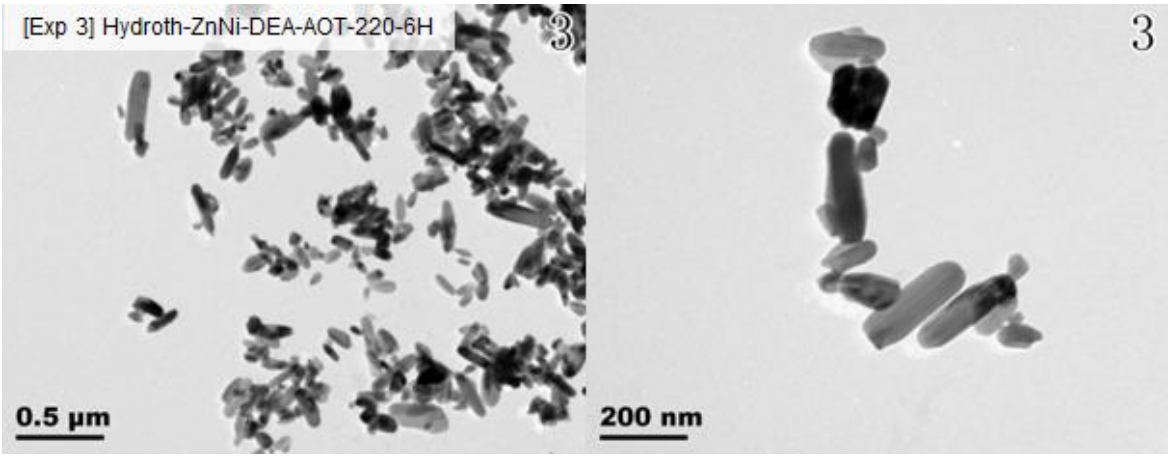

Figure 5-42: TEM micrograph of the particles prepared by the reactions between DEA and $Zn(NO_3)_2$ in the presence of PEG followed by hydrothermal treatment at 220°C for 6 hours (Experiment 3)

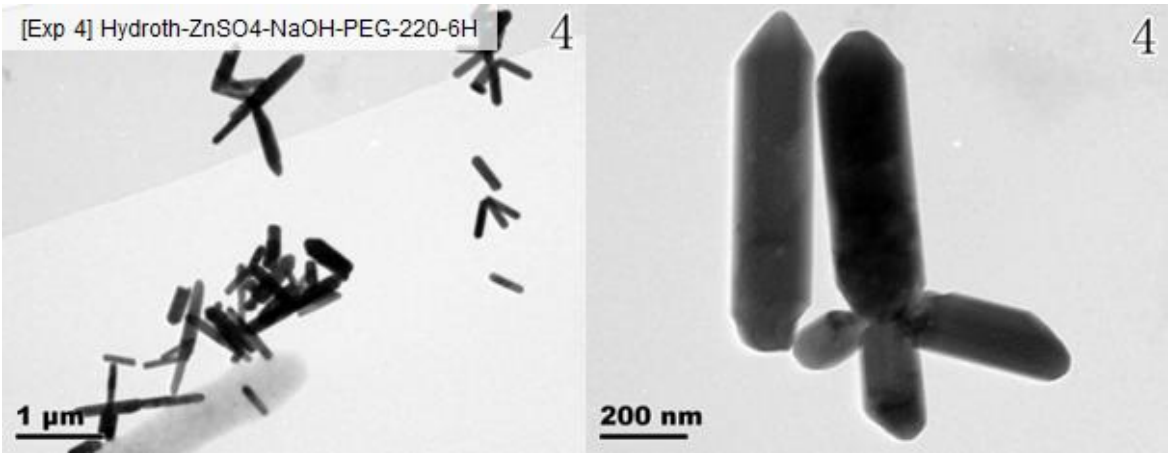

Figure 5-43: TEM micrograph of the particles prepared by the reactions between NaOH and $ZnSO_4$ in the presence of PEG followed by hydrothermal treatment at 220°C for 6 hours (Experiment 4)

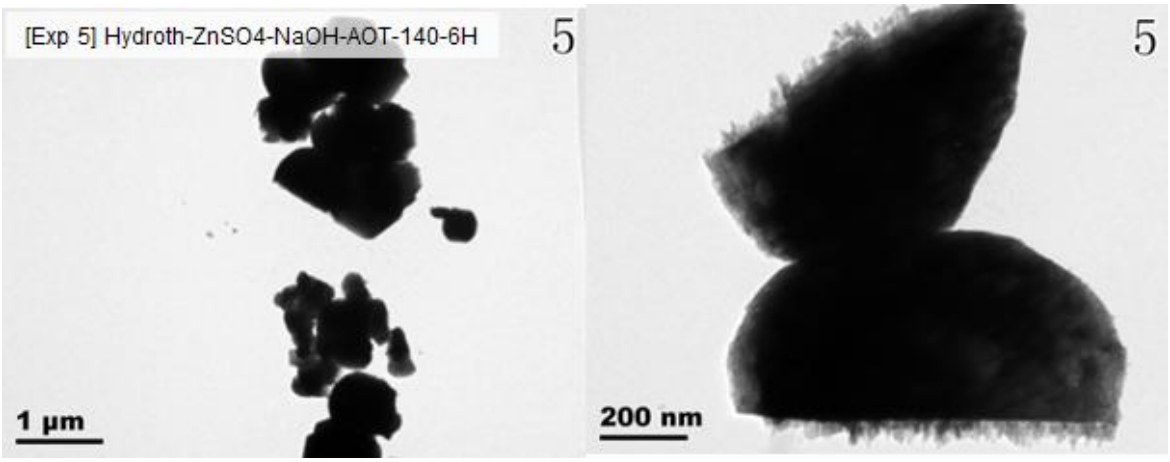

Figure 5-44: TEM micrograph of the particles prepared by the reactions between NaOH and $ZnSO_4$ in the presence of AOT followed by hydrothermal treatment at 140°C for 6 hours (Experiment 5)

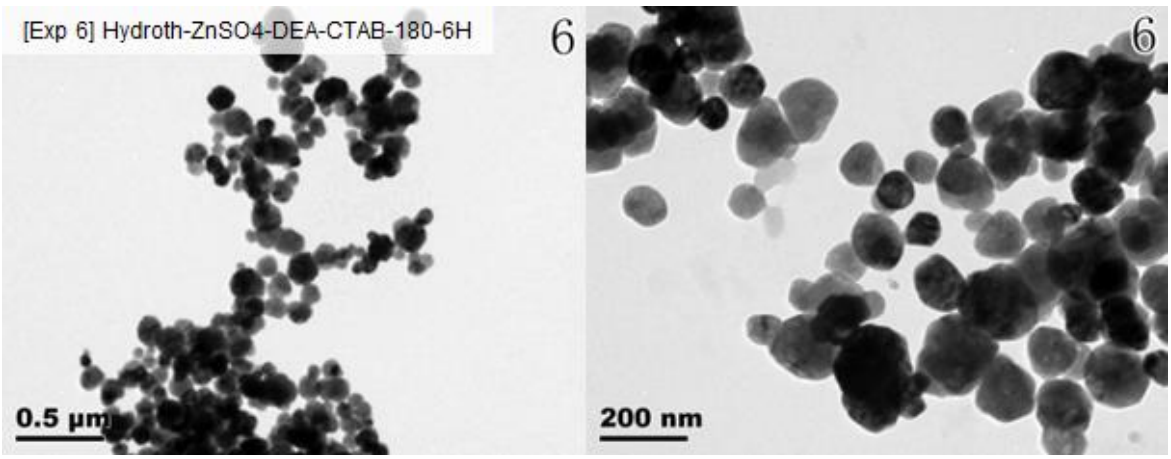

Figure 5-45: TEM micrograph of the particles prepared by the reactions between DEA and $ZnSO_4$ in the presence of CTAB followed by hydrothermal treatment at 180°C for 6 hours (Experiment 6)

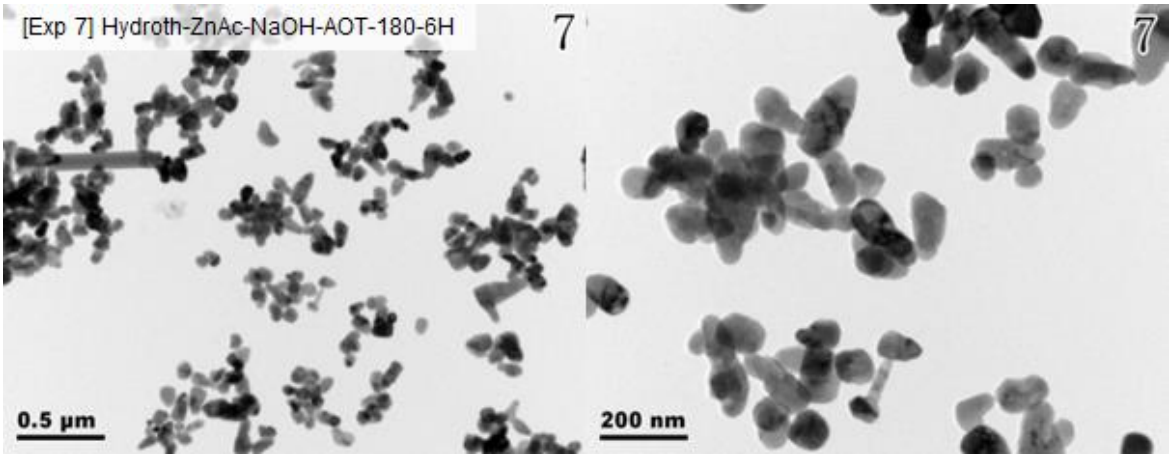

Figure 5-46: TEM micrograph of the particles prepared by the reactions between NaOH and $Zn(CH_3COO)_2 \cdot 2H_2O$ in the presence of AOT followed by hydrothermal treatment at 180°C for 6 hours (Experiment 7)

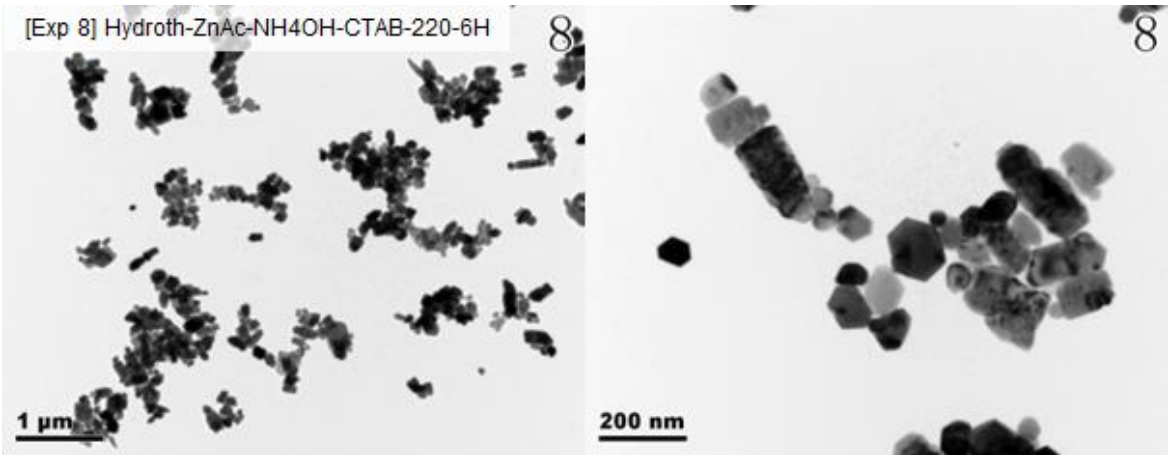

Figure 5-47: TEM micrograph of the particles prepared by the reactions between NH_4OH and $Zn(CH_3COO)_2 \cdot 2H_2O$ in the presence of CTAB followed by hydrothermal treatment at 220°C for 6 hours (Experiment 8)

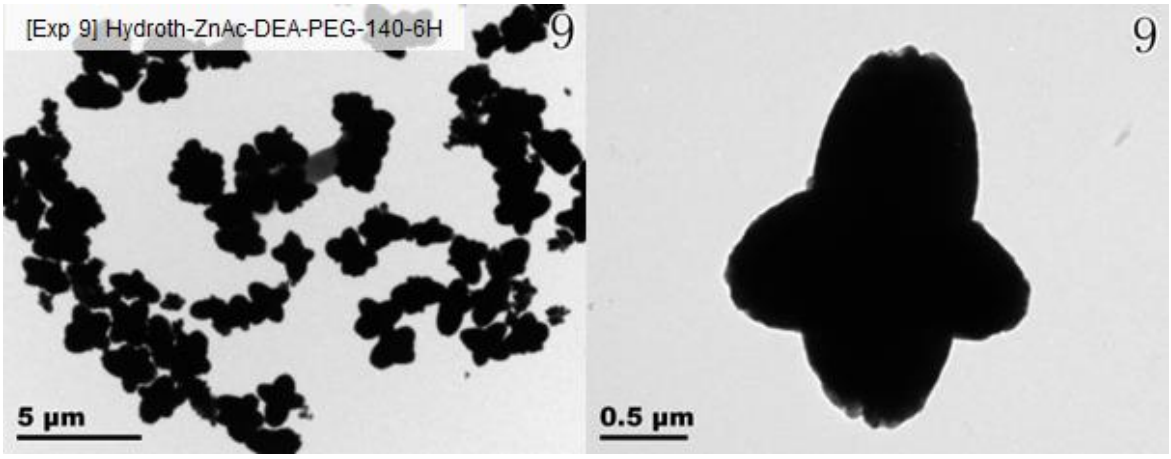

Figure 5-48: TEM micrograph of the particles prepared by the reactions between DEA and $Zn(CH_3COO)_2 \cdot 2H_2O$ in the presence of PEG followed by hydrothermal treatment at 140°C for 6 hours (Experiment 9)**.**

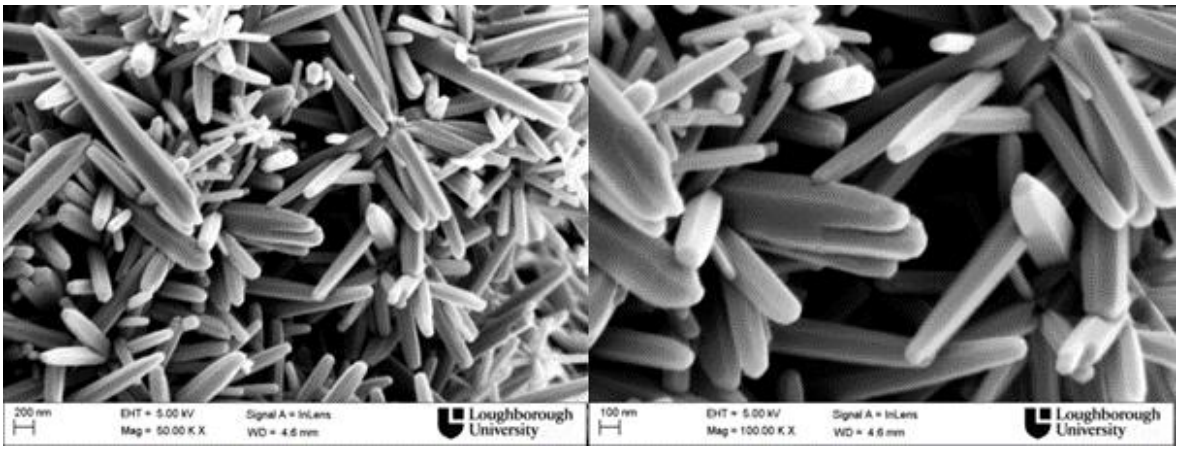

Figure 5-49: FEGSEM micrographs of the synthesized ZnO nanorods in prepared by the reactions between NaOH and $ZnSO_4$ in the presence of PEG followed by hydrothermal treatment at 220°C for 6 hours (Experiment 4)

It can be seen from these TEM and FEGSEM micrographs that ZnO with different sizes and morphologies including spindle-like (Figure 5-40), rod-like (Figure 5-41, Figure 5-42, Figure 5-43), semicircle shape (Figure 5-44), anisotropic nanoparticles (Figure 5-45, Figure 5-46, Figure 5-47), nanoellipse (Figure 5-48) were synthesized by varying hydrothermal processing parameters.

A summary of the particle sizes and morphologies of the first group of orthogonal design via hydrothermal is given in Table 6-12. The aspect ratio (average length/average width L/D) was used as the criteria for selection of optimising combination of the synthetic conditions to produce the ZnO particles with controlled particle size and, in particular, morphology, which is presented in Table 5-6 including the analysis of the experimental results based on orthogonal design approach.

Table 5-6: Summary of results of the first orthogonal experiments.

Figure	Morphology	Average length (L) (nm)	Average width (D) (nm)
Figure 5-40	Flower-like	850	600
Figure 5-41	Rod-like	2170	270
Figure 5-42	Rod-like	270	90
Figure 5-43	Rod-like	820	182
Figure 5-44	Semicircle-like	920	480
Figure 5-45	spherical-like	100	96
Figure 5-46	spherical-like	120	48
Figure 5-47	Spherical /small rod-like	100	66
Figure 5-48	Ellipse-like	2500	1000

From the analysis results in Table 5-7 the δ values show that the change of the surfactant (factor C) has the most significant effect on the aspect ratio of the particles synthesized. The K values indicate that the most influence to the aspect ratio of the particles for a single factor with corresponding levels is C2: surfactant PEG, then A1: zinc salt precursor [$Zn(NO_3)_2 \cdot 6H_2O$], B2: NH_4OH base solution and hydrothermal temperature at 180°C.

Therefore, it can be concluded from the first group that the influences of factors on the L/W ratios decrease in the sequence of surfactant, zinc salt, temperature and base. The

combination of optimum parameters that affects the L/W ratio of synthesized ZnO most is $Zn(NO_3)_2 \cdot 6H_2O$, NH_4OH, PEG, 180 °C.

Table 5-7: The aspect ratios of the particles and analysis of Orthogonal array 1.

Fact / Expt. No.	A [Zinc salt]	B [Base]	C [Surfactant]	D [Temp. °C]	Aspect Ratio (L/D)
Figure 5-40	$Zn(NO_3)_2 \cdot 6H_2O$	NaOH	CTAB	140	1.4
Figure 5-41		NH_4OH	PEG	180	8.0
Figure 5-42		DEA	AOT	220	3.0
Figure 5-43	$ZnSO_4 \cdot 7H_2O$	NaOH	PEG	220	4.5
Figure 5-44		NH_4OH	AOT	140	1.9
Figure 5-45		DEA	CTAB	180	1.0
Figure 5-46	$Zn(C_2H_4O_2)_2 \cdot 2H_2O$	NaOH	AOT	180	2.5
Figure 5-47		NH_4OH	CTAB	220	1.5
Figure 5-48		DEA	PEG	140	2.5
K_1	12.4	8.4	3.9	5.8	
K_2	7.4	11.4	15.0	11.5	
K_3	6.5	6.5	7.4	9.0	
k_1	4.13	2.80	1.30	1.93	
k_2	2.47	3.80	5.00	3.83	
k_3	2.17	2.17	2.47	3.00	
δ	1.96	1.63	3.70	1.90	
Rank of δ	C > A > D > B				
Optimum parameter	A_1	B_2	C_2	D_2	

Two optimum parameter: surfactant of PEG and hydrothermal temperature of 180°C plus two other "moderate" parameters: $ZnSO_4 \cdot 7H_2O$ as the zinc salt precursor and NaOH as the base solution were chosen for another group of orthogonal design experiment in order to investigate other factors including hydrothermal time, amount of surfactant and pH value as the three factors in the second group and each of them had 3 different levels as listed in Table 5-8 and the subsequent $L_9(3^3)$ array for the second group was presented in Table 5-9. These 9 experiments used $ZnSO_4 \cdot 7H_2O$, NaOH and PEG as starting materials and were conducted at 180 °C.

Table 5-8: Three factors with their corresponding levels chosen in the 2nd group

Level		1	2	3
Factor	Time	2h	4h	6h
	Surfactant amount	0.00025mol	0.0005 mol	0.001 mol
	pH value	≈ 11.5	≈ 10.5	≈ 12.5

Table 5-9: The details of the experiment - $L_9(3^3)$ array designed for the 2nd group

Expt. number	Time (h)	Surfactant Amount (mol)	pH value
1	2	0.00025	11.5±0.2
2		0.0005	10.0±0.2
3		0.001	12.8±0.2
4	4	0.00025	10.0±0.2
5		0.0005	12.8±0.2
6		0.001	11.5±0.2
7	6	0.00025	12.8±0.2
8		0.0005	11.5±0.2
9		0.001	10.0±0.2

Figure 6-24 shows the micrographs of the ZnO particles synthesised based on the 2nd group if orthogonal design and a FEGSEM micrograph of the particles prepared using conditions for experiment 2 is shown in Figure 6-25.

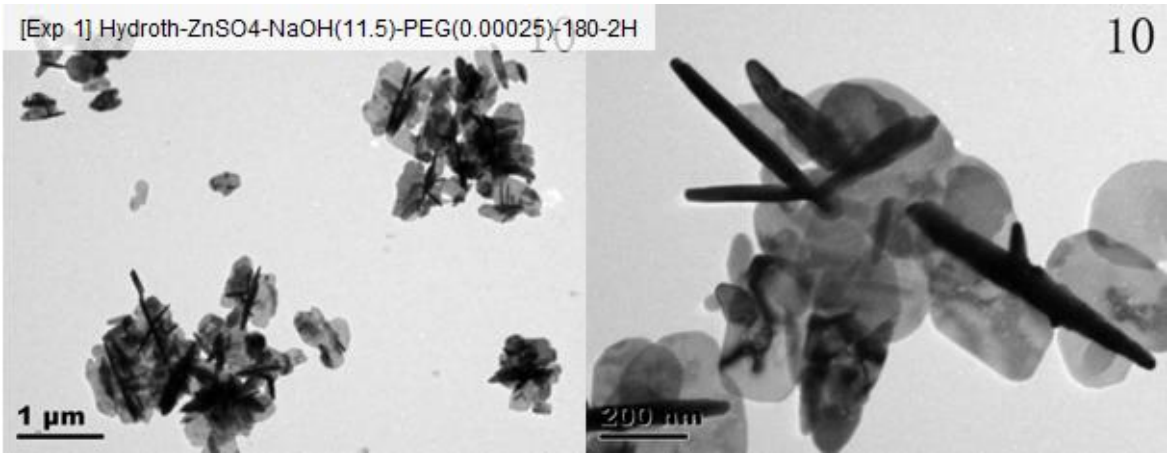

Figure 5-50: TEM micrograph of the particles prepared by the reactions between NaOH (ph = 11.5) and $Zn(SO)_4$ in the presence of PEG (0.00025 mol.) followed by hydrothermal treatment at 180°C for 2 hours (Experiment 1)

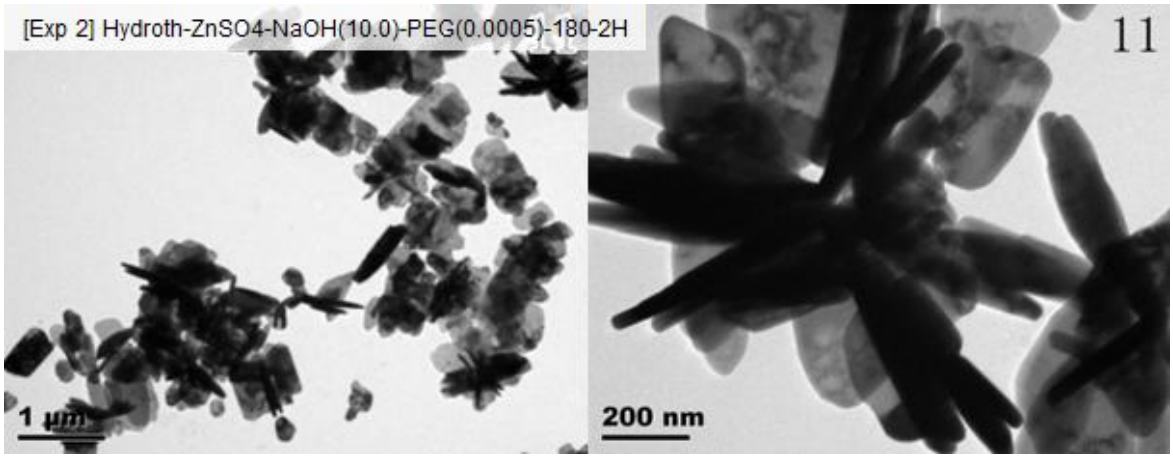

Figure 5-51: TEM micrograph of the particles prepared by the reactions between NaOH (ph = 10.0) and $Zn(SO)_4$ in the presence of PEG (0.0005 mol.) followed by hydrothermal treatment at 180°C for 2 hours (Experiment 2)

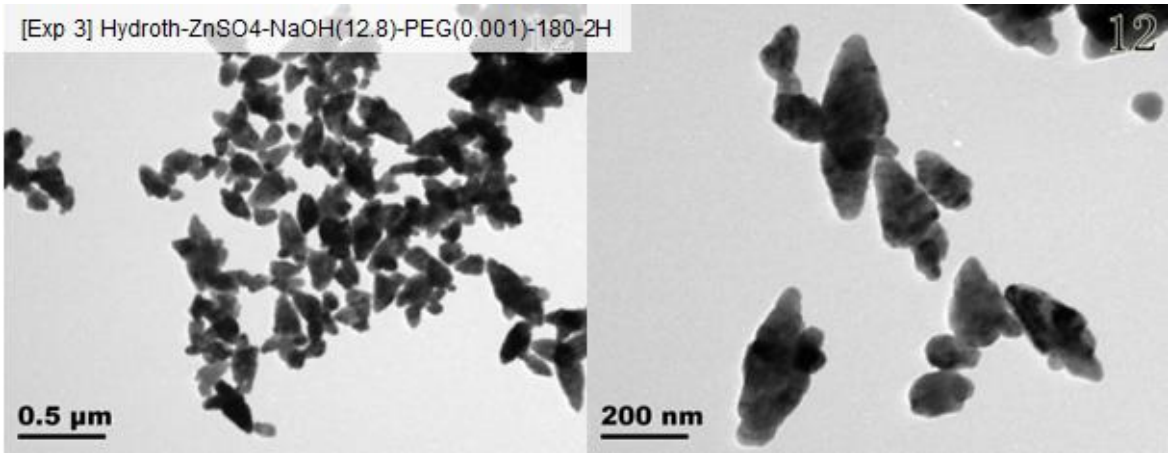

Figure 5-52: TEM micrograph of the particles prepared by the reactions between NaOH (ph = 12.8) and $Zn(SO)_4$ in the presence of PEG (0.001mol.) followed by hydrothermal treatment at 180°C for 2 hours (Experiment 3)

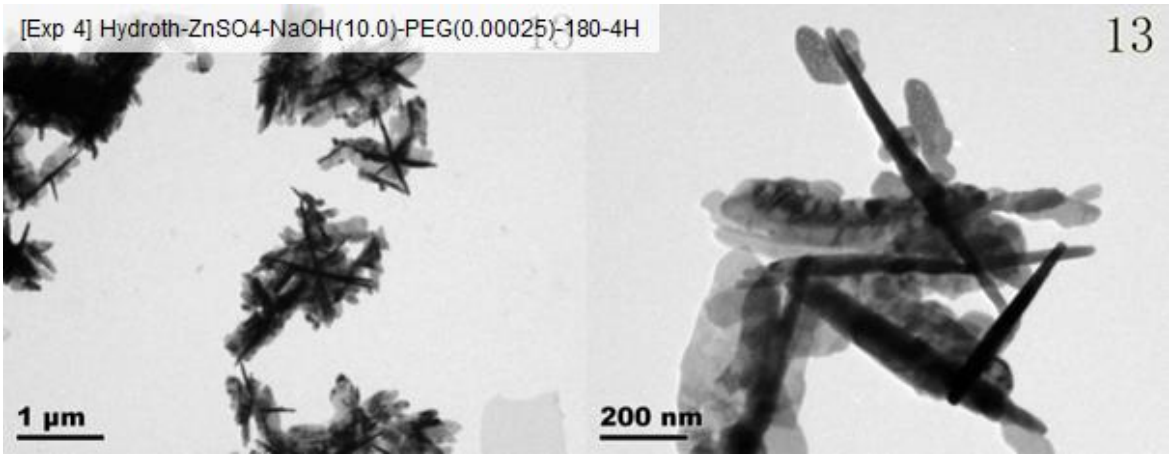

Figure 5-53: TEM micrograph of the particles prepared by the reactions between NaOH (ph = 10.0) and $Zn(SO)_4$ in the presence of PEG (0.00025 mol.) followed by hydrothermal treatment at 180°C for 4 hours (Experiment 4)

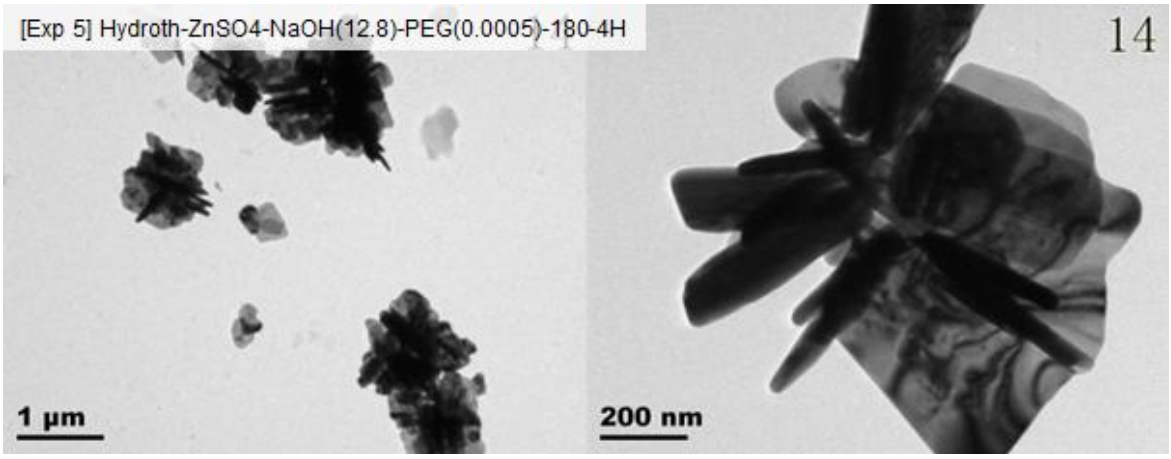

Figure 5-54: TEM micrograph of the particles prepared by the reactions between NaOH (ph = 12.8) and $Zn(SO)_4$ in the presence of PEG (0.0005mol.) followed by hydrothermal treatment at 180°C for 4 hours (Experiment 5)

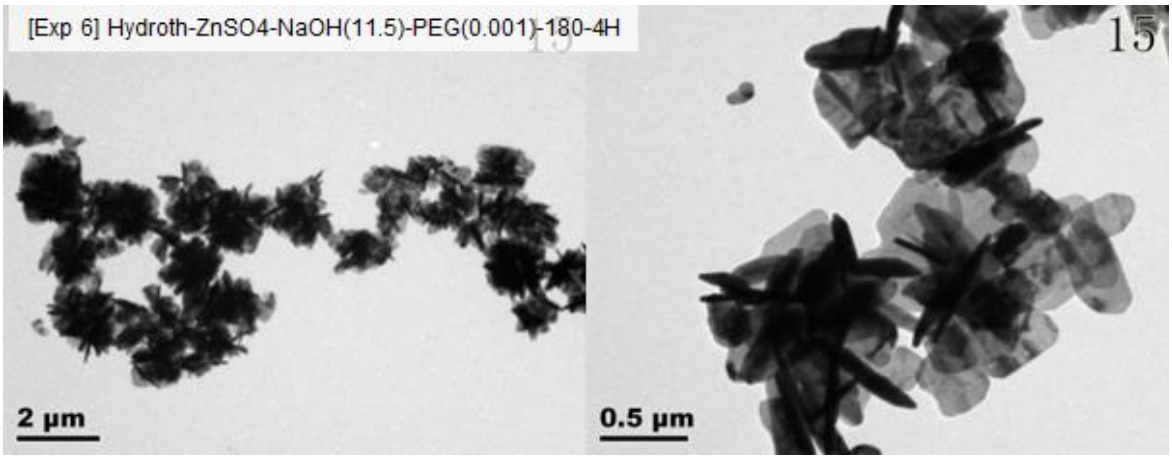

Figure 5-55: TEM micrograph of the particles prepared by the reactions between NaOH (ph = 11.5) and $Zn(SO)_4$ in the presence of PEG (0.001mol.) followed by hydrothermal treatment at 180°C for 2 hours (Experiment 6)

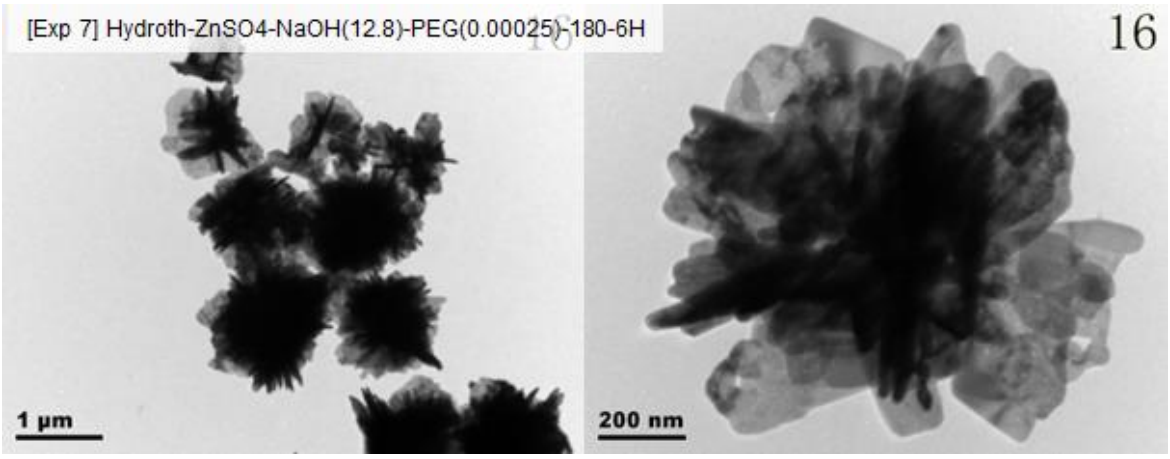

Figure 5-56: TEM micrograph of the particles prepared by the reactions between NaOH (ph = 12.8) and $Zn(SO)_4$ in the presence of PEG (0.00025mol.) followed by hydrothermal treatment at 180°C for 6 hours (Experiment 7)

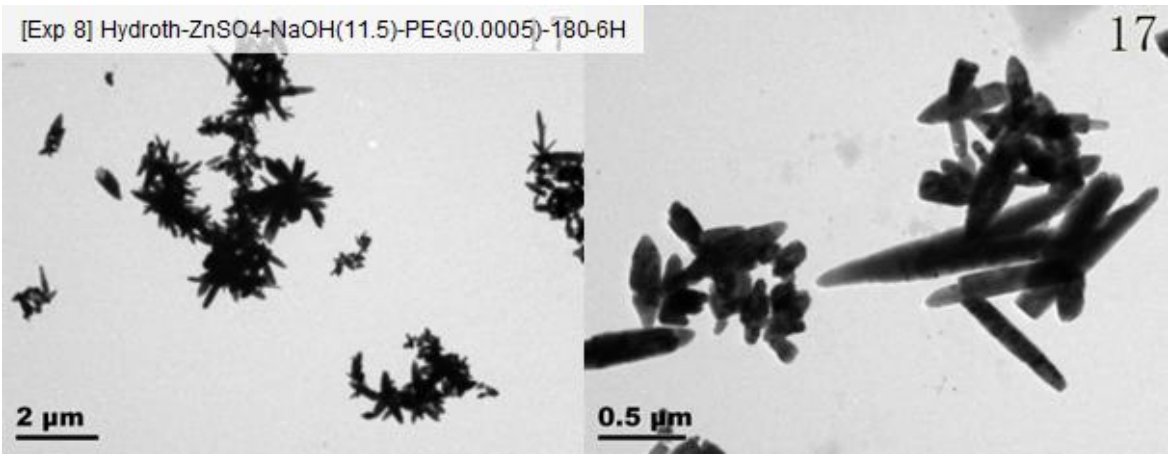

Figure 5-57: TEM micrograph of the particles prepared by the reactions between NaOH (ph = 11.5) and $Zn(SO)_4$ in the presence of PEG (0.0005mol.) followed by hydrothermal treatment at 180°C for 6 hours (Experiment 8)

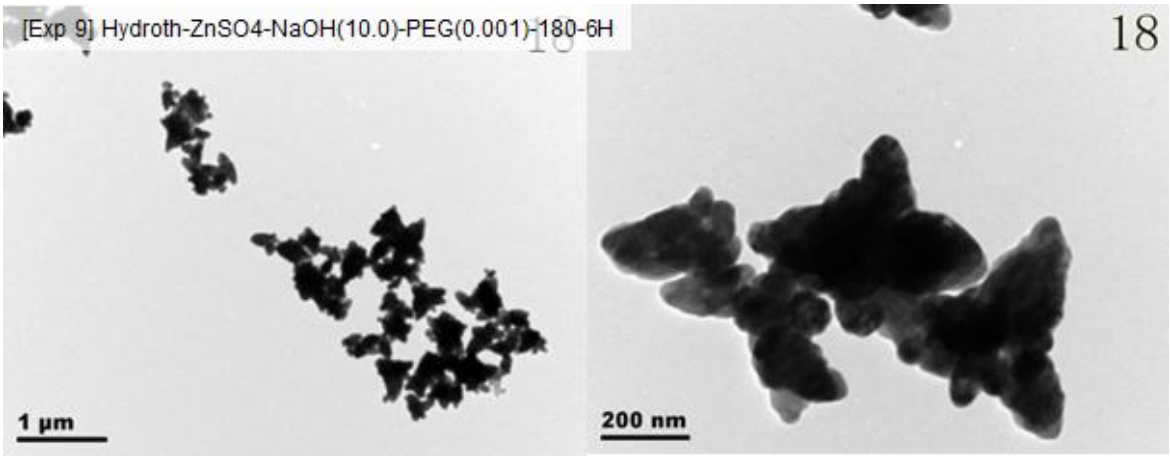

Figure 5-58: TEM micrograph of the particles prepared by the reactions between NaOH (ph = 10.0) and $Zn(SO)_4$ in the presence of PEG (0.001mol.) followed by hydrothermal treatment at 180°C for 6 hours (Experiment 3)

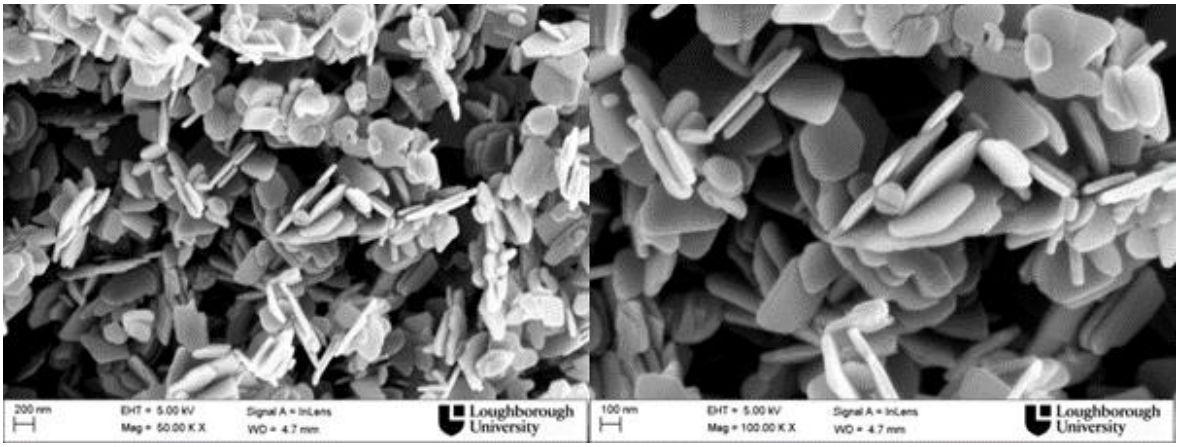

Figure 5-59: FEGSEM micrographs of the synthesized flake-like ZnO prepared TEM micrograph of the particles prepared by the reactions between NaOH (ph = 10.0) and $Zn(SO)_4$ in the presence of PEG (0.0005 mol.) followed by hydrothermal treatment at 180°C for 2 hours (Experiment 2)

It can be seen from these TEM and FEGSEM micrographs that ZnO with different sizes and morphologies including flake-like (Figure 5-50, Figure 5-51, Figure 5-53, Figure 5-54, Figure 5-55), tip-like anisotropic nanoparticles (Experiment No. Figure 5-52, Figure 5-58) were synthesized by varying hydrothermal processing parameters such as precursors, time, temperature, pH and surfactants. A summary of the particle size and morphology of the particles synthesised is presented in Table 5-10. The aspect ratio of the particles and the analysis results of 2nd group of orthogonal design are given in Table 5-11.

Table 5-10: A summary of results of the first orthogonal experiments.

Figure	Morphology	Average length (L) (nm)	Average width (D) (nm)
Figure 5-50	Flake-like / Rod-like	420	144
Figure 5-51	Flake-like / Rod-like	450	127
Figure 5-52	Tip-like	267	127
Figure 5-53	Flake-like / Rod-like	680	120
Figure 5-54	Flake-like / Rod-like	480	145
Figure 5-55	Flake-like / Rod-like	570	220
Figure 5-56	Spherical-like	1200	1000
Figure 5-57	Rod-like	720	180
Figure 5-58	Tip-like	310	130

Table 5-11: The aspect ratios of the particles and analysis of Orthogonal Array 2.

Factor / Expt. No.	E [Time (h)]	F [Surfactant Amount (g)]	G [pH value]	R (L/W ratio)
Figure 5-50	E_1 [2]	F_1 [0.1]	G_1 [≈ 11.5]	2.9
Figure 5-51		F_2 [0.2]	G_2 [≈ 10.5]	3.5
Figure 5-52		F_3 [0.4]	G_3 [≈ 12.5]	2.1
Figure 5-53	E_2 [4]	F_1	G_2	5.7
Figure 5-54		F_2	G_3	3.3
Figure 5-55		F_3	G_1	2.6
Figure 5-56	E_3 [6]	F_1	G_3	1.2
Figure 5-57		F_2	G_1	4.0
Figure 5-58		F_3	G_2	2.4
K1	8.5	9.8	9.9	
K2	11.6	10.8	11.6	
K3	7.6	7.1	6.6	
k1	2.8	3.3	3.3	
k2	3.9	3.6	3.9	
k3	2.5	2.4	2.2	
Δ	1.4	1.2	1.7	
Rank	G > E> F			
Optimum parameter	E_2	F_2	G_2	

It can be seen from both Table 5-10 and Table 5-11 the change of hydrothermal temperature, the pH value and the amount of surfactant all has effect on the particle size, morphology and aspect ratio of the ZnO particles hydrothermally synthesised. The L/W ratio of the particles decreased with the increase of pH value but had an optimum surfactant amount and hydrothermal time for achieving highest aspect ratio. The combination of optimum parameters that influences the L/W ratios most is 4h, 0.0005mol PEG, pH ≈ 10.5.

The confirmation experiment was carried out using the optimum parameters obtained from the two groups of orthogonal experiments (Table 4-4, Table 5-11) using hydrothermal processing (Table 5-12). TEM micrographs of the confirmation experiment are displayed in Figure 6-26. ZnO particles with the morphology of nanorods were synthesized.

Table 5-12: Processing conditions of the confirmation experiment

Zinc salt	Base	Surfactant & amount	Temperature	Time	pH value
$Zn(NO_3)_2 \cdot 6H_2O$	NH_4OH	0.0005 mol PEG	180 °C	6h	10.0±0.2

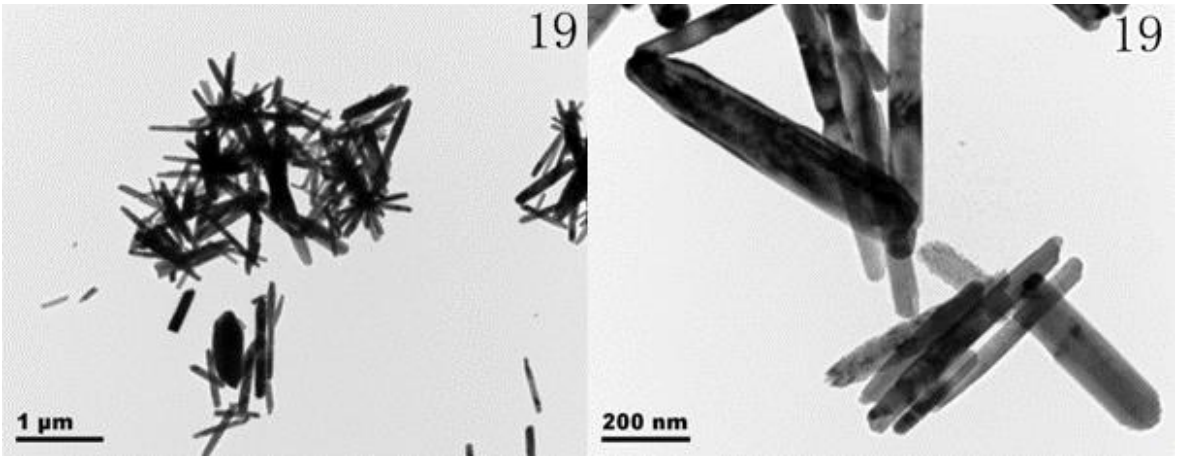

Figure 5-60: TEM micrographs of ZnO nanorods synthesized in the confirmation experiment

The L/D ratio of ZnO nanorods obtained in this confirmation experiment is 9.4. This value is larger than the L/D ratios of ZnO nanoparticles synthesized in orthogonal experiments which range from 1.0 to 8.0. This result is in good agreement with the prediction. This successfully proves the applicability of orthogonal experiment design used in the hydrothermal synthesis of ZnO nanomaterials to analyse the effect of varying processing parameters on the sizes and morphologies of ZnO.

The phase structure of the as-obtained ZnO products was characterised by XRD. A typical XRD pattern of the as-synthesized ZnO is displayed in Figure 6-27.

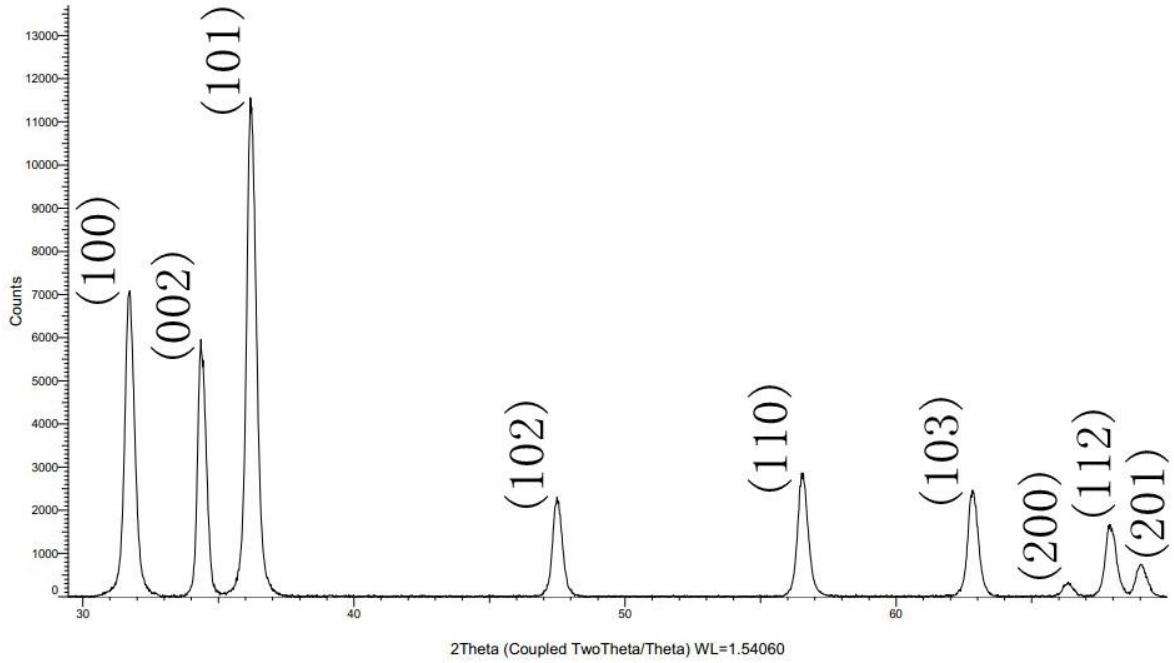

Figure 5-61: XRD pattern of synthesized ZnO product (Confirmation experiment)

All the detected peaks in Figure 6-26 can be well indexed to the typical crystallised hexagonal wurzite structure of ZnO (lattice constants a = 0.325 nm and c = 0.521 nm), which are in good conformity with the values in Joint Committee on Powder Diffraction Standards (JCPDS) No. 36-1451 [8, 47]. More specifically, the nine peaks detected at 31.8, 34.50, 36.3, 47.6, 56.7, 63.0, 68.0 and 19.2° 2θ in Figure 6-26 are in consistence with the diffraction from the (1 0 0), (0 0 2), (1 0 1), (1 0 2), (1 1 0), (1 0 3), (2 0 0), (1 1 2), (2 0 1) planes of the hexagonal structure of ZnO respectively [52, 53]. The narrow but strong diffraction peaks detected suggest that the as-synthesized ZnO nanomaterials have good crystallinity. The full width at half maximum (FWHM) of the (1 0 1) peak is the narrowest

among all the detected peaks. This means the growth of ZnO nanomaterials is preferred along the direction of (1 0 1) plane. No characteristic peaks from precursors (such as NaOH) and intermediates (such as $Zn(OH)_2$) are observed from the pattern within the XRD detection limit.

5.3 Synthesis of Aluminium Doped ZnO (AZO) via hydrothermal

AZO nanomaterials were synthesized using $ZnSO_4 \cdot 7H_2O$ as zinc salt precursor, $AlCl_3 \cdot 6H_2O$ as aluminium salt precursor and NaOH as the base solution (pH = 10±0.2). PEG was used as the non-ionic surfactant and the solution was hydrothermally treated at 220 °C for 6 h. The Al/Zn ratios fixed at 3 at.%, 5 at.% and 10 at.% respectively, as presented in

Table 5-13: The experimental details of synthesising AZO via hydrothermal

Sample	Zinc salt	Base	Surfact	Temp (℃)	Time (h)	pH	Dopant
AZO-1HT	0.005 mol	NaOH	0.0005 mol	220	6	10.0±0.2	0.00015 mol
AZO-2HT	0.005 mol	NaOH	0.0005 mol	220	6	10.0±0.2	0.00025 mol
AZO-3TH	0.005 mol	NaOH	0.0005 mol	220	6	10.0±0.2	0.0005 mol

TEM micrographs of the AZO nanoparticles synthesized with Al/Zn ratio of 3 at.%, 5 at.% and 10 at.% are shown in Figure 5-64, Figure 5-63 and Figure 5-64, respectively.

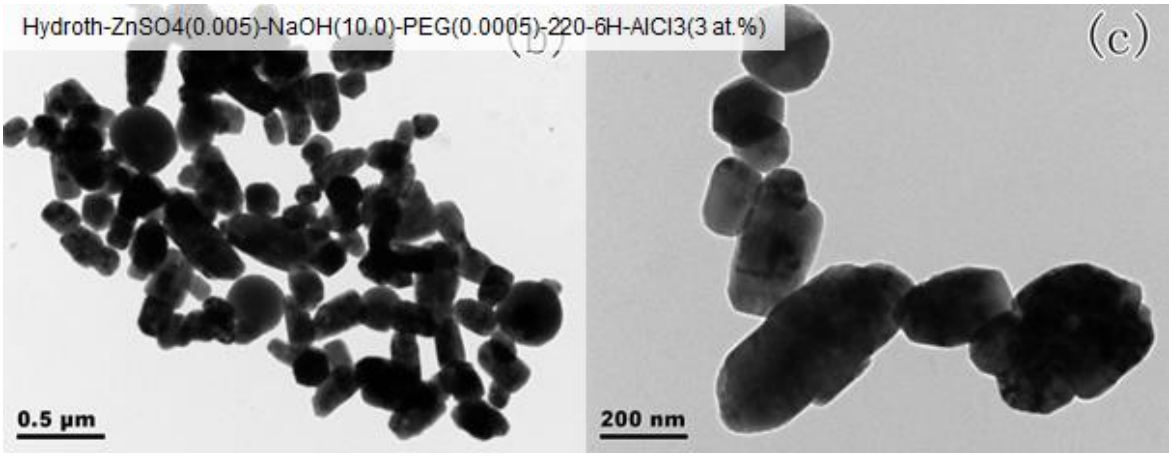

Figure 5-62: TEM micrographs of AZO nanomaterials with Al/Zn ratio of 3 at.%

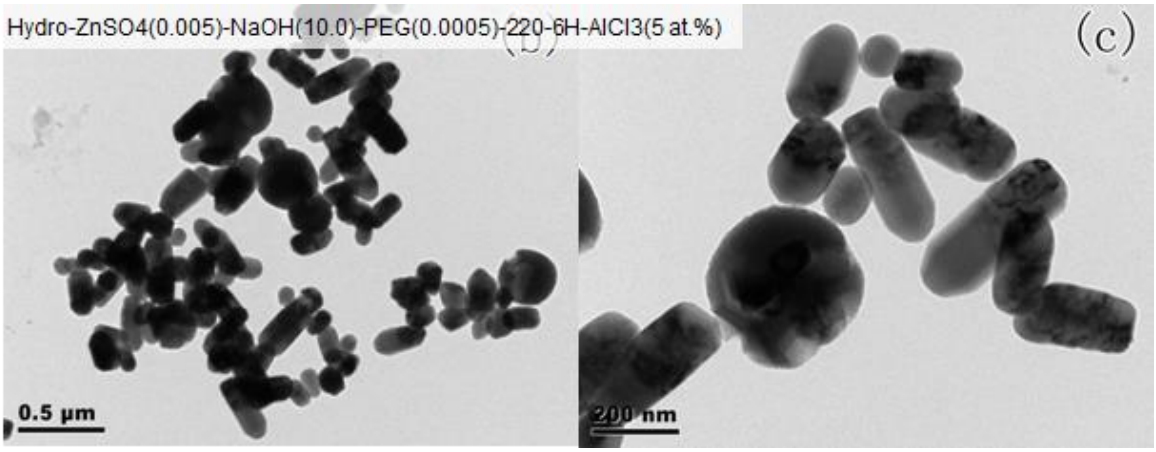

Figure 5-63: TEM micrographs of AZO nanomaterials with Al/Zn ratio of 5 at.%

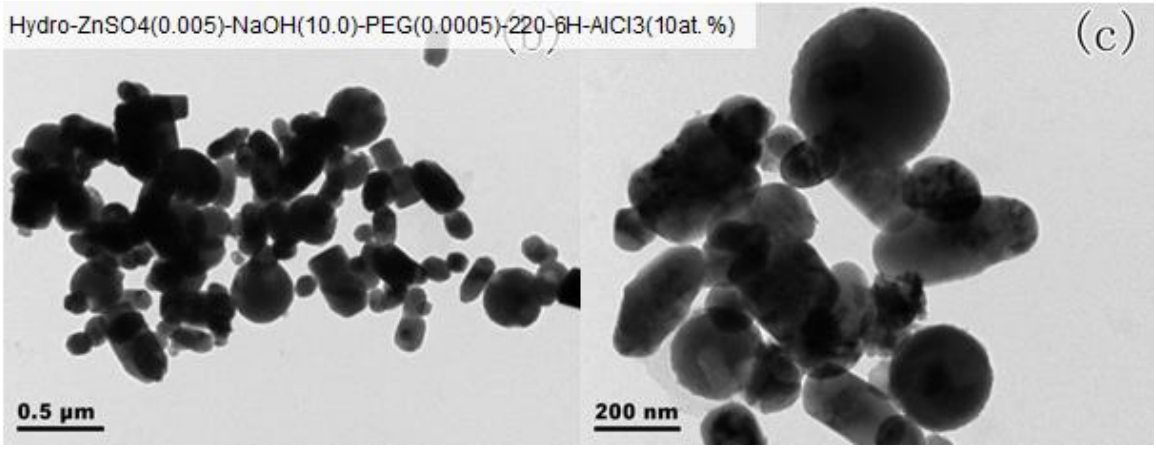

Figure 5-64: TEM micrographs of AZO nanomaterials with Al/Zn ratio of 10 at.%

It can be seen that AZO with different morphologies were obtained when different concentration of the aluminium atomic content was used. Two different shapes of the

synthesized AZO are observed from the TEM micrographs above: nanorod and nanosphere, with the nanosphere particles well dispersed among nanorods. It can be seen that the percentage of the observed nanospheres increases with the increasing Al/Zn atomic ratios.

Energy-dispersive X-ray (EDX) spectroscopy was carried out to examine the elemental information about these two morphologies and sample AZO-3HT was taken as the example. EDX is a technique which utilises backscatted electrons from an electron microscopy beam to identify particular elements and their relative portions. Figure 5-65 is the TEM image of the area chosen to be analysed by EDX. The red circles marked in Figure 6-31 illustrate the two parts of the morphologies examined. Correspondingly, the two EDX spectra generated from the nanorod and nanosphere morphologies are displayed in Figure 5-66 (a) and (b) respectively.

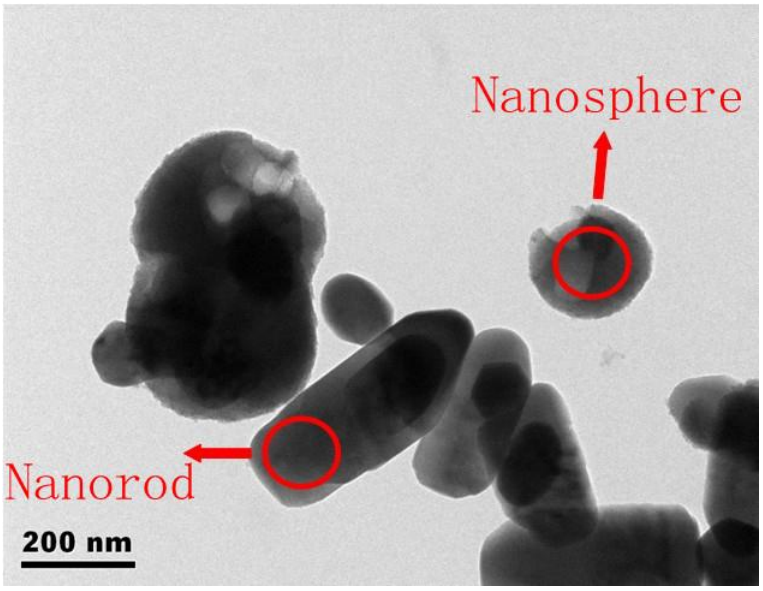

Figure 5-65: TEM image with two selected morphologies for EDX analysis

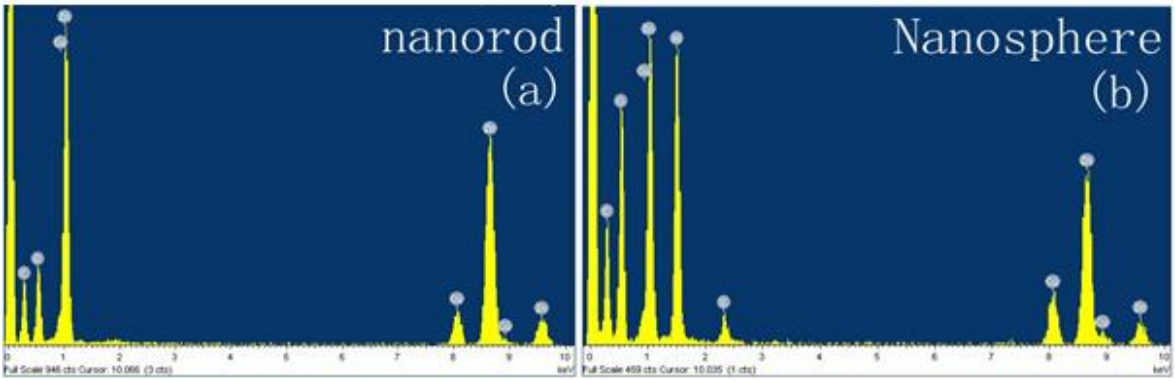

Figure 5-66: EDX spectra of: (a) nanorod morphology; (b) nanosphere morphology

It can be seen from the above two EDX spectra that only zinc, oxygen, copper and carbon were detected in the nanorod morphology while zinc, oxygen, aluminium, sulphur, copper and carbon were detected in the nanosphere morphology. The copper and carbon detected come from the carbon film coated brass grid used in TEM sample preparation. EDX patterns show that there is a small amount of sulphur presented in the spectrum of the nanosphere structure, which probably comes from the starting zinc salt $ZnSO_4 \cdot 7H_2O$, probably due to unreacted parts of the zinc salt which were not removed completely during the washing procedure. The weight and atomic percentages of all detected elements in nanorod and nanosphere morphologies from the EDX analysis are listed in Table 5-14.

Table 5-14: Weight and atomic percentages of detected elements in nanorod and nanosphere morphologies

Element	Nanorod		Nanosphere	
	Weight (%)	Atomic (%)	Weight (%)	Atomic (%)
O	17.18	45.81	29.93	52.79
Al	0.12	0.20	25.85	27.03
S	0.04	0.06	2.43	2.14
Zn	82.65	53.94	41.79	18.04
Total	100		100	

From Table 5-14 the atomic ratio of Al:Zn:O:S is calculated as 0.0037 : 1 : 0.85 : 0.0011 in the nanorod morphology and 1.50 : 1 : 2.93 : 0.12 in nanosphere morphology.

It can be seen from the TEM and EDX analysis that aluminium predominantly exists in the nanosphere morphology of the as-synthesized AZO particles while zinc and oxygen exists in both nanorod and nanosphere morphologies. The randomly and evenly distributed nanospheres among nanorods indicate the dopant aluminium is very well dispersed in ZnO. The increasing amount of nanospheres with increasing Al/Zn atomic ratios (3 at.% to 10 at.%) identified in the TEM results indicate that a larger amount of aluminium is doped in ZnO when more aluminium salt is added at the beginning of the synthesis process.

XRD patterns of the as-synthesized AZO nanomaterials with Al/Zn ratio of 3 wt.%, 5 wt.% and 10 wt.% are displayed in Figure 5-67. No characteristic peaks of Al_2O_3 or impurities such as $ZnSO_4 \cdot 7H_2O$ were detected from the pattern within the XRD detection limit.

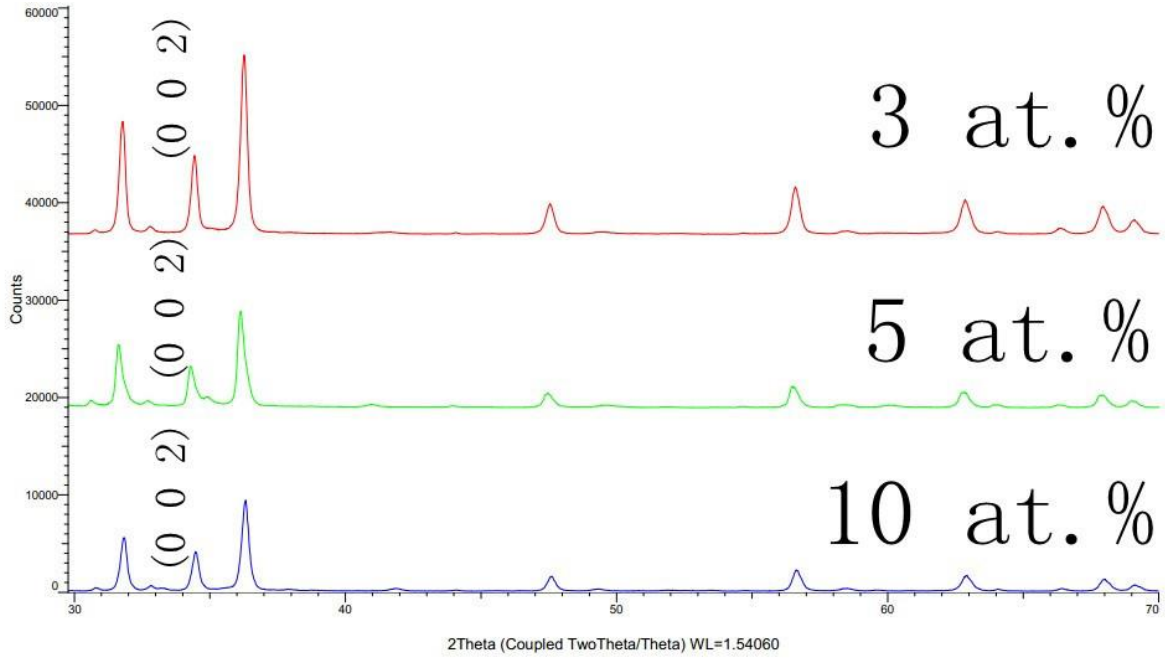

Figure 5-67: XRD patterns of AZO with 3 different Al/ZnO ratio: 3 at.%, 5 at.% and 10 at.%

Comparing Figure 5-67 for AZO with Figure 5-61 for pure ZnO, the detected diffraction peaks in AZO pattern are less sharp and strong than those observed in ZnO patterns. This indicates the presence of dopant Al in ZnO reducing crystallinity [60]. It can also be observed in Figure 5-67, the larger the Al/Zn ratio is, the less sharp and strong the detected diffraction peaks are, which indicates the increasing amount of Al atomic content in AZO reduces crystallinity [60].

The characteristic peaks in XRD patterns can be used to estimate the mean grain size of the synthesized AZO nanoparticles. If the estimation is based on one single peak, the chosen peak is best located between 30 and 50° 2θ. According to literature, the (0 0 2) plane is a commonly selected plane to investigate the grain size of AZO [60]. The estimation is calculated using the Scherrer formula and the crystal size of the particles are given in Table 5-15.

Table 5-15: Crystal size of the AZO particles calculated by Scherrer formula

Sample	Crystal Size
AZO-1HT	31.9
AZO-2HT	29.4
AZO-3HT	29.1

The comparison of three values shows the average grain size of AZO nanoparticles decreases with increasing Al atomic content. The sizes of AZO nanoparticles observed in TEM micrographs (Figure 5-62, Figure 5-63 and Figure 5-64) range from about one hundred to several hundred nanometres. The calculated grain sizes are smaller than the particle sizes observed in TEM images. This is probably because an AZO particle is made up of more than one grain [60].

Chapter 6 Discussion

The effects of synthetic conditions, surfactants, starting salts, types of base solution and hydrothermal parameters on the particle size, crystalline phases and morphologies of the ZnO particles synthesised are discussed below.

6.1 The formation mechanism of ZnO crystals

The XRD patterns (Figure 4-1 to Figure 4-3) obtained via co-precipitation indicated that Zn-O, Zn-O-H and secondary and unknown phases were obtained. The lattice structure of zinc blende and wurtzite ZnO is shown in Figure 6-1B and Figure 6-1C, respectively along with the rocksalt lattice (Figure 6-1A) [15, 19].

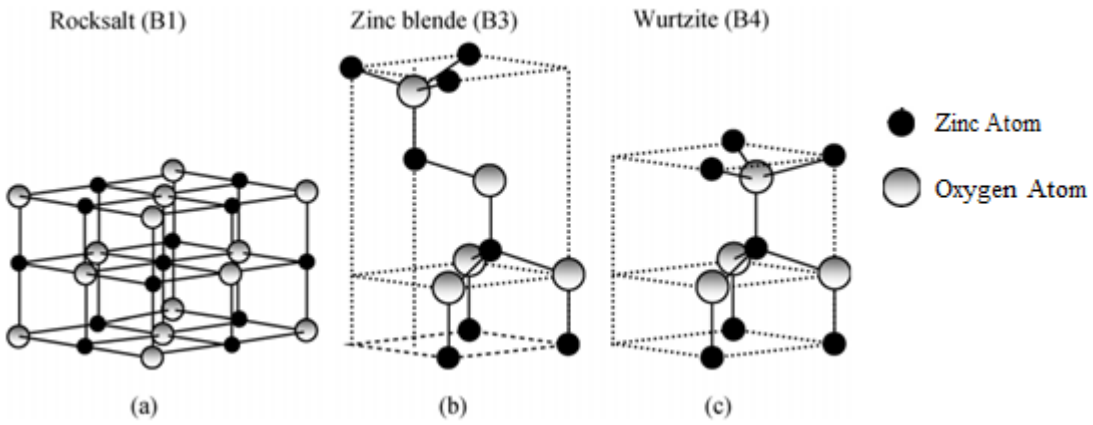

Figure 6-1: Ball and stick model of lattice structures of ZnO compounds: (a) rocksalt, (b) zinc blende, and (c) wurtzite [15, 19]. The black dots represent Zinc atoms and the white dots represent Oxygen atoms

The general concept involved in the synthesis of ZnO nanoparticles through co-precipitation is homogeneous nucleation and crystal growth [8, 69, 105]**.** This is initiated by the nuclei unit ($Zn(OH)_2$) and the growth unit ($[Zn(OH)_4]^{2-}$), separately and obtained according to the equations below [67-69]:

$$Zn^{2+} + 2OH^- \rightarrow Zn(OH)_2\downarrow \quad (6\text{-}1)$$

$$Zn^{2+} + 4OH^- \rightarrow [Zn(OH)_4]^{2-} \quad (6\text{-}2)$$

$$[Zn(OH)_4]^{2-} \rightarrow Zn(OH)_2 \downarrow + 2OH^- \quad (6\text{-}3)$$

$$Zn(OH)_2 \rightarrow ZnO \downarrow + H_2O \quad (6\text{-}4)$$

$$[Zn(OH)_4]^{2-} \rightarrow ZnO \downarrow + 2H_2O + 2OH^- \quad (6\text{-}5)$$

It is known that if the growth rate dominates the nucleation rate, the crystallite size increases. Conversely, if the nucleation rate dominates the growth rate, the crystallite size decreases. With regards to the formation of ZnO, the nucleation rate and growth rate is primarily governed by the Zn:OH ratio in the solution.

As the zinc concentration was fixed, the nucleation and growth rates could have only been changed by the pH of the solution. However, as reported following the co-precipitation orthogonal experiments (Section 4.2.5), it was the zinc source (e.g. $Zn(CH_3COO)_2$•$2H_2O$, $Zn(NO_3)_2$•$6H_2O$) which was found to be more influential. As the availability of Zn^{2+} was fixed, it is considered the anions e.g. CH_3COO^-, NO_3^-, and Cl^- were the primary cause of any influence on the compounds formed and where formed, ZnO particle aspect ratio.

This growth habit can be explained by a dissolution / re-precipitation mechanism [106, 107]. When zinc source is mixed with a base, $Zn(OH)_2$ precipitates **(6-1)** are formed. With the addition of more OH^- ions into the solution, some of the $Zn(OH)_2$ will transform to $[Zn(OH)_4]^{2-}$ (6-2), which means both $Zn(OH)_2$ and $[Zn(OH)_4]^{2-}$ are generated.

During the co-precipitation process, $Zn(OH)_2$ is formed by the dehydration of the $[Zn(OH)_4]^{2-}$ ions. (**6-3**) and for the $Zn(OH)_2$, the precipitates will dissolve to form Zn^{2+} and OH^-. When the concentration of Zn^{2+} and OH^- is greater than a critical value, ZnO crystals will be generated and precipitate from the solution. Due to the solubility of ZnO crystals being much lower than that of $Zn(OH)_2$, ZnO crystals are formed by the transformation of $Zn(OH)_2$

precipitates during the precipitation process **(6-4)**. It is likely that the formation of secondary and unknown phases was due to the critical value not being met (Figure 4-1C).

Where Zn-O was synthesised and confirmed by XRD (Figure 4-1A, Figure 4-1B), the difference in particle shape has been explained by H.Usui [108]. The ZnO crystals, and the ions generated or present within the solution, react on the crystals surfaces. For example, anions present in the solution (counter-ions), CH_3COO^-, NO_3^-, and Cl^- can influence the degree of aggregation and re-arrangement of primary particles. These anions are present due to the dissolution of the zinc salt in water [2]**.** The different anions from the different starting salts have their own individual properties. In addition, they can affect the chemistry at the crystal face (influence on the electrical double layer). This can lead to changes in energy distribution of the surface leading to subsequently changes in growth behaviour and morphologies [109].

In the formation of ZnO, when the concentration of Zn^{2+} and OH^- reach the super-saturation degree of ZnO, ZnO nuclei are considered to form. After the formation of ZnO nuclei, subsequent growth of the crystal occurs.

Figure 6-2 represents the effect of monomer concentration on crystal growth over time (La Mers principle) [110]. When the monomer concentration (in this case the growth unit $[Zn(OH)_4]^{2-}$) reaches a supersaturation level, seed nucleation occurs, with the monomer continuously aggregating. During these nucleation and growth stages, C_{Sat} and C_{Equil} control the control of growth parameters and phase. For example, when F68 and P123 were used as the surfactant, the $Zn(OH)_2$ phase was predominant, suggesting that C_{sat} had been raised to a level where nucleation of ZnO could not occur.

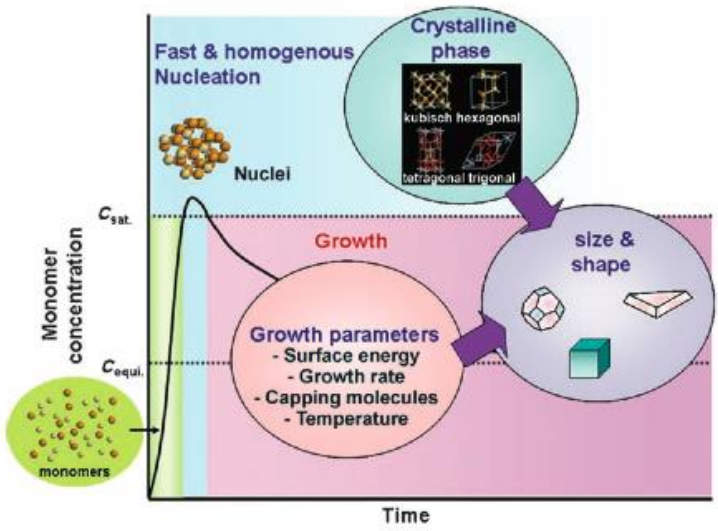

Figure 6-2: General representation of the effect of monomer concentration over time [110].

When zinc salt is dissolved in water, it exists in the form of Zn^{2+} and the anions (e.g. CH_3COO). Zn^{2+} reacts with OH^- when a base solution is added and forms $Zn(OH)_2$ white precipitates and the growth unit $[Zn(OH)_4]^{2-}$ (Equation 6-1, 6-2). $Zn(OH)_2$ and $[Zn(OH)_4]^{2-}$ are responsible for the homogeneous nucleation and crystal growth of ZnO respectively. After the appearance of $Zn(OH)_2$ units, the nucleation unit grew around the nuclei sites along the quickest growth plane. The equations indicate that in the solution, the supersaturated $Zn(OH)_2$ re-dissolves in solution and forms the $[Zn(OH)_4]^{2-}$by the attraction of ions.

The conversion between $Zn(OH)_2$ and $[Zn(OH)_4]^{2-}$ is affected by several processing variables such as temperature and pH value . The dissolution of $Zn(OH)_2$ in the solution provides Zn^{2+} and OH^-. ZnO will be crystallised from the solution and begin to grow when the concentration of Zn^{2+} and OH^- reaches the critical value that is required for the formation of ZnO (Equation 6-4, 6-5). $Zn(OH)_2$ is preferentially converted into ZnO because ZnO is much less soluble than $Zn(OH)_2$ in the solution [67, 69, 111, 112]

One possible reason is that $Zn(OH)_2$ and ZnO are formed simultaneously at first in the solution in co-precipitation process based on the mechanism discussed above. Hence, when the concentration of Zn^{2+} and OH^- was over the supersaturation degree of forming ZnO, $Zn(OH)_2$ phase can be transformed to ZnO phase at room temperature **(**6-4**)**. Another possible reason, investigated by Peterson et al. [113], is based on Figure 6-3 which suggests

that the formation of ZnO solid particles depended on both reaction pH and concentration of the zinc salt.

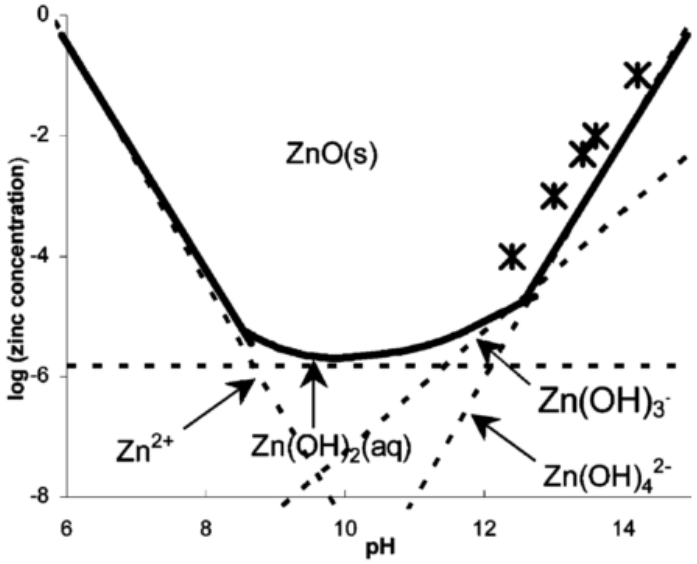

Figure 6-3: Phase transformation diagram of ZnO-H2O system at 25°C[113]

In this project, the concentration of the soluble Zn^{2+} was low. With the addition of the base solution, the pH value of the reactions was increased to around 10.0 to 12.8, depending on the amount of base solution added.

In comparison between the base sources, NaOH and TMAH are both regarded as “strong bases”. DEA is considered as a “weak base”. This difference was highlighted in the measured pH of the solutions. Solutions prepared with the strong bases had a pH recorded in the range of pH = 12.8±0.2. The solutions prepared with DEA were recorded in the range of pH = 10.0±0.2.

Based upon Figure 6-3 this would suggest that in the reaction with NaOH and TMAH, $[Zn(OH)_4]^{2-}$ would have been formed. The reaction with DEA would have led to the formation of $Zn(OH)_2$. In both case ZnO would not have formed. Li et al [114] have discussed that in solution, the growth unit can only dehydrate to $Zn_xO_y(OH)_z^{(z+2y-2x)-}$ (which forms clusters that eventually formed ZnO nuclei) under heat convection and subsequent diffusion of ions and deregulation movement among molecules and ions in the solution. It is presumed that the formation of ZnO was due to the vigorous stirring of the solution (4000 rpm for 30 minutes)

that generated the heat, diffusion and movement needed for the synthesis of ZnO. However, this theory could not be accurately measured and subsequently verified.

6.2 Comparison of co-precipitation and hydrothermal process

The morphology, the size, the crystallinity and the homogeneity of particles synthesised via hydrothermal treatment were different from the particles synthesised via co-precipitation process.

6.2.1 Comparison on morphology and size

The TEM images in Figure 6-4 clearly show the effects of hydrothermal treatment on the morphology and size of ZnO particles. The particle size synthesised by hydrothermal are much larger than that of co-precipitation. The particles synthesised via co-precipitation were short rod-like with a plain end or tip-like while the particles synthesised via hydrothermal showed long rod-like with a plain end or sword-like. In addition, the outline of the particles synthesised via hydrothermal were much smoother than that of co-precipitation.

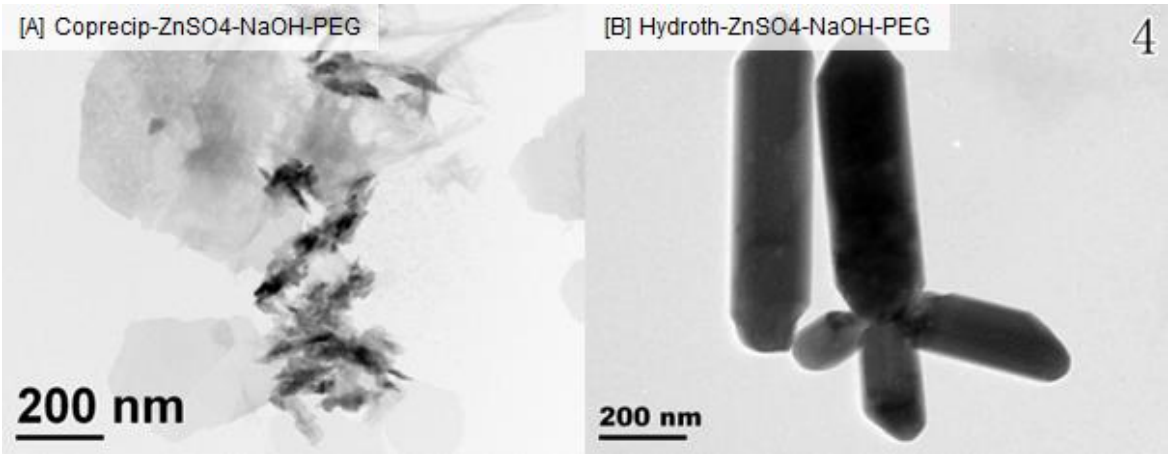

Figure 6-4: Comparison of ZnO synthesised by [A] co-precipitation [B] hydrothermal

In the first orthogonal experiment, with increasing temperature, the ZnO particles generally first tended to be pseudo-spherical-like (co-precipitation) and then a rod-like morphology.

This morphological change is similar to investigations by Zhang, Raoufi, Chen, Hong et al. [115-118].

Table 6-1: Resulting co-precipitation and hydrothermal morphologies from the first co-precipitation experiment

Co-precipitation morphology	Hydrothermal Morphology	Hydrothermal Temperature
Flower-like	Spindle-like	140
Rectangle-like	Rod-like	180
Spherical-like	Rod-like	220
Small needle/rod-like	Rod-like	220
Small rod-like	Semicircle-like	140
Spherical-like	Spherical-like	180
Spherical-like	Spherical-like	180
Spherical /small rod-like	Spherical /small rod-like	220
Spindle/rod-like	Ellipse-like	140

The possible mechanism for the formation of the rod-like particle is that the higher temperature supplied by the hydrothermal process provided sufficient activation energy which was above the free energy barrier. The provided energy dissolved the small nuclei and the dissolved small nuclei mostly tended to grow on the (0001) preferred crystal face of ZnO. Further discussion on the formation of rod-like particles is given in Section 6.3.3.

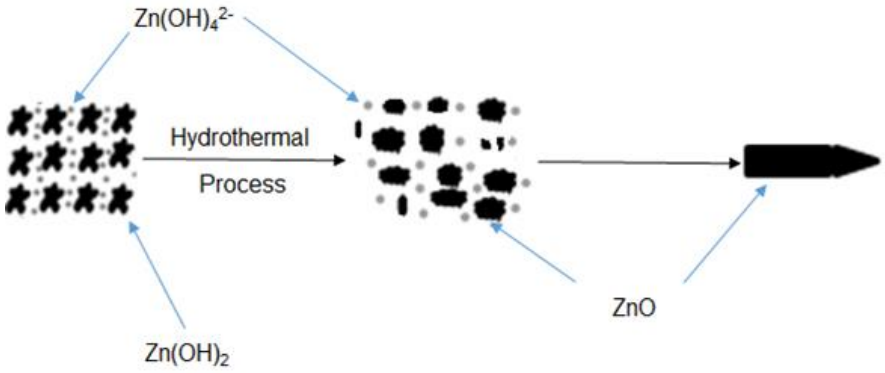

Figure 6-5: Illustration of possible mechanism in hydrothermal process.

The degree of supersaturation in La Mer's condition introduced in Section 6.1 (Figure 6-2) had an influence on the growth of the particles. With increasing temperature, the solubility of precipitating material decreased and subsequently a higher degree of supersaturation was acquired to drive particles to grow. The growth process continued until the supersaturation was eliminated and equilibrium solubility was acquired.

The hydrothermal process was carried out in an autoclave under higher temperature and pressure. The temperature and pressure were required to be higher than 25°C and 100kPa, respectively.

The Telfon lined autoclave used for hydrothermal synthesis in this project is showed in Figure 6-6 .The following parameters are pertinent to the hydrothermal process:

- The autoclave volume was 30ml and two-thirds volume of aqueous solution was added to it (20ml).
- The minimum and maximum temperature used were 120 °C and 200 °C respectively.
- An ideal gas condition has been assumed.

Therefore, the pressure can be calculated according to the ideal gas law (Boyle's law) given below [119, 120]:

$$PV = nRT \quad (6\text{-}6)$$

Where, P is the pressure of the gas (Pa); V is the practical volume (m^3); n is the number of moles (mol); R is the ideal gas constant (8.314J/mol·K); T is the temperature (Kelvin).

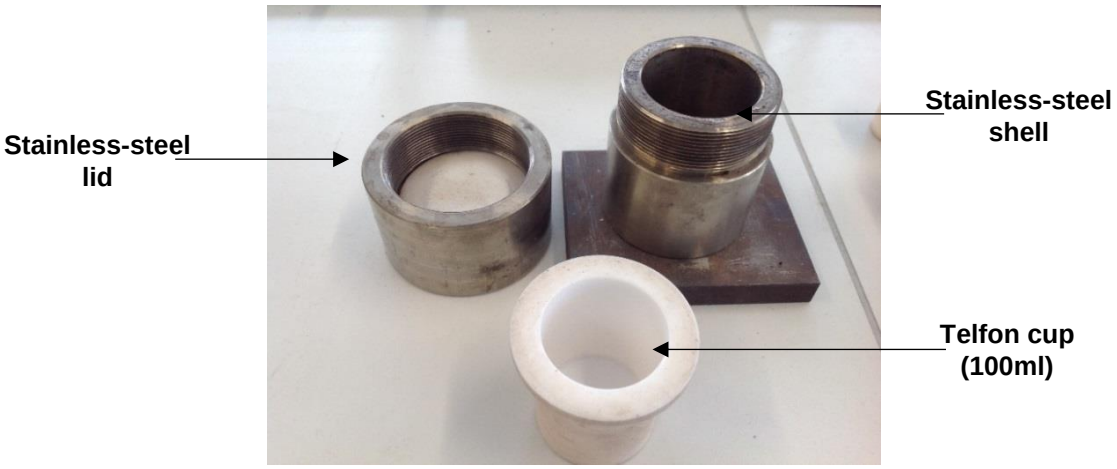

Figure 6-6: The Telfon hydrothermal autoclave used in the experiment.

Based on the equations (6-1 to 6-5) presented previously, the number of moles is 1.1 mol and is equal to the quantity of water in mol. The theoretical pressure in the Telfon autoclave for the minimum (140 °C) and maximum temperature (220 °C) is shown below:

$$p = \frac{nRT}{V} = \frac{1.1\ mol \times 8.314 J/mol{\cdot}K \times (140+273.15)K}{0.03\ m^3} = 125.95kPa \quad (6\text{-}7)$$

$$p = \frac{nRT}{V} = \frac{1.1\ mol \times 8.314 J/mol{\cdot}K \times (220+273.15)K}{0.03\ m^3} = 150.34kPa \quad (6\text{-}8)$$

The resultant calculated pressure is higher than the minimum hydrothermal pressure requirement (100kPa). However, the actual pressure is lower than the theoretical value since the solution was not pure aqueous solution due the presence of a base. The OH^- in the solution would have accelerated the concentration association degree and subsequently reduced the pressure in the autoclave.

The XRD pattern (Figure 4-1 to Figure 4-3) obtained via co-precipitation indicated the phases of Zn-O and Zn-O-H were synthesised. One possible reason is that Zn-O and Zn-O-H are formed simultaneously at first in the solution in co-precipitation process based on the mechanisms previously discussed; when the concentration of Zn^{2+} and OH^- was greater than the super saturation point for forming ZnO, $Zn(OH)_2$ phase can be transformed to ZnO phase at room temperature. The formation of ZnO was likely aided by the stirring of the solution

Another possible reason is based on Figure 6-3. Peterson et al. [113] reported the concentration of the soluble Zn^{2+} was lower than 1×10^{-6}mol/L at the beginning of the reaction indicating at first, $Zn(OH)_2$ were obtained in the solution. Then, with increasing concentration of Zn^{2+} and increasing pH until reached around 10.5.

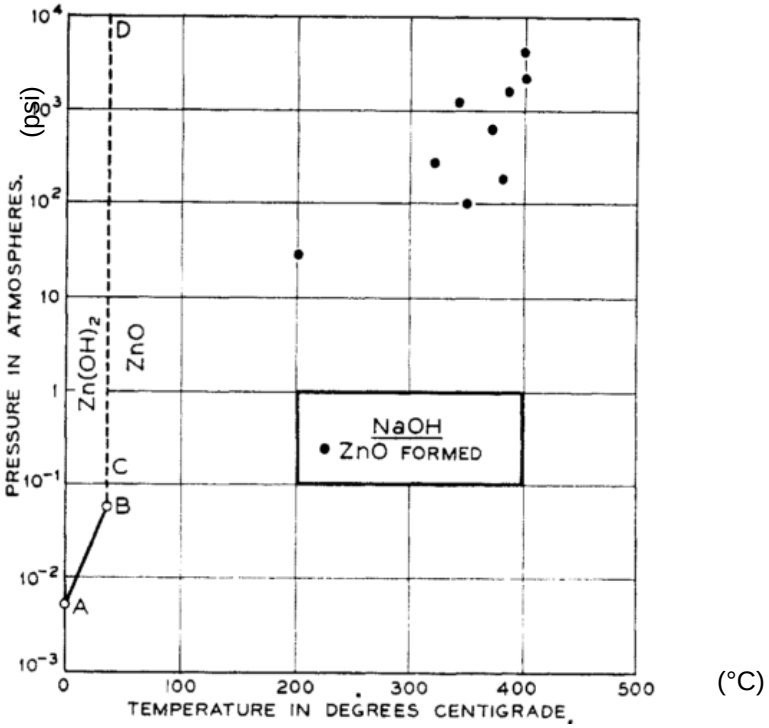

Figure 6-7: Phase transformation diagram of ZnO-H_2O system under different temperature and pressure [121].

In order to fully transform the $Zn(OH)_2$ phase to ZnO phase, enough activation energy should be applied to overcome the free energy barrier caused by the homogeneous nucleation occurred in solution. In Figure 6-7, the phase transformation boundary with the required temperatures and pressures are illustrated. As investigated by Laudise and

Ballman [121] when the pressure was higher than approximately 0.6kPa (the pressure at point B) and temperature higher than 35°C, $Zn(OH)_2$ can be totally transformed to ZnO. However, though the atmospheric pressure of the co-precipitation experiments was a standard pressure (2 psi) and met the required minimum value, the temperature was only 17-23°C. At these conditions, $Zn(OH)_2$ phase still cannot be fully transformed to ZnO phase under room temperature without optimum pH (10.5) and/or enough pressure (above 0.6 kPa). This was confirmed by the XRD pattern (Figure 5-11) with mixed phases synthesised via co-precipitation with “weak bases”.

With regards to the phase transforming from zinc blende to wurtzite, Figure 6-8 indicates the transform required relative low temperature and pressure. With decreasing pressure, the required minimum temperature to transform between zinc blende and wurtzite tends to become lower. It can be extrapolated from the boundary line in the diagram that under 7MPa (7000 kPa) with temperatures as high as 200°C is enough for the zinc blende phase transforming to wurtzite, [122] [123]. ZnO with an entirely wurtzite structure was and proved by the XRD pattern (Figure 6-12) under these conditions.

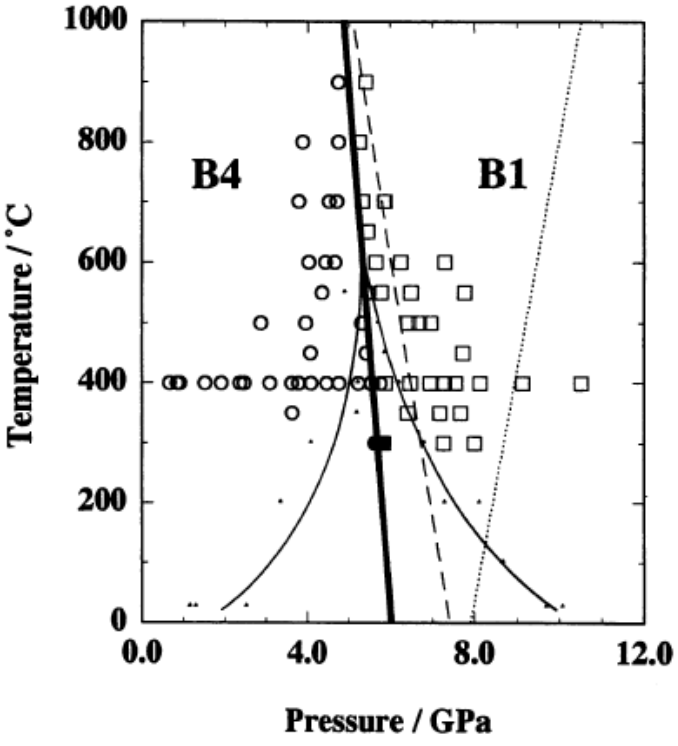

Figure 6-8. Phase transformation diagram between zinc blende, wurtzite and rocksalt [122].

For the phase transformation in ZnO, phases can not be transformed from wurtzite to rocksalt. The rock salt structure is only stable under pressure [124]. Figure 6-9 shows the transformation point. The red line is the theory value and the dash lines are the resulted obtained by Kusaba et al. and Inoue [125]. The calculated pressure (approximately 1- 2 MPa) is much lower than the phase transformation requirement, of around 7 GPa. The temperatures are also significantly different (300 ^{o}C versus 17 – 25 ^{o}C).

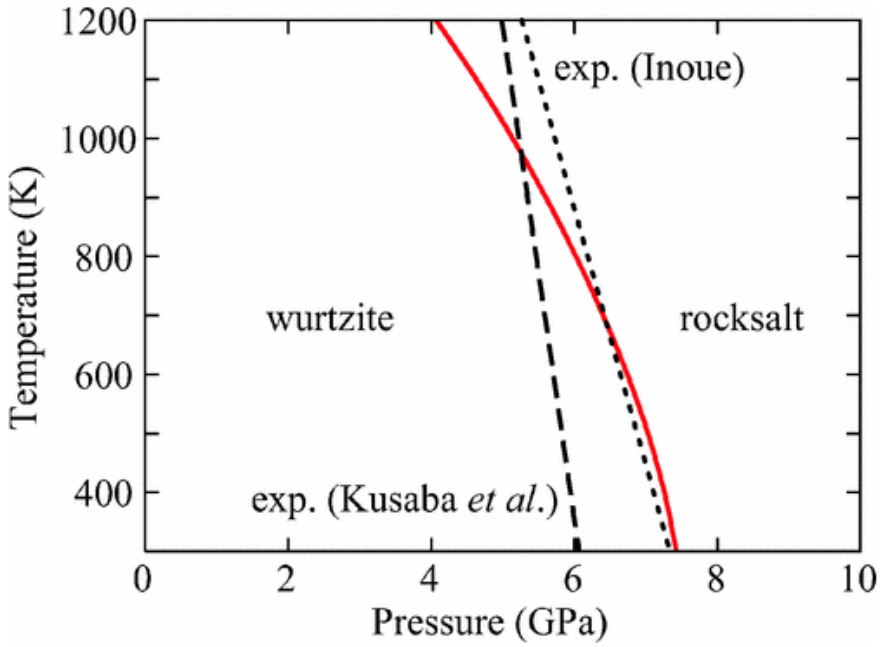

Figure 6-9: Phase transformation diagram between wurtzite and rocksalt [125].

In summary, Figure 6-4 shows the same morphology with different particle size indicated the particles were modified by the hydrothermal process. The homogeneous nucleation and grain growth mechanism resulted in the modification of the particles.

6.2.2 Comparison on crystal phase and crystallinity

The crystal phases of ZnO compounds, Al_2O_3 compounds and AZO via hydrothermal treatment were identified by XRD. The intensity of the peak indicated the crystallinity degree.

XRD results of the samples prepared with NaOH (Figure 6-10) and TMAH (Figure 6-11) with each of the surfactants showed the same correlation of results, with Zn-O compounds forming with L64 and Zn-O-H compounds forming with F68 and P123. This is compared to Zn-O compounds formed with both bases sources when there was no surfactant present. The difference in chemistry and morphology could be due to the interactions between the different polymers and growth of ZnO.

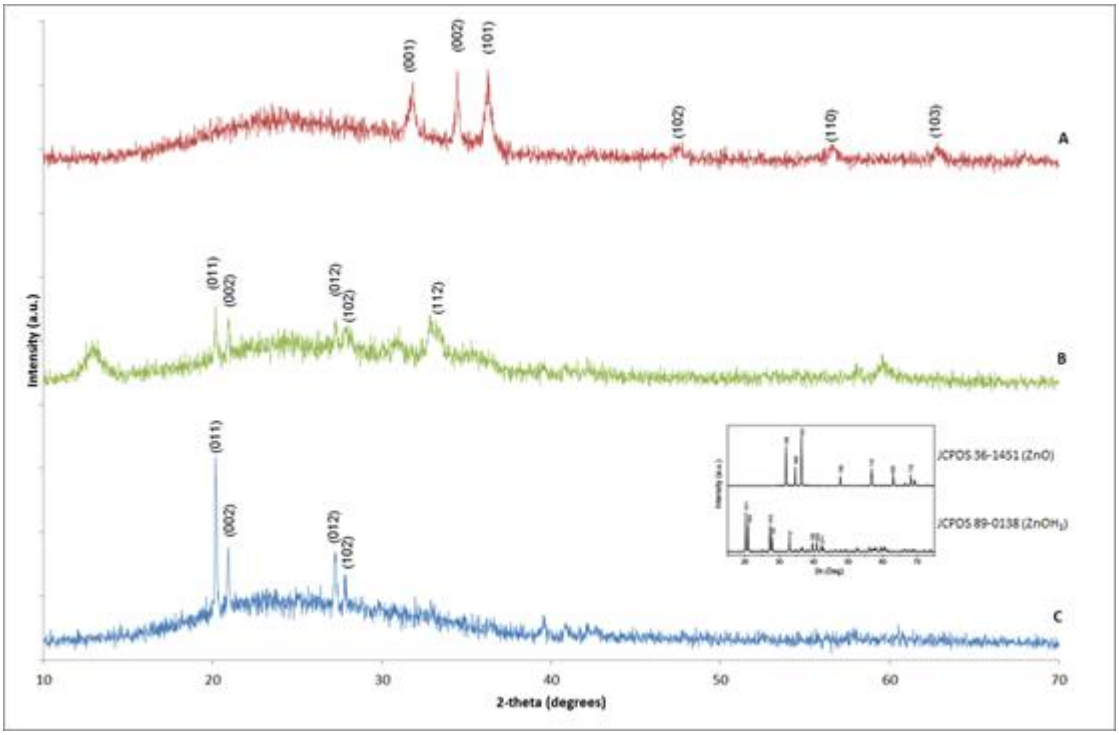

Figure 6-10: X-Ray diffractogram of the particles synthesised by the reactions between $Zn(CH_3COO)_2 \cdot 2H_2O$ and NaOH with different Pluronic surfactants [A] L64 [B] F68 [C] P123

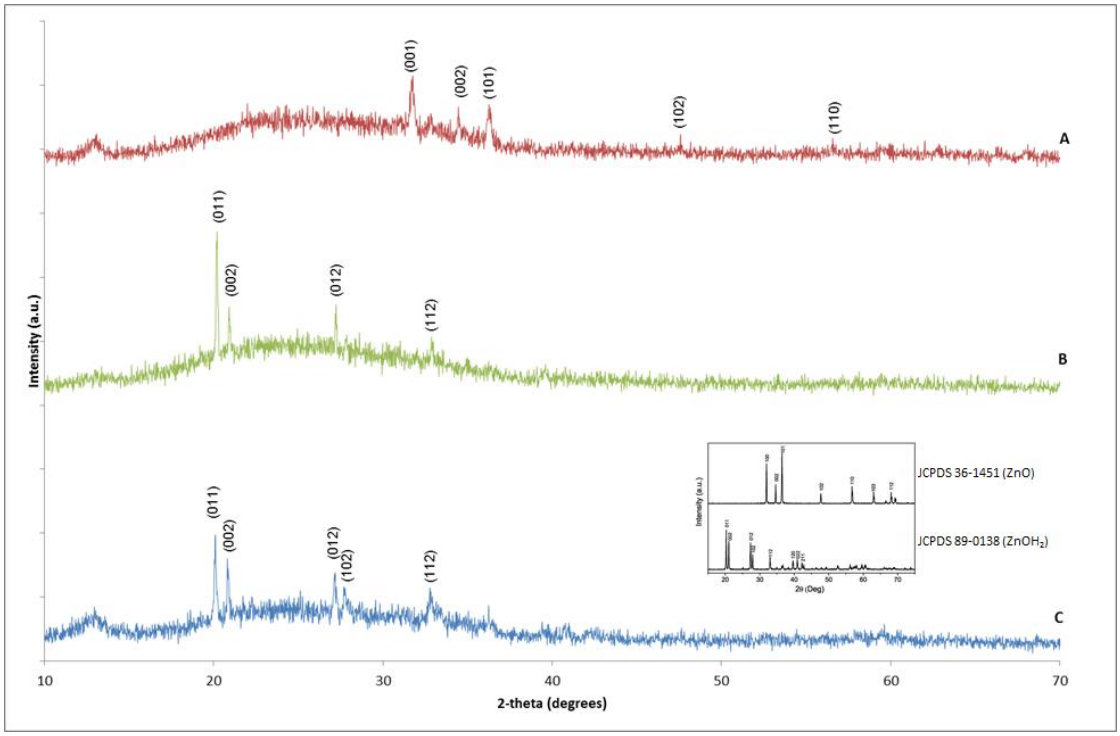

Figure 6-11: X-Ray diffractogram of the particles synthesised by the reactions between $Zn(CH_3COO)_2 \cdot 2H_2O$ and TMAH with different Pluronic surfactants [A] L64 [B] F68 [C] P123

For the Zn-O compound sample synthesised after hydrothermal process, ZnO was obtained confirmed by the XRD results showed in Figure 6-12.

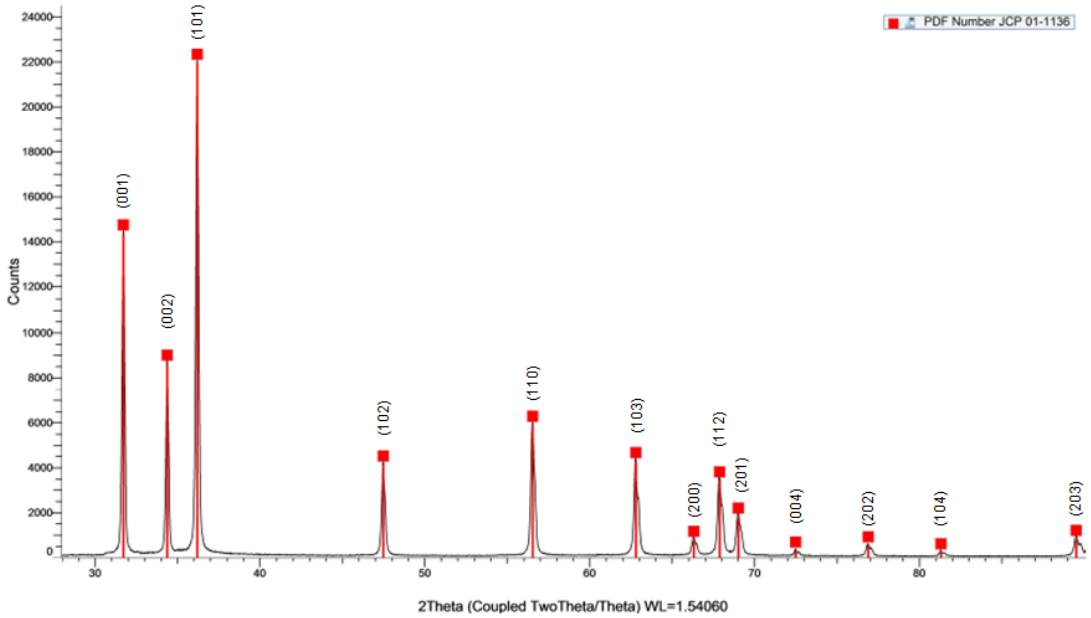

Figure 6-12: XRD pattern of synthesised ZnO powder via hydrothermal process.

The acquired peaks were all the same as the standard values of hexagonal ZnO without other characteristic peaks of impurities. The detected narrow and strong peaks showed in the pattern indicated that the synthesised ZnO nanoparticles have good crystallinity. The peak with highest intensity (above 20000 counts) shows that the preferential growth plane is (101).

According to the matched standard PDF card of ZnO (JCP 01-1136), pure hexagonal wurtzite ZnO was acquired with a= 3.24Å, c=5.18Å and c/a ratio was 1.6. This indicated that the phase was totally transformed from zinc blende to wurtzite.

Comparing the intensity of Zn-O compounds via co-precipitation (Figure 6-10, Figure 6-11) and hydrothermal (Figure 6-12), the sample synthesised via hydrothermal reported higher intensities. The high intensity shows that the crystallinity was improved after the hydrothermal process. In addition, the phases were transformed from the mixture of Zn-O compounds (blende and wurtzite) to pure ZnO. This is because the crystallinity of the pure wurtzite structure is higher than that of the mixed phases. In addition, the wurzite crystal structure is more compact than zinc blende resulting in a higher crystallinity [126].

For the aluminum oxides compounds synthesized via hydrothermal process, part of the detected peaks (red peaks in Figure 6-13) were in accordance with the acquired $Al(OH)_3$, and the other characteristic peaks matched with AlOOH (PDF number: JCP 48-0890) [127]. Comparing the XRD pattern of synthesized $Al(OH)_3$ in Figure 6-13 the sharper and stronger peaks detected via hydrothermal process indicated higher crystallinity. In addition, the phase was partially transformed from $Al(OH)_3$ to AlOOH. This is because the higher temperature provided higher energy for $Al(OH)_3$ phase to transform.

10 at% doped aluminium (AZO-3HT) was characterised by XRD showed in Figure 6-14.

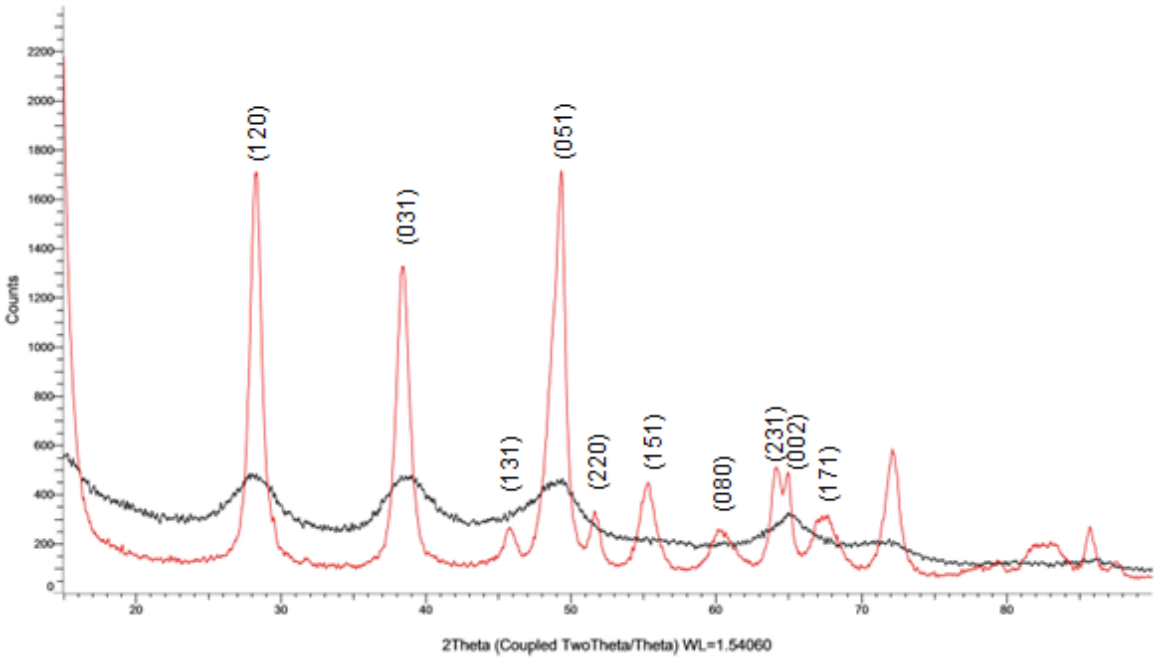

Figure 6-13: XRD pattern of synthesised $Al(OH)_3$ and AlOOH compounds[127].

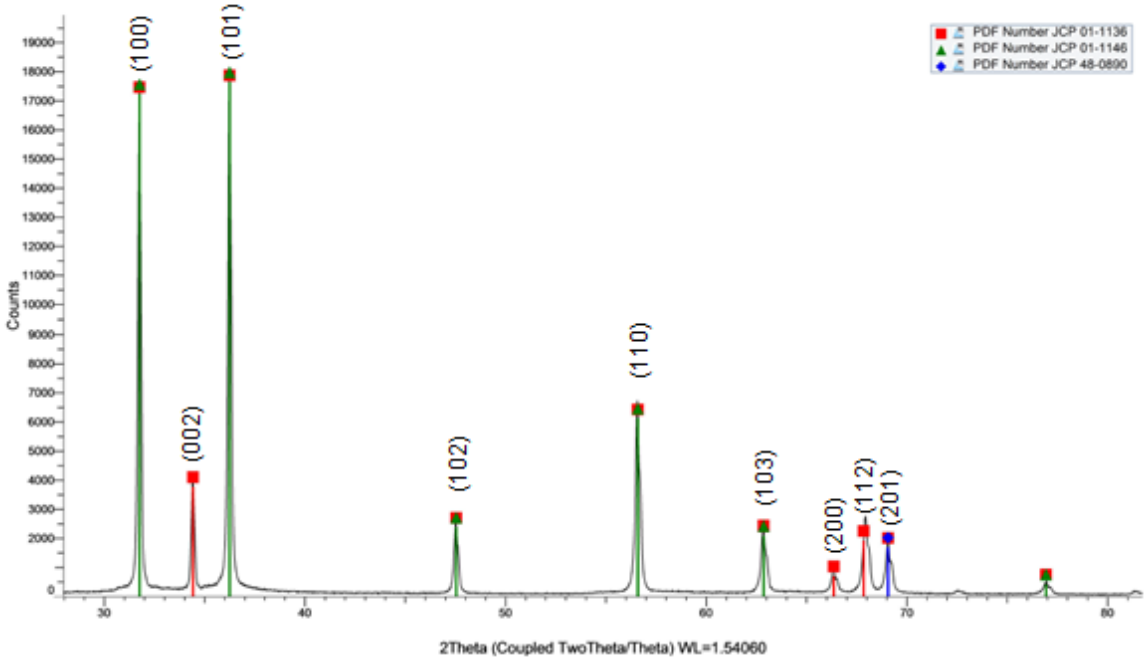

Figure 6-14: XRD pattern of synthesised AZO (10% at., AZO-3HT) [128].

The detected peaks in Figure 6-14 matched well with the standard peak values of ZnO (JCP 01-1136), AZO or $ZnAl_2O_4$ (gahnite) (JCP 01-1146) and AlOOH (JCP 48-0890)[128]. Therefore, aluminum doped ZnO was confirmed to be acquired in the sample. The characteristic peak of AlOOH was rarely detected due to the relative broad peaks with weak intensities.

Compared with the intensities of the characteristic peaks of detected ZnO in AZO with pure ZnO displayed in Figure 6-12 the intensity of the peaks of ZnO in AZO were lower than the pure ZnO.

6.3 Growth mechanism concerning particle size and morphology

ZnO particles with particle size ranging from several hundred nanometres to a few micrometres were obtained both using co-precipitation and hydrothermal methods. The size of the synthesized ZnO particles is controlled by the rates of nucleation and crystal growth [116, 129]. According to Equation (6-2) and (6-3) previously described in Section 6.1, $Zn(OH)_2$ and $[Zn(OH)_4]^{2-}$ exist in the reactions in equilibrium. When there is a large amount of ZnO nuclei and a small amount of the growth unit $[Zn(OH)_4]^{2-}$ in the reaction solution, the nucleation rate is high and the crystal growth rate is low. In this case particles with relatively small size are obtained. In contrast, when there is a small amount of ZnO nuclei and a large amount of the growth unit $[Zn(OH)_4]^{2-}$ in the solution, the nucleation rate is low and the crystal growth rate is high. In this case relatively large particles are synthesized [116].

The growth mechanism concerning the synthesized ZnO particles with different morphologies is a very complex topic. In this project ZnO particles with different morphologies such as flower-like, nanorod and tip-like anisotropic particles were synthesised via co-precipitation and hydrothermal methods in this project.

6.3.1 Formation of flower-like particles

Flower-like particles were observed, with an example shown in Figure 6-15. A possible growth mechanism for the as-synthesised flower-like ZnO particles is as follows.

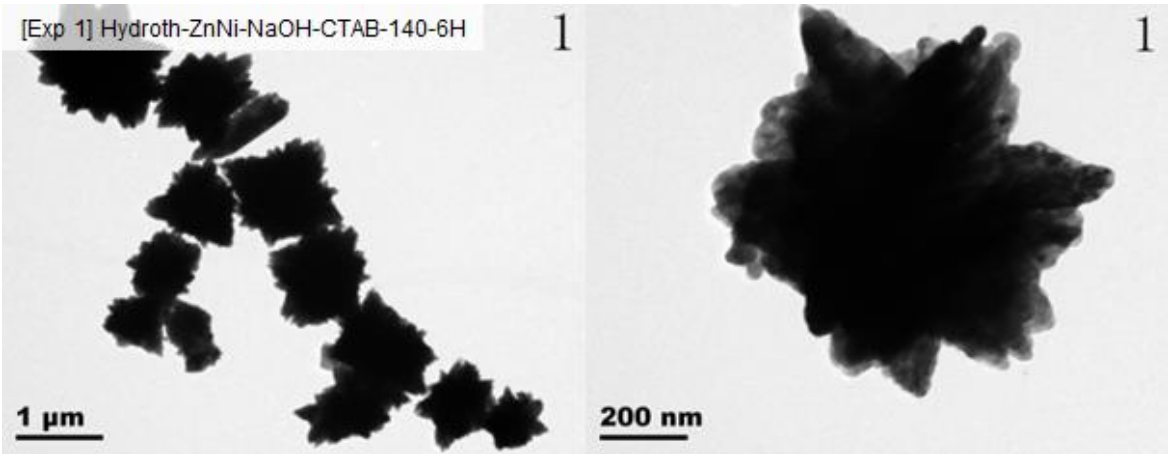

Figure 6-15: Example of a synthesised flower-like particle

At the beginning of the synthesis process, aggregates of ZnO multinuclei spontaneously crystallised from the preferred formation of growth unit $[Zn(OH)_4]^{2-}$ in the reaction solution due to excess OH^- [130]. These aggregates act as the growth sites for ZnO particles along the (0001) direction and as a consequence, flower-like ZnO is obtained under thermal conditions as the reaction continues [68].

A similar mechanism for flower-like ZnO synthesized at high temperatures is given by Zhang et al. The mechanism focused on the effect of the hydrothermal temperature rather than the presence of excess OH- ions. When the hydrothermal synthesis is carried out at high temperatures such as 200 °C it is reported that Equation (6-2) (formation of $[Zn(OH)_4]^2$) is preferred to occur in the hydrothermal reaction than Equation (6-3) (formation of $Zn(OH_2)$ from formation of $[Zn(OH)_4]^{2-}$. As a result, though there are many growth units $[Zn(OH)_4]^{2-}$ available, there are not enough for the formation of ZnO nanorods [69]. The competition between growth and nucleation is also reported by other authors. At higher temperature the superstation level increase in solution because of faster alkaline decomposition, making the nucleation more favourable [62, 114, 131, 132].

Moreover, Zhang et al discussed that at high temperatures, active sites are formed around ZnO nuclei on which further ZnO growth is preferred. As a result, flower-like ZnO structures are synthesized [69]. A schematic graph for this proposed mechanism is illustrated in Figure 6-16.

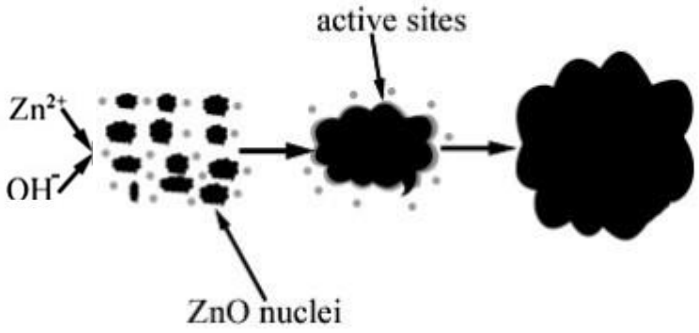

Figure 6-16: Schematic graph of the possible mechanism for flower-like ZnO [69].

6.3.2 Formation of anistropic particles

A possible growth mechanism for the synthesized anisotropic ZnO particles can also be described on the basis of Zhang et al.'s work. When a large amount of ZnO nuclei and a small amount of the growth unit $[Zn(OH)_4]^{2-}$ is available in the hydrothermal solution, anisotropic ZnO nanoparticles is formed attributing to anisotropic growth preference of ZnO [69]. An example of an anistropic particles formed is given in Figure 6-17 and the mechanism is described schematically in Figure 7-5.

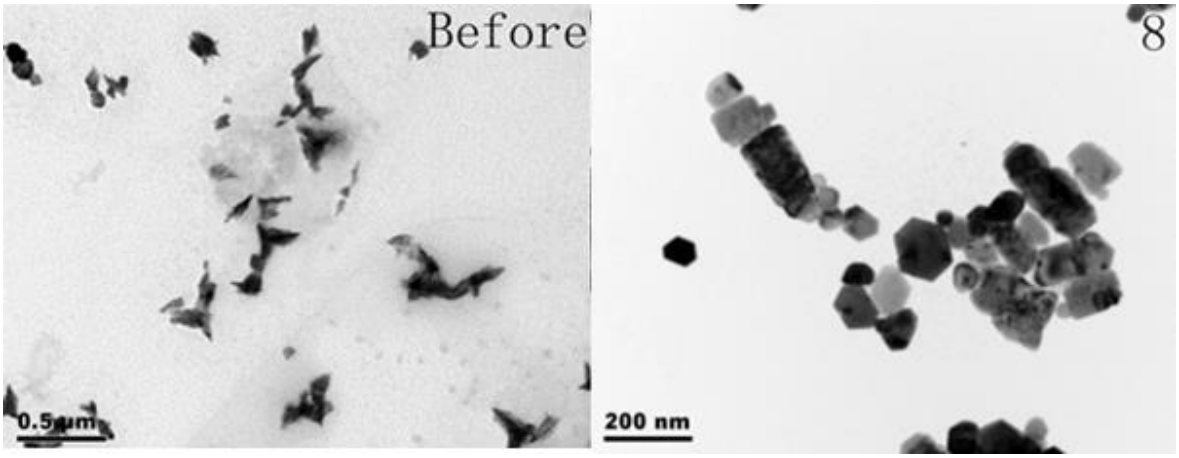

Figure 6-17: Example of a synthesised anistropic particles

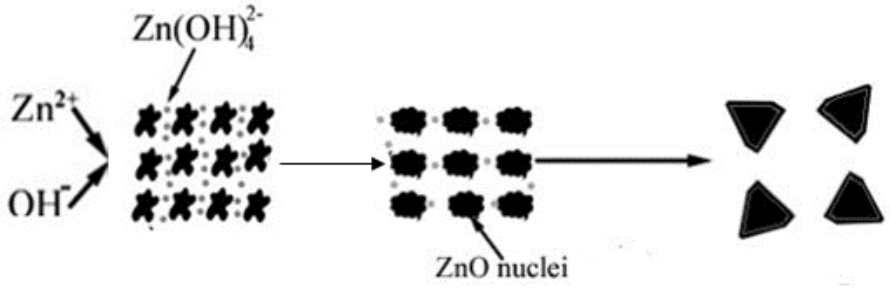

Figure 6-18: Schematic graph of the possible mechanism for ZnO anisotropic nanoparticles [69].

6.3.3 Formation of nanorods

The formation of nanorods (Figure 6-19) is considered to have occurred due to arrangement of the zinc and oxygen ions.

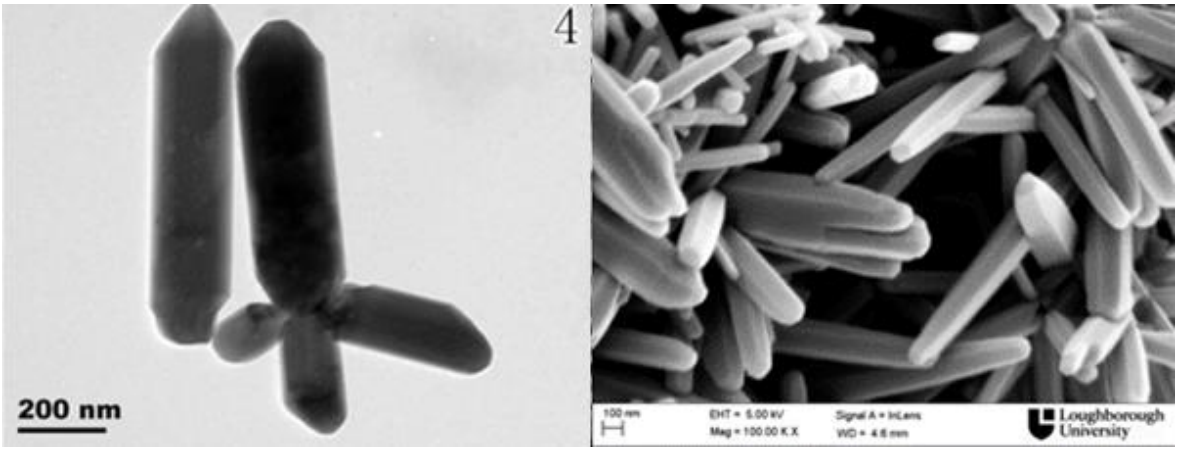

Figure 6-19: Example of a synthesised nanorod particle

The zinc and oxygen ions situate themselves tetrahedrally in the planes of the hexagonal wurtzite structure of ZnO, resulting in the large amount of zinc in the positive polar plane and the large amount of oxygen in the negative plane [67]. This polar structure is used to describe the formation mechanism of ZnO nanorods.

Active sites, which are controlled by processing parameters such as temperature and pH, are formed around ZnO nuclei, resulting in the preferential growth of ZnO nanorods on them along the direction of (0 0 0 1) plane. Therefore the mechanism can be schematically described combining the growth habit and the preferential growth on active sites together, as shown in Figure 6-20 [67].

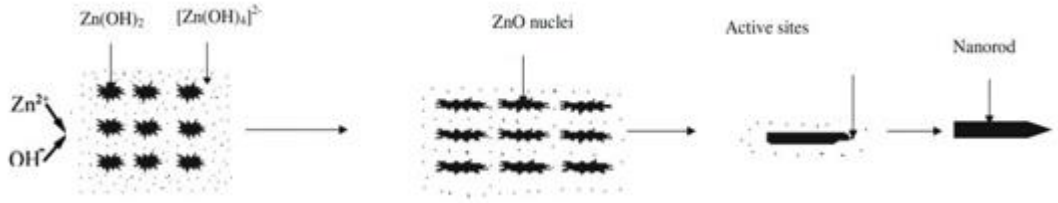

Figure 6-20: Schematic graph of the possible mechanism for ZnO nanorods [67]

The formation of the tip can be attributed to by the polar plane growth rates. The different growth rates of polar planes are controlled by the growth unit $[Zn(OH)_4]^{2-}$ in reaction solution, decreasing in the sequence of (0 0 0 1), (0 1 -1 0) and (0 0 0 -1). How fast a polar plane disappears is determined by how fast the growth rate of that plane is. So the plane with the rapidest growth rate, (0 0 0 1), is the first to disappear in synthesis process, resulting in the formation of a sharp end along the c axis. In contrast, the plane with the slowest growth rate, (0 0 0 -1), is left during the hydrothermal treatment, resulting in the formation of a plain end along the c axis. This growth habit of ZnO nanorods is displayed in Figure 6-21, illustrating the ZnO structure with sharp shape at one end of the c axis and plane shape on the other end [67, 133].

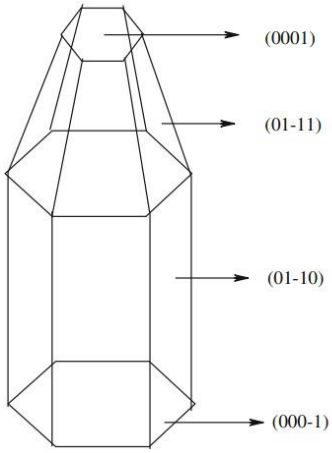

Figure 6-21: Growth habit of ZnO nanorods with one sharp end and one plain end along the c axis [67].

6.3.4 Formation of platelets

The formation of the platelets (Figure 6-22) can be explained by the relationship between the OH- ions and the $Zn_xO_y(OH)_z^{(z+2y-2x)-}$ [114]. During the dehydration reaction a part of the

OH- ligands of the surface of the growth complex $Zn_xO_y(OH)_z^{(z+2y-2x)-}$ can be shielded by the other ions in the solution, forming a cationic surface with H_2O or other ions in the structure. In a neutral medium, there is little effect on the OH- ligands at the interface and so cations within the structure are formed leading to crystal growth. However in a alkali solution, the growth unit is shielded by OH- ions forming a complex such as $Zn(OH)_{4-x}(ONa)_x^{2-}$. This means that the $Zn_xO_y(OH)_z^{(z+2y-2x)-}$clusters formed have a cation surface with ONa^- ions at the interface. For continuation of the growth, these ONa^- ions must be removed and replaced with OH^-, which is an endothermic process, thus slowing the growth rate down [114, 134-136].

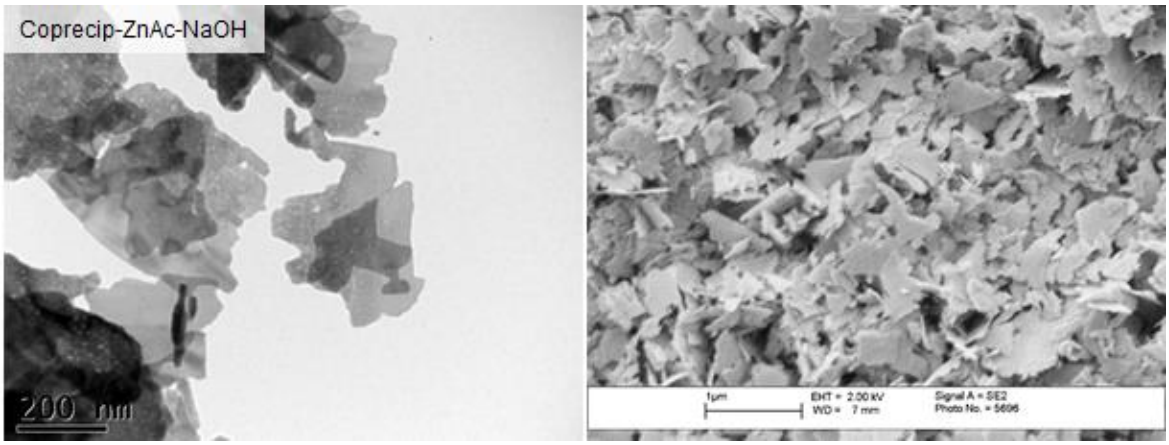

Figure 6-22: Example of a synthesised platelet particle

The growth could be also directional. It is well known that ZnO is a polar crystal with zinc-rich positive polar plane and oxygen-rich negative polar plane, the most rapid growth rate plane, (0001), was the intrinsic preferential growth plane of ZnO [137]. However, due to the inhibition of shielding effect of OH- at the (0001) and ($V_{(\bar{1}0\bar{1}\bar{1})}$ and $V_{(\bar{1}010)}$) faces the other directions grow, causing a large surface area on the other two surfaces, forcing the ZnO into a shape of a platelet [114, 138, 139].

Music et al, suggests that the formation of platelets could be due to adsorption of CH_3COO^- ions onto the (0001) surface, suppressing growth of the surface [41]. Xu et al [140] showed that when large amounts of CH_3COO^- ions were present when ZnO films were electrodeposited from a $Zn(NO_3)_2$ solution, that they would be adsorbed onto the positive polar face of the (0001) surface which prevented contact of $[Zn(OH)_4]^{2-}$ on the (0001) surface and limited the crystal growth along the c-axis. However Mcbride et al. suggested that the counter-ion

had little effect on the morphology of ZnO even when the starting zinc source concentration was doubled and that the only change occurred when the base solution concentration was changed [40].

6.3.5 Formation of microflowers

In the present work, when the zinc source was changed from $Zn(CH_3COO)_2 \cdot 2H_2O$ to $Zn(NO_3)_2 \cdot 6H_2O$, platelets were formed suggesting the lack of effect that the counter-ion has on the morphology. However when the zinc source was changed to $ZnCl_2$ there was a change in morphology to microflowers (Figure 6-23). This suggests that either the Cl^- ion did not inhibit the (0001) plane or there was a change in the growth speed of the ZnO. Xu et al suggests that the $ZnCl_2$ has a higher degree of ionization, which leads to a faster reaction [30].

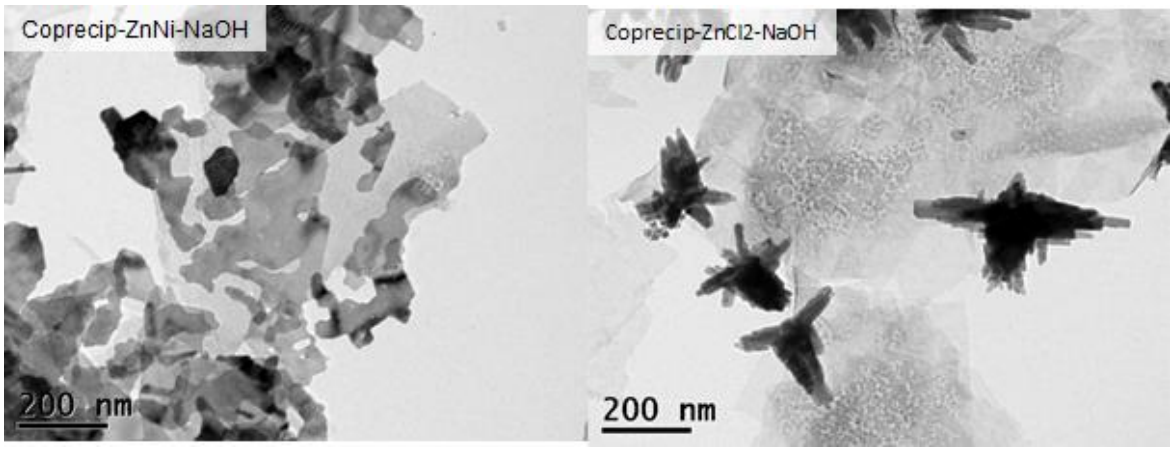

Figure 6-23: Change in morphology following a change in zinc source from $Zn(NO_3)_2 \cdot 6H_2O$ to $ZnCl_2$.

Microflowers of ZnO are generally formed when the growth rate is fast. Wahab et al [39] suggests that with energy, the aggregates form a big core sphere, which provide the surface energy for the attachment of active molecules of ZnO. These active molecules of ZnO, also known as stems or rachis, attach themselves to the core sphere and arrange themselves in such a way that requires the minimum amount of surface energy to keep the symmetry of the wurtzite crystal structure. These steams then can grow in the (0001) direction, forming the microflower. Figure 6-24 shows this process.

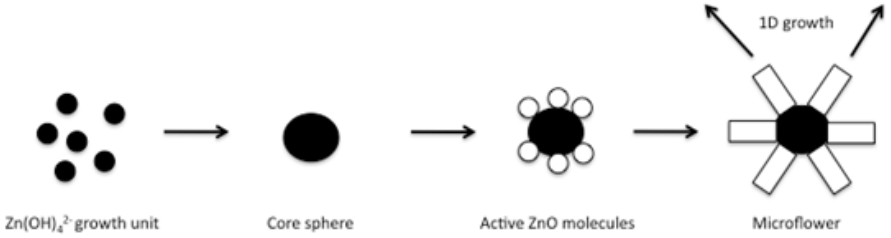

Figure 6-24: Representation of the growth of ZnO microflowers

Xu et al. [30] speculates that the high degree of ionization from $ZnCl_2$ leads to a faster reaction. It is possible that the Cl^- ions in the solution help in the removal of the ONa- ions from the surface of the (0001) face, greatly increase the speed of the reaction.

When $ZnCl_2$ was used as the zinc source and TMAH as the base solution, a mix of $Zn(OH)_2$ polyhedral structures and microflowers of ZnO was formed, though XRD suggests that $Zn(OH)_2$ / $Zn_5(CO_3)_2(OH)_6$ (Hydrozincite) was the majority phase. According to Zabinski et al, [141] the microstructure of hydrozincite consists of $Zn_3(OH)_6O_2^{4-}$ sheets with additional Zn atoms and counter-ions above and below these sheets. It is the counter-ion groups that hold these sheets together. It is also a defiency of counter-ions that leads to a disorder in the layer sequence and the random polyol shape seen in the FEGSEM image. The micrograph also shows the formation of some small microflowers of ZnO. This suggests that there were active clusters of growth unit in the solution.

6.4 Effect of surfactants

The effect of surfactants on the particle size, the crystalline phases and the morphology of zinc compounds were investigated through the addition of the surfactant and change of different surfactants as presented in section 4.1 and 4.2.

The role of the surfactant is dual. At low concentrations, the surfactant provokes agglomeration due to lowering of the energy of the coated surface, which subsequently lead to a reduction of the total surface area of the system. The strength of this factor is proportional to the type and amount of the surfactant with respect to any given amount of the non-coated material [142].

On the other hand, the coated surface becomes inactive, which inhibits agglomeration [143]. Since a larger amount of the surfactant allows for coating of the larger surface, this factor limits the size increase of the particles. These two opposing factors determine the role of the surfactant in the arrangement of the coated nanoparticles. In particular, at low concentrations of the surfactant, an increase in its quantity leads to acceleration of the aggregation, whereas the total coated surface remains small. At some critical level of surfactant quantity, all the agglomerates are coated, hence stabilized. Further increase of the surfactant concentration can only reduce the size of the agglomerates, which allows for coating of all the initial particles [142].

Surfactant can be used to control particle size and hinder aggregation. Three Pluronic surfactants (L64, F68 and P123) and various base solutions were used with $Zn(CH_3COO)_2 \cdot 2H_2O$. It was found that these had a significant effect on the chemistry, morphology and size of the particle compared to the sample prepared without any additive. A visual representation of the different block lengths and a summary of the compositions of the three Pluronic surfactants is given in Figure 6-25 and Table 6-2, respectively.

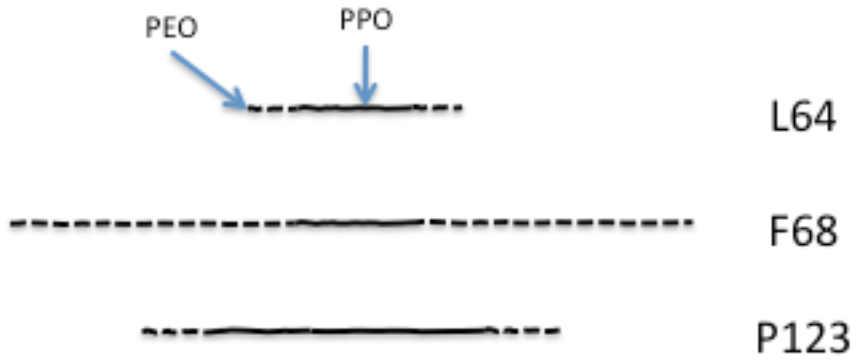

Figure 6-25: Visual representation of the different block lengths of L65, F68 and P123

Table 6-2: Compositions of PEO-PPO-PEO copolymers and critical micellisation temperatures (CMT) of 5% aqueous solutions [144-146]

Pluronic	Mw	PEO (wt-%)	PPO block (M_w)	PEO block (M_w)	cmc [mM] (25°C)	CMT (°C) (5 wt%)
L64	2900	40	1740	1160	26.3	26.5
F68	8400	80	1680	6720	320.5	40
P123	5750	30	4025	1725	0.05	12.5

It is well documented that block copolymers like the PEO-PPO-PEO can exist in various phases when dissolved in a solvent such as H_2O. There are three important parameters that help decide the morphology of block copolymer, CMC (Critical Micelle Concentration), CMT (Critical Micelle Temperature) and CP (Cloud point). It is at both the CMC and CMT points that the surfactant will orient itself so that the insoluble block will shield itself from the soluble block of the surfactant. If either the CMC or CMT parameters are not met then self-assembly will not occur. While CP does not have a direct effect on the morphology, it is useful to know at what temperature the surfactant would saturate out of the solvent.

As previously noted, crystal formation happens in two stages: crystal nucleation and growth rate. The non-ionic surfactant has an effect on both of these stages. When the $Zn(CH_3COO)_2 \cdot 2H_2O$ solution is added to the surfactant solution, the Zn^{2+} metal cations bind to two oxygen atoms in the PEO block as shown in Figure 6-26, which is known as a pseudo crown ether [147, 148]. This is important to the crystal nucleation stage. When the NaOH solution is added to the solution, $Zn(OH)_2^{4-}$ growth units are formed at these growth ethers. In the case of L64, these growth units act as a point as which other $Zn(OH)_2^{4-}$ growth units can cluster to. As discussed earlier, the clustering of these growth units followed by anisotropic growth from the c-axis forms microflowers. However in the case of F68 and P123, $Zn(OH)_2$ was formed with an anisotropic and aggregated polyol morphology. The reason for this could be the way the polymer affects the second stage of the crystal formation, growth rate [145, 148-150]

The difference in morphology of the $Zn(OH)_2$ phase can be explained by the nature of the surfactants. In solution, due to the temperature and concentration of the surfactants, P123 should exist in a micellar state and F68 in a unimer state. Micelle cores provide a relatively more favourable environment to poor soluble compounds in aqueous solutions. As P123 is the only surfactant to form a core (due to its large PPO content), $Zn(OH)_2$ can aggregate into large polyol structures. However for F68, in the unimer state the $[Zn(OH)_4]^{2-}$ growth units cannot aggregate to supersaturation levels to form ZnO due to the size of the surfactant, and form $Zn(OH)_2$ which more stable but poorly soluble and so exists in an anisotropic crystal structure.

With the introduction of NaOH, growth units of $[Zn(OH)_4]^{2-}$ are formed at the Zn^{2+} sites in the pseudo crown ether [147, 148]. An example of a pseudo crown ether is given in Figure 6-26.

These are then replaced with the Na^+ cations formed when the salt is dissolved. The $[Zn(OH)_4]^{2-}$ small clusters are formed on the methyl groups in the PPO chain due to steric hindrance. Steric hindrance causes ionized groups to absorb onto the nucleating ZnO particles, imparting a positive surface charge preventing each other from approaching by columb repulsion. As L64 is a small unimer, this repulsion is small and so small clusters can form, eventually forming ZnO with the addition of multiple growth units. Sun et al [151] and Hao et al [152] discuss that with a surfactant in solution, the surface tension of the solution is reduced. This means that the energy required for the formation of a new phase is lower and therefore ZnO crystal can form in at lower supersaturation.

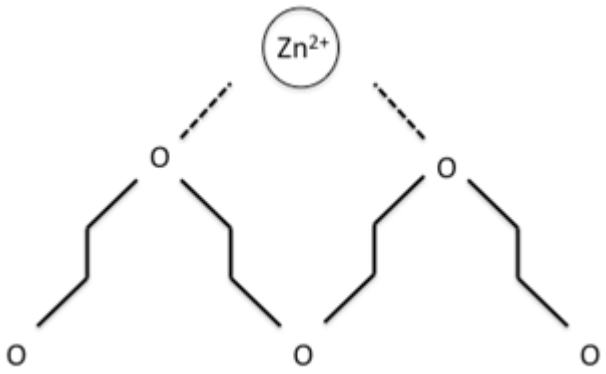

Figure 6-26: Representation of the binding of Zn^{2+} with Oxygen atoms in a the PEO block

When F68 was used, aggregated polyol $Zn(OH)_2$ was formed. Compared to L64, F68 has double the percentage of PEO blocks, but with the same amount of PPO blocks [153]. Therefore it could be suggested that the PEO block has a profound effect on the formation of ZnO. With the increase in PEO block size, the Zn^{2+} cations are encapsulated. At room temperature, with the addition of NaOH, there is no enough energy for the replacement of the Zn^{2+} with the Na^+ cation and so $Zn(OH)_2$ molecules are formed within the cavities. As these molecules cannot escape or interact with other $Zn(OH)_2$ due to the encapsulation. The anisotropic growth seen in the micrograph could be due to some anisotropic growth during stirring

In contrast, P123 has the approximately the same percentage of PEO blocks as L64, but a much higher amount of PPO. It is this hydrophobic setup that forces the surfactant into a micelle in the experimental conditions. This big increase in PPO size means that the steric resistance also increases. This means that more of the growth units adsorb onto the methyl

groups instead of onto other growth units. Along the hexagonal axis, crystals grew fast and was promoted by the crystal face in polar plane <0 0 1>, however, along the lateral axis, ZnO grew slow and was restrained because of the adsorption of the positively charged PEO molecules. When PEO was absorbed by the surface of ZnO in the medium, it could impede the further growth of the precipitate in the course of hydrothermal process [154]. However, the ZnO prepared without surfactant grew asymmetrically and the particles were not in the nanosize range. This indicates PEO as a surfactant has an inhibition influence on the growth of nanorods, which can be used to control the particle size.

Nanosized ZnO with double ended acicular structure was obtained through hydrothermal process (Figure 5-41). One underlying explanation was analysed by Tzeng et al. [155] At first, most Zn^{2+} ions are chelated on the PEG polymer chain, the rest of Zn^{2+} forms $Zn(OH)_2$, which OH^- ions are supported by NH_4OH. With more NH_4OH added in, both $Zn(OH)_4^{2}$ ions and $Zn(OH)_2$ form. During the hydrothermal treatment, a little amount of ZnO grows on the surface of PEG. However, most Zn^{2+} ions are free and can support the secondary growth. Since ZnO grows faster on the positive polar plane (0001) than any other polar plane, which has mentioned before, ZnO with acicular structure on one end generated. In addition, the higher the growth rate of a facet, the smaller the area of the facet is, thereby ZnO with acicular structure generates [155]. Due to the required amount of Zn^{2+} ions and sufficient hydrothermal time, the secondary growth takes place on the other end of ZnO crystals [155]. The growth habit of double ended acicular ZnO nanocrystals is shown below in Figure 6-27.

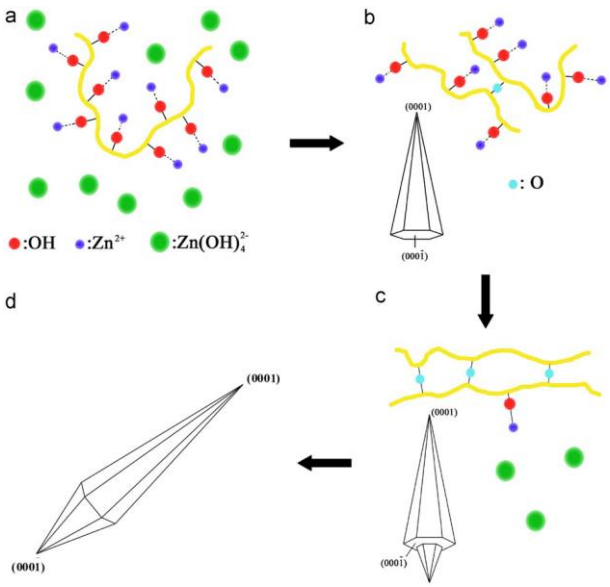

Figure 6-27: The growth habit of ZnO nanocrystals with double ended acicular structure [155].

This effect was pronounced when the concentration of L64 in a [$Zn(CH_3COO)_2$•$2H_2O$ /NaOH] solution was modified (Figure 4-22, Figure 5-29). It was observed that there was no change in morphology as the concentration increased from 1% to 28% with a star-like structure being synthesised. When the concentration increased to 53% a change to an agglomerated platelet structure was observed. This is probably due to a change in the structure of the surfactant in the solution. The phase diagram for L64 in solution is shown in Figure 6-28 and suggests that at a 53 wt% the non-ionic surfactant could be considered to be in a hexagonal phase [156, 157].

In the case of the three surfactants used, Table 6-2 shows that at room temperature at a concentration of 5%, the only polymer that would achieved self-assembly would be P123. However in the experiments rather than a set weight percentage, a set concentration was used in 40ml of water, meaning that the actual weight percentage of surfactant used was 4.5%, 13% and 9% for L64, F68 and P123 respectively. From the data available, it is possible to state that both L64 and F68 are in a unimer state and P123 in a micelle state in solution [157].

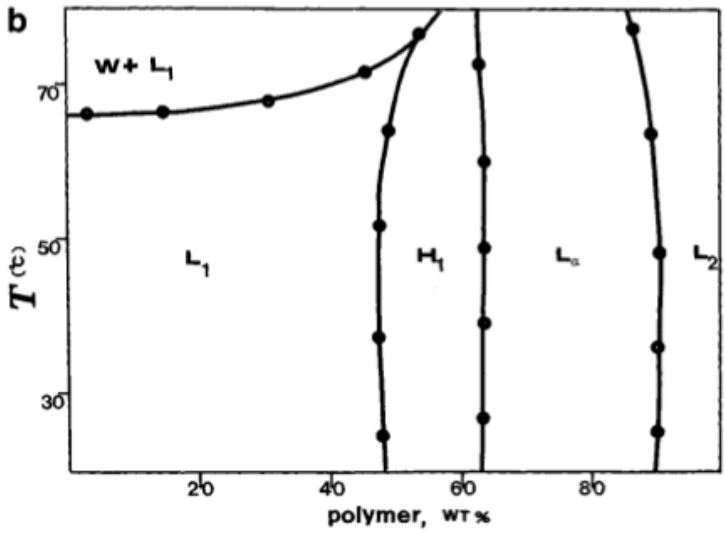

Figure 6-28: Partial phase diagram (temperature versus polymer composition as weight per cent) for L64/water. The notations are as follows L_1, L_2 isotropic solution phases, H_1 hexagonal phase [157].

It is considered that the formation of platelets at a concentration of 53 wt.% was probably due the hexagonal structure of the L64 confining or suppressing the growth rate in the (0001) direction.

When SDS and CTAB were used as the surfactants in the co-precipitation solutions with $Zn(CH_3COO)_2 \bullet 2H_2O$ and NaOH, the morphologies of the particles were changed. Instead of the platelet particles formed without surfactant, aggregated blocks were synthesised with SDS and a tape like structure with CTAB. In order to investigate the role of each of the surfactants, it is necessary to discuss their individual structures. Figure 6-29 shows the molecular structures of both surfactants.

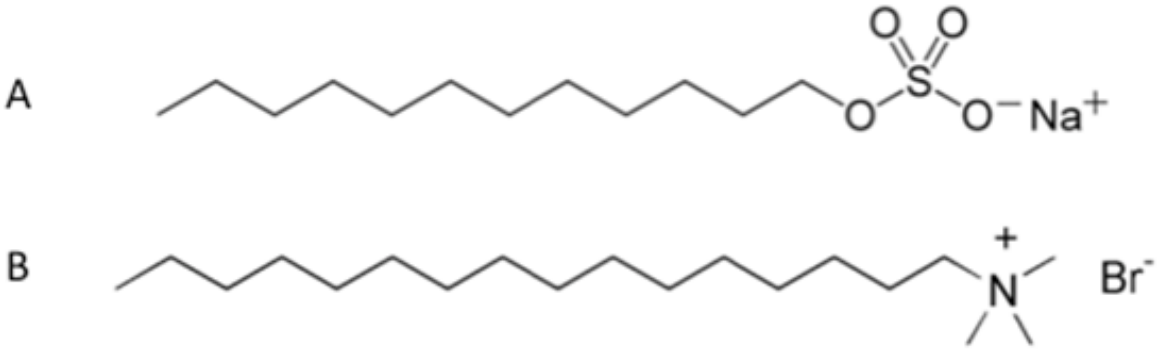

Figure 6-29: Structures of [A] SDS [B] CTAB

It is well known that SDS is a typical anionic surfactant [158, 159]. There are three ways in which SDS may have an influence on the growth of the particles. SDS may have an influence on precursor nucleation, on phase transformation and in the final agglomeration in bigger particles [160]. In this case the SDS caused the synthesis or aggregation blocks/polygonal shapes, which is presumed to be $Zn(OH)_2$ due to the crystal shape. In a alkaline solution, SDS are in competition with the OH- ions and if overcome the anionic surfactant could repel the $[Zn(OH)_4]^{2-}$ building block of ZnO [161]. This repulsion could lead to the aggregation of $[Zn(OH)_4]^{2-}$ which will lead to the formation of large polyols of chemically stable $Zn(OH)_2$.

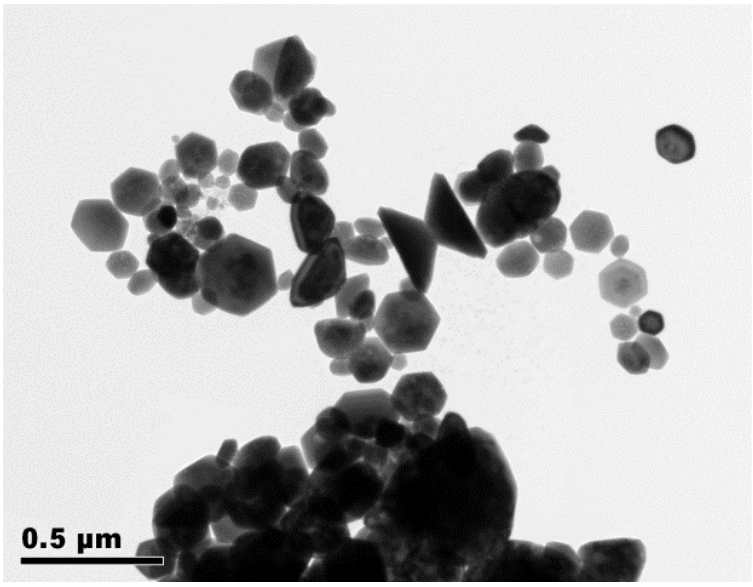

Figure 6-30: TEM images ZnO nanohexagons

ZnO nano hexagons were synthesized with SDS at hydrothermal temperature 140°C (Figure 6-30). The anionic surfactant SDS and hydrothermal temperature (140°C) play important roles in the formation of ZnO with hexagonal structure. The low hydrothermal temperature, which was the lowest of the temperatures used, may not have benefited further growth of ZnO and would have likely inhibited the growth of particles to form the preferred rod-like ZnO.

In addition to the low hydrothermal temperature, one explanation about the formation of the hexagonal ZnO structure was discussed G. K. Pradhan.et al; the agglomeration of ZnO crystals in every direction leads to the formation of the hexagonal structure. [162]. From the figure it can be seen, some particles are well shaped, others may not. The particles with hexagonal structure were fully grown, while others were not completed crystal growth [162]. This was due to the use of SDS as a surfactant, which can reduce surface tension. [163, 164]. During the hydrothermal process, because of steric hindrance, it can inhibit particles aggregating together [165, 166].

CTAB on the other hand is a cationic surfactant that in an aqueous system is positively charged with a tetrahedral head with a long hydrophobic tail. In this case the CTAB may provide a long chain reaction interface and induce growth in a definite direction [167, 168].

When the concentration of CTAB is much higher than that of its CMC (0.033%), the surfactant forms lamellar/layered hybrids. In this case 6.8% of CTAB was used [72]. Shen et al discusses that the zinc species/CTAB molar ratio is key factor for controlling the mineralization of zinc species on the micelles of CTAB and solidifying the agglomerates of micelles. Theoretically, lamellar/layered hybrids are easily formed when the Zn^{2+}/CTAB molar ratio is close to 1. At this ratio, exfoliation and rolling of the inorganic layers causes the formation of tubes. However in this case the ratio was 2.7, which meant there was an excess of Zn^{2+}. This could have led to the formation of thicker lamellar sheets that were unable to roll into a tube [72].

CTAB was selected as the optimum surfactant for synthesising rod-like particles. CTAB was used in this project since it can increase the reaction rate and lead to a product with higher crystallinity [151]. As a cationic surfactant, CTAB ionizes in the solution [169]. The ionized equation is [169]:

$$\mathrm{CTAB} \rightarrow \mathrm{CTA}^{+} + B^{-}$$

The mechanism of accelerating long particles is that CTA^+, ionized in the solution from CTAB, attached with $[Zn(OH)_4]^{2-}$ electrostatically. So, the ionized ions aided the landing of the growth unit $[Zn(OH)_4]^{2-}$ which had tetrahedron geometry, to form ion-pairs suggested by Sun et al. [48, 151, 170].

This step accelerated the growth of ZnO particles on the (0001) crystal face. Figure 6-31 (a) shows clearly that CTA^+ is also tetrahedron with a positive charge and a long tail which is hydrophobic [151, 171]. The forming and landing process are showed clearly in Figure 6-31. CTAB accelerated the orientated growth of (0001) ZnO crystal face was also approved by Wang et al. Moulahi et al. notes that since CTAB favours to form a film in which the molecules tend to be perpendicular to the absorbed surface, the growth units would tend to face-land onto the growing surface [172].

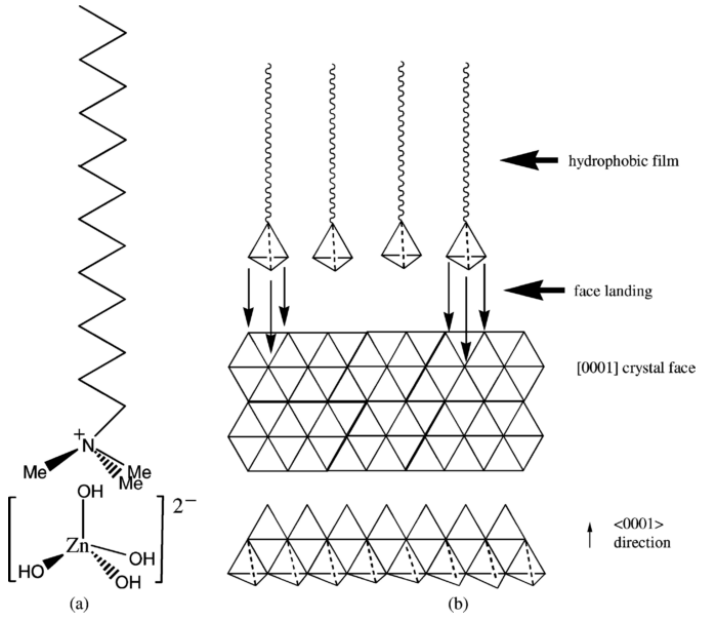

Figure 6-31: (a) Illustration of formed ion-pair between CTA+ and $[Zn(OH)_4]^{2-}$ (b) Illustration of landing process on the (0001) crystal face of ZnO [151].

6.5 Effect of hydrothermal processing variables on the sizes and morphologies of ZnO particles

6.5.1 Effect of hydrothermal treatment

The products obtained before and after hydrothermal synthesis in Experiment No. 3 in the orthogonal array experiments were characterised by TEM and the micrographs are displayed in Figure 6-32.

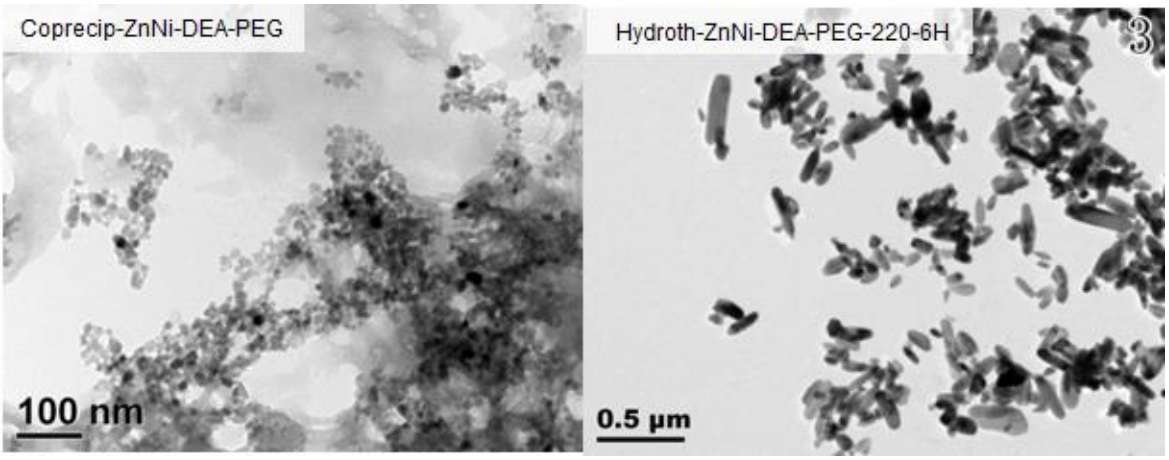

Figure 6-32: TEM micrographs of the products obtained before and after hydrothermal synthesis

As can be seen from Figure 6-32, the size of the particles with hydrothermal treatment is smaller than that of the particles without hydrothermal treatment. The particles observed in the before hydrothermal TEM micrograph takes the morphology of tip-like anisotropic nanoparticles. The outline of the particles is rough. The morphology of the hydrothermally synthesized ZnO is anisotropic nanoparticles with very smooth outline. This indicates the size and morphology is modified by the hydrothermal treatment. This modification is achieved through homogeneous nucleation and grain growth during the reaction process [69, 173].

6.5.2 Effect of hydrothermal time

The ranking result suggested that the type of surfactant was the most influential factor in the control of aspect ratio. This was to be expected and is considered to be due to both the nucleation and growth rate control the surfactant has over the size and morphology. As previously discussed the control is provided both directly (i.e. attachment of Zn^{2+}) and indirectly (i.e. counter-ion interaction).

The results showed that for the smallest and largest hydrothermal times (2 hours and 12 hours), the smallest and largest aspect ratios were formed, respectively. In addition, the optimum parameter was noted to be 12 hours. These affects are regarded to be due to a process called Ostwald ripening.

Ostwald ripening [43], also known as coarsening, is a mechanism driven by an increase in chemical potentiation of a particle with a subsequent decrease in particle size [174]. The process causes the continued growth of larger particles by the dissolution of smaller ones [165]. In general, particle size increases with increasing reaction time as more material is added to the particle surfaces. In addition the rate of addition of material to existing nuclei increases [175].

At an optimum time of 12 hours, the smaller particles of ZnO would have been re-dissolved. This would have reduced the variance in the obtained morphologies, controlling the aspect ratios. They would then have re-deposited upon the c-axis, increasing the length of a rod-like or star-like branch. This is therefore considered to have increased the aspect ratio of the branch.

6.5.3 Effect of temperature

Hydrothermal temperature is an important factor to influence the size and morphology. The hydrothermal temperature is noted as a more influential factor compared to the type of surfactant.

ZnO morphologies were synthesised at 100^{o}C, 160^{o}C and 200^{o}C for 6 hours (Figure 5-38). The FEGSEM results showed with the exception of one result, a star-like morphology was obtained (the use of F68 and 200^{o}C led to a whisker like morphology forming). The results also showed a variation in size from structures of 750 nm to >10 µm. An increase in particle size is noticeable for ZnO precipitated with L64 and F68. In the case of P123, no visible increase in size was observed within the micrographs.

The particle size increase can be explained by a kinetic ripening mechanism. An increase of temperature introduces a high solubility of ZnO and re-dissolution of all crystals until a new solubility limit is reached within the solution. Small crystals are likely to resolve in in the solution whereas large crystals may slight reduce in size. The cooling of the autoclave would restore the original solubility and the solute is considered to redeposit on the surface of the remaining particles. This would have resulted in the formation of larger particles with the increase of hydrothermal temperature.

An experiment was conducted and compared to explore the effect of temperature on the sizes and morphologies of the hydrothermally prepared ZnO nanomaterials. These two experiments were carried out under the same synthesizing conditions except for temperature. Experiment No. 4 was conducted at 220 °C while No. 20 was carried out at 140 °C. The synthesizing details are listed in Table 6-3. TEM micrographs of ZnO nanomaterials synthesized at 220°C and 140°C are presented in Figure 6-33.

Table 6-3: Details of synthesizing conditions in for the comparison of two hydrothmeral temperatures

Zinc salt	Base	Surfactant	Time	pH value	Temperature (°C)
$ZnSO_4 \cdot 7H_2O$	NaOH	PEG	6h	10.0±0.2	220
					140

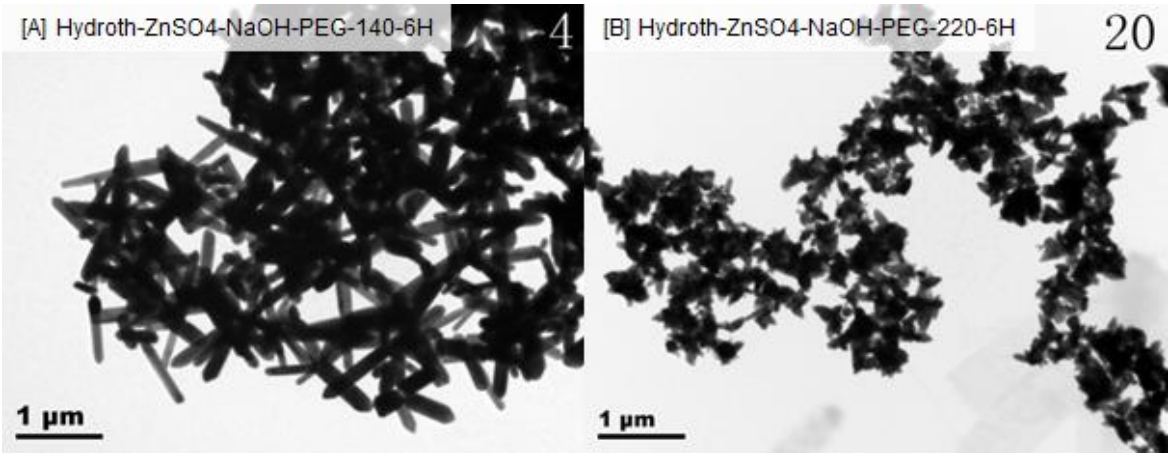

Figure 6-33: TEM micrographs of ZnO nanomaterials synthesized in: (a) 140 °C; (b) 220 °C

ZnO nanorods are observed in the TEM micrographs particles synthesised at 140°C and particles prepared at 220 °C take the morphology of tip-like anisotropic nanoparticles. This indicates hydrothermal temperature has an influence on the morphologies of the synthesized ZnO nanomaterials.

The underlying mechanism can be explained based on the research of Zhang et al. [69]. It is assumed that the nuclei $Zn(OH)_2$ and the growth unit $[Zn(OH)_4]^{2-}$ coexist in the starting hydrothermal solution. The former is responsible for the homogeneous nucleation and the

latter takes responsibility for the crystal growth in hydrothermal synthesis. ZnO grows in an anisotropic manner at 140 °C because of the lack of active sites around ZnO nuclei and enough $[Zn(OH)_4]^{2-}$ to stimulate nuclei growth at relatively low temperatures. Therefore tip-like anisotropic ZnO nanoparticles are prepared at 140 °C. When the hydrothermal synthesis process is carried out at relatively high temperatures such as 220 °C, there are enough active sites around nuclei for ZnO to grow. In addition, the transformation of $Zn(OH)_2$ into $[Zn(OH)_4]^{2-}$ takes place through the reaction:

$$Zn(OH)_2 + 2OH^- = [Zn(OH)_4]^{2-}$$ [69]

The increased amount of the growth unit $[Zn(OH)_4]^{2-}$ makes it possible to form and grow ZnO nanorods from nuclei. Therefore instead of tip-like anisotropic nanoparticles, ZnO nanorods are obtained at 200 °C [69].

It can be concluded from the analysis above that hydrothermal temperature has an effect on the morphologies of the synthesized ZnO nanoparticles. This influence is achieved by the effect of temperature on the number of active sites, ZnO nuclei, and the growth unit $[Zn(OH)_4]^{2-}$ [69].

Chapter 7 Conclusions and Future Work

7.1 Conclusions

The following conclusions can be drawn from the experimental results and discussion

- Zn-O, Zn-O-H compounds and other secondary and unknown phases of either compound were synthesized by co-precipitation and hydrothermal methods. In the precipitation process, Zn-O and Zn-O-H compounds were synthesised with the use of a “strong” base solutions such as NaOH and TMAH. Zn-O-H and other unknown phases were observed for the reactions between “weak” base solutions (pH =10.0±0.2, DEA and NH_4OH). With the exception of the use of $ZnCl_2$ as the salt precursor platelet particles (irregular or elongated) approximately 200 – 400nm in length were synthesised.

- Hydrothermal treatment (140 °C / 6 hours) of the co-precipitated samples without the presence of surfactants synthesised with a “strong” base solution showed an increase in crystallinity were Zn-O compounds had been previously synthesized. Samples Zn-O-H and other unknown phases were synthesized (*e.g.* with a “weak” base source) were converted to Zn-O compounds. Elliptical and spherical particles (200 to 800 nm) were synthesised with DEA and large aggregated bundles of rod-like structures (< 1000 nm) were synthesised with NH_4OH as the base solution.

- A mixture of of Zn-O and Zn-O-H was observed when non-ionic surfactants L64, F68 and P123 were added to a reaction between $Zn(CH_3COO)_2 \cdot 2H_2O$ and a “strong” base solution. ZnO was identified when surfactant L64 was added and a mixture of Zn-O and Zn-O-H was obtained with the addition of F68 and P123. A change in morphology in the nanoparticles was observed with the addition of L64. A change from platelet to star-like and aggregate platelets with the use of NaOH and TMAH as the “strong” base solution, respectively.

- Co-precipitated samples in presence of surfactants L64, F68 and P123 were hydrothermally treated (140 °C / 6 hours) and showed a change in compound from

Zn-O-H to Zn-O when F68 and P123 were used. For the use of NaOH as the base solution, a change in morphology also resulted from the aggregated polyols to bundles of rod-like structures. When TMAH was used as a base solution large aggregated bundles of Zn-O were formed with F68 and P123. There was no change in the morphology or size of the particles synthesised with L64, with a flower like morphology and aggregated platelet morphology formed with NaOH and TMAH, respectively. In the synthesis with "weak" base solutions there was a change in compound (Zn-O-H to Zn-O) but little change of morphology.

- In the case of the reaction between $Zn(CH_3COO)_2 \cdot 2H_2O$, NaOH and L64, until the concentration of the surfactant was greater than 53 wt%, there was no effect on the morphology of the star-like particles. At a concentration greater than 53% an aggregated platelet morphology was obtained. There was no change in this outcome following hydrothermal synthesis.

- A change of zinc salt in a reaction with NaOH and in the presence of non-ionic surfactants had a varying effect. The particles synthesised with $Zn(NO_3)_2 \cdot 6H_2O$ showed a change in morphology from platelets to large plank like-structures and aggregated irregular shaped particles. Conversely the change in zinc salt to $ZnCl_2$ resulted in little change in morphology from an aggregated bundle of rods to a platelet morphology.

- Following hydrothermal treatment, a change of zinc salt in a reaction with NaOH and in the presence of non-ionic surfactant had a limited effect on morphology. Though the hydrothermal treatment led to the formation of Zn-O, the presence of surfactant only led to a change from a platelet morphology to an aggregated rod-like morphology when $Zn(NO_3)_2 \cdot 6H_2O$ was the zinc salt. Following hydrothermal treatment, no change in morphology resulted when $ZnCl_2$ was used in the presence of non-ionic surfactants.

- Ionic surfactants were also used as the additive to investigate their effects on the particle size and morphology of -particles with a fixed starting salt ($Zn(CH_3COO)_2 \cdot 2H_2O$ and both "strong" and "weak" base solutions. Large (< 2 μm) aggregated block and tape like structures were synthesised with SDS and CTAB, respectively and NaOH as the base source. This was in contrast to the use of TMAH, which lead to the formation

of a flower-like (CTAB) and fern-like structure (SDS). The use of either “weak” base solution led to a thin platelet like structure which was not indicative of the formation of ZnO.

- Hydrothermal synthesis of samples prepared with CTAB and SDS. All the samples showed conversion to a Zn-O compound. Nanorods, agglomerated platelet and microflower morphologies were synthesised with both “strong” base solutions. Spherical and elliptical particles were synthesised with DEA. Hexagonal and needle/plank-like particles were formed with CTAB. The particle size for both base solutions ranged from 200nm (DEA/SDS) to > 1 µm (SDS/NaOH and CTAB/NH_4OH).

- The effects of synthesis conditions were investigated with through the hydrothermal treatment of Zn-O compounds co-precipitated with $Zn(CH_3COO)_2 \bullet 2H_2O$, NaOH and non-ionic surfactants. In general, when the hydrothermal temperature was modified between 2 to 12 hours, star-like structures between 1µm to 10µm were synthesised. An increase in particle size was noticeable for non-ionic surfactants L64 and F68, but not P123. The effect of hydrothermal time was examined with co-precipitated samples synthesised with $Zn(CH_3COO)_2 \bullet 2H_2O$ and DEA. The results showed a significant increase in particle size from 450 nm (2 hours) to 4200nm (6 hours)

- An orthogonal experiment based around the results of the singular experiments showed the optimum parameter for the formation largest aspect ratio (5.1) under co-precipitation conditions was attained with $Zn(NO_3)_2 \cdot 6H_2O$ reacted with NH_4OH and PEG as the surfactant. The XRD pattern reported that a mixture of $Zn(OH)_2$ and ZnO was formed. The parameter for the formation of the lowest aspect ratio (1.1) was attained with $Zn(Ac)_2 \cdot 2H_2O$ reacted with DEA using AOT as the surfactant. The calculated particles size of ZnO and $Zn(OH)_2$ was 11 and 28 nm, respectively.

- Hydrothermal treatment of the orthogonal designed experiment showed a change in optimum parameters. Flower-like, rod-like and spherical/elliptical-like morphologies were synthesised. The optimum for the formation under hydrothermal conditions (8.0) was attained with $ZnSO_4 \cdot 7H_2O$ reacted with DEA and CTAB. The hydrothermal treatment was ranked 3rd in the influence of the aspect ratio. The effect of surfactant

was still ranked the most influential, but the influence of salt (2nd most influential) and base (4th most influential) were reversed in comparison to the co-precipitated samples.

- Two optimum parameters and two moderate parameters were chosen for another group of orthogonal design experiments to investigate the influence of hydrothermal time, amount of surfactant and pH. The orthogonal experiment used $ZnSO_4 \cdot 7H_2O$, NaOH and PEG and a hydrothermal temperature of 180 °C. The results indicated that the pH value of the solution had the most influence, with hydrothermal time (2nd) and surfactant amount (3rd) less influential. The combination of optimum parameters that had the most influences on the L/W ratios was 4h, 0.0005mol PEG, pH ≈ 10.5

- A confirmation experiment using the optimum parameters obtained from the two groups of hydrothermal orthogonal experiments resulted in a L/W aspect ratio of 9.4. This was larger than the L/D ratios of nanoparticles synthesised in orthogonal experiments which ranged from 1.0 to 9.0. The morphology of the particles synthesised in the confirmation experiments was nanorods. The XRD pattern confirmed the as-synthesised particles as ZnO.

- Comparison of the effect of hydrothermal temperature and hydrothermal time from the results of the orthogonal experiments showed an increase in particle size due to either parameter. This was in line with the outcome of the effect of the hydrothermal parameters investigated with the single experiments.

- The size of hydrothermally synthesised ZnO nanoparticles was shown to decrease with increasing pH of the solution. Comparison of two experiments from the hydrothermal orthogonal experiments showed a decrease from a particles size of serval microns to a particle size of several hundred nanometers when the pH increased from 8.1±0.2 to 10.0±0.2.

- AZO with either nanorods or nanosphere morphologies were obtained when different concentration of the aluminum atomic content (3 at.%, 5 at.% and 10 at.%) was used. XRD analysis showed that the average crystal size of AZO nanoparticles decreased with increasing Al atomic content and was likely due to the AZO particle being made up of more than one grain.

7.2 Future Work

The following areas related to this project could be investigated further:

1. In the present work, the role of the surfactant was reported to be the most influential. Of the surfactants used, PEG was reported to be the optimum surfactant. PEG can be synthesised in various different molecular weights [176, 177]. It is expected that further improvement on the aspect ratio can be achieved by investigation into the hydrothermal synthesis with various different PEG molecular weights [178].

2. The present work has focused upon the use of H_2O as the synthesis medium. It is known that the use of solvents (*e.g.* ethanol) can have an effect on particle size [55, 179, 180]. The change of synthesis medium should be investigated

3. Though the effect on particle size and morphology has been investigated in this work, the effectiveness of the ZnO particles in a particle sense has not. Further work could be conducted on the casting of the particles and the characterisation of the room temperature optical properties by photoluminescence spectroscopy[181]. The gas-sensing properties could also be investigated [182].

REFERENCES

1. Look, D. C. Recent advances in ZnO materials and devices. Materials Science and Engineering: B 80, 383-387 (2001).

2. Rajeswari Yogamalar, N. & Chandra Bose, A. Tuning the aspect ratio of hydrothermally grown ZnO by choice of precursor. Journal of Solid State Chemistry 184, 12-20 (2011).

3. Arya, S. K. et al. Recent advances in ZnO nanostructures and thin films for biosensor applications: review. Anal. Chim. Acta 737, 1-21 (2012).

4. Edelstein, A. S. & Cammaratra, R. in Nanomaterials: synthesis, properties and applications (CRC Press, 1998).

5. Rotello, V. M. in Nanoparticles: building blocks for nanotechnology (Springer Science & Business Media, 2004).

6. Cao, G. in Synthesis, Properties and Applications (World Scientific, 2004).

7. Whitesides, G. M., Kriebel, J. K. & Mayers, T. B. in Nanoscale Assembly Chemical Techniques 217 (Springer, 2005).

8. Bréchignac, C., Houdy, P. & Lahmani, M. in Nanomaterials and nanochemistry (Springer Science & Business Media, 2008).

9. Tseng, A. A. in Nanofabrication: fundamentals and applications (World Scientific, 2008).

10. Wang, Z. L. Zinc oxide nanostructures: growth, properties and applications. Journal of Physics: Condensed Matter 16, R829 (2004).

11. Moezzi, A., McDonagh, A. M. & Cortie, M. B. Zinc oxide particles: Synthesis, properties and applications. Chem. Eng. J. 185, 1-22 (2012).

12. Baruah, S. & Dutta, J. Hydrothermal growth of ZnO nanostructures. Science and Technology of Advanced Materials 10, 013001 (2009).

13. Yogamalar, R. & Bose, A. C. Synthesis, Dopant Study and Device Fabrication of Zinc Oxide Nanostructures: Mini Review. Progress in Nanotechnology and Nanomaterials.

14. Cauda, V. et al. in Handbook of Nanomaterials Properties 137-177 (Springer, 2014).

15. Yogamalar, N. & Bose, A. C. Synthesis, dopant study and device fabrication of zinc oxide nanostructures: mini review. Progress in Nanotechnology and Nanomaterials 2, 1-20 (2013).

16. Akermi, M., Sakly, N., Chaabane, R. B. & Ouada, H. B. Effect of PEG-400 on the morphology and electrical properties of ZnO nanoparticles application for gas sensor. Materials Science in Semiconductor Processing 16, 807-817 (2013).

17. Jagadish, C. & Pearton, S. J. in Zinc oxide bulk, thin films and nanostructures: processing, properties, and applications (Elsevier, 2011).

18. Kahouli, M., Barhoumi, A., Bouzid, A., Al-Hajry, A. & Guermazi, S. Structural and optical properties of ZnO nanoparticles prepared by direct precipitation method. Superlattices and Microstructures 85, 7-23 (2015).

19. Özgür, Ü. et al. A comprehensive review of ZnO materials and devices. J. Appl. Phys. 98, 041301 (2005).

20. Chittofrati, A. & Matijević, E. Uniform particles of zinc oxide of different morphologies. Colloids and Surfaces 48, 65-78 (1990).

21. Farnsworth, M. & Kline, C. Zinc Chemicals, Their Properties and Applications. International Lead Zinc Research Organization, New York (1968).

22. Tynell, T. & Karppinen, M. Atomic layer deposition of ZnO: a review. Semiconductor Science and Technology 29, 043001 (2014).

23. Sirelkhatim, A. et al. Review on zinc oxide nanoparticles: antibacterial activity and toxicity mechanism. Nano-Micro Letters 7, 219-242 (2015).

24. Prescott, W. V. & Schwartz, A. I. in Nanorods, nanotubes, and nanomaterials research progress (Nova Publishers, 2008).

25. Gomez, J. L. & Tigli, O. Zinc oxide nanostructures: from growth to application. J. Mater. Sci. 48, 612-624 (2013).

26. Fan, Z. & Lu, J. G. Zinc oxide nanostructures: synthesis and properties. Journal of nanoscience and nanotechnology 5, 1561-1573 (2005).

27. Lee, B. & Komarneni, S. in Chemical processing of ceramics (CRC Press, 2005).

28. Rahaman, M. N. in Ceramic processing (CRC Press, 2007).

29. Hu, Z., Oskam, G., Penn, R. L., Pesika, N. & Searson, P. C. The influence of anion on the coarsening kinetics of ZnO nanoparticles. The Journal of Physical Chemistry B 107, 3124-3130 (2003).

30. Xu, X. et al. Preparation of multi-interfacial ZnO particles and their growth mechanism. Advanced Powder Technology 22, 634-638 (2011).

31. Shaporev, A., Ivanov, V., Baranchikov, A., Polezhaeva, O. & Tret'yakov, Y. D. ZnO formation under hydrothermal conditions from zinc hydroxide compounds with various chemical histories. Russian Journal of Inorganic Chemistry 52, 1811-1816 (2007).

32. Degen, A. & Kosec, M. Effect of pH and impurities on the surface charge of zinc oxide in aqueous solution. Journal of the European Ceramic Society 20, 667-673 (2000).

33. Li, P., Liu, H., Zhang, Y., Wei, Y. & Wang, X. Synthesis of flower-like ZnO microstructures via a simple solution route. Mater. Chem. Phys. 106, 63-69 (2007).

34. Wahab, R., Ansari, S., Kim, Y. S., Song, M. & Shin, H. The role of pH variation on the growth of zinc oxide nanostructures. Appl. Surf. Sci. 255, 4891-4896 (2009).

35. Vaishampayan, M. V., Mulla, I. S. & Joshi, S. S. Low temperature pH dependent synthesis of flower-like ZnO nanostructures with enhanced photocatalytic activity. Mater. Res. Bull. 46, 771-778 (2011).

36. Richardson, J. J. & Lange, F. F. Controlling low temperature aqueous synthesis of ZnO. 1. Thermodynamic analysis. Crystal Growth and Design 9, 2570-2575 (2009).

37. Musić, S., Dragčević, Đ., Popović, S. & Ivanda, M. Precipitation of ZnO particles and their properties. Mater Lett 59, 2388-2393 (2005).

38. Ge, M. et al. Nanostructured ZnO: from monodisperse nanoparticles to nanorods. J. Cryst. Growth 305, 162-166 (2007).

39. Wahab, R., Kim, Y. & Shin, H. Fabrication, characterization and growth mechanism of heterostructured zinc oxide nanostructures via solution method. Current Applied Physics 11, 334-340 (2011).

40. McBride, R. A., Kelly, J. M. & McCormack, D. E. Growth of well-defined ZnO microparticles by hydroxide ion hydrolysis of zinc salts. Journal of Materials Chemistry 13, 1196-1201 (2003).

41. Musić, S., Dragčević, Đ. & Popović, S. Influence of synthesis route on the formation of ZnO particles and their morphologies. J. Alloys Compounds 429, 242-249 (2007).

42. Hou, Z. et al. Synthesis of dumbbell-like ZnO microcrystals via a simple solution route. Nanoscale research letters 7, 1-7 (2012).

43. Voorhees, P. W. The theory of Ostwald ripening. Journal of Statistical Physics 38, 231-252 (1985).

44. Samanta, P. K. & Chaudhuri, P. R. Wet chemical growth of zinc oxide octahedrons and their optical property. Mater Lett 68, 510-512 (2012).

45. Seow, Z. et al. Controlled synthesis and application of ZnO nanoparticles, nanorods and nanospheres in dye-sensitized solar cells. Nanotechnology 20, 045604 (2009).

46. Li, P., Wei, Y., Liu, H. & Wang, X. Growth of well-defined ZnO microparticles with additives from aqueous solution. Journal of Solid State Chemistry 178, 855-860 (2005).

47. Hou, X., Zhou, F., Yu, B. & Liu, W. PEG-mediated synthesis of ZnO nanostructures at room temperature. Mater Lett 61, 2551-2555 (2007).

48. Anas, S., Mangalaraja, R. & Ananthakumar, S. Studies on the evolution of ZnO morphologies in a thermohydrolysis technique and evaluation of their functional properties. J. Hazard. Mater. 175, 889-895 (2010).

49. Lee, J. & Choi, S. Crystallization behavior of nano-ceria powders by hydrothermal synthesis using a mixture of H< sub> 2</sub> O< sub> 2</sub> and NH< sub> 4</sub> OH. Mater Lett 58, 390-393 (2004).

50. Piticescu, R., Monty, C., Taloi, D., Motoc, A. & Axinte, S. Hydrothermal synthesis of zirconia nanomaterials. Journal of the European Ceramic Society 21, 2057-2060 (2001).

51. Mihaiu, S. et al. Thermal behavior of ZnO precursor powders obtained from aqueous solutions. Rev Roum Chim 58, 335-345 (2013).

52. Chen, J. et al. The effect of Al doping on the morphology and optical property of ZnO nanostructures prepared by hydrothermal process. Appl. Surf. Sci. 255, 3959-3964 (2009).

53. Suchanek, W. L., Lencka, M. M. & Riman, R. E. Hydrothermal synthesis of ceramic materials. Aqueous Systems at Elevated Temperatures and Pressures: Physical Chemistry in Water, Steam, and Hydrothermal Solutions, Edited by DA Palmer, R.Fernández-Prini, and AH Harvey.Elsevier Ltd.London, UK, 717-744 (2004).

54. Podrezova, L., Porro, S., Cauda, V., Fontana, M. & Cicero, G. Comparison between ZnO nanowires grown by chemical vapor deposition and hydrothermal synthesis. Applied Physics A 113, 623-632 (2013).

55. Ehrentraut, D. et al. Solvothermal growth of ZnO. Progress in crystal growth and characterization of materials 52, 280-335 (2006).

56. Zhu, H., Yang, D. & Zhang, H. A simple and novel low-temperature hydrothermal synthesis of ZnO nanorods. Inorganic materials 42, 1210-1214 (2006).

57. Xu, H. et al. Hydrothermal synthesis of zinc oxide powders with controllable morphology. Ceram. Int. 30, 93-97 (2004).

58. Litster, J. in Design and Processing of Particulate Products (Cambridge University Press, 2016).

59. Zhang, Y. & Mu, J. Controllable synthesis of flower-and rod-like ZnO nanostructures by simply tuning the ratio of sodium hydroxide to zinc acetate. Nanotechnology 18, 075606 (2007).

60. Polsongkram, D. et al. Effect of synthesis conditions on the growth of ZnO nanorods via hydrothermal method. Physica B: Condensed Matter 403, 3713-3717 (2008).

61. Zhang, J. et al. Hydrothermal synthesis and growth mechanisms of different ZnO nanostructures and their gas-sensing properties. J. Mater. Sci. : Mater. Electron. 26, 1347-1353 (2015).

62. Zhang, J. et al. Control of ZnO morphology via a simple solution route. Chemistry of Materials 14, 4172-4177 (2002).

63. Shi, W., Guo, G. & Xiang, L. Synthesis of ZnO whiskers via hydrothermal decomposition route. Transactions of Nonferrous Metals Society of China 20, 1049-1052 (2010).

64. Wang, H., Xie, J., Yan, K. & Duan, M. Growth mechanism of different morphologies of ZnO crystals prepared by hydrothermal method. Journal of Materials Science & Technology 27, 153-158 (2011).

65. Kiomarsipour, N. & Razavi, R. S. Characterization and optical property of ZnO nano-, submicro-and microrods synthesized by hydrothermal method on a large-scale. Superlattices and Microstructures 52, 704-710 (2012).

66. Wang, Y., Yang, J., Kong, J., Jia, H. & Yu, M. ZnO microspheres: Controllable preparation and optical properties. Superlattices and Microstructures 86, 228-235 (2015).

67. Nagaraju, G., Ashoka, S., Chithaiah, P., Tharamani, C. & Chandrappa, G. Surfactant free hydrothermally derived ZnO nanowires, nanorods, microrods and their characterization. Materials Science in Semiconductor Processing 13, 21-28 (2010).

68. Jiang, L., Li, G., Ji, Q. & Peng, H. Morphological control of flower-like ZnO nanostructures. Mater Lett 61, 1964-1967 (2007).

69. Zhang, H. et al. Synthesis of flower-like ZnO nanostructures by an organic-free hydrothermal process. Nanotechnology 15, 622 (2004).

70. Mao, Y. et al. Synthesis of porous small-sized ZnO nanoparticles and their gas-sensing performance. Mater Lett 157, 151-154 (2015).

71. Ni, Y. et al. Hydrothermal preparation, characterization and property research of flowerlike ZnO nanocrystals built up by nanoflakes. Mater. Res. Bull. 43, 2919-2928 (2008).

72. Shen, L. et al. Organic molecule-assisted hydrothermal self-assembly of size-controlled tubular ZnO nanostructures. The Journal of Physical Chemistry C 111, 7280-7287 (2007).

73. Shi, X. et al. Zn (II)-PEG 300 globules as soft template for the synthesis of hexagonal ZnO micronuts by the hydrothermal reaction method. Langmuir 25, 5940-5948 (2009).

74. Guo, W., Li, X., Qin, H. & Wang, Z. PEG-20000 assisted hydrothermal synthesis of hierarchical ZnO flowers: Structure, growth and gas sensor properties. Physica E: Low-dimensional Systems and Nanostructures 73, 163-168 (2015).

75. Zhang, H. et al. Controllable growth of ZnO microcrystals by a capping-molecule-assisted hydrothermal process. Crystal growth & design 5, 547-550 (2005).

76. Zhou, Y., Wu, W., Hu, G., Wu, H. & Cui, S. Hydrothermal synthesis of ZnO nanorod arrays with the addition of polyethyleneimine. Mater. Res. Bull. 43, 2113-2118 (2008).

77. Pal, M., Bera, S., Sarkar, S. & Jana, S. Influence of Al doping on microstructural, optical and photocatalytic properties of sol–gel based nanostructured zinc oxide films on glass. RSC Advances 4, 11552-11563 (2014).

78. Nunes, P. et al. Effect of different dopant elements on the properties of ZnO thin films. Vacuum 64, 281-285 (2002).

79. Henni, A., Merrouche, A., Telli, L. & Karar, A. Studies on the structural, morphological, optical and electrical properties of Al-doped ZnO nanorods prepared by electrochemical deposition. J Electroanal Chem 763, 149-154 (2016).

80. Rao, M. R. & Okada, T. in ZnO nanocrystals and allied materials (Springer, 2014).

81. Schuler, T. & Aegerter, M. A. Optical, electrical and structural properties of sol gel ZnO: Al coatings. Thin Solid Films 351, 125-131 (1999).

82. Ratana, T., Amornpitoksuk, P. & Suwanboon, S. The wide band gap of highly oriented nanocrystalline Al doped ZnO thin films from sol–gel dip coating. J. Alloys Compounds 470, 408-412 (2009).

83. Shukla, R., Srivastava, A., Srivastava, A. & Dubey, K. Growth of transparent conducting nanocrystalline Al doped ZnO thin films by pulsed laser deposition. J. Cryst. Growth 294, 427-431 (2006).

84. Chang, J. & Hon, M. The effect of deposition temperature on the properties of Al-doped zinc oxide thin films. Thin Solid Films 386, 79-86 (2001).

85. Romero, R., López, M., Leinen, D., Martın, F. & Ramos-Barrado, J. Electrical properties of the n-ZnO/c-Si heterojunction prepared by chemical spray pyrolysis. Materials Science and Engineering: B 110, 87-93 (2004).

86. Lee, J. & Park, B. Transparent conducting ZnO: Al, In and Sn thin films deposited by the sol–gel method. Thin Solid Films 426, 94-99 (2003).

87. Dawber, M. Sputtering techniques for epitaxial growth of complex oxides. Epitaxial Growth of Complex Metal Oxides, 31 (2015).

88. Kim, K. H., Park, K. C. & Ma, D. Y. Structural, electrical and optical properties of aluminum doped zinc oxide films prepared by radio frequency magnetron sputtering. J. Appl. Phys. 81, 7764-7772 (1997).

89. Minami, T., Nanto, H. & Takata, S. Highly conductive and transparent aluminum doped zinc oxide thin films prepared by RF magnetron sputtering. Japanese Journal of Applied Physics 23, L280 (1984).

90. Pei, Z. et al. Transparent conductive ZnO: Al thin films deposited on flexible substrates prepared by direct current magnetron sputtering. Thin Solid Films 497, 20-23 (2006).

91. Willey, R. R. in Practical design and production of optical thin films (CRC Press, 2002).

92. Mattox, D. M. Physical vapor deposition (PVD) processes. Met Finish 100, 394-408 (2002).

93. Pierre, A. C. in Introduction to sol-gel processing (Springer Science & Business Media, 2013).

94. Kim, Y. & Tai, W. Electrical and optical properties of Al-doped ZnO thin films by sol–gel process. Appl. Surf. Sci. 253, 4911-4916 (2007).

95. Brinker, C. J. & Scherer, G. W. in Sol-gel science: the physics and chemistry of sol-gel processing (Academic press, 2013).

96. Chandekar, A., Sengupta, S. K., Barry, C. M. F., Mead, J. L. & Whitten, J. E. Template-directed adsorption of block copolymers on alkanethiol-patterned gold surfaces. Langmuir 22, 8071-8077 (2006).

97. Farley, S., Oom, M., Terrien, B. & Zalewski, J. Design of experiments via Taguchi methods: Orthogonal Arrays. (2007).

98. Hu, X., Zhang, J. & Zhong, J. An enhanced genetic algorithm with orthogonal design (Evolutionary Computation, 2006. CEC 2006. IEEE Congress on, IEEE, 2006).

99. Chung, Y. T., Ba-Abbad, M. M., Mohammad, A. W., Hairom, N. H. H. & Benamor, A. Synthesis of minimal-size ZnO nanoparticles through sol–gel method: Taguchi design optimisation. Mater Des 87, 780-787 (2015).

100. Srivastava, A. & Jain, K. Study on ZnO-doped tin oxide thick film gas sensors. Mater. Chem. Phys. 105, 385-390 (2007).

101. Musić, S., Šarić, A. & Popović, S. Dependence of the microstructural properties of ZnO particles on their synthesis. J. Alloys Compounds 448, 277-283 (2008).

102. Li, P., Liu, H., Xu, F. & Wei, Y. Controllable growth of ZnO nanowhiskers by a simple solution route. Mater. Chem. Phys. 112, 393-397 (2008).

103. Akbari, B., Tavandashti, M. P. & Zandrahimi, M. Particle Size Characterization of Nanoparticles–A Practicalapproach. Iranian Journal of Materials Science and Engineering 8, 48-56 (2011).

104. Thongsuriwong, K., Amornpitoksuk, P. & Suwanboon, S. The effect of aminoalcohols (MEA, DEA and TEA) on morphological control of nanocrystalline ZnO powders and its optical properties. Journal of Physics and Chemistry of Solids 71, 730-734 (2010).

105. Ring, T. A. in Fundamentals of ceramic powder processing and synthesis (Academic Press, 1996).

106. Shang, Y., Liu, H. & Hu, Y. Synthesis and Characterization of Needle-Like ZnO by Gemini Surfactant-Assisted Hydrothermal Process. J. Dispersion Sci. Technol. 27, 1-3 (2006).

107. Xie, J., Li, P., Li, Y., Wang, Y. & Wei, Y. Morphology control of ZnO particles via aqueous solution route at low temperature. Mater. Chem. Phys. 114, 943-947 (2009).

108. Usui, H. The effect of surfactants on the morphology and optical properties of precipitated wurtzite ZnO. Mater Lett 63, 1489-1492 (2009).

109. Srikanth, C. K. & Jeevanandam, P. Effect of anion on the homogeneous precipitation of precursors and their thermal decomposition to zinc oxide. J. Alloys Compounds 486, 677-684 (2009).

110. Jun, Y., Choi, J. & Cheon, J. Shape control of semiconductor and metal oxide nanocrystals through nonhydrolytic colloidal routes. Angewandte Chemie International Edition 45, 3414-3439 (2006).

111. Jagadish, C. & Pearton, S. ZnO bulk, thin films, and nanostructures. (2006).

112. Moulahi, A. & Sediri, F. ZnO nanoswords and nanopills: Hydrothermal synthesis, characterization and optical properties. Ceram. Int. 40, 943-950 (2014).

113. Peterson, R. B., Fields, C. L. & Gregg, B. A. Epitaxial chemical deposition of ZnO nanocolumns from NaOH solutions. Langmuir 20, 5114-5118 (2004).

114. Li, W., Shi, E., Zhong, W. & Yin, Z. Growth mechanism and growth habit of oxide crystals. J. Cryst. Growth 203, 186-196 (1999).

115. Zhang, J., Zhang, W., Zhao, E. & Jacques, H. J. Study of high-density AZO ceramic target. Materials Science in Semiconductor Processing 14, 189-192 (2011).

116. Raoufi, D. Synthesis and microstructural properties of ZnO nanoparticles prepared by precipitation method. Renewable Energy 50, 932-937 (2013).

117. Chen, C., Liu, P. & Lu, C. Synthesis and characterization of nano-sized ZnO powders by direct precipitation method. Chem. Eng. J. 144, 509-513 (2008).

118. Hong, R., Pan, T., Qian, J. & Li, H. Synthesis and surface modification of ZnO nanoparticles. Chem. Eng. J. 119, 71-81 (2006).

119. Schubert, U. & Hüsing, N. in Synthesis of inorganic materials (John Wiley & Sons, 2012).

120. Salman, N. et al. Effect of temperature and time in the hydrothermal treatment of HY zeolite. Microporous and Mesoporous materials 90, 339-346 (2006).

121. Laudise, R. & Ballman, A. HYDROTHERMAL SYNTHESIS OF ZINC OXIDE AND ZINC SULFIDE1. J. Phys. Chem. 64, 688-691 (1960).

122. KUSABA, K., SYONO, Y. & KIKEGAWA, T. Phase transition of ZnO under high pressure and temperature. Proceedings of the Japan Academy.Ser.B: Physical and Biological Sciences 75, 1-6 (1999).

123. Decremps, F., Zhang, J. & Liebermann, R. New phase boundary and high-pressure thermoelasticity of ZnO. EPL (Europhysics Letters) 51, 268 (2000).

124. Klingshirn, C. ZnO: From basics towards applications. physica status solidi (b) 244, 3027-3073 (2007).

125. Seko, A., Oba, F., Kuwabara, A. & Tanaka, I. Pressure-induced phase transition in ZnO and Zn O− Mg O pseudobinary system: A first-principles lattice dynamics study. Physical Review B 72, 024107 (2005).

126. Morkoç, H. & Özgür, Ü. in Zinc oxide: fundamentals, materials and device technology (John Wiley & Sons, 2008).

127. Hou, H., Xie, Y., Yang, Q., Guo, Q. & Tan, C. Preparation and characterization of γ-AlOOH nanotubes and nanorods. Nanotechnology 16, 741 (2005).

128. Wu, R. et al. Investigation of aluminum and gallium co-doped ZnO powders and their effects on the properties of targets. Materials Science in Semiconductor Processing 19, 24-31 (2014).

129. Shi, R., Yang, P., Dong, X., Ma, Q. & Zhang, A. Growth of flower-like ZnO on ZnO nanorod arrays created on zinc substrate through low-temperature hydrothermal synthesis. Appl. Surf. Sci. 264, 162-170 (2013).

130. Kuriakose, S., Bhardwaj, N., Singh, J., Satpati, B. & Mohapatra, S. Structural, optical and photocatalytic properties of flower-like ZnO nanostructures prepared by a facile wet chemical method. Beilstein journal of nanotechnology 4, 763-770 (2013).

131. Cunha, D. M. & Souza, F. L. Facile synthetic route for producing one-dimensional zinc oxide nanoflowers and characterization of their optical properties. J. Alloys Compounds 577, 158-164 (2013).

132. Li, Z. et al. Growth and comparison of different morphologic ZnO nanorod arrays by a simple aqueous solution route. Mater Lett 61, 4362-4365 (2007).

133. Zhao, J., Jin, Z., Liu, X. & Liu, Z. Growth and morphology of ZnO nanorods prepared from Zn (NO 3) 2/NaOH solutions. Journal of the European Ceramic Society 26, 3745-3752 (2006).

134. Sun, L. et al. Alkali-dependent synthesis of flower-like ZnO structures with enhanced photocatalytic activity via a facile hydrothermal method. Appl. Surf. Sci. 258, 5455-5461 (2012).

135. Kiomarsipour, N. & Razavi, R. S. Hydrothermal synthesis and optical property of scale- and spindle-like ZnO. Ceram. Int. 39, 813-818 (2013).

136. Demoisson, F., Piolet, R. & Bernard, F. Hydrothermal growth of ZnO nanostructures in supercritical domain: Effect of the metal salt concentration (Zn (NO 3) 2) in alkali medium (KOH). The Journal of Supercritical Fluids 97, 268-274 (2015).

137. Zhang, H. et al. Low temperature synthesis of flowerlike ZnO nanostructures by cetyltrimethylammonium bromide-assisted hydrothermal process. The Journal of Physical Chemistry B 108, 3955-3958 (2004).

138. Zhao, X., Li, M. & Lou, X. Sol–gel assisted hydrothermal synthesis of ZnO microstructures: morphology control and photocatalytic activity. Advanced Powder Technology 25, 372-378 (2014).

139. Xiao, Q., Huang, S., Zhang, J., Xiao, C. & Tan, X. Sonochemical synthesis of ZnO nanosheet. J. Alloys Compounds 459, L18-L22 (2008).

140. Xu, L., Guo, Y., Liao, Q., Zhang, J. & Xu, D. Morphological control of ZnO nanostructures by electrodeposition. The Journal of Physical Chemistry B 109, 13519-13522 (2005).

141. Line, I. S. THE PROBLEM OF STACKING. ORDER IN NATURAL HYDROZINCITE. (1966).

142. Prozorov, T., Kataby, G., Prozorov, R. & Gedanken, A. Effect of surfactant concentration on the size of coated ferromagnetic nanoparticles. Thin Solid Films 340, 189-193 (1999).

143. Bumajdad, A., Eastoe, J. & Mathew, A. Cerium oxide nanoparticles prepared in self-assembled systems. Adv. Colloid Interface Sci. 147, 56-66 (2009).

144. Jia, L. et al. Mechanism of PEO–PPO–PEO micellization in aqueous solutions studied by two-dimensional correlation FTIR spectroscopy. J. Colloid Interface Sci. 345, 332-337 (2010).

145. Alexandridis, P. Gold nanoparticle synthesis, morphology control, and stabilization facilitated by functional polymers. Chem. Eng. Technol. 34, 15-28 (2011).

146. Tsui, H., Hsu, Y., Wang, J. & Chen, L. Novel behavior of heat of micellization of Pluronics F68 and F88 in aqueous solutions. Langmuir 24, 13858-13862 (2008).

147. Kohut, A., Voronov, A., Samaryk, V. & Peukert, W. Amphiphilic invertible polyesters as reducing and stabilizing agents in the formation of metal nanoparticles. Macromolecular rapid communications 28, 1410-1414 (2007).

148. Alexandridis, P. & Tsianou, M. Block copolymer-directed metal nanoparticle morphogenesis and organization. European Polymer Journal 47, 569-583 (2011).

149. Pokhrel, S., Simion, C. E., Teodorescu, V. S., Barsan, N. & Weimar, U. Synthesis, Mechanism, and Gas-Sensing Application of Surfactant Tailored Tungsten Oxide Nanostructures. Advanced Functional Materials 19, 1767-1774 (2009).

150. Sakai, T. & Alexandridis, P. Mechanism of gold metal ion reduction, nanoparticle growth and size control in aqueous amphiphilic block copolymer solutions at ambient conditions. The Journal of Physical Chemistry B 109, 7766-7777 (2005).

151. Sun, X., Chen, X., Deng, Z. & Li, Y. A CTAB-assisted hydrothermal orientation growth of ZnO nanorods. Mater. Chem. Phys. 78, 99-104 (2003).

152. Hao, C. et al. Hydrothermal synthesis of flower cluster-shaped ZnO microstructures with sodium lignosulfonate as structure-directing agent. J. Mater. Sci. : Mater. Electron. 26, 9171-9177 (2015).

153. da Silva, R. C. & Loh, W. Effect of additives on the cloud points of aqueous solutions of ethylene oxide–propylene oxide–ethylene oxide block copolymers. J. Colloid Interface Sci. 202, 385-390 (1998).

154. Tang, E., Tian, B., Zheng, E., Fu, C. & Cheng, G. Preparation of zinc oxide nanoparticle via uniform precipitation method and its surface modification by methacryloxypropyltrimethoxysilane. Chem. Eng. Commun. 195, 479-491 (2008).

155. Tzeng, S., Hon, M. & Leu, I. Growth characteristics of ultra long double-ended acicular ZnO synthesized by a hydrothermal process. J. Cryst. Growth 311, 4510-4517 (2009).

156. Li, Y., Xu, G., Zhu, Y., Wang, Y. & Gong, H. Aggregation behavior of Pluronic copolymer in the presence of surfactant: Mesoscopic simulation. Colloids Surf. Physicochem. Eng. Aspects 334, 124-130 (2009).

157. Coppola, L., Oliviero, C., Pogliani, L., Ranieri, G. & Terenzi, M. A self-diffusion study in aqueous solution and lyotropic mesophases of amphiphilic block copolymers. Colloid Polym. Sci. 278, 434-442 (2000).

158. Li, F. et al. Structural and luminescent properties of ZnO nanorods and ZnO/ZnS nanocomposites. J. Alloys Compounds 474, 531-535 (2009).

159. Sun, G. et al. Anionic surfactant-assisted hydrothermal synthesis of high-aspect-ratio ZnO nanowires and their photoluminescence property. Mater Lett 60, 2777-2782 (2006).

160. Oliveira, A. P. A., Hochepied, J., Grillon, F. & Berger, M. Controlled precipitation of zinc oxide particles at room temperature. Chemistry of materials 15, 3202-3207 (2003).

161. Samaele, N., Amornpitoksuk, P. & Suwanboon, S. Effect of pH on the morphology and optical properties of modified ZnO particles by SDS via a precipitation method. Powder Technol 203, 243-247 (2010).

162. Pradhan, G. K. & Parida, K. Fabrication, growth mechanism, and characterization of α-Fe2O3 nanorods. ACS applied materials & interfaces 3, 317-323 (2011).

163. Zhang, Y. et al. Preparation of ZnO nanoparticles by a surfactant-assisted complex sol–gel method using zinc nitrate. J. Sol Gel Sci. Technol. 51, 198-203 (2009).

164. Moghadam, T. F. & Azizian, S. Effect of ZnO nanoparticles on the interfacial behavior of anionic surfactant at liquid/liquid interfaces. Colloids Surf. Physicochem. Eng. Aspects 457, 333-339 (2014).

165. Burda, C., Chen, X., Narayanan, R. & El-Sayed, M. A. Chemistry and properties of nanocrystals of different shapes. Chem. Rev. 105, 1025-1102 (2005).

166. Tang, E., Cheng, G., Ma, X., Pang, X. & Zhao, Q. Surface modification of zinc oxide nanoparticle by PMAA and its dispersion in aqueous system. Appl. Surf. Sci. 252, 5227-5232 (2006).

167. Sun, Z., Liu, L., Zhang, L. & Jia, D. Rapid synthesis of ZnO nano-rods by one-step, room-temperature, solid-state reaction and their gas-sensing properties. Nanotechnology 17, 2266 (2006).

168. Jakubowska, A. Interactions of different counterions with cationic and anionic surfactants. J. Colloid Interface Sci. 346, 398-404 (2010).

169. Maiti, U., Nandy, S., Karan, S., Mallik, B. & Chattopadhyay, K. Enhanced optical and field emission properties of CTAB-assisted hydrothermal grown ZnO nanorods. Appl. Surf. Sci. 254, 7266-7271 (2008).

170. Chen, J., Hu, Y. & Zheng, X. Surfactant-assisted self-assembly growth of single-crystalline ZnO microflowers at low temperature. Colloids Surf. Physicochem. Eng. Aspects 313, 576-580 (2008).

171. Yadav, R. S., Pandey, A. C. & Sanjay, S. S. ZnO porous structures synthesized by CTAB-assisted hydrothermal process. Structural Chemistry 18, 1001-1004 (2007).

172. Moulahi, A., Sediri, F. & Gharbi, N. Hydrothermal synthesis of nanostructured zinc oxide and study of their optical properties. Mater. Res. Bull. 47, 667-671 (2012).

173. Wang, D., Zhao, Y. & Song, C. Synthesis and properties of cuboid-shaped ZnO hierarchical structures. Solid State Sciences 12, 776-782 (2010).

174. Penn, R. L. Kinetics of oriented aggregation. The Journal of Physical Chemistry B 108, 12707-12712 (2004).

175. Tsai, J., Meen, T., Wu, T., Lai, Y. & He, Y. Morphology and optical properties of ZnO microrods grown by high-temperature hydrothermal method. Microelectronic Engineering 148, 55-58 (2015).

176. Samodi, A., Rashidi, A., Marjani, K. & Ketabi, S. Effects of surfactants, solvents and time on the morphology of MgO nanoparticles prepared by the wet chemical method. Mater Lett 109, 269-274 (2013).

177. Liufu, S., Xiao, H. & Li, Y. Investigation of PEG adsorption on the surface of zinc oxide nanoparticles. Powder Technol 145, 20-24 (2004).

178. Wang, F. et al. PEG-assisted hydrothermal synthesis and photoluminescence of flower-like ZnO microstructures. Mater Lett 117, 131-133 (2014).

179. Adhyapak, P. V., Meshram, S. P., Amalnerkar, D. P. & Mulla, I. S. Structurally enhanced photocatalytic activity of flower-like ZnO synthesized by PEG-assited hydrothermal route. Ceram. Int. 40, 1951-1959 (2014).

180. Lu, F., Cai, W. & Zhang, Y. ZnO hierarchical micro/nanoarchitectures: solvothermal synthesis and structurally enhanced photocatalytic performance. Advanced Functional Materials 18, 1047-1056 (2008).

181. Liu, X. et al. In-situ observation of hydrothermal growth of ZnO nanowires on patterned Zn substrate and their photocatalytic performance. Appl. Surf. Sci. 356, 240-248 (2015).

182. Sun, H. et al. Facile template-free hydrothermal fabrication of ZnO hollow microspheres for gas sensing applications. Ceram. Int. 40, 16465-16473 (2014).

Appendix A: Calculations

The calculation for K, k and δ in Orthogonal 1

For factor A in orthogonal 1,

$$K_{A1} = R_{S1} + R_{S2} + R_{S3} = 1.8 + 5.1 + 1.3 = 8.2;\ k_{A1} = \frac{K_{A1}}{3} = \frac{8.2}{3} = 2.7$$

$$K_{A2} = R_{S4} + R_{S5} + R_{S6} = 4.4 + 2.3 + 1.1 = 7.8;\ k_{A2} = \frac{K_{A2}}{3} = \frac{7.8}{3} = 2.6$$

$$K_{A3} = R_{S7} + R_{S8} + R_{S9} = 1.2 + 2.1 + 4.0 = 7.3;\ k_{A3} = \frac{K_{A3}}{3} = \frac{7.3}{3} = 2.4$$

δ_{kA} is defined as the biggest difference between k_{A1}, k_{A2} and k_{A3}.

So, $\delta_{kA} = 2.7\text{-}2.4 = 0.3$

For factor B,

$$K_{B1} = R_{S1} + R_{S4} + R_{S7} = 1.8 + 4.4 + 1.2 = 7.4;\ k_{B1} = \frac{K_{B1}}{3} = \frac{7.4}{3} = 2.5$$

$$K_{B2} = R_{S2} + R_{S5} + R_{S8} = 5.1 + 2.3 + 2.1 = 9.5;\ k_{B2} = \frac{K_{B2}}{3} = \frac{9.5}{3} = 3.2$$

$$K_{B3} = R_{S3} + R_{S6} + R_{S9} = 1.3 + 1.1 + 4.0 = 6.3;\ k_{B3} = \frac{K_{B3}}{3} = \frac{6.3}{3} = 2.1$$

$$\delta_{kB} = 3.2\text{-}2.1 = 1.1$$

Similarly, for factor C,

$$K_{C1} = R_{S1} + R_{S6} + R_{S8} = 1.8 + 1.1 + 2.1 = 5.0;\ k_{C1} = \frac{K_{C1}}{3} = \frac{5.0}{3} = 1.7$$

$$K_{C2} = R_{S2} + R_{S4} + R_{S9} = 5.1 + 4.4 + 4.0 = 13.5;\ k_{C2} = \frac{K_{C2}}{3} = \frac{13.5}{3} = 4.5$$

$$K_{C3} = R_{S3} + R_{S5} + R_{S7} = 1.3 + 2.3 + 1.2 = 4.8;\ k_{C3} = \frac{K_{C3}}{3} = \frac{4.8}{3} = 1.6$$

$$\delta_{kC} = 4.5\text{-}1.6 = 2.9$$

The calculation processes of K, k and δ in Orthogonal 2

For factor A in Orthogonal 2,

$$K_{A1} = R_{S1} + R_{S2} + R_{S3} = 8.28 + 10.85 + 1.38 = 20.51;\ k_{A1} = \frac{K_{A1}}{3} = \frac{20.51}{3} = 6.84$$

$$K_{A2} = R_{S4} + R_{S5} + R_{S6} = 9.86 + 1.60 + 3.43 = 14.88;\ k_{A2} = \frac{K_{A2}}{3} = \frac{14.88}{3} = 4.96$$

$$K_{A3} = R_{S7} + R_{S8} + R_{S9} = 1.47 + 13.21 + 2.16 = 16.84;\ k_{A3} = \frac{K_{A3}}{3} = \frac{16.84}{3} = 5.61$$

$$\delta_{kA} = 6.84\text{-}5.61 = 13.71$$

For factor B,

$$K_{B1} = R_{S1} + R_{S4} + R_{S7} = 8.28 + 9.86 + 1.47 = 19.61;\ k_{B1} = \frac{K_{B1}}{3} = \frac{19.61}{3} = 6.54$$

$$K_{B2} = R_{S2} + R_{S5} + R_{S8} = 10.85 + 1.60 + 2.16 = 25.66;\ k_{B2} = \frac{K_{B2}}{3} = \frac{25.66}{3} = 8.55$$

$$K_{B3} = R_{S3} + R_{S6} + R_{S9} = 1.38 + 3.43 + 2.16 = 6.97;\ k_{B3} = \frac{K_{B3}}{3} = \frac{6.97}{3} = 2.32$$

$$\delta_{kB} = 8.54\text{-}2.32 = 6.23$$

For factor C,

$$K_{C1} = R_{S1} + R_{S6} + R_{S8} = 8{,}28 + 3.43 + 13.21 = 24.93;\ k_{C1} = \frac{K_{C1}}{3} = \frac{24.93}{3} = 8.31$$

$$K_{C2} = R_{S2} + R_{S4} + R_{S9} = 10.85 + 9.86 + 2.16 = 22.86;\ k_{C2} = \frac{K_{C2}}{3} = \frac{22.86}{3} = 7.62$$

$$K_{C3} = R_{S3} + R_{S5} + R_{S7} = 1.38 + 1.60 + 1.47 = 4.44;\ k_{C3} = \frac{K_{C3}}{3} = \frac{4.44}{3} = 1.48$$

$$\delta_{kC} = 8.31\text{-}1.48 = 6.83$$

For factor D,

$$K_{D1} = R_{S1} + R_{S5} + R_{S9} = 8.28 + 1.60 + 2.16 = 12.04;\ k_{D1} = \frac{K_{D1}}{3} = \frac{12.04}{3} = 4.01$$

$$K_{D2} = R_{S2} + R_{S6} + R_{S7} = 10.85 + 3.43 + 1.47 = 15.74;\ k_{D2} = \frac{K_{D2}}{3} = \frac{15.74}{3} = 5.25$$

$$K_{D3} = R_{S3} + R_{S4} + R_{S8} = 1.38 + 9.86 + 13.21 = 24.45;\ k_{D3} = \frac{K_{D3}}{3} = \frac{24.45}{3} = 8.15$$

$$\delta_{kD} = 8.15\text{-}4.01 = 4.1$$

APPENDIX B: EXPERIMENTAL DETAILS

Experiment No.	Type	Zinc Precursor	Base	Surfactant	pH	Hydro. Temp (°C)	Hydro. Time (hours)
1	Co-precipitation	Zn(CH3COO)2•2H2O	NaOH	N/A	12.8±0.2		
2	Hydrothermal	Zn(CH3COO)2•2H2O	NaOH	N/A	12.8±0.2	140	6
3	Co-precipitation	$Zn(NO_3)_2 \cdot 6H_2O$	NaOH	N/A	12.8±0.2		
4	Hydrothermal	$Zn(NO_3)_2 \cdot 6H_2O$	NaOH	N/A	12.8±0.2	140	6
5	Co-precipitation	$ZnCl_2$	NaOH	N/A	12.8±0.2		
6	Hydrothermal	$ZnCl_2$	NaOH	N/A	12.8±0.2	140	6
7	Co-precipitation	Zn(CH3COO)2•2H2O	TMAH	N/A	12.8±0.2		
8	Hydrothermal	Zn(CH3COO)2•2H2O	TMAH	N/A	12.8±0.2	140	6
9	Co-precipitation	$Zn(NO_3)_2 \cdot 6H_2O$	TMAH	N/A	12.8±0.2		
10	Hydrothermal	$Zn(NO_3)_2 \cdot 6H_2O$	TMAH	N/A	12.8±0.2	140	6
11	Co-precipitation	$ZnCl_2$	TMAH	N/A	12.8±0.2		
12	Hydrothermal	$ZnCl_2$	TMAH	N/A	12.8±0.2	140	6
13	Co-precipitation	Zn(CH3COO)2•2H2O	DEA	N/A	10.0±0.2		
14	Hydrothermal	Zn(CH3COO)2•2H2O	DEA	N/A	10.0±0.2	140	6
15	Co-precipitation	$Zn(NO_3)_2 \cdot 6H_2O$	DEA	N/A	10.0±0.2		
16	Hydrothermal	$Zn(NO_3)_2 \cdot 6H_2O$	DEA	N/A	10.0±0.2	140	6
17	Co-precipitation	$ZnCl_2$	DEA	N/A	10.0±0.2		
18	Hydrothermal	$ZnCl_2$	DEA	N/A	10.0±0.2	140	6
19	Co-precipitation	Zn(CH3COO)2•2H2O	NH4OH	N/A	10.0±0.2		
20	Hydrothermal	Zn(CH3COO)2•2H2O	NH4OH	N/A	10.0±0.2	140	6
21	Co-precipitation	$Zn(NO_3)_2 \cdot 6H_2O$	NH4OH	N/A	10.0±0.2		
22	Hydrothermal	$Zn(NO_3)_2 \cdot 6H_2O$	NH4OH	N/A	10.0±0.2	140	6

Experiment No.	Type	Zinc Precursor	Base	Surfactant	pH	Hydro. Temp (°C)	Hydro. Time (hours)
23	Co-precipitation	$ZnCl_2$	NH4OH	N/A	10.0±0.2		
24	Hydrothermal	$ZnCl_2$	NH4OH	N/A	10.0±0.2	140	6
25	Co-precipitation	Zn(CH3COO)2•2H2O	NaOH	L64 (10%)	12.8±0.2		
26	Hydrothermal	Zn(CH3COO)2•2H2O	NaOH	L64	12.8±0.2	140	6
27	Co-precipitation	Zn(CH3COO)2•2H2O	NaOH	F68	12.8±0.2		
28	Hydrothermal	Zn(CH3COO)2•2H2O	NaOH	F68	12.8±0.2	140	6
29	Co-precipitation	Zn(CH3COO)2•2H2O	NaOH	P123	12.8±0.2		
30	Hydrothermal	Zn(CH3COO)2•2H2O	NaOH	P123	12.8±0.2	140	6
31	Co-precipitation	Zn(CH3COO)2•2H2O	TMAH	L64	12.8±0.2		
32	Hydrothermal	Zn(CH3COO)2•2H2O	TMAH	L64	12.8±0.2	140	6
32	Co-precipitation	Zn(CH3COO)2•2H2O	TMAH	F68	12.8±0.2		
34	Hydrothermal	Zn(CH3COO)2•2H2O	TMAH	F68	12.8±0.2	140	6
35	Co-precipitation	Zn(CH3COO)2•2H2O	TMAH	P123	12.8±0.2		
36	Hydrothermal	Zn(CH3COO)2•2H2O	TMAH	P123	12.8±0.2	140	6
37	Co-precipitation	Zn(CH3COO)2•2H2O	DEA	L64	10.0±0.2		
38	Hydrothermal	Zn(CH3COO)2•2H2O	DEA	L64	10.0±0.2	140	6
39	Co-precipitation	Zn(CH3COO)2•2H2O	DEA	F68	10.0±0.2		
40	Hydrothermal	Zn(CH3COO)2•2H2O	DEA	F68	10.0±0.2	140	6
41	Co-precipitation	Zn(CH3COO)2•2H2O	DEA	P123	10.0±0.2		
42	Hydrothermal	Zn(CH3COO)2•2H2O	DEA	P123	10.0±0.2	140	6
43	Co-precipitation	Zn(CH3COO)2•2H2O	NH4OH	L64	10.0±0.2		
44	Hydrothermal	Zn(CH3COO)2•2H2O	NH4OH	L64	10.0±0.2	140	6
45	Co-precipitation	Zn(CH3COO)2•2H2O	NH4OH	F68	10.0±0.2		
46	Hydrothermal	Zn(CH3COO)2•2H2O	NH4OH	F68	10.0±0.2	140	6

Experiment No.	Type	Zinc Precursor	Base	Surfactant	pH	Hydro. Temp (°C)	Hydro. Time (hours)
47	Co-precipitation	$Zn(CH_3COO)_2•2H_2O$	NH4OH	P123	10.0±0.2		
48	Hydrothermal	$Zn(CH_3COO)_2•2H_2O$	NH4OH	P123	10.0±0.2	140	6
49	Co-precipitation	$Zn(CH_3COO)_2•2H_2O$	NaOH	L64 (1%)	12.8±0.2		
50	Hydrothermal	$Zn(CH_3COO)_2•2H_2O$	NaOH	L64 (1%)	12.8±0.2		
51	Co-precipitation	$Zn(CH_3COO)_2•2H_2O$	NaOH	L64 (28%)	12.8±0.2		
52	Hydrothermal	$Zn(CH_3COO)_2•2H_2O$	NaOH	L64 (28%)	12.8±0.2		
53	Co-precipitation	$Zn(CH_3COO)_2•2H_2O$	NaOH	L64 (53%)	12.8±0.2		
54	Hydrothermal	$Zn(CH_3COO)_2•2H_2O$	NaOH	L64 (53%)	12.8±0.2		
55	Co-precipitation	$Zn(NO_3)_2·6H_2O$	NaOH	L64	12.8±0.2		
56	Hydrothermal	$Zn(NO_3)_2·6H_2O$	NaOH	L64	12.8±0.2	140	6
57	Co-precipitation	$Zn(NO_3)_2·6H_2O$	NaOH	F68	12.8±0.2		
58	Hydrothermal	$Zn(NO_3)_2·6H_2O$	NaOH	F68	12.8±0.2	140	6
59	Co-precipitation	$Zn(NO_3)_2·6H_2O$	NaOH	P123	12.8±0.2		
60	Hydrothermal	$Zn(NO_3)_2·6H_2O$	NaOH	P123	12.8±0.2	140	6
61	Co-precipitation	$ZnCl_2$	NaOH	L64	12.8±0.2		
62	Hydrothermal	$ZnCl_2$	NaOH	L64	12.8±0.2	140	6
63	Co-precipitation	$ZnCl_2$	NaOH	F68	12.8±0.2		
64	Hydrothermal	$ZnCl_2$	NaOH	F68	12.8±0.2	140	6
65	Co-precipitation	$ZnCl_2$	NaOH	P123	12.8±0.2		
66	Hydrothermal	$ZnCl_2$	NaOH	P123	12.8±0.2	140	6
67	Co-precipitation	$Zn(CH_3COO)_2•2H_2O$	NaOH	SDS	12.8±0.2		
68	Hydrothermal	$Zn(CH_3COO)_2•2H_2O$	NaOH	SDS	12.8±0.2	140	6
69	Co-precipitation	$Zn(CH_3COO)_2•2H_2O$	NaOH	CTAB	12.8±0.2		
70	Hydrothermal	$Zn(CH_3COO)_2•2H_2O$	NaOH	CTAB	12.8±0.2	140	6

Experiment No.	Type	Zinc Precursor	Base	Surfactant	pH	Hydro. Temp (°C)	Hydro. Time (hours)
71	Co-precipitation	$Zn(CH_3COO)_2•2H_2O$	TMAH	SDS	12.8±0.2		
72	Hydrothermal	$Zn(CH_3COO)_2•2H_2O$	TMAH	SDS	12.8±0.2	140	6
73	Co-precipitation	$Zn(CH_3COO)_2•2H_2O$	TMAH	CTAB	12.8±0.2		
74	Hydrothermal	$Zn(CH_3COO)_2•2H_2O$	TMAH	CTAB	12.8±0.2	140	6
75	Co-precipitation	$Zn(CH_3COO)_2•2H_2O$	DEA	SDS	10.0±0.2		
76	Hydrothermal	$Zn(CH_3COO)_2•2H_2O$	DEA	SDS	10.0±0.2	140	6
77	Co-precipitation	$Zn(CH_3COO)_2•2H_2O$	DEA	CTAB	10.0±0.2		
78	Hydrothermal	$Zn(CH_3COO)_2•2H_2O$	DEA	CTAB	10.0±0.2	140	6
79	Co-precipitation	$Zn(CH_3COO)_2•2H_2O$	NH4OH	SDS	10.0±0.2		
80	Hydrothermal	$Zn(CH_3COO)_2•2H_2O$	NH4OH	SDS	10.0±0.2	140	6
81	Co-precipitation	$Zn(CH_3COO)_2•2H_2O$	NH4OH	CTAB	10.0±0.2		
82	Hydrothermal	$Zn(CH_3COO)_2•2H_2O$	NH4OH	CTAB	10.0±0.2	140	6
83	Hydrothermal	$Zn(CH_3COO)_2•2H_2O$	NaOH	L64	12.8±0.2	140	2
84	Hydrothermal	$Zn(CH_3COO)_2•2H_2O$	NaOH	L64	12.8±0.2	140	4
85	Hydrothermal	$Zn(CH_3COO)_2•2H_2O$	NaOH	L64	12.8±0.2	140	12
86	Hydrothermal	$Zn(CH_3COO)_2•2H_2O$	NaOH	F68	12.8±0.2	140	2
87	Hydrothermal	$Zn(CH_3COO)_2•2H_2O$	NaOH	F68	12.8±0.2	140	4
88	Hydrothermal	$Zn(CH_3COO)_2•2H_2O$	NaOH	F68	12.8±0.2	140	12
89	Hydrothermal	$Zn(CH_3COO)_2•2H_2O$	NaOH	P123	12.8±0.2	140	2
90	Hydrothermal	$Zn(CH_3COO)_2•2H_2O$	NaOH	P123	12.8±0.2	140	4
91	Hydrothermal	$Zn(CH_3COO)_2•2H_2O$	NaOH	P123	12.8±0.2	140	12
92	Hydrothermal	$Zn(CH_3COO)_2•2H_2O$	NaOH	L64	12.8±0.2	120	6
93	Hydrothermal	$Zn(CH_3COO)_2•2H_2O$	NaOH	L64	12.8±0.2	160	6
94	Hydrothermal	$Zn(CH_3COO)_2•2H_2O$	NaOH	L64	12.8±0.2	200	6

Experiment No.	Type	Zinc Precursor	Base	Surfactant	pH	Hydro. Temp (°C)	Hydro. Time (hours)
95	Hydrothermal	$Zn(CH_3COO)_2•2H_2O$	NaOH	F68	12.8±0.2	120	6
96	Hydrothermal	$Zn(CH_3COO)_2•2H_2O$	NaOH	F68	12.8±0.2	160	6
97	Hydrothermal	$Zn(CH_3COO)_2•2H_2O$	NaOH	F68	12.8±0.2	200	6
98	Hydrothermal	$Zn(CH_3COO)_2•2H_2O$	NaOH	P123	12.8±0.2	120	6
99	Hydrothermal	$Zn(CH_3COO)_2•2H_2O$	NaOH	P123	12.8±0.2	160	6
100	Hydrothermal	$Zn(CH_3COO)_2•2H_2O$	NaOH	P123	12.8±0.2	200	6
101	Hydrothermal	$ZnSO_4·7H_2O$	NaOH	PEG	10.0±0.2	140	6
102	Co-precipitation	$Zn(NO_3)_2·6H_2O$	NaOH	CTAB	10.0±0.2		
103	Co-precipitation	$Zn(NO_3)_2·6H_2O$	NH4OH	PEG	10.0±0.2		
104	Co-precipitation	$Zn(NO_3)_2·6H_2O$	DEA	AOT	10.0±0.2		
105	Co-precipitation	ZnSO4·6H2O	NaOH	PEG	10.0±0.2		
106	Co-precipitation	ZnSO4·6H2O	NH4OH	AOT	10.0±0.2		
107	Co-precipitation	ZnSO4·6H2O	DEA	CTAB	10.0±0.2		
108	Co-precipitation	$Zn(CH_3COO)_2•2H_2O$	NaOH	AOT	10.0±0.2		
109	Co-precipitation	$Zn(CH_3COO)_2•2H_2O$	NH4OH	CTAB	10.0±0.2		
110	Co-precipitation	$Zn(CH_3COO)_2•2H_2O$	DEA	PEG	10.0±0.2		
111	Co-precipitation	Zn(NO3)2·6H2O	NH4OH	PEG	10.0±0.2		
112	Co-precipitation	$Zn(CH_3COO)_2•2H_2O$	DEA	AOT	10.0±0.2		
113	Hydrothermal	$Zn(NO_3)_2·6H_2O$	NaOH	CTAB	10.0±0.2	140	6
114	Hydrothermal	$Zn(NO_3)_2·6H_2O$	NH4OH	PEG	10.0±0.2	180	6
115	Hydrothermal	$Zn(NO_3)_2·6H_2O$	DEA	AOT	10.0±0.2	220	6
116	Hydrothermal	ZnSO4·7H2O	NaOH	PEG	10.0±0.2	220	6
117	Hydrothermal	ZnSO4·7H2O	NH4OH	AOT	10.0±0.2	140	6
118	Hydrothermal	ZnSO4·7H2O	DEA	CTAB	10.0±0.2	180	6
119	Hydrothermal	$Zn(CH_3COO)_2•2H_2O$	NaOH	AOT	10.0±0.2	180	6

Experiment No.	Type	Zinc Precursor	Base	Surfactant	pH	Hydro. Temp (°C)	Hydro. Time (hours)
120	Hydrothermal	$Zn(CH_3COO)_2•2H_2O$	NH4OH	CTAB	10.0±0.2	220	6
121	Hydrothermal	$Zn(CH_3COO)_2•2H_2O$	DEA	PEG	10.0±0.2	140	6
122	Hydrothermal	ZnSO4·7H2O	NaOH	PEG	11.5±0.2	180	2
123	Hydrothermal	ZnSO4·7H2O	NaOH	PEG	10.0±0.2	180	2
124	Hydrothermal	ZnSO4·7H2O	NaOH	PEG	12.8±0.2	180	2
125	Hydrothermal	ZnSO4·7H2O	NaOH	PEG	10.0±0.2	180	4
126	Hydrothermal	ZnSO4·7H2O	NaOH	PEG	12.8±0.2	180	4
127	Hydrothermal	ZnSO4·7H2O	NaOH	PEG	11.5±0.2	180	4
128	Hydrothermal	ZnSO4·7H2O	NaOH	PEG	12.8±0.2	180	6
129	Hydrothermal	ZnSO4·7H2O	NaOH	PEG	11.5±0.2	180	6
130	Hydrothermal	ZnSO4·7H2O	NaOH	PEG	10.0±0.2	180	6
131	Hydrothermal	$Zn(NO_3)_2·6H_2O$	NH_4OH	PEG	10.0±0.2	180	6